

ABSTRACT

Title of Thesis:

FEASIBILITY ANALYSIS AND FDS
MODELING OF WATER MIST FIRE
SUPPRESSION SYSTEMS FOR
PROTECTION OF AIRCRAFT HANGARS

Karolyn M. Steranka, Master of Science, 2021

Thesis Directed By:

Dr. James A. Milke
Department of Fire Protection Engineering
Dr. Arnaud Trouvé, Co-Advisor
Department of Fire Protection Engineering

Concern about PFAS containing foam fire suppression agents' negative environmental impact motivated the U.S. Air Force to perform a two-phase feasibility analysis of water mist systems for protection of aircraft hangars. Phase I involved a feasibility analysis of COTS water mist technologies based on manufacturer specifications, literature, and previous test data. Phase I identified seven manufacturers who have developed systems with potential for successful protection of aircraft hangars. Phase II used FDS to model two low pressure and one high pressure system identified in Phase I. Phase II completed an analysis and validation simulations of the Lagrangian particle, extinction, and evaporation model in FDS. Following validation simulations each nozzle was tested in a full-scale hangar configuration for protection of a JP-8 spill fire. The results found the

DISTRIBUTION E: Distribution authorized to DoD Components only. Administrative or Operational Use. Proprietary Information. 16 April 2021. Other request for this document shall be referred to AFCEC/CXA 139 Barnes Dr. Suite 2, Tyndall AFB 32403

high-pressure mist system was able to extinguish the fire and earlier activation times lead to less damage to the aircraft and hangar compartment.

FEASIBILITY ANALYSIS AND FDS MODELING OF WATER MIST FIRE
SUPPRESSION SYSTEMS FOR PROTECTION OF AIRCRAFT HANGARS

by

Karolyn M. Steranka

Thesis submitted to the Faculty of the Graduate School of the
University of Maryland, College Park, in partial fulfillment
of the requirements for the degree of
Master of Science
2021

Advisory Committee:

Dr. James A. Milke, Chair

Dr. André W. Marshall

Dr. Arnaud Trouvé, Co-Advisor

DISTRIBUTION E: Distribution authorized to DoD Components only. Administrative or
Operational Use. Proprietary Information. 16 April 2021. Other request for this document
shall be referred to AFCEC/CXA 139 Barnes Dr. Suite 2, Tyndall AFB 32403

Acknowledgements

I am extremely grateful for all of the support I have received throughout this research project. First, I want to express my deepest appreciation to both of my advisors Dr. Milke and Dr. Trouvé who despite being remote dedicated countless hours to guide me through both technical and mental challenges associated with research. Dr. Milke has provided constant support throughout not only this past year, but my entire undergraduate career at UMD, his extensive knowledge in the industry has helped me connect with numerous industry leading professionals and advance my personal development. Dr. Trouvé was instrumental in helping me navigate challenges in FDS, interpret results, and understand how to systematically make changes in my FDS input file to get clear results. I would also like to extend my sincere thanks to Dr. Marshall for participating as a member on my thesis defense board.

I would like to thank the Air Force and Battelle for funding this research project. I also wish to thank everyone who has contributed to our monthly meetings, particularly Dr. Heather Luckarift and Dr. Bridgett Ashley.

I would like to recognize all of the water mist manufacturers and their respective representatives who contributed to this research effort, particularly Henrik Abrahamansen, from VID Fire-Kill, and Dr. Kati Laakkonen, from Marioff.

I would like to acknowledge the University of Maryland supercomputing resources (<http://hpcc.umd.edu>) made available for conducting the research reported in

this paper. Thanks also to the numerous leading industry professionals who took the time to answer my questions through emails and zoom meetings.

A very special thank you to all of my friends and family who have supported me (and fed me) through the long days and nights. I would especially like to thank my sister, Kristin, and her husband, Mark, for giving me a quiet place to work during these unprecedented times being stuck at home; my boyfriend Jack, for his unwavering support of both my research and my new coffee addiction; and my parents, for introducing me to the STEM field and encouraging me to pursue higher education.

Table of Contents

CHAPTER 1 INTRODUCTION.....	1
1.1 MOTIVATION	2
1.2 COMPUTATIONAL MODELING BACKGROUND	3
1.3 SCOPE OF WORK	5
CHAPTER 2 LITERATURE REVIEW	6
2.1 LOW PRESSURE WATER MIST SYSTEMS	6
2.2 INTERMEDIATE PRESSURE WATER MIST SYSTEMS	8
2.3 HIGH PRESSURE WATER MIST SYSTEM	9
2.4 HYBRID EXTINGUISHING SYSTEMS	12
CHAPTER 3 FEASIBILITY ANALYSIS	13
3.1 FEASIBILITY CRITERIA	13
3.2 DOWN SELECTION JUSTIFICATION	15
3.3 COTS RECOMMENDATIONS	17
CHAPTER 4 FDS MODELS AND VALIDATION SIMULATIONS.....	20
4.1 FUEL MODEL	20
4.1.1 Fuel Characteristics	20
4.1.2 Combustion and Pyrolysis Model Description	22
4.1.3 Radiation Model Description	23
4.1.4 Fuel Validation Simulations.....	25
4.2 WATER MIST MODEL.....	32
4.2.1 Nozzle and Lagrangian Particle Model Description	32
4.2.2. Water Mist Characteristics & Validation Simulations	35
4.3 EXTINGUISHMENT AND EVAPORATION MODEL.....	46
4.3.1 Extinction Model Description	47
4.3.2 Extinction Model Verification Simulations	49
4.3.4 Evaporation Model Description	51
4.3.5 Evaporation Verification Simulations	52
CHAPTER 5 MODEL INPUTS.....	56
5.1 COMPARTMENT GEOMETRY	56
5.2 DESIGN FIRE	58
5.4 NOZZLE INPUTS AND SPACING.....	60
5.4 INSTRUMENTATION DEVICES.....	62
5.5 SIMULATED SCENARIOS.....	63
5.6. FDS GRID ANALYSIS AND SELECTION.....	64
5.6.1 Critical Length Scales Analysis	64
5.6.2 Final Grid Selection.....	73
5.7 MODEL LIMITATIONS.....	75
CHAPTER 6 RESULTS.....	75
6.1 NOZZLE A FINAL SIMULATIONS.....	77
6.2 NOZZLE B FINAL SIMULATIONS.....	92
6.2.1 Simulations B.1: 30 second activation time	92
6.2.2 Simulation B.2: 50 second water mist activation	107
6.3 NOZZLE C FINAL SIMULATIONS.....	114
6.3.1 Simulation C.1: 30 second activation time.....	114

6.3.2 Simulation C.2: 50 second activation time.....	122
CHAPTER 7 CONCLUSION	128
7.1 SUMMARY.....	128
7.2 FUTURE WORK.....	130
APPENDIX A: ADDITIONAL MANUFACTURER INFORMATION.....	130
A.1 DANFOSS FIRE SAFETY.....	130
A.2 FIKE	131
A.3 FOGTEC	132
A.4 GW SPRINKLERS A/S.....	132
A.5 HYDROCORE	133
A.6 JOHNSON CONTROL INTERNATIONAL.....	134
A.7 MARIOFF	134
A.8 MINIMAX.....	135
A.9 PHIREX AUSTRALIA	136
A.10 RG SYSTEMS	137
A.11 SECURIPLEX.....	137
A.12 ULTRA FOG	138
A.13 VICTAULIC.....	139
A.14 VID FIRE-KILL.....	139
APPENDIX B: FLAME DETECTOR RESPONSE AND WATER MIST ACTIVATION TIME	140
APPENDIX C: AIR ENTRAINMENT VERIFICATION SIMULATIONS	141
APPENDIX D: NOZZLE A & B GRID SENSITIVITY ANALYSIS	144
D.1 NOZZLE A GRID SENSITIVITY.....	144
D.2. NOZZLE B GRID SENSITIVITY ANALYSIS	145
APPENDIX E: HANGAR DRAWINGS	149
APPENDIX F: NOZZLE B SMALL SCALE EXTINCTION SIMULATIONS	149
F.1 DROPLETS PER SECOND ANALYSIS.....	149
F.2 GRID SIZE ANALYSIS	151
APPENDIX G: FDS INPUT FILE	152
F.1 NOZZLE A FDS INPUTS	169
F.2 NOZZLE B FDS INPUTS	175
F.2.1 Side Ignition Source Grid.....	178
F.2.2 Center ignition source Grid.....	179
F.3 NOZZLE C FDS INPUTS	181
APPENDIX H: ADDITIONAL INCIDENT HEAT FLUX RESULTS	206
H.1 NOZZLE A RESULTS.....	206
H.2 NOZZLE B RESULTS.....	210
H.3 NOZZLE C RESULTS.....	217
REFERENCES	223

List of Tables

Table 2-1 Low Pressure Water Mist Systems Summary7
Table 2-2 Intermediate Pressure Water Mist Systems Summary9
Table 2-3 High Pressure Water Mist Systems Summary10
Table 2-4 Hybrid Extinguishing Systems Summary13
Table 3-1: COTS Water Mist Recommendations.....19
Table 4-1: JP-8 values for MLRPUA calculations21
Table 4-2: JP-8 Fuel Properties22
Table 4-3 FDS Input for Nozzle A40
Table 4-4 FDS Inputs for modeling Nozzle B44
Table 4-5 FDS Input for Single Micronozzle in Multi-Orifice Nozzle C46
Table 4-6 FDS Extinction Criteria Inputs.....48
Table 4-7 Blower Vent Inputs in FDS49
Table 5-1 Hangar Construction & Obstruction Thermal Properties [15-19].....56
Table 5-2 Fuel FDS Input Values for Final Simulations in the Hangar Configuration.....59
Table 5-3 Summary of final FDS input parameters for Nozzle A, B, & C61
Table 5-4 Composite Performance Criteria.....63

List of Figure

Figure 4-1 Average net heat flux at pool surface versus radial distance from fire origin. Varying radiant fraction and soot yield = 0.0.	27
Figure 4-2. Average net heat flux at pool surface versus radial distance from fire origin. Varying soot yield and radiant fraction= 0.0.	27
Figure 4-3 Average net heat flux at pool surface versus radial distance from fire origin. Varying radiant fraction and soot yield = 0.03.	28
Figure 4-4 Average net heat flux at the pool surface over initial 30 seconds of flame spread versus distance from fire origin for 12 m x 24 m fire source, open burning.	30
Figure 4-5 Average net heat flux at the pool surface over initial 30 seconds of flame spread versus distance from fire origin for a 12 m x 24 m fire source in the hangar configuration.	31
Figure 4-6 Nozzle A spray head image	36
Figure 4-7 Cumulative Number Function predicted by FDS and measured by RISE report for Nozzle A	38
Figure 4-8 Average velocity versus height for varying initial velocity for Nozzle A with offset = 0.3., and specified CNF droplet distribution.....	39
Figure 4-9 Nozzle B spray head image.....	40
Figure 4-10 CNF and CVF for Nozzle B.....	43
Figure 4-11 Velocity versus radial distance, 1 m below the nozzle, for varying grid sizes for Nozzle C	45
Figure 4-12 Diameter (D10) versus radial distance, 1 m below the nozzle, for varying grid sizes for Nozzle C.....	46
Figure 4-13 Combustion efficiency versus oxygen mole fraction in the incoming oxidizer stream	50
Figure 4-14 Mass Fraction of Water Vapor in air flow versus time for simulation with mass flow rate of air 0.742 kg/s and incoming air temperature of 200 °C	54
Figure 4-15 Heat flow of air versus time for simulation with mass flow rate of air 0.742 kg/s and incoming air temperature of 200 °C	54
Figure 4-16 Mass Fraction of Water Vapor in air flow versus time for simulation with mass flow rate of air 0.23 kg/s and incoming air temperature of 500 °C	55
Figure 4-17 Heat flow of air versus time for simulation with mass flow rate of air 0.23 kg/s and incoming air temperature of 500 °C	55
Figure 5-1 Smokeview animation of hangar configuration, view from YMIN.....	58
Figure 5-2 Smokeview animation of hangar configuration, view from XMAX.....	58
Figure 5-3 Diameter (D10) vs vertical distance from nozzle for small mesh and hybrid mesh with Nozzle A. Nozzle located at z = 5 m.	66
Figure 5-4 Velocity vs vertical distance from nozzle for small mesh and hybrid mesh with Nozzle A. Nozzle located at z = 5 m.	66
Figure 5-3 Diameter vs vertical distance from nozzle for small mesh and hybrid mesh with Nozzle A. Nozzle located at z = 5 m.	66
Figure 5-4 Velocity vs vertical distance from nozzle for small mesh and hybrid mesh with Nozzle A. Nozzle located at z = 5 m.	66
Figure 5-5 Diameter (D10) vs radial distance for small mesh and hybrid mesh with Nozzle A. Measurements at z = 3.5 m below nozzle.....	66
Figure 5-6 Velocity vs radial distance for small mesh and hybrid mesh with Nozzle A. Measurements at z = 3.5 m below nozzle.....	66
Figure 5-5 Diameter vs radial distance for small mesh and hybrid mesh with Nozzle A. Measurements at z = 3.5 m below nozzle.....	66
Figure 5-6 Velocity vs radial distance for small mesh	

and hybrid mesh with Nozzle A. Measurements at $z = 3.5$ m below nozzle.....	66
Figure 5-7 Gas velocity vector SLCF through center of spray for Nozzle A, $dx = 0.1$ m	67
Figure 5-8 Gas velocity vector SLCF through center of spray for Nozzle A, hybrid mesh.....	67
Figure 5-9 Diameter (D10) vs horizontal distance from nozzle for small mesh and hybrid meshes with Nozzle B. Nozzle located at $x = 0$ m	68
Figure 5-10 Velocity vs horizontal distance from nozzle for small mesh and hybrid meshes with Nozzle B. Nozzle located at $x = 0$ m	68
Figure 5-11 Gas velocity vector SLCF through center of spray for Nozzle B, $dx = 0.05$ m.....	69
Figure 5-12 Gas velocity vector SLCF through center of spray for Nozzle B, hybrid mesh with grid size 0.05 m close to nozzle and 0.1 m above nozzle	69
Figure 5-13 Gas velocity vector SLCF through center of spray for Nozzle B, hybrid mesh with grid size 0.05 m close to nozzle and 0.1 m downstream	70
Figure 5-14 Diameter (D10) vs vertical distance from nozzle for small mesh and hybrid meshes with Nozzle C. Nozzle located at $z = 3$ m.	71
Figure 5-15 Velocity vs vertical distance from nozzle for small mesh and hybrid meshes with Nozzle C. Nozzle located at $z = 3$ m.	71
Figure 5-16 Diameter (D10) vs radial distance for small mesh and hybrid meshes with Nozzle C. Measurements at $Z = 3.2$ m below nozzle.	71
Figure 5-17 Velocity vs radial distance for small mesh and hybrid meshes with Nozzle C. Measurements at $z = 3.2$ m below nozzle.....	71
Figure 5-18 Gas velocity vector SLCF through center of spray for Nozzle C, $dx = 0.02$ m.....	72
Figure 5-19 Gas velocity vector SLCF through center of spray for Nozzle C, hybrid mesh with dx $= 0.02$ m to 0.04 m.....	72
Figure 5-20 Gas velocity vector SLCF through center of spray for Nozzle C, hybrid mesh with dx $= 0.02$ m to 0.08 m.....	73
Figure 6-1 Designations of various ‘targets’ in hangar compartment for results and analysis	76
Figure 6-2 Visual representation of incident heat flux device locations for results and analysis ..	77
Figure 6-3 FDS measured and expected HRR versus time for simulation A.1	78
Figure 6-4 MLR fuel and evaporation rate of water mist versus time for simulation A.1	78
Figure 6-6 Incident Heat Flux versus time low on the side of the fuselage for simulation A.1	78
Figure 6-5 Incident Heat Flux versus time across the center of the fuselage ($Y = 13$) for simulation A.1	78
Figure 6-8 Incident Heat Flux versus time to the right wing ($X = 15$) for simulation A.1	79
Figure 6-7 Incident Heat Flux versus time to the left wing ($X = 7.8$) for simulation A.1.....	79
Figure 6-10 Temperature versus time at various heights on Beam 2 for simulation A.1.....	79
Figure 6-9 Temperature versus time at various heights on Beam 1 for simulation A.1.....	79
Figure 6-11 Temperature versus time for various horizontal locations on Beam 3 for simulation A.1	80
Figure 6-12 Incident heat flux versus time at each electrical box for simulation A.1.....	80
Figure 6-13 Temperature SLCF at (a) $t = 30.5$ seconds, (b) $t = 40$ seconds, (c) $t = 60$ seconds, (d) t $= 90$ seconds, (e) $t = 120$ seconds for simulation A.1	81
Figure 6-14 Sprinkler Water Vapor Mass Fraction SLCF at (a) $t = 30.5$ seconds, (b) $t = 40$ seconds, (c) $t = 60$ seconds, (d) $t = 90$ seconds, (e) $t = 120$ seconds for simulation A.1.....	82
Figure 6-15 Oxygen Volume Fraction SLCF at (a) $t = 30.5$ seconds, (b) $t = 40$ seconds, (c) $t = 60$ seconds, (d) $t = 90$ seconds, (e) $t = 120$ seconds for simulation A.1	83
Figure 6-17 MLR fuel and evaporation rate of water mist versus time for simulation A.2.....	85
Figure 6-16 FDS measured and expected HRR versus time for simulation A.2.....	85
Figure 6-18 Incident heat flux versus time for various locations across the center of the fuselage ($Y=13$) for simulation A.2.....	86

Figure 6-19 Incident heat flux versus time for various location along the bottom of the left wing (X = 7.8) for simulation A.2	86
Figure 6-20 Incident Heat flux versus time for various locations along the bottom of the right wing (X = 15) for simulation A.2	86
Figure 6-22 Temperature versus time at various heights on Beam 2 for simulation A.2	87
Figure 6-21 Temperature versus time at various heights on Beam 1 for simulation A.2	87
Figure 6-23 Temperature versus time for various horizontal locations on Beam 3 for simulation A.2	87
Figure 6-24 Incident heat flux versus time at each electrical box for simulation A.2	88
Figure 6-25 Temperature SLCF at (a) t = 50.5 seconds, (b) t = 60 seconds, (c) t = 80 seconds, (d) t = 120 seconds for simulation A.2	89
Figure 6-26 Sprinkler Water Vapor Mass Fraction SLCF at (a) t = 50.5 seconds, (b) t = 60 seconds, (c) t = 80 seconds, (d) t = 120 seconds for simulation A.2	90
Figure 6-27 Oxygen Volume Fraction SLCF at (a) t = 50.5 seconds, (b) t = 60 seconds, (c) t = 80 seconds, (d) t = 120 seconds for simulation A.2	91
Figure 6-29 MLR fuel and evaporation rate of water mist versus time for simulation B.1.a	92
Figure 6-28 FDS measured and expected HRR versus time for simulation B.1.a	92
Figure 6-32 Incident Heat Flux versus time at various locations along fuselage (X = 13) for simulation B.1.a	93
Figure 6-33 Incident Heat Flux versus time at various locations on the left wing (X=11) for simulation B.1.a	93
Figure 6-30 Incident Heat Flux versus time at various locations along the low side of the fuselage for simulation B.1.a	93
Figure 6-31 Incident Heat Flux versus time at various locations on the right wing (X=15) for simulation B.1.a	93
Figure 6-34 Temperature versus time at various heights on Beam 1 for simulation B.1.a	94
Figure 6-35 Temperature versus time at various heights on Beam 2 for simulation B.1.a	94
Figure 6-36 Temperature versus time at various horizontal locations on Beam 3 for simulation B.1.a	94
Figure 6-37 Incident heat flux versus time at each electrical box for simulation B.1.a	95
Figure 6-38 Temperature SLCF at (a) t = 30.5 seconds, (b) t = 40 seconds, (c) t = 60 seconds, (d) t = 90 seconds, (e) t = 120 seconds for simulation B.1.a	96
Figure 6-39 Sprinkler Water Vapor Mass Fraction SLCF at (a) t = 30.5 seconds, (b) t = 40 seconds, (c) t = 60 seconds, (d) t = 90 seconds, (e) t = 120 seconds for simulation B.1.a	97
Figure 6-40 Oxygen Volume Fraction SLCF at (a) t = 30.5 seconds, (b) t = 40 seconds, (c) t = 60 seconds, (d) t = 90 seconds, (e) t = 120 seconds for simulation B.1.a	98
Figure 6-41 FDS measured and expected HRR versus time for simulation B.1.b	100
Figure 6-42 MLR Fuel and evaporation rate versus time for simulation B.1.b	100
Figure 6-44 Incident Heat Flux versus time to high side of fuselage for simulation B.1.b	101
Figure 6-45 Incident Heat Flux versus time to various locations on the left wing (X = 7.8) for simulation B.1.b	101
Figure 6-46 Incident Heat Flux versus time to various locations on the right wing (X = 15) for simulation B.1.b	101
Figure 6-43 Incident Heat Flux versus time to center of fuselage (Y = 13) for simulation B.1.b	101
Figure 6-48 Temperature versus time at various heights on Beam 2 for simulation B.1.b	102
Figure 6-47 Temperature versus time at various heights on Beam 1 for simulation B.1.b	102
Figure 6-49 Temperature versus time at various horizontal locations on Beam 3 for simulation B.1.b	102
Figure 6-50 Incident heat flux versus time at each electrical box for simulation B.1.b	103

Figure 6-51 Temperature SLCF at (a) t = 30.5 seconds, (b) t = 40 seconds, (c) t = 60 seconds, (d) t = 90 seconds, (e) t = 114 seconds for simulation B.1.b.....	104
Figure 6-52 Sprinkler Water Vapor Mass Fraction SLCF at (a) t = 30.5 seconds, (b) t = 40 seconds, (c) t = 60 seconds, (d) t = 90 seconds, (e) t = 114 seconds for simulation B.1.b.....	105
Figure 6-53 Oxygen Volume Fraction SLCF at (a) t = 30.5 seconds, (b) t = 40 seconds, (c) t = 60 seconds, (d) t = 90 seconds, (e) t = 114 seconds for simulation B.1.b	106
Figure 6-54 FDS measured and expected HRR versus time for simulation B.2	108
Figure 6-55 MLR Fuel and evaporation rate versus time for simulation B.2	108
Figure 6-59 Incident Heat Flux versus time to various locations on the right wing (X = 15) for simulation B.2.....	109
Figure 6-58 Incident Heat Flux versus time to various locations on the left wing (X = 11) for simulation B.2.....	109
Figure 6-56 Incident Heat Flux versus time to various down the center of the fuselage (X=13) for simulation B.2.....	109
Figure 6-57 Incident Heat Flux versus time to various locations on the low side of the fuselage for simulation B.2.....	109
Figure 6-60 Temperature versus time at various heights on Beam 1 for simulation B.2	110
Figure 6-61 Temperature versus time at various heights on Beam 2 for simulation B.2.....	110
Figure 6-62 Temperature versus time at various horizontal locations on Beam 3 for simulation B.2.....	110
Figure 6-63 Incident heat flux versus time at each electrical box for simulation B.2.....	111
Figure 6-64 Temperature SLCF at (a) t = 50.5 seconds, (b) t = 60 seconds, (c) t = 80 seconds, (d) t = 120 seconds for simulation B.2	112
Figure 6-65 Sprinkler Water Vapor Mass Fraction SLCF at (a) t = 50.5 seconds, (b) t = 60 seconds, (c) t = 80 seconds, (d) t = 120 seconds for simulation B.2	113
Figure 6-66 Oxygen Volume Fraction SLCF at (a) t = 50.5 seconds, (b) t = 60 seconds, (c) t = 80 seconds, (d) t = 120 seconds for simulation B.2.....	114
Figure 6-67 FDS measured and expected HRR versus time for simulation C.1	115
Figure 6-68 MLR fuel and evaporation rate of water mist versus time for simulation C.1	115
Figure 6-70 Incident Heat Flux versus time to various locations on the low side of the fuselage for simulation C.1	116
Figure 6-69 Incident Heat Flux versus time to various locations down the center of the fuselage (X=13) for simulation C.1	116
Figure 6-72 Incident Heat Flux versus time to various locations on the right wing (X =15) for simulation C.1	116
Figure 6-71 Incident Heat Flux versus time to various locations on the left wing (X = 7.8) for simulation C.1	116
Figure 6-73 Temperature versus time at various heights on Beam 1 for simulation C.1	117
Figure 6-74 Temperature versus time at various heights on Beam 2 for simulation C.1	117
Figure 6-75 Temperature versus time at various horizontal locations on Beam 3 for simulation C.1.....	117
Figure 6-76 Incident heat flux versus time at each electrical box for simulation C.1	118
Figure 6-77 Temperature SLCF at (a) t = 30.5 seconds, (b) t = 40 seconds, (c) t = 60 seconds, (d) t = 70 seconds for simulation C.1	119
Figure 6-78 Sprinkler Water Vapor Mass Fraction SLCF at (a) t = 30.5 seconds, (b) t = 40 seconds, (c) t = 60 seconds, (d) t = 70 seconds for simulation C.1	120
Figure 6-79 Oxygen Volume Fraction SLCF at (a) t = 30.5 seconds, (b) t = 40 seconds, (c) t = 60 seconds, (d) t = 70 seconds for simulation C.1	121
Figure 6-80 FDS measured and expected HRR versus time for simulation C.2	122

Figure 6-81 MLR fuel and evaporation rate of water mist versus time for simulation C.2	122
Figure 6-82 Incident Heat Flux versus time to various locations down the center of the fuselage (X=13) for simulation C.2	123
Figure 6-83 Incident Heat Flux versus time to various locations on the low side of the fuselage for simulation C.2.....	123
Figure 6-85 Incident Heat Flux versus time to various locations on the right wing (X = 17.5) for simulation C.2.....	123
Figure 6-84 Incident Heat Flux versus time to various locations on the left wing (X = 7.8) for simulation C.2.....	123
Figure 6-87 Temperature versus time at various heights on Beam 2 for simulation C.2	124
Figure 6-86 Temperature versus time at various heights on Beam 1 for simulation C.2	124
Figure 6-88 Temperature versus time at various horizontal locations on Beam 3 for simulation C.2.....	124
Figure 6-89 Incident heat flux versus time at each electrical box for simulation C.2.....	125
Figure 6-90 Temperature SLCF at (a) t = 50.5 seconds, (b) t = 60 seconds, (c) t =80 seconds, (d) t = 90 seconds for simulation C.2	126
Figure 6-91 Sprinkler Water Vapor Mass Fraction SLCF at (a) t = 50.5 seconds, (b) t = 60 seconds, (c) t =80 seconds, (d) t = 90 seconds for simulation C.2	126
Figure 6-92 Oxygen Volume Fraction SLCF at (a) t = 50.5 seconds, (b) t = 60 seconds, (c) t =80 seconds, (d) t = 90 seconds for simulation C.2.....	127
Figure 11-1 FDS particle velocity and expected particle velocity with $C_d = 0$	142
Figure 11-2 FDS particle velocity and expected terminal velocity versus height with $C_d = 0.8$..	143
Figure 11-3 FDS particle velocity and expected terminal velocity versus height with $C_d = 5$	144
Figure 12-1 Velocity versus vertical height for Nozzle A with varying grid size and final droplet size distribution and nozzle characteristics.....	145
Figure 12-2 Diameter versus vertical height for Nozzle A with varying grid size and final droplet size distribution and nozzle characteristics.....	145
Figure 12-3 Velocity versus horizontal distance from the center of Nozzle B for varying grid size with uniform velocity and droplet size.	146
Figure 12-4 Diameter versus horizontal distance from the center of Nozzle B for varying grid size with uniform velocity and droplet size.	147
Figure 12-5 Velocity versus horizontal distance from the center of Nozzle B for varying grid size with final droplet size distribution and input characteristics	148
Figure 12-6 Velocity versus horizontal distance from the center of Nozzle B for varying grid size with final droplet size distribution and input characteristics	148
Figure 14-1 HRR versus time for small scale extinction simulations using Nozzle B and varying the number of droplets representing the flow	150
Figure 14-2 Evaporation rate versus time for small scale extinction simulations using Nozzle B and varying the number of droplets representing the flow	150
Figure 14-3 HRR versus time for small scale extinction simulations using Nozzle B and varying the vertical location of grid size increase	151
Figure 14-4 Evaporation rate versus time for small scale extinction simulations using Nozzle B and varying the vertical location of grid size increase	152
Figure 16-1 Incident Heat Flux versus time for various locations along the fuselage (X=13) for simulation A.1	206
Figure 16-2 Incident Heat Flux versus time for various locations along the high side of the fuselage for simulation A.1.....	206
Figure 16-3 Incident Heat Flux versus time for various locations along the Nose of the aircraft (Y = 20) for simulation A.1	206

Figure 16-4 Incident Heat Flux versus time for various locations on the left wing (X = 10) for simulation A.1	207
Figure 16-5 Incident Heat Flux versus time for various locations on the left wing (X = 11) for simulation A.1	207
Figure 16-6 Incident Heat Flux versus time for various locations on the right wing (X = 17.5) for simulation A.1	207
Figure 16-7 Incident Heat Flux versus time for various locations on the right wing (X = 18.2) for simulation A.1	208
Figure 16-8 Incident Heat Flux versus time for various locations along the fuselage (X=13) for simulation A.2	208
Figure 16-9 Incident Heat Flux versus time for various locations along the Nose of the aircraft (Y = 20) for simulation A.2	208
Figure 16-10 Incident Heat Flux versus time for various locations on the left wing (X = 10) for simulation A.2	209
Figure 16-11 Incident Heat Flux versus time for various locations on the left wing (X = 11) for simulation A.2	209
Figure 16-12 Incident Heat Flux versus time for various locations on the right wing (X = 17.5) for simulation A.2	209
Figure 16-13 Incident Heat Flux versus time for various locations on the right wing (X = 18.2) for simulation A.2	210
Figure 16-14 Incident Heat Flux versus time for various locations across the center of the fuselage (Y=13) for simulation B.1.a	210
Figure 16-15 Incident Heat Flux versus time for various locations along the high side of the fuselage for simulation B.1.a.....	211
Figure 16-16 Incident Heat Flux versus time for various locations along the Nose of the aircraft (Y = 20) for simulation B.1.a	211
Figure 16-17 Incident Heat Flux versus time for various locations on the left wing (X = 7.8) for simulation B.1.a	211
Figure 16-18 Incident Heat Flux versus time for various locations on the left wing (X = 10) for simulation B.1.a	212
Figure 16-19 Incident Heat Flux versus time for various locations on the right wing (X = 17.5) for simulation B.1.a	212
Figure 16-20 Incident Heat Flux versus time for various locations on the right wing (X = 18.2) for simulation B.1.a	212
Figure 16-21 Incident Heat Flux versus time for various locations along the fuselage (X=13) for simulation B.1.b.....	213
Figure 16-22 Incident Heat Flux versus time for various locations along the low side of the fuselage for simulation B.1.b.....	213
Figure 16-23 Incident Heat Flux versus time for various locations along the Nose of the aircraft (Y = 20) for simulation B.1.b	213
Figure 16-24 Incident Heat Flux versus time for various locations on the left wing (X = 10) for simulation B.1.b.....	214
Figure 16-25 Incident Heat Flux versus time for various locations on the left wing (X = 11) for simulation B.1.b.....	214
Figure 16-26 Incident Heat Flux versus time for various locations on the right wing (X = 17.5) for simulation B.1.b.....	214
Figure 16-27 Incident Heat Flux versus time for various locations on the right wing (X = 18.2) for simulation B.1.b.....	215
Figure 16-28 Incident Heat Flux versus time for various locations across the center of the	

fuselage (Y=13) for simulation B.2.....	215
Figure 16-29 Incident Heat Flux versus time for various locations along the high side of the fuselage for simulation B.2.....	215
Figure 16-30 Incident Heat Flux versus time for various locations along the Nose of the aircraft (Y = 20) for simulation B.2	216
Figure 16-31 Incident Heat Flux versus time for various locations on the left wing (X = 7.8) for simulation B.2.....	216
Figure 16-32 Incident Heat Flux versus time for various locations on the left wing (X = 10) for simulation B.2.....	216
Figure 16-33 Incident Heat Flux versus time for various locations on the right wing (X = 17.5) for simulation B.2.....	217
Figure 16-34 Incident Heat Flux versus time for various locations on the right wing (X = 18.2) for simulation B.2.....	217
Figure 16-35 Incident Heat Flux versus time for various locations across the center of the fuselage (Y=13) for simulation C.1	217
Figure 16-36 Incident Heat Flux versus time for various locations along the high side of the fuselage for simulation C.1.....	218
Figure 16-37 Incident Heat Flux versus time for various locations along the Nose of the aircraft (Y = 20) for simulation C.1	218
Figure 16-38 Incident Heat Flux versus time for various locations on the left wing (X = 10) for simulation C.1.....	218
Figure 16-39 Incident Heat Flux versus time for various locations on the left wing (X = 11) for simulation C.1.....	219
Figure 16-40 Incident Heat Flux versus time for various locations on the right wing (X = 17.5) for simulation C.1.....	219
Figure 16-41 Incident Heat Flux versus time for various locations on the right wing (X = 18.2) for simulation C.1.....	219
Figure 16-42 Incident Heat Flux versus time for various locations across the center of the fuselage (Y=13) for simulation C.2.....	220
Figure 16-43 Incident Heat Flux versus time for various locations along the high side of the fuselage for simulation C.2.....	220
Figure 16-44 Incident Heat Flux versus time for various locations along the Nose of the aircraft (Y = 20) for simulation C.2	220
Figure 16-45 Incident Heat Flux versus time for various locations on the left wing (X = 10) for simulation C.2.....	221
Figure 16-46 Incident Heat Flux versus time for various locations on the left wing (X = 11) for simulation C.2.....	221
Figure 16-47 Incident Heat Flux versus time for various locations on the right wing (X = 15) for simulation C.2.....	221
Figure 16-48 Incident Heat Flux versus time for various locations on the right wing (X = 18.2) for simulation C.2.....	222

List of Abbreviations

- AHJ:** Authority Having Jurisdiction
- AIT:** Auto Ignition Temperature
- CFD:** Computational Fluid Dynamics
- CFT:** Critical Flame Temperature
- CNF:** Cumulative number function
- COTS:** Commercial Off the Shelf
- CVF:** Cumulative volume function
- DoD:** Department of Defense
- FDS:** Fire Dynamics Simulator
- FM:** FM Global
- HC-1:** Hazard Category 1
- HRR:** Heat Release Rate
- IMO:** International Maritime Organization
- LA:** local application
- LES:** Large-Eddy Simulation
- MLRPUA:** Mass Loss Rate Per Unit Area
- NIST:** National Institute of Standards and Technology
- NFPA:** National Fire Protection Association
- SINTEF:** Foundation for Scientific and Industrial Research at the Norwegian Institute of Technology
- SCLF:** Slice file
- SOLIT:** Safety of Life in Tunnels
- TVD:** Total Variation Diminishing
- UPTUN:** Engineering Guidance for Water Based Fire Fighting Systems in Tunnels

Chapter 1 Introduction

Aircraft hangars house very expensive aircraft and are used for a variety of purposes ranging from parking or storage of aircraft to hazardous maintenance and repair procedures. During these procedures, the potential exists for a jet fuel spill which is subsequently ignited to cause a very large fire. Foam fire suppression agents currently protect many aircraft hangars worldwide; these effectively extinguish and prevent the re-ignition of fuel spill fires. Concern about foam fire suppression agents' environmental impact is motivating the U.S. Air Force to consider alternative fire suppression solutions for aircraft hangars. This concern has been enhanced due to the frequency of inadvertent activations of the suppression systems, i.e., activations without a fire being present [1].

This report explores the feasibility of using water mist and hybrid fire extinguishing systems for the protection of jet fuel pool fires in aircraft hangars. The research conducted is divided into two sequential phases. Phase I includes a comprehensive review of market research and manufacturer data to provide an initial assessment of the technical feasibility of commercial off the shelf (COTS) water mist and hybrid technologies. Phase I identifies seven water mist manufacturers totaling ten combined water mist systems that demonstrate potential success in a hangar application. Phase II analyzes three mist systems deemed feasible in Phase I through computational fluid dynamics (CFD) modeling, utilizing NIST's Fire Dynamics Simulator (FDS), to model full scale fire scenarios and justify the conclusions from phase I. The simulations provide direct comparisons for water mist activation time on the effectiveness of

suppression, high pressure versus low pressure mist systems, and ceiling versus floor nozzles for protection. The results show that high pressure water mist is more effective at a 12 m ceiling height than low pressure, floor nozzles significantly impact the flame structure which can sometimes lead to higher incident heat fluxes to the aircraft, and an earlier activation time leads to less damage to the aircraft.

These simulations provide a basis for further down selection of nozzles based on the performance of high pressure versus low pressure, and ceiling versus floor-oriented nozzles. Based upon the results of Phase I and Phase II a full-scale test plan matrix is devised for the U.S. Air Force.

1.1 Motivation

Jet fuel yields a high potential fire hazard in aircraft hangars to produce fires with heat release rates up to hundreds of megawatts, damaging aircraft, expensive equipment, and the building structure. Currently, this hazard is commonly protected by foam fire protection systems. These systems have the ability to quickly suppress large hydrocarbon fires and prevent re-ignition by forming a thin film separating the fuel and heat while cooling the fuel surface. Though effective, the foam in these systems was recently identified as containing the chemical compound, C-8, which is unable to be broken down by humans or biodegrade in the environment. According to the National Fire Protection Association (NFPA), foams pose toxicity, biodegradability, persistence, treatability in wastewater treatment plants, and nutrient loading risks [1,2].

In addition to negative environmental impacts inadvertent foam discharges can have a costly impact through direct damage to the aircraft and unnecessary loss of

business continuity. A study conducted by the University of Maryland determined on an annual basis there was an average of 11.8 times the number of accidental foam system discharges versus those responding to fire in DoD and commercial aircraft hangars. The study found that of 205 foam system discharges with known causes between 2004 – 2020, only 1 incident involved a fire [1]. Due to environmental concerns and the costly impact of inadvertent foam discharges, the U.S. Air Force is considering water mist as an alternative fire suppression solution for aircraft hangars.

Over the past two decades, water mist has become a popular alternative to gaseous fire protection systems and sprinklers due to its unique suppression mechanisms, efficient water use, and environmental impact. Water mist utilizes cooling effects, radiation attenuation, and oxygen displacement through the rapid vaporization of small water particles to steam to extinguish fires. Many experiments have been done on the effectiveness of mist in small enclosed spaces, particularly for spaces on ships; however, to date a small number of studies have been conducted on the effectiveness of water mist systems in large un-enclosed spaces such as aircraft hangars.

1.2 Computational Modeling Background

Computational fire modeling in phase II of this research is performed using the program FDS, version 6.7.4, developed by the National Institute of standards and technology (NIST). Smokeview, version 6.7.14, is used for visual representation of the output from the fire models. The newest release of FDS is not used in this research due to issues with the particle model, particularly in regard to evaporation. These issues were identified through evaporation verification simulations and led to the decision to use an older model

of FDS for this research where the particle model and evaporation process is fundamental to the research question.

FDS software is designed to numerically solve a modified version of the Navier-Stokes equation that is appropriate for thermally driven fluid flow with low Mach number. The default version of FDS, utilized in this research, is a large-eddy simulation (LES) model. The LES governing equations apply a low-pass filter to the transportation of mass, momentum, and energy equations to explicitly solve for large scale fluid dynamics and employ additional terms to account for modeled sub grid scale dynamics. The equations are solved using a time integrated total variation diminishing (TVD) scheme based on the grid size in the simulation. A thorough description of the modelling capabilities, governing equations, and numerical algorithms be found in the FDS Technical Reference Guide [4].

FDS has been developed and validated for many fully developed and well-ventilated fire scenarios to predict smoke and heat transport from fires. However, under-ventilated fires and extinction via oxygen depletion and sub-grid scale kinetic effects has minimal validation and imposes very specific constraints. Information on all validated uses for FDS simulations can be found in the FDS Validation Reference Guide [5]. Because of the uncertainty associated with these calculations each aspect of the simulation must be carefully analyzed to ensure accurate physical behavior in the model and appropriate input values. Chapter 4 discusses the combustion and radiation model for simulating the fuel, the Lagrangian particle model for simulating water mist and the extinction and evaporation model for simulating flame sheet interaction.

1.3 Scope of Work

This work provides a focused effort on the evaluation, market analysis, and down select process of COTS water mist systems for possible use in Department of Defense (DoD) aircraft hangars. The information collected for Phase I is limited to publicly available information and voluntary manufacturer participation for additional material.

Modeling of select COTS products is tailored to specific Air Force hangar dimensions and evaluated based on DoD specific extinguishment criteria. Modeling of water mist nozzles for Phase II is limited to availability and reliability of manufacturer provided data. Modeling scenarios included in this study are limited to:

- Low Ceiling hangar (12 m height) with a 10,500 L fuel spill
 - Nozzle A
 - 30 second activation time
 - 50 second activation time
 - Nozzle B
 - 30 second activation time
 - Ignition in center of fuel spill
 - Ignition at edge of fuel spill
 - 50 second activation time
 - Nozzle C
 - 30 second activation time
 - 50 second activation time

Modeling scenarios are designed to determine the feasibility of water mist for aircraft hangar protection, using Manufacturer recommended nozzle spacing and flow requirements. Nozzle A is a ceiling mounted multi-orifice low pressure water mist nozzle, nozzle B is a floor pop-up multi-orifice low-pressure water mist nozzle, and

nozzle C is a high-pressure multi-orifice ceiling mounted water mist nozzle. The scenarios investigate the effect of quick detection and activation time on the effectiveness of the water mist and compare ceiling versus floor nozzles and high pressure versus low pressure nozzles. Data gathered from Phase I and II is utilized to assess system performance versus rated specifications and serves as the foundations for operational field testing and system validation. The outcome of the study is used to aid USAF in the generation of requirements for water mist fire suppression as a replacement for aqueous film forming foams (AFFF) in aircraft hangars.

Chapter 2 Literature Review

2.1 Low Pressure Water Mist Systems

NFPA 750 defines a low pressure water mist system as any water mist system where the pipe pressure does not exceed 12 bar. Low pressure water mist systems produce larger water droplets which can penetrate more challenging fire plumes with their high momentum. The larger drops are limited in suppressing obstructed fires due to high fallout rates from mist, which reduces the mixture of mist in the air. Low pressure systems can use ordinary sprinkler components and require less maintenance than other mist systems [6].

Table 2-1 summarizes manufacturers' key aspects of low pressure water mist systems for protection against Class B, shielded pool or running fuel fires. Many of the systems in Table 2-1 are FM approved for protection of data centers, non-storage HC-1 occupancies, wet bench, industrial cookers, etc.; however, only approvals with Class B fire tests are included as relevant to hangar applications. FM approvals are important,

despite the type of approval, to demonstrate the product has endured rigorous testing for each of the components involved.

Table 2-1 Low Pressure Water Mist Systems Summary

Manufacturer	Applications	Advantages^a	Disadvantages^a	Approvals^b
Fike: Duraquench (K6 nozzle) [Fike, 2020]	Machinery & Turbine Enclosures, Local Application	Capable of extinguishing concealed spray fires. Preliminary LA tests show extinguishment with no volume limit. Multiple pumps have potential to protect large volume space. Recent hangar protection webinar with solutions.	No published test results from Class B fires. Not tested in hangar application, no current installations of floor nozzles. Single pump is limited to a 4,596 m ³ space.	FM5560 – Turbine and Machinery Enclosures < 4,610 m ³ and 12 m
GW Sprinklers A/S: M5 nozzle [GWSprinkler, 2020]	Machinery & Turbine Enclosures Paint Booths, Local Application	Suitable for protection of pool fire and spray fire applications. Can be installed up to 14.4 m above hazard.	Max nozzle to ceiling distance is 1 meter. Nozzle obstructions must be less than 20 degrees of nozzle spray. Only supply nozzles, not entire configuration.	N/A
Minimax: ProCon [Minimax, 2020]	Local Application, Paint Shops, Machine Tools, Hydraulic Units, Diesel Generators	Effective in unenclosed spaces. Swirling nozzle capabilities for mist distribution. Effective under tough environmental conditions.	Need to be installed at several levels for tall equipment.	N/A

Securiplex: Fire Scope 2000 [Securiplex, 2020]	Machinery & Turbine Enclosures, Local Application, Material Handling	Air impingement creates droplets < 200 μm at low pressure. Full-scale tested in 3 rd party research applications for machinery spaces.	Limited protection volume due to required compressed air storage. No floor nozzle applications. Limited success with small, obstructed fires.	FM5560 – Turbine and Machinery Enclosures < 260 m ³ and 5 m, Local Application
VID Fire-Kill [VidAps, 2020]	Aircraft Hangars, Local Application, Tunnels, Total Flooding Machinery Space	Approved for ceiling heights up to 12 m for machinery spaces. Local application nozzles listed up to 11 m above hazard. Previous testing in aircraft hangars and with floor nozzles.	Floor nozzles must be installed flush with floor and risk being inoperable due to movable obstructions. Large droplets do not vaporize as quickly in fire, potential for splashing of fuel.	FM5560 – Turbine and Machinery Enclosures < 4,610 m ³ and 12 m

^a See relevant manufacturer discussion in Annex A for additional details.

^b [7]

2.2 Intermediate Pressure Water Mist Systems

NFPA 750 defines an intermediate pressure water mist system as any system with an operating pressure greater than 12 bar and less than 34 bar. Intermediate pressure systems can provide the larger water droplets at a higher velocity than low pressure systems. Intermediate pressure water mist systems require some specialized piping and fittings due to the higher operating pressure than typical sprinkler components.

Table 2-2 summarizes manufacturers' key aspects of intermediate pressure water mist systems for protection against Class B, shielded pool fires. Many of the systems in Table 2-2 are FM approved for protection of data centers, non-storage HC-1 occupancies, wet bench, industrial cookers, etc.; however, only approvals with Class B fire tests are relevant to hangar applications.

Table 2-2 Intermediate Pressure Water Mist Systems Summary

Manufacturer	Applications	Advantages^a	Disadvantages^a	Approvals^b
Fike: Micromist [Fike, 2020]	Turbine and Machinery Enclosures, Hydraulic Piping Equipment, Chemical Processes	Successfully tested to protect flammable liquid processes. Can be wall or ceiling mounted.	Only available in two Nitrogen cylinder size configurations. Nozzles only designed for total flooding.	FM5560 – Turbine and Machinery Enclosures < 260 m ³ and 4.9 m
JCI: Aquamist ULF (AM4 & AM10 nozzle) [Tyco, 2020]	Turbine and Machinery Enclosures	AM10 nozzle full scale tested by U.S. Navy for ship machinery spaces.	Limited in success extinguishing concealed pool fires. No floor nozzles or floor applications have been explored. Narrow mist discharge has difficulty in extinguishing fires between nozzles.	FM5560 - Turbine and Machinery Enclosures < 1,280 m ³ and 8 m (only AM4 nozzle)

^a See relevant manufacturer discussion in Annex A for additional details.

^b [7]

2.3 High Pressure Water Mist System

NFPA 750 defines a high pressure water mist system as a system with an operating pressure greater than 34 bar. High pressure systems produce very fine water droplets which are easily converted to steam to cool hot gases and locally displace oxygen. High pressure water mist systems have higher potential to lack the momentum needed to penetrate the fire plume in a tall ceiling application but are easily transported through natural and forced air flow in the building. By following air movement patterns, small droplets from high pressure systems are not impacted by obstructions as much as lower

pressure water mist systems. In general, high pressure systems require specialized piping, fittings, and power supply.

Table 2-3 summarizes manufacturers’ key aspects of high pressure water mist systems for protection against Class B, shielded pool fires. Many of the systems in Table 2-3 are FM approved for protection of data centers, non-storage HC-1 occupancies, wet bench, industrial cookers, etc.; however, only approvals with Class B fire tests are included as relevant to hangar applications.

Table 2-3 High Pressure Water Mist Systems Summary

Manufacturer	Applications	Advantages^a	Disadvantages^a	Approvals^c
Danfoss: SEM-SAFE [Danfoss, 2020]	Machinery Enclosures, Local Application, Metro Lines, Train Stations	Tested to IMO standards for marine applications. Floor level application for cable tunnels.	Most widely used for marine applications. No published information on nozzles.	FM5560 – Machinery Enclosures < 800 m ³ and 8 m
Fogtec [Fogtec International, 2020]	Turbines and Machinery Enclosures, Tunnels, Paint Shops/Coating Lines, Storage and Production of Flammable Liquids.	Full scale tested for tunnel fires up to 150 MW. Rooms not required to be sealed. Machinery test video available. Successful in tunnels up to 9 m.	Able to contain but not extinguish tunnel fires.	FM5560 – Turbine Enclosures < 270 m ³ (no height limit specified)
Hydrocore [Hydrocore, 2020]	Turbine and Machinery Enclosures, Local Application, Tunnels	3 rd party witness to full scale testing for tunnel fires 50-100 MW.	Not yet into integrated in the U.S. No nozzle characteristics.	FM5560 – Turbine and Machinery Enclosure < 260 m ³ and 5 m, Local Application
JCI: Aquamist Fog	Turbine and Transformer	Optimized nozzles available	Not a lot of testing and	FM5560 – Turbine and

[Tyco, 2020]	Rooms, Diesel Engines and Alternators, Paint Spray Booth, Local Application	for different hazards. Cylinder or pump power options for system.	capabilities known by company representatives or published on website.	Machinery Enclosures < 260 m ³ and 5 m
Marioff: Hi-Fog [Marioff, 2020]	Aircraft Hangars, Turbines and Machinery Enclosures, Local Application, Manufacturing, Flammable Liquid Storage	Test summary's available for hangar, shipboard machinery, and local application protection. Full-scale tested by U.S. Navy for ship machinery spaces.	Floor nozzles must be flush with floor and are difficult to be retrofit into existing building.	FM5560 - Turbine and Machinery Enclosures < 1,375 m ³ and 11 m, Local Application
Minimax: ProCon XP [Minimax, 2020]	Machinery and Turbine Enclosures, Diesel Generators, Hydraulic Rooms	Approved for enclosures with ceiling heights up to 13.5 m. Protection for large spaces.	Effective in enclosed spaces.	FM5560 – Turbine and Machinery Enclosures < 2,430 m ³ and 13.5 m
Phirex Australia: FOGEX [Phirex Australia, 2020]	Aircraft Hangars, Machinery and Turbine Enclosures, Military and Naval Applications	Local Application tests effective up to 11.1 m above floor. Ceiling only aircraft hangar protection with ceiling heights up to 12 m. No need for room sealing.	No third party reviewed or public test results available. No commercial floor nozzles available but could be developed upon request.	FM5560 – Turbine and Machinery Enclosures < 500 m ³ and 5 m
RG Systems [RG Systems, 2020]	Local Application Machinery and Turbine, Flammable Liquids	Wide variety of nozzles for adaptability of specific hazards. Turbine protection tested to 16 fire scenarios by SINTEF.	No public test results available. No known floor nozzles developed or available.	FM5560 ^b – Turbine and Machinery Enclosures < 260 m ³ and 5 m

Securiplex: Fire Scope 5000 Securiplex, 2020]	Turbine and Machinery Enclosures, Propulsion Engines, Tunnels, Aircraft Hangars	Worked with U.S. Armed forces to protect aircraft hangars with local application nozzle. Tested and approved for use by U.S. Navy and Coast Guard.	No public test data available. Local application nozzles for hangars are not floor mounted.	FM 5560 – Turbine Enclosures < 1,200 m ³ and 11 m, Machinery Enclosures < 500 m ³ and 5 m
Ultra fog [Ultra Fog, 2020]	Aircraft Hangars, Turbine and Machinery Enclosures, Tunnels	Have installed floor nozzles for aircraft hangars. Approved for heights up to 12 m in machinery enclosures.	No public test data or nozzle characteristics available.	FM5560 – Turbine and Machinery Enclosures < 1,329 m ³ and 12 m

^a See relevant manufacturer discussion in Annex A for additional details.

^b Decaying pressure system only.

^c [7]

2.4 Hybrid Extinguishing Systems

Hybrid extinguishing systems use a combination of inert gas and water mist to extinguish fire hazards. These systems are generally used in water sensitive areas because they utilize lower water flow rates. Hybrid systems rely on inerting the atmosphere more than water mist systems for extinguishment which poses challenges in unenclosed large open spaces. Hybrid systems utilize piping for both water and inert gas. These systems generally operate at low water pressure, meaning no high pressure water pumps are required.

Table 2-4 summarizes manufacturers' key aspects of hybrid extinguishing systems for protection against Class B, shielded pool fires. Many of the systems in Table 2-4 are FM approved for protection of data centers, non-storage HC-1 occupancies, wet

bench, industrial cookers, etc.; however, only approvals with Class B fire tests are included as relevant to hangar applications.

Table 2-4 Hybrid Extinguishing Systems Summary

Manufacturer	Applications	Advantages^a	Disadvantages^a	Approvals^b
Victaulic [Victaulic, 2020]	Turbine and Machinery Enclosures, Local Application, Picking Lines, Flammable Liquid Storage	Extinguishment aided by inert atmosphere through dense mist mixture. Single emitter can protect up to 70.7 m ³ .	Requires large amount of stored Nitrogen. Larger openings in room have lower duration of protection after discharge.	FM5580- Turbine and machinery Enclosures < 3,600 m ³ and 7.5 m
JCI: Aquamist Sonic [Tyco, 2020]	Turbine and Machinery Enclosures	Two atomizers create 1.5 trillion water droplets per second. Sidewall atomizers are available.	Requires large amount of stored nitrogen for atomization.	FM 5580 – Turbine and Machinery Enclosures < 1,040 m ³ and 8 m

^a See relevant manufacturer discussion in Annex A for additional details.

^b [7]

Chapter 3 Feasibility Analysis

3.1 Feasibility Criteria

This report analyzes the feasibility of COTS water mist and hybrid technologies to protect aircraft hangars given a pool or running jet fuel fire. Assessing each system’s feasibility is conducted by referencing previous test data for class B fires, including those aspects related to performance in extinguishing obstructed fires, performance in unenclosed spaces, nozzle characteristics, marketed applications, and relevant approvals.

Previous test data assessing water mist systems’ ability to control class B fires can be utilized to demonstrate the potential capability of mist systems to suppress or control a

fire in a hangar given the similarity in the type of fuel. Successful performance of extinguishing obstructed fires demonstrates the capability and potential of a ceiling only water mist system to navigate around obstructions, such as an aircraft, through moving with airflow throughout the space to extinguish the fire. Performance in large unenclosed spaces demonstrates the lack of dependence on enclosure effects to extinguish a fire. A large area such as a hangar cannot utilize enclosure effects; therefore, it is important to ensure the mist system's extinguishing properties without these effects. Nozzle characteristics are needed for future modeling and allow mist systems to be compared with those successful in similar market research applications.

Currently, there are no standardized third-party tests for the protection of aircraft hangars with water mist so no nozzle can be approved for this application. However, nozzles that have been approved from third-party testing facilities, such as FM Global (FM) and International Maritime Organization (IMO), still have merit for this application. FM approved nozzles demonstrate the rigorous testing nozzles and system configurations have endured through component and fire testing. FM approvals for machinery, turbine, and local application all involve combustible liquid fires, which easily translate to a fuel load in an aircraft hangar. FM approvals for Hazard Category 1 (HC-1), data centers, etc. still show the nozzle has successfully completed rigorous testing but does not demonstrate the ability to suppress class B fires. Hazard Categories are used by FM Global to determine the level of sprinkler protection needed for non-storage occupancies, HC-1 corresponds to the lowest overall combustible load rating possible.

IMO guideline MSC/CIRC. 1165, approval of equivalent water-based fire extinguishing systems for machinery spaces and cargo pump rooms, demonstrates a similar level of protection to FM approval 5560, approval for machinery space protection. Both approvals require extinction of obstructed and non-obstructed pool fires, spray fires, and wood crib fire scenarios. IMO 1387, approval of fixed water-based local application firefighting systems, is significantly less comprehensive than FM approval 5560, approval for local application protection. IMO 1387 requires significantly less fire scenarios to be tested than FM 5560 and approval based on IMO 1387 does not directly correlate to sufficient protection for land-based applications. Comparing IMO approvals to hangar applications must be carefully reviewed.

3.2 Down Selection Justification

After an initial review of COTS water mist manufacturers and their respective systems, some manufacturers are excluded from further consideration. They are excluded due to a lack of published information to verify the criteria in section 3.1 of this report or due to nozzles designed for dissimilar fire load applications. The following manufacturers are excluded.

Viking, a fire suppression manufacturer, developed one water mist nozzle to protect particle board presses where flammable liquids or wood shavings are present. Due to the singular nozzle application and lack of FM approvals, Viking's water mist system is not considered feasible for hangar applications.

TomCO2 Systems, Deluge Supply Pte, and Shanghai Mansion Wananda Fire Systems Co all have FM approved water mist systems but have no published websites or

data on water mist systems. Due to a lack of available information these systems are not explored further in this report.

Kington Process Systems Ltd manufactures high pressure water mist systems but is limited in applications and is only FM approved for the protection of industrial oil cookers. Due to Kington Process Systems' focus on kitchen hazard protection this system is not evaluated further in this report.

Novenco Fire Fighting has one FM approved water mist system, Xflow, for the protection of HC-1 occupancies. All other applications published on the manufacturers' website are for the protection of various spaces on ships and tested to IMO standards. Marine based approvals for these applications do not accurately translate to land-based applications; therefore, Xflow is not evaluated further in this report.

TankTech is a fire suppression manufacturer based in Korea and has an FM approved water mist system for turbine and machinery spaces less than 260 cubic meters. The TankTech website has no data sheets or application information and only contains two product videos relevant to mist. Due to the low FM approval volume compared to other mist systems and lack of product information this system is not evaluated further in this report.

Siemens developed one hybrid extinguishing system, Sinorix H2O Gas, utilizing nitrogen gas to propel water mist and inert the area. This system is marketed for the protection of storage of combustible liquids and turbines; however, most installed applications are for libraries, museums, and HC-1 occupancies. Due to the limited public information, lack of FM approvals, and focus on class A deep seated fires, this system is not evaluated further in this report.

3.3 COTS Recommendations

Through a preliminary review of COTS water mist and hybrid extinguishing systems, eight manufacturers were initially dismissed due to lack of public information, testing, approvals, or dissimilar applications. Justification for dismissal is given in section 3.2 of this report. Further evaluation was performed on the remaining systems based upon marketed applications, industry installations, test results, approvals, water mist characteristics, and public literature. This evaluation is presented in chapter 2.

Following the evaluation in Chapter 2, Marioff, Phirex Australia, Securiplex, Ultra Fog, and VID Fire-Kill are identified as leading manufacturers who have marketed water mist solutions for the protection of aircraft hangars. With the exception of Securiplex, all of these manufacturers have installed their respective systems in operating industry hangars that have been approved by local AHJ's. These approvals are subjective and dependent on the hangar configuration, assumed fuel load, and acceptable level of protection required. Of these solutions, Marioff, VID Fire-Kill, and Ultra Fog are the only manufacturers that have developed floor nozzle solutions. Phirex Australia utilized ceiling only protection for heights up to 12 meters. Securiplex designed a movable grid system with local application nozzles to be placed under the aircraft for protection. This system was designed in conjunction with the U.S. Armed Forces but was never installed for undisclosed reasons.

Based upon the success of ceiling only water mist systems, Fike and Minimax are included as potentially feasible for hangar applications due to their high ceiling height FM approval. Minimax has similar mist characteristics to the Marioff nozzle C and is FM approved for use in machinery spaces with ceiling heights above 12 meters. Fike utilizes

the same nozzle as VID Fire-Kill, which has been utilized in hangar protection but Fike has performed less testing with their system configuration.

Neither of the hybrid extinguishing systems are recommended due to the lack of developed floor nozzles, importance of room integrity, and large storage requirements of inert gas. Hybrid systems rely on reducing the oxygen content in the vicinity of the fire. In a large space such as an aircraft hangar, where the large doors may be open, global reduction of the oxygen concentration is not viable. Otherwise, because the droplet size produced from the nozzles is larger than that from water mist nozzles, the hybrid extinguishing system will not have the cooling efficiency as that from a water mist system with small droplets.

Table 3-1 compiles available nozzle characteristics from each manufacturer that have either been used for hangar applications or have been identified as potentially successful in large open spaces. When available, water mist characteristics specifically for hangar applications are compiled. When application specific characteristics are not available, information is taken from the FM approvals guide for machinery and turbine protection.

Table 3-1: COTS Water Mist Recommendations

Parameter	VID Fire-Kill		Ultra Fog	Securiplex	Phirex Australia	Minimax	Marioff			Fike ^a
Nozzle	A	B	202-209-O	Fire Scope 5000	FOGEX	Marine XP	C	D	E	A
Max Height [m]	12	N/A	14	11	12	10.3	11	5	N/A	12
Operating Pressure [bar]	16	8	100	51.7	100	60	50	50	75	16 ^a
Flow Rate [LPM]	22.4	28.2	20.9	15.1	6.4	15.1	27.5	12.7	18.2	22.4
K-Factor [LPM/bar ^{1/2}]	5.6	10	2.09	2.1	0.64	1.9	3.9	1.8	2.1	5.6
Spacing [m]	3x3	2x8	5x5	2.5x2.5	-	4x4	4x4	4x4	2.5 m	3x3
Review Summary	Video of floor nozzle test shows extinguishment of medium-large pool fire in under 3 minutes and extinguishment of 1 m ² JP-8 fire with hangar doors open.		General instillation on military base in Sweden; however, no full-scale resting results or nozzle characteristics are publicly available. Floor pop-up nozzles use same nozzle as ceiling nozzle.	Tested by the U.S. Navy for machinery spaces, all fires extinguished in less than 5 minutes. Coast Guard approved system for spaces up to 4,500 m ³ .	Installed at ceiling, 11-12 m high, for protection of fighter jets and military helicopters. No videos provided.	Tested and approved to IMO 1387. Not tested for success in extinguishing obstructed fires. No floor nozzles.	Full scale hangar testing report summary showed 4 different fire scenarios (under the mockup) to be extinguished within 3.2 minutes of activation. Two fire scenarios in a difficult location were unable to be extinguished but the HRR was significantly reduced.			Video of concealed spray fire extinguished by ceiling only nozzles. Simulations of floor and ceiling nozzles protection in hangar.

^a Fike shares nozzle with VID APS

Chapter 4 FDS Models and Validation Simulations

FDS simulations are conducted to assess the ability of water mist to protect against jet fuel fires and determine full-scale test criteria. Water mist systems considered in the FDS simulations were based on the designs identified in the COTS feasibility analysis. Due to time and resource constraints only three nozzles developed by two manufacturers in Table 3-1 are modelled.

4.1 Fuel Model

4.1.1 Fuel Characteristics

The fuel load used in this model consists of military grade JP-8 jet fuel. JP-8 is composed of varying percentages of hydrocarbon components, each of which has different thermal properties and contributes to the overall material properties of JP-8. Due to the complex composition of JP-8 a simple gas burner pyrolysis model, single step combustion model, and specified radiative fraction model are used to simulate the fuel. To invoke these models, FDS only requires the fuel mass loss rate per unit area (MLRPUA), post combustion soot yield, and radiative fraction. Additional information about the pyrolysis, combustion, and radiation models can be found in section 4.1.2 and 4.1.3.

Literature and experimental results for the MLRPUA of JP-8 provide a wide range of values that are dependent on parameters such as the depth of the spill, quantity of liquid spilled, floor material, and fuel temperature. The MLRPUA value used in these simulations is determined by correlations in the SFPE Handbook and verified with experimental results from NIST. The maximum MLRPUA is estimated by correlations from Gottuk and White [8],

$$\dot{m}''_{\infty} = \frac{\Delta H_c}{h_v} * 0.001 \quad \text{Eq. 1}$$

where ΔH_c , the heat of combustion of JP-8, and h_v , the latent heat of vaporization of JP-8, are defined in Table 4-1. The MLRPUA for the fire size of interest, accounting for the impact of fuel depth on the burning rate, is estimated by correlations from Gottuk and White [8],

$$\dot{m}'' = C_{\delta} * \frac{\Delta H_c}{h_v} * 0.001 * (1 - \exp(-k\beta D)), \quad \text{Eq. 2}$$

where C_{δ} , the depth correction factor, $k\beta$, the mean absorption length, and D, the diameter of the spill, are defined in Table 4-1.

Table 4-1: JP-8 values for MLRPUA calculations

ΔH_c [kJ/kg]	h_v [kJ/kg]	C_{δ}	$k\beta$ [m ⁻¹]	D [m]	\dot{m}''_{∞} [kg/s/m ²]	\dot{m}'' [kg/s/m ²]
42,800 ^a	441 ^b	0.69 ^c	3.1 ^c	12 ^d	0.09	0.06

^a [10]

^b [11]

^c [8]

^d Based on assumed fuel spill size determined in section 5.2

Due to limited published data, the radiative fraction for JP-8 is estimated based on radiative fraction values for kerosene. JP-8 is a kerosene-based fuel and has similar chemical and physical properties to kerosene. Radiative fraction values for kerosene vary from 0.4 to 0.04 with variation in diameter from 1 m to 50 m [9]. Given the large fire size in these simulations any radiant fraction between 0.05 and 0.3 is feasible. The soot yield for JP-8 is estimated based on soot yield values from experiments with dodecane, which range from 0.01 to 0.2.

Large jet fuel pool fires, i.e. those with a diameter greater than 3 m, transition to fully developed steady state fires after a transient period following the time to full pool involvement. For jet fuel fires with diameters larger than 3 m the time to full pan involvement plus the transient phase can have a duration greater than 100 seconds duration [13]. Because activation of the water mist system with flame detectors occurs within 50 seconds (see annex B for detection and activation justification), a flame spread rate is specified to model the transient behavior of the fire during activation. The flame spread rate is a function of pool surface temperature and depth, but for the purpose of these simulations a single

Table 4-2: JP-8 Fuel Properties

	FDS Input Statement	Value
value of 0.03 m/s is assumed.		
This flame spread value	MLRPUA	0.06
assumes liquid phase-	[kg/s/m ²]	
controlled flame spread over	RADIATIVE_FRACTION	0.1
the surface of the pool for the	SOOT_YIELD	0.03
time frame of interest. Table	SPREAD_RATE	0.03
4-2 summarizes the fuel	[m/s]	
	HEAT_OF_COMBUSTION	42,800
	[kJ/kg]	

properties used in the final fire engineering configuration simulations, described in chapter 6.

4.1.2 Combustion and Pyrolysis Model Description

Due to the complex composition of JP-8 a user defined MLRPUA pyrolysis model is employed for the FDS simulation. This model greatly simplifies the pyrolysis process and

neglects the material properties of JP-8. The model prescribes a fixed MLRPUA of fuel vapor at the pool surface that is independent of radiation absorption and emission effects.

The default single step infinitely fast, mixing controlled combustion model is used in the simulations. The simple combustion model lumps all species present in the simulation into either fuel, oxygen, or products of combustion. The model requires a representative fuel chemical composition and post-combustion soot yield to generate a balanced global combustion equation. The representative chemical composition for JP-8 used in these simulations is $C_{11}H_{21}$ [11]. The combustion process assumes that inside the flame region there is no air and outside the flame region there is no fuel. The combustion model assumes infinitely fast chemistry, meaning the entire chemical reaction takes place instantaneously at the flame sheet. This instantaneous reaction assumes that the mixing of fuel and oxygen governs the combustion process. Additional details about the combustion chemistry and relationship between primitive species and lumped species can be found in the FDS technical reference guide [4].

4.1.3 Radiation Model Description

Due to the large grid cell size in comparison to the size of a flame sheet, the flame temperature (T_f) in FDS is not accurately resolved by the grid. Consequently, the radiation source term T_f^4 dependence is not accurately predicted in the flame region. For this reason, FDS generally uses models to predict the radiation heat transfer.

4.1.3.1 Radiation Model 1: Optically Thick, Specified Radiative Fraction

One of the radiation models used in the validation simulations in section 4.1.4 is the LES default optically thick model with a specified radiative fraction, which corresponds to radiation model 3 in the FDS Users Guide [12]. This radiation model prescribes a fraction

of the global HRR that is emitted in the form of radiation from the fire. The radiation model only uses this calculation for radiative heat emission in the flame region, radiation emission not in the flame region is calculated using the temperature to the fourth power dependence based on average cell temperature. The user-specified radiative fraction times the global HRR gives the source term for the radiative transport equation.

Radiation absorption and emission effects are governed by the absorption coefficient, κ , which is a function of temperature and CO₂, H₂O, and soot mass fractions. The thermal feedback to the pool surface is a function of both the radiative fraction and absorption coefficient. The radiative fraction dictates the thermal feedback from inside the fuel dome and the average cell temperature dictates the thermal feedback from the smoke layer and soot particles outside of the fuel dome.

4.1.3.2 Radiation Model 2: Optically Thin, Specified Radiative Fraction

The second radiation model used in the validation simulations in section 4.1.4 and in the final simulations, is the optically thin model with a specified radiative fraction, which corresponds to radiation model 2 in the FDS Users Guide [12]. This radiation model also uses the radiative fraction to determine the amount of radiant heat emitted from the flame zone and to calculate the source term in the radiative transport equation.

This model neglects radiation absorption effects by forcing the absorption coefficient, κ , equal to 0. The thermal feedback to the fuel surface is controlled solely by the radiative fraction; FDS does not attempt to calculate re-absorption of energy by the products of combustion. Large hydrocarbon fires generally produce large amounts of soot which absorb radiation and shield outer objects from thermal radiation. This phenomenon is difficult to replicate with large grid cells and specifying an optically thin model can

prevent FDS from overestimating the radiative heat transfer from the products of combustion in the flame and smoke plume. Additional information about the two radiation models and numerical solutions to the radiative transport equation can be found in the FDS technical users guide [4].

4.1.4 Fuel Validation Simulations

4.1.4.1 Small Fire Tests – Open Environment

The first validation simulation analyzes a 1 m diameter pool fire in the center of a 6 m x 6 m x 5 m computational domain. The ceiling and the walls of the domain are open to the environment and the floor is constructed of concrete. A grid size of 10 cm is used in order to resolve the dynamics at the pool surface with at least 10 grid cells. An angular resolution of 100 angles is used to solve the radiation transport equation.

Hydrocarbon pool fires greater than 1 m in diameter are driven by radiation heat transfer; therefore, it is important to correctly capture the radiant heat from the fire to accurately determine the gas phase interaction of water mist with the flame sheet. In order to validate the fuel model, a series of simulations were conducted looking at the absorption and emission radiation effects by analyzing the net heat flux at the pool surface. These simulations examine the relationship between soot yield, radiant fraction, and thermal feedback with each radiation model for a 1 m fire in an open environment. Results of these simulations are provided in figures 4-1 through 4-3 and are compared to the expected net heat flux at the fuel surface which is depicted by a dashed line. The expected net heat flux is estimated to be 32 kW/m² using a heat balance at the fuel surface with a 20 % increase to account for heat losses to the fuel pan,

$$\dot{q}_{net}'' = 1.2 * (\dot{m}_{fuel}'' * h_v), \quad Eq. 3$$

where $\dot{m}_{fuel}'' = 0.06 \frac{kg}{s * m^2}$ and $h_v = 441 \text{ kJ/kg}$.

Figures 4-1 and 4-2 show the net heat flux versus radial position on the fuel surface for simulations using radiation model 1, described in 4.1.3.1. Figure 4-1 plots the net heat flux at the pool surface for varying radiant fractions with a constant soot yield of zero. Figure 4-1 reveals that as the radiant fraction approaches zero, the average net heat flux due to gas radiation reaches a constant value of approximately 30 kW/m². Increasing the post-combustion soot yield will increase the net heat flux from the minimum value of 30 kW/m², attained when assuming small radiation emission inside the flame zone and assuming no soot production.

Figure 4-2 plots the net heat flux at the pool surface for varying soot yield with a constant radiant fraction of 0. By setting the radiant fraction to 0 the radiation model switches from the default optically thick with a specified radiative fraction to the optically thick with an unspecified radiative fraction model. This model corresponds to radiation model 4 in the FDS Users Guide [12]. These two models are identical in emission calculations outside of the flame zone and absorption calculations throughout the domain; however, this model calculates radiation emission inside the flame zone based on the average cell temperature. This plot proves that as the soot yield increases the net heat flux to the fuel surface rises above 30 kW/m² due to additional radiation absorption and emission effects of added soot particles. Based on these results, the fuel can be modeled by modelling radiation inside the flame zone with a T_f^4 dependence, by specifying a radiant fraction of zero, and by specifying a low post combustion soot yield of 0.01.

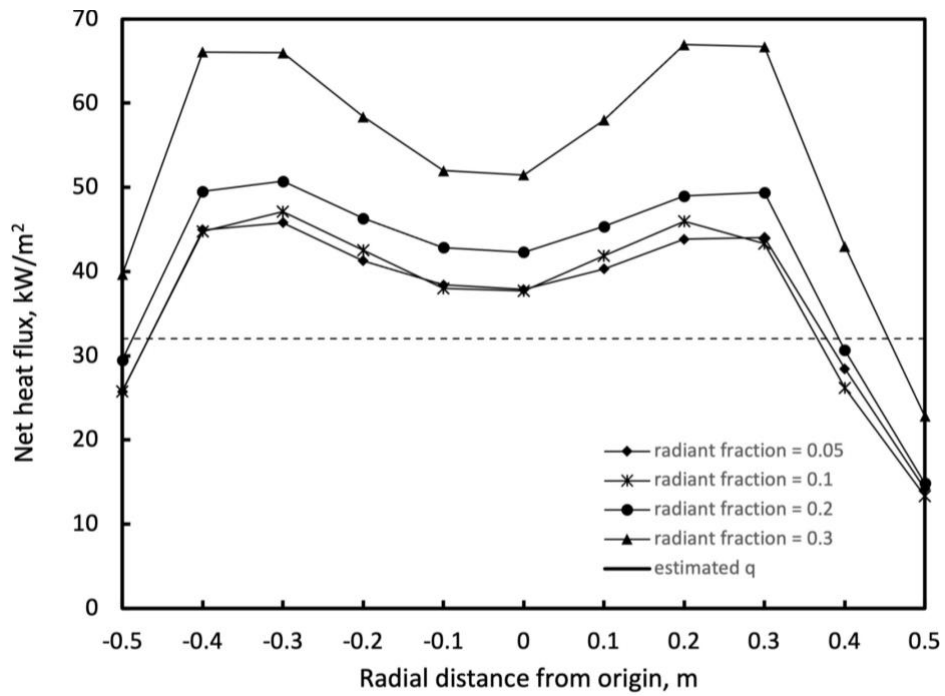


Figure 4-1 Average net heat flux at pool surface versus radial distance from fire origin. Varying radiant fraction and soot yield = 0.0.

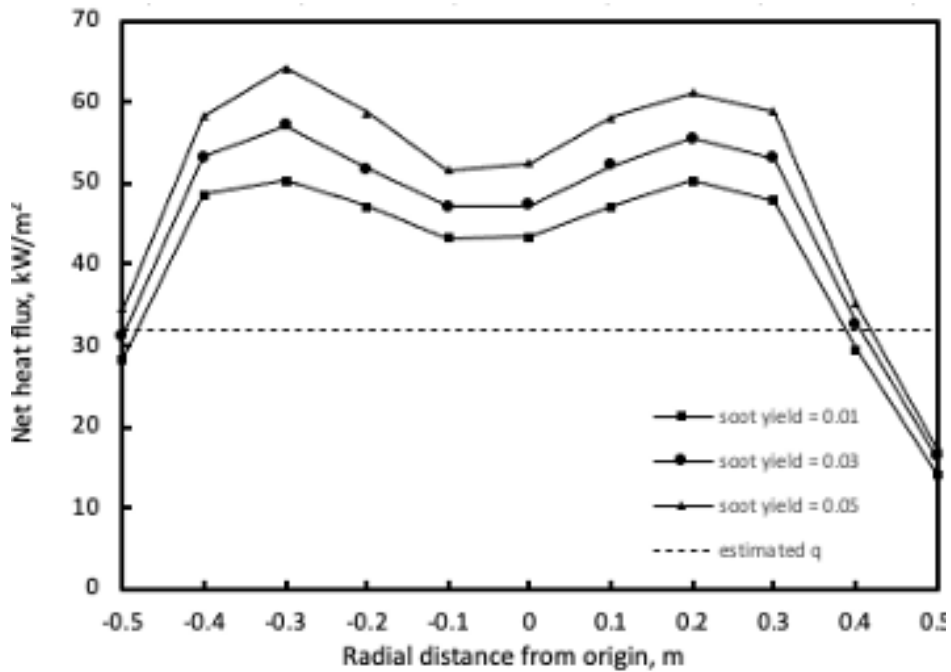


Figure 4-2. Average net heat flux at pool surface versus radial distance from fire origin. Varying soot yield and radiant fraction = 0.0.

Figure 4-3 shows the net heat flux versus radial position on the fuel surface for simulations with radiation model 2. As described in 4.1.3.2 radiation model 2 only accounts for radiation emission inside the flame sheet and neglects gas radiation emission effects and all radiation absorption effects at the pool surface. Because the only contribution to radiation from the fire comes from the prescribed radiant fraction, as the radiant fraction approaches 0 the net heat flux to the surface decreases. These results are shown in Figure 4-3. These results show that radiation to the pool surface can be more

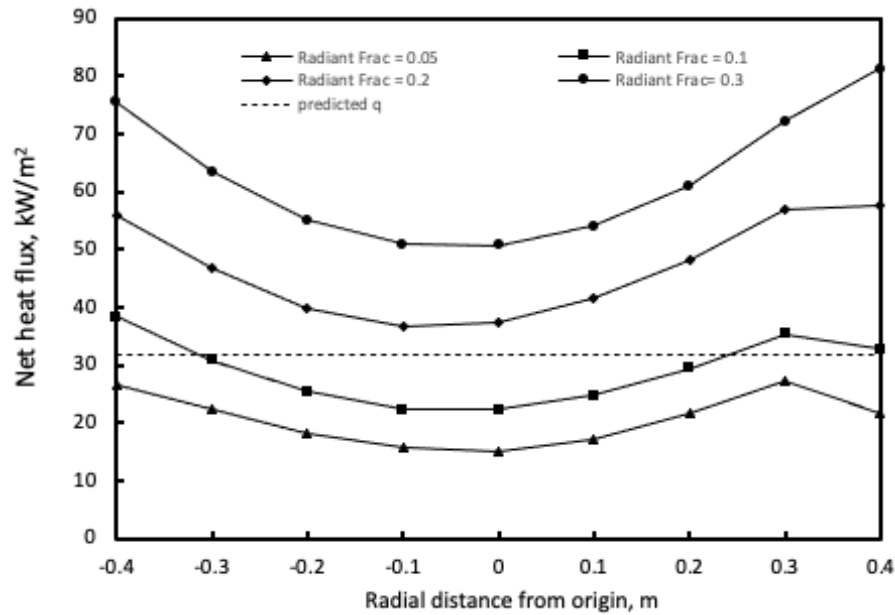


Figure 4-3 Average net heat flux at pool surface versus radial distance from fire origin. Varying radiant fraction and soot yield = 0.03.

accurately predicted by neglecting absorption effects; however, this model neglects the physics associated with soot particle radiation absorption.

The results from these validation simulations provide two ways to model the fuel which are outlined in Table 4-3.

Table 4-3: Fuel Modeling Options

	Fuel Model 1	Fuel Model 2
Radiation Model	1 (optically thick)	2 (optically thin)
RADIATIVE_FRACTION	0.0	0.1
SOOT_YIELD	0.01	0.03

4.1.4.2 Large Fire – Open Environment

Following the results from the small diameter fire simulations, larger fire simulations in an open environment are conducted using the two acceptable modeling methods. These simulations provide an intermediate step to compare to the small fire simulations before examining results for the final compartment geometry.

This simulation analyzes a 12 m x 24 m pool fire that spreads radially at 0.3 m/s from the center of the pool in a 26 m x 26 m x 12 m computational domain. This simulation uses a greater flame spread rate than the final simulations in chapter 5; however, this change effectively only alters the duration of growth, the net radiation at different fire sizes as the fire develops deviates by less than 10 % from simulations with a lower spread rate. The higher spread rate allows a less computationally expensive simulation to be compared to the final configuration. The ceiling and the walls of the domain are open to the environment and the floor is constructed of concrete. A grid size of 50 cm is used in order to resolve the dynamics at the pool surface. An angular resolution of 100 angles is used to solve the radiation transport equation.

The net heat flux at the pool surface versus radial distance from the fire center for each radiation model is provided in Figure 4-4. The results are averaged over the first 30 seconds of fire spread where the flame does not yet consume the entire fuel area. After the first 30 seconds of fire spread the fire becomes very large and the heat flux to the surface becomes significantly overpredicted. Because activation of the water mist will occur before the fire covers a 12 m x 18 m area, which corresponds to the spread within 30 seconds with 0.3 m/s flame spread, analysis of the first 30 seconds of free burning is sufficient. Fire model 1 shows net heat flux values that are double those found in the small pool fire tests (i.e. 32 kW/m²). Fire model 2 shows net heat flux values comparable to those found in the small pool fire tests.

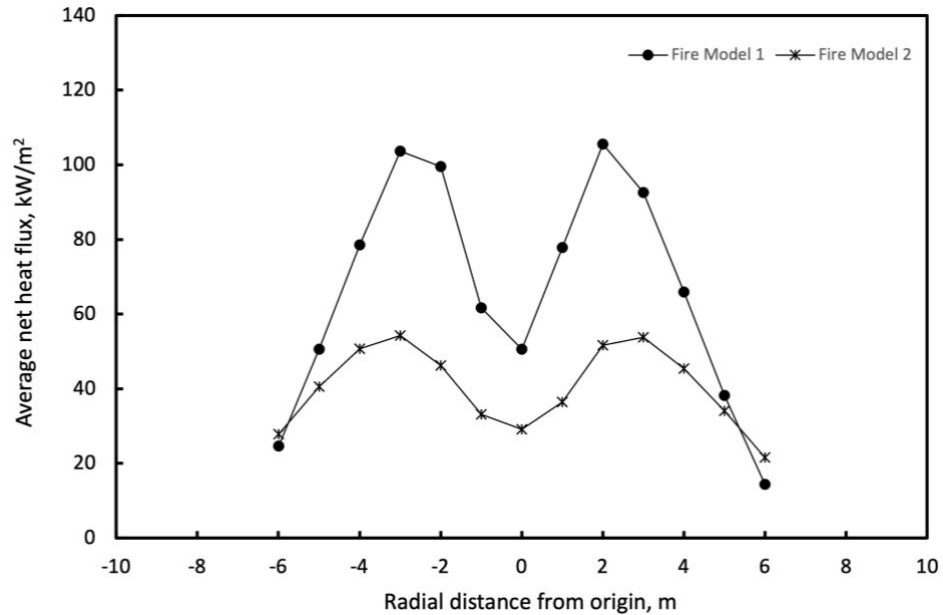


Figure 4-4 Average net heat flux at the pool surface over initial 30 seconds of flame spread versus distance from fire origin for 12 m x 24 m fire source, open burning.

4.1.4.3 Large Fire – Inside Hangar

The final step in fuel verification is to review the results of the fire burning inside of the hangar configuration. This simulation analyzes a 12 m x 24 m pool fire that spreads

radially at 0.3 m/s from the center of the pool in a 26 m x 26 m x 12 m hangar with a 12 m x 7 m door opening. See section 4.1.4.2 for justification of this spread rate value. An additional open mesh of 6 m x 26 m x 12 m is attached to the door opening to account for air entrainment into the hangar. The ceiling and the walls of the hangar are constructed of corrugated metal and the floor is constructed of concrete. A grid size of 50 cm is used in order to resolve the dynamics at the pool surface. An angular resolution of 100 angles is used to solve the radiation transport equation.

Figure 4-5 plots the results of the neat heat flux versus radial position for each fuel model burning inside of the hangar compartment. The results are analyzed in a similar manner to the results in 4.1.4.2 and the same conclusions can be made. Fire model 1 shows net flux values that are over double those found in the small pool fire tests (i.e.

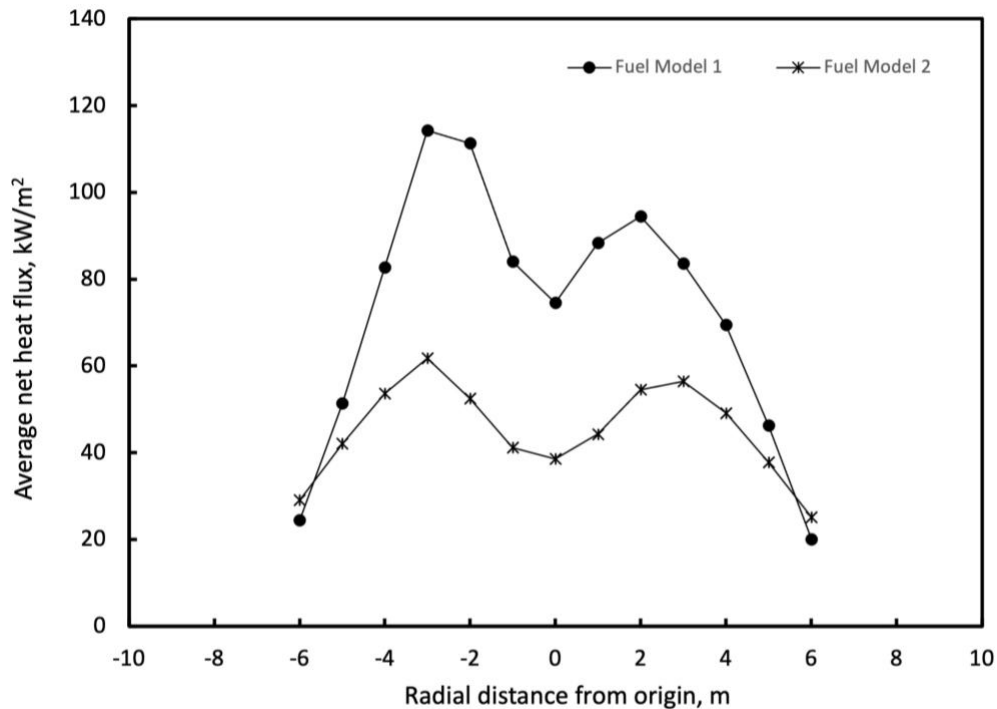


Figure 4-5 Average net heat flux at the pool surface over initial 30 seconds of flame spread versus distance from fire origin for a 12 m x 24 m fire source in the hangar configuration.

32 kW/m²). Fire model 2 shows net heat flux values comparable to those found in the small pool fire tests.

Based on the results from the three validation simulations, fuel model 2 provides a better representation of the fire scenario. All simulations for the remainder of this report will use fire model 2.

4.2 Water Mist Model

Water mist nozzles are difficult to simulate in FDS due to the complex atomization process that occurs at the nozzle, the number and size of water droplets produced by the nozzle, complex spray patterns and characteristics, lack of detailed spray characterization, and coupling of the gas phase and water mist droplets.

This section outlines different models and devices used in FDS to simulate a water mist spray and validation tests conducted to best replicate three water mist nozzles given limited experimental test data for spray characterization.

4.2.1 Nozzle and Lagrangian Particle Model Description

FDS has multiple options for introducing particles into the computational domain; however, this project will only focus on introduction from a nozzle. A nozzle is a term in FDS that has pre-defined input parameters such as initial velocity, spray angle, k-factor, and pressure. These input parameters describe the initial conditions of water droplets into the computational domain. Values for the k-factor and pressure can be taken from manufacturer data. Values for initial velocity and spray angle can be obtained from experimental data when available or estimated by numerical techniques. Methods to estimate these values are discussed in section 4.2.2.

The spray angle in FDS specifies two angles through which droplets are introduced into the domain. Multi-orifice water mist nozzles can be modelled by placing multiple nozzles at a single point with varying orientation based on the orifice direction or by specifying a single nozzle with a complex spray pattern. Both techniques are used in modelling different water mist nozzles in this report.

The particles are inserted into the domain at a prescribed radial distance, r_o , from the nozzle along the sphere created by the specified spray angles. Particles are inserted at a distance from the nozzle in order to assume that the break-up of the water jet into a spray is complete. Inserting the particles at a distance from the nozzle avoids numerical instabilities associated with having all of the droplets originate in one grid cell and avoids simulating the atomization process.

Once particles are introduced into the domain they are tracked as Lagrangian particles because they are too small to be resolved by the numerical grid. Water mist nozzles produce millions of water particles per second; however, it is too computationally heavy to track every particle from a nozzle. A single numerical droplet in FDS represents a collection of physical water droplets with similar characteristics in an actual water mist spray. The position and acceleration of the particle are determined from the following equations

$$\frac{dx}{dt} = u_p \quad \text{Eq. 4}$$

$$\frac{du_p}{dt} = g - \frac{\rho^* C_d^* A_{p,c}}{2 * m_p} (u_p - u) |u_p - u| \quad \text{Eq. 5}$$

where u and u_p represent bulk particle and gas velocities for a given grid cell and $A_{p,c}$ is the cross sectional area of the particle. The drag coefficient is a function of the local

Reynolds number based on particle diameter and is given as

$$C_d = \begin{cases} \frac{24}{Re_d}, & Re_d < 1 \\ 24 * \frac{0.85 + 0.15 * Re_d^{0.687}}{Re_d}, & 1 < Re_d < 1000 \\ 0.44, & 1000 < Re_d \end{cases} \quad Eq. 6.$$

The local Reynolds number is a function of the bulk cell particle and gas velocity, corresponding to the fact that FDS assumes that the particles in a cell represent a bulk mass dragging on the gas.

In cells where the local droplet volume fraction is less than 1×10^{-5} FDS neglects aerodynamic effects between particles and assumes two way coupling between Lagrangian particles and the gas phase. In cells where the local droplet volume fraction exceeds 1×10^{-5} a drag reduction model is automatically activated in FDS. This model accounts for aerodynamic interactions between particles by modeling the drag on a trailing particle with a reduced drag coefficient,

$$C_d = C_{d,0} * \frac{F}{F_0}, \quad Eq. 7$$

where $C_{d,0}$ is the single particle drag coefficient and F/F_0 is the hydrodynamic force ratio of the trailing particle to an isolated particle. A full description of the hydrodynamic force ratio can be found in the FDS technical reference guide [4].

An important characteristic for water mist nozzles is the size and distribution of water droplets produced. The default droplet size distribution in FDS is the Rosin-Rammler lognormal distribution,

$$F_v(D) = \begin{cases} \frac{1}{\sqrt{2\pi}} \int_0^D \frac{1}{\sigma D'} \exp\left(-\frac{\left[\ln\left(\frac{D'}{D_{v,0.5}}\right)\right]^2}{2\sigma^2}\right) dD' & (D \leq D_{v,0.5}) \\ 1 - \exp\left(-0.693 * \left(\frac{D}{D_{v,0.5}}\right)^\gamma\right) & (D > D_{v,0.5}) \end{cases} \quad Eq. 8$$

where $D_{v,0.5}$ is the volumetric median diameter, and γ and σ are empirically determined to be 2.4 and $1.15/\gamma$ respectively. The γ and σ parameters can be user controlled to change the width of the distribution, the user can define both γ and σ ; however, by default $\sigma=1.15/\gamma$ to ensure a smooth transition between the two functions. Another method of inputting the droplet size distribution is by a user specified cumulative number function (CNF). Each of these two methods are used to describe droplet distributions for different nozzles in the following sections.

The Lagrangian particle model is coupled with LES governing equations through bulk cell values, summing all of the water mist in a given grid cell and dividing by the volume. Additional details and complete equations for transfer of mass, momentum, and energy of Lagrangian particles can be found in the FDS technical reference guide [4].

4.2.2. Water Mist Characteristics & Validation Simulations

Due to time constraints only two VID Fire-Kill nozzles and one Marioff nozzle are modelled in this study. Each of the water mist nozzles have different spray characteristics and each nozzle has different experimental data for validation. Each nozzle is characterized and validated based on available information and previous testing.

Before delving into the characterization of each nozzle, simulations to verify the particle terminal velocity and air entrainment were conducted and compared to hand calculations. Results of these simulations can be found in Appendix C. The results verify that FDS is able to predict the terminal velocity of the particles given non-quiescent gas conditions due to air entrainment through the activation of the water mist nozzle.

4.2.2.1 Nozzle A

Nozzle A is a ceiling mounted multi-orifice low pressure water mist nozzle developed by VID Fire-Kill. The nozzle contains 7 orifices, one oriented directly downwards and 6 oriented at a 45-degree angle as shown in Figure 4-6. These orifices are modelled in FDS using a single nozzle and a spray pattern table assuming equal flow out



Figure 4-6 Nozzle A spray head image

of each orifice. The k-factor and pressure are taken from the product data sheet to be $5.6 \frac{L}{min \cdot \sqrt{bar}}$ and 16 bar respectively. The spray angle of each nozzle was taken from manufacturer data; each orifice has an equal spray angle of 80°.

Previously acquired experimental data on this nozzle has been collected, by the RISE Research Institute of Sweden, which characterized the water mist spray through interferometric techniques. The results of the report include the droplet size distribution and average velocity at a location $z = 300$ mm downstream of the exit nozzle and $r = 0$ mm from the spray axis. The experimental data was collected at a fixed injection pressure of 16 bar. Validation simulations in FDS compare results obtained with the PDPA diagnostic in FDS to the results of the RISE experimental data.

A series of simulations were conducted to determine the input parameters for the offset, initial velocity, and droplet size distribution. Each validation simulation is conducted in a 3 m x 3 m x 3 m domain with a grid size of 0.1 m. A grid analysis, which

can be found in Appendix D, determined negligible discrepancies between a grid size of 5 cm and 10 cm for this nozzle. All of the boundaries except for ZMAX are constructed as open vents. The flow is represented by 5×10^4 droplets per second. These simulations use a higher number of droplets to represent the flow than in the final simulations. The number of droplets was decreased in the final simulations due to the high computation time associated with an increased number particles. The nozzle is located 0.1 m below the ceiling in the center of the domain. The humidity is set to 100 % to prevent evaporation of droplets for the duration of the simulation. Simulations varying the offset values from 0.1 m to 0.3 m, with a monodisperse droplet diameter of 80 μm and initial velocity 20 m/s, impacted the velocity results downstream by less than 25 percent. An offset value of 0.3 m was chosen because the experimental data was taken at this location and the input parameters can be developed based on the experimental results.

The droplet size distribution was determined from the experimental data and inserted with a user specified CNF. Figure 4-7 shows the measured CNF from the RISE report versus the CNF predicted by FDS.

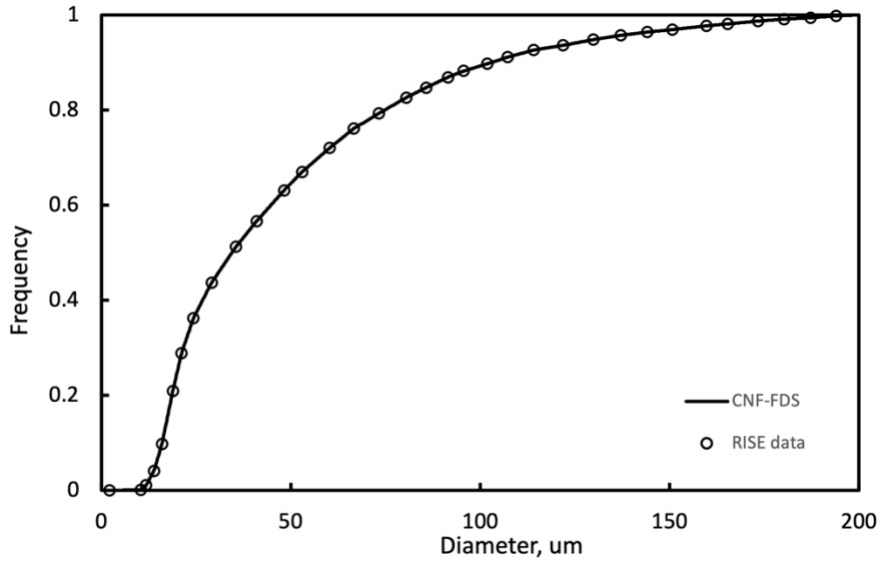


Figure 4-7 Cumulative Number Function predicted by FDS and measured by RISE report for Nozzle A

The maximum initial velocity from the nozzle can be estimated by the modified Bernoulli equation

$$V = \sqrt{\frac{2 \cdot \Delta P}{\rho}} \quad \text{Eq. 9}$$

to be 57 m/s. The RISE data found the average velocity of particles at a location 300 mm downstream of the nozzle to be 0.8 m/s. A series of simulations were conducted varying the initial velocity at the offset value of 0.3 m, with the specified droplet distribution shown in figure 4-8, from 0.5 m/s to 50 m/s. Figure 4-8 plots the average velocity versus height for the varying initial velocities.

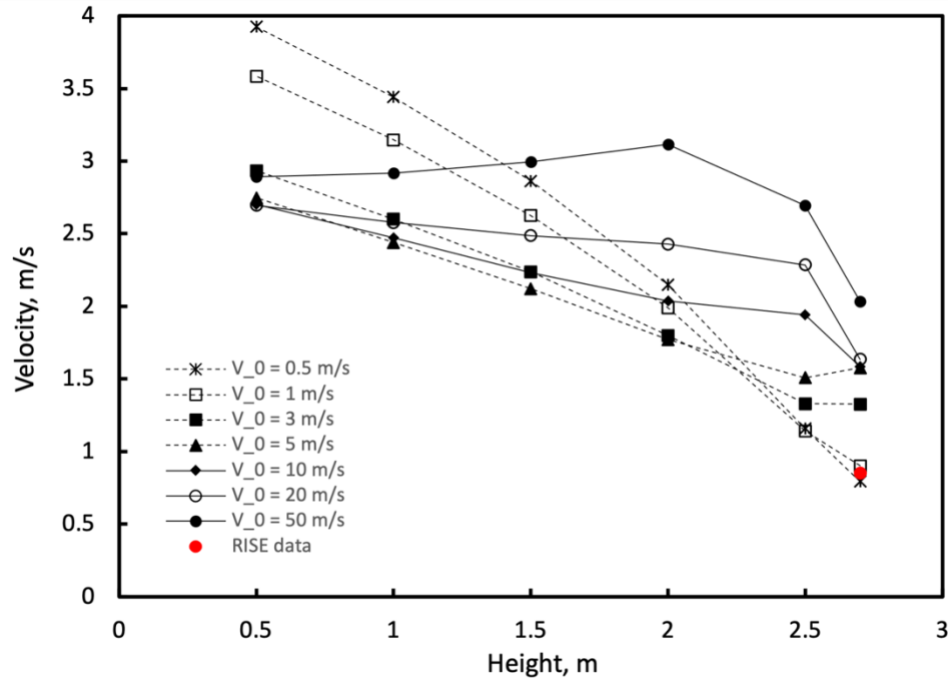


Figure 4-8 Average velocity versus height for varying initial velocity for Nozzle A with offset = 0.3., and specified CNF droplet distribution

The results show that an initial velocity less than 3 m/s yields the best accuracy with the experimental data and initial velocities greater than 10 m/s begin to converge downstream of the nozzle. Although the low velocities match the RISE data more accurately, inserting droplets at this slow speed neglects the transfer of momentum that occurs between the water mist nozzles and the air. Additionally, initial velocities from 5 to 20 m/s are less than a factor of 2 overpredicted; given the uncertainties associated with each of the measurements this is within reasonable error. For these reasons, 10 m/s was chosen as the initial velocity input. The final FDS inputs for Nozzle A are summarized in Table 4-3.

Table 4-3 FDS Input for Nozzle A

k-factor [L/min/bar ^{1/2}]	Operating pressure [bar]	V_0 [m/s]	ϕ [degrees]	Number of Perimeter Micronozzles & Orientation	Droplet Size Distribution ^a	r ₀ [m]
5.6	16	10	80	6 45°	See figure 4-7	0.3

^aUser Specified CNF

4.2.2.2 Nozzle B

Nozzle B is a low pressure, multi-orifice floor pop up nozzle, designed by VID Fire-Kill specifically for aircraft hangar protection. The nozzle contains four orifices, one centered facing directly horizontal, and 3 oriented at a 45-degree angle as shown in Figure 4-9. These orifices are modelled in FDS using a single nozzle and a



Figure 4-9 Nozzle B spray head image

spray pattern table assuming equal flow out of each orifice. The k-factor and pressure are taken from the product data to sheet to be $10 \frac{L}{min \cdot \sqrt{bar}}$ and 8 bar respectively. The spray angle from each micro-nozzle is assumed to be equal and was estimated by analyzing spray images with the software ImageJ. The spray angle was found to be 60 degrees.

This nozzle has had no previous experimental droplet characterization. Input values are determined through hand calculation estimates and iterative testing in FDS. Each monodisperse validation simulation is conducted in a 5 m x 3 m x 1.5 m domain with a grid size of 0.1 m. A grid analysis, which can be found in Appendix D, determined small discrepancies between a grid size of 5 cm and 10 cm for this nozzle with monodisperse droplets and significant discrepancies between a grid size of 5 cm and 10 cm for this nozzle with a droplet distribution. All of the boundaries, except for ZMAX and ZMIN, are constructed of open vents. The flow is represented by $5 \cdot 10^4$ droplets per second. These simulations use a greater number of droplets to represent the flow than in the final simulations. The number of droplets was decreased in the final simulations due to the high computation time associated with an increased number of particles. The nozzle is centered 0.2 m above the ground, 0.1 m from XMIN, and oriented in the positive x direction. The humidity is set to 100 % to prevent evaporation of droplets for the duration of the simulation. Initial tests varied the offset value from 0.1 m to 0.3 m, with monodisperse droplets of 150 μm , and an initial velocity of 35 m/s. The results found less than a 25 % difference in the nearfield velocity results and no discrepancy for the velocity further than 1 m away from the nozzle. An offset value of 0.1 m is used for characterization of this nozzle.

The initial velocity is estimated by assuming equal flow out of each nozzle

$$Q_{total} = 4 * q_{micronozzle} \quad \text{Eq. 10}$$

where Q_{total} , the total flow from the nozzle, is 471 g/s. This equation gives a constant flow of 117 g/s from each micro-nozzle. The corresponding velocity can be determined from a conservation statement,

$$V = \frac{q_{nozzle}}{\rho \cdot \frac{\pi}{4} \cdot d^2} \quad Eq. 11$$

where ρ is the density of water, and d is the diameter of the micro-nozzle. The diameter of the center micro-nozzle is 2.0 mm, and the diameter of the perimeter micro-nozzles are 2.8 mm. Solving for each velocity based on the diameter of the orifice gives 38 and 20 m/s respectively for the center and perimeter nozzles. These initial velocity values are checked against the velocity estimate using the modified Bernoulli equation, equation 9, which gives 40 m/s. This confirms that the center nozzle is in agreement with the Bernoulli equation estimate and the perimeter micro-nozzles have a lower velocity due to the larger orifice size.

The only spray distribution data for the nozzle is that D_{v90} is less than 350 microns. The default FDS Rosin-Rammler Lognormal distribution is used to estimate the droplet distribution. Iterative testing through small scale extinction simulations compared to experimental extinction data was completed to determine the distribution characteristics. The median diameter, gamma, and sigma for the distribution were determined to be 200 microns, 2, and 1.7 respectively. The final assumed CNF for this nozzle is shown in Figure 4-10.

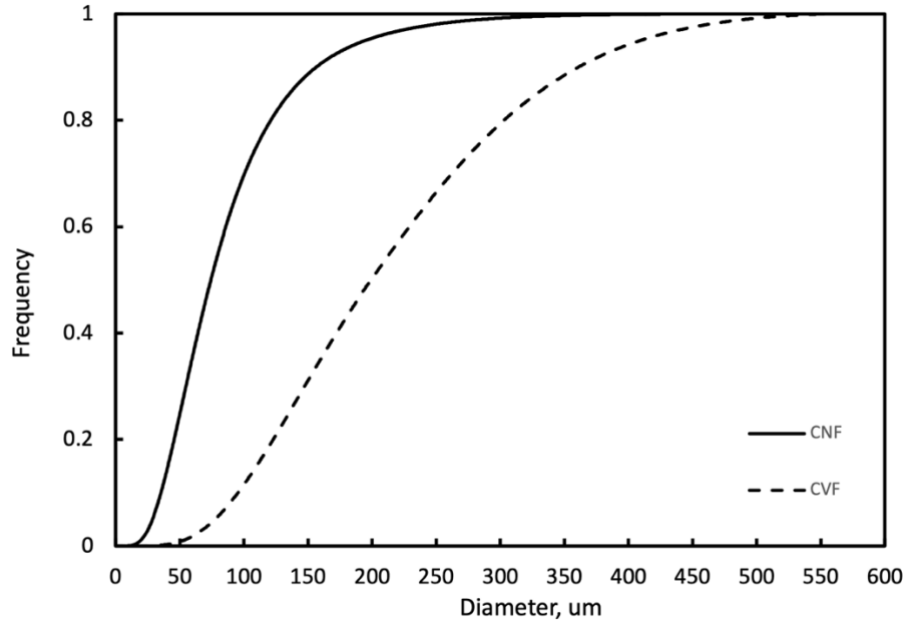


Figure 4-10 CNF and CVF for Nozzle B

The small-scale extinction simulations were conducted in a 5 m x 5 m x 4 m domain with a hybrid grid size of 0.05 m below 3 m in the space and 0.1 m above 3 m in the space. This hybrid mesh is due to the grid dependency of the nozzle with a droplet distribution, as shown in Appendix D. A 1 m diameter JP-8 fire source, with characteristics as outlined in section 4.1, is located in the center of the room and four floor nozzles were equally spaced around the fire at 2 m x 2 m spacing. The spray is represented by 2×10^4 droplets per second. The extinction model for these simulations used the default LOI of 0.135, a CFT of 1527 °C, an AIT of 330 °C everywhere in the domain, and a fuel surface temperature ramp for ignition. Details for each of these inputs can be found in section 4.3.

The FDS simulation for this nozzle could be improved with experimental characterization of the nozzle and a droplet size distribution analysis. The final FDS inputs for Nozzle B are summarized in Table 4-4.

Table 4-4 FDS Inputs for modeling Nozzle B

k-factor [L/min/bar ^{1/2}]	Operating pressure [bar]	V_0 [m/s]	ϕ [degrees]	Number of Perimeter Micronozzles & Orientation	Droplet Size Distribution ^a			r ₀ [m]
					D _{v50} [um]	γ	σ	
10	8	35 ^b	60	3	200	2	0.58	0.1
		20 ^c		45°				

^a default Rosin Rammler Lognormal distribution

^b center nozzle

^c perimeter nozzles

4.2.2.3 Nozzle C

Nozzle C is a ceiling mounted, multi-orifice high pressure water mist nozzle developed by Marioff. The nozzle contains nine orifices one oriented directly downwards and eight oriented at a 30-degree angle. The orifices are modelled in FDS using nine individual water mist nozzles with varying orientations located at a single point. The k-factor and pressure are taken from the product data sheet to be $3.9 \frac{L}{min*\sqrt{bar}}$ and 70 bar respectively, the k-factor of each individual micro nozzle is assumed to be 0.433

$\frac{L}{min*\sqrt{bar}}$, which is consistent with assuming equal flow out of each orifice.

Due to time constraints a full analysis of this water mist nozzle was not possible. Detailed characteristics were taken from a previous VTT research project [14]. The VTT research found the results of the high-pressure nozzle to be highly grid dependent. A series of simulations were conducted to verify similar results to the previous VTT results and verify if the grid dependency still exists in newer versions of FDS. The simulations were conducted in a 0.5 m x 0.5 m x 1.5 m domain with varying grid sizes as noted. The nozzle is placed 0.1 m from the ceiling and all boundaries, except for ZMAX, are composed of open vents. The flow is represented by $1*10^5$ droplets per second, in

accordance with the VTT inputs. The simulations only characterize one singular micronozzle of the multi-orifice nozzle. By default, `PARTICLE_CFL = .FALSE.` in FDS, which means that particles can traverse more than one grid cell in a time step. Due to the high velocities associated with the high pressure nozzle, `PARTICLE_CFL=.TRUE.` must be specified to accurately resolve the spray near the nozzle. This diagnostic is used for all future simulations with this nozzle.

Figures 4-11 and 4-12 show the results of the nozzle obtained with VTT inputs compared to experimental data. These results match within reasonable error to the results published by VTT and are still very grid dependent [14].

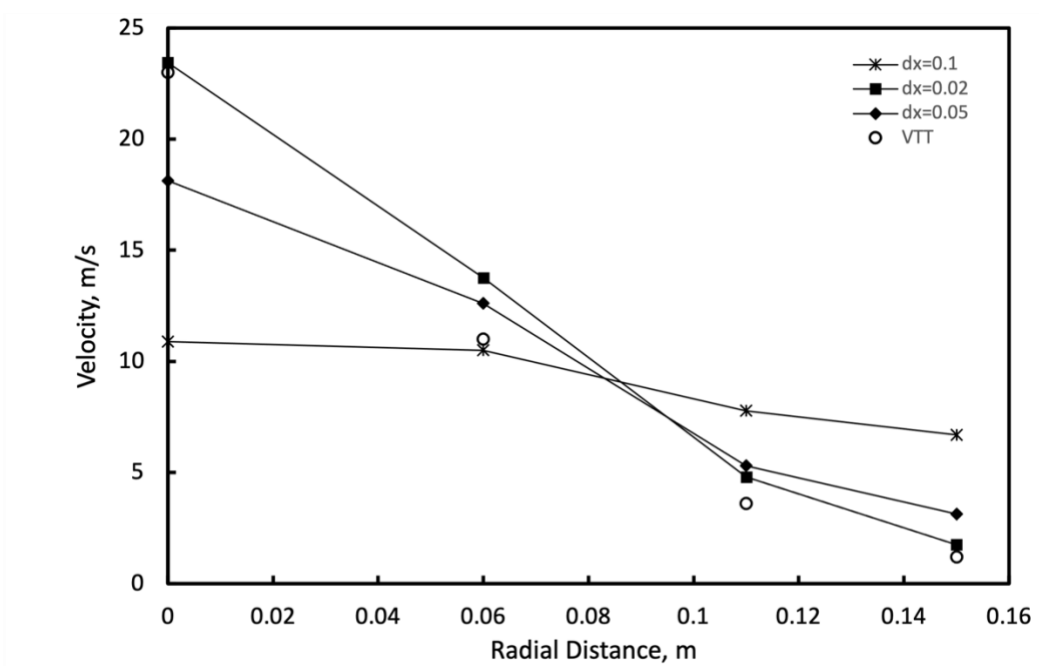


Figure 4-11 Velocity versus radial distance, 1 m below the nozzle, for varying grid sizes for Nozzle C

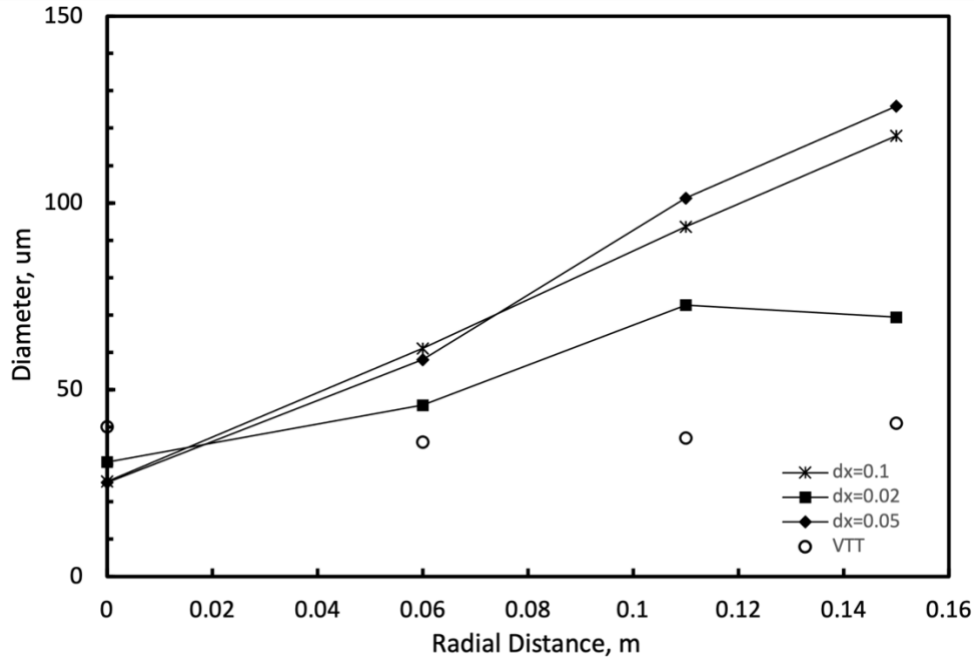


Figure 4-12 Diameter (D10) versus radial distance, 1 m below the nozzle, for varying grid sizes for Nozzle C

The FDS inputs for a single micro-nozzle are summarized in Table 4-5. The multi-orifice Nozzle C is created from 9 micro-nozzles located at a single point with varying orientation vectors based on the nozzle configuration described above.

Table 4-5 FDS Input for Single Micronozzle in Multi-Orifice Nozzle C

k-factor [L/min/bar ^{1/2}]	Operating pressure [bar]	V ₀ [m/s]	φ [degrees]	Number of perimeter micronozzles & Orientation	Droplet Size Distribution ^a			r ₀ [m]
					D _{v50} [μm]	γ	σ	
0.433	70	118	24	8	79	2.26	0.5	0.1

30 °

^a default Rosin Rammler Lognormal distribution

4.3 Extinction and Evaporation Model

For water mist nozzles extinction and evaporation are closely related; however, it is important to note that these processes involve two separate models in FDS. This

section will explain how extinction and evaporation are modelled by FDS and report the results of verification simulations for each model individually.

Because FDS was initially developed for modeling combustion in well ventilated conditions, the extinction model is quite simplified and can sometimes be hindered by the default combustion conditions. Extinction in FDS with a prescribed MLRPUA and default mixing-controlled combustion model predicts extinction as a binary process. In reality extinction with water mist is a complex process that involves temperature reduction due to evaporation, localized oxygen depletion through expansion of water droplets during evaporation, reduction in the fuel pyrolysis rate due to reduced re-radiation to the fuel surface and radiation attenuation, and direct cooling of the fuel surface. The importance of each of these extinction effects is weighted differently depending on the nozzle characteristics, room configuration, and fuel characteristics.

In an open environment where global oxygen reduction is not possible, the main extinguishing mechanism of water mist is flame cooling due to evaporation and sub-grid scale kinetic effects. Therefore, for the configuration of interest, with no enclosure effects, it is sufficient to govern extinction conditions with the simplified models in FDS which are based on fuel content, oxygen content, and flame temperature.

4.3.1 Extinction Model Description

There are two extinction models available in FDS; however, this research will only focus on Extinction Model 2. Extinction Model 2 determines if combustion is viable in a given grid cell based on the initial temperature, oxygen content, and fuel content. If the oxygen and fuel at the initial grid cell conditions can raise the temperature of the grid cell to the

critical flame temperature, then combustion occurs in the cell at the given time step. If the oxygen and fuel at the initial temperature cannot raise the temperature of the grid cell to the critical flame temperature, then local combustion does not occur in the grid cell for the given time step. FDS interprets the critical flame temperature (CFT) as a function

based on the limiting oxygen index (LOI). For the purpose of this research the default LOI and a modified CFT are

Table 4-6 FDS Extinction Criteria Inputs

LOI [mol/mol]	CFT [°C]
0.135	1527

used for extinction criteria; values for these criteria are shown in Table 4-6. The theory behind the critical flame temperature can be found in Beyler’s chapter of the SFPE handbook [9] and technical details of the critical flame temperature and limiting oxygen index relationship within FDS can be found in the FDS technical reference guide [4].

In its default setting FDS assumes that everywhere fuel vapor and oxygen mix combustion occurs, despite the local temperature. This assumption is sufficient for well-ventilated combustion problems; however, this can impact the extinction model and combustion can unphysically begin in a grid cell that had previously been extinguished and cooled to ambient temperature when fuel reaches sufficient oxygen. To stop unphysical burning of fuel and oxygen an auto-ignition temperature (AIT) of 310 °C is specified everywhere in the domain and an increased fuel surface temperature is used for ignition. This AIT is higher than values found in literature for JP-8 and was determined through iterative extinction tests with Nozzle B compared to experimental data. The AIT is grid dependent and simulations with grid sizes less than and greater than 10 cm in this report use a modified AIT.

By implementing an AIT, FDS no longer assumes everywhere fuel and oxygen mix combustion occurs, consequently an ignition source is no longer assumed. A fuel surface ramp function is used to facilitate ignition of the pool fire. The fuel surface ramps up to 700 °C for the first 8 seconds of the simulation and then ramps down to the flashpoint of JP-8, 38 °C, for the remaining duration of the simulation. The fuel is assumed to be at the flashpoint because this is the greatest fuel temperature that facilitates liquid phase-controlled flame spread over the fuel surface. Additional information about the AIT, fuel surface temperature, and extinction model can be found in the FDS users guide [12].

4.3.2 Extinction Model Verification Simulations

A series of simulations were conducted to verify the extinction model in a reduced oxygen environment. The simulations model a 1 m diameter pool fire located in the center of the domain, a vent blowing varying mass fractions of nitrogen located at the XMIN boundary and an open vent located at the XMAX boundary. Initial conditions for the vent source are specified in Table 4-7. The

Table 4-7 Blower Vent Inputs in FDS

vent activates at $t = 15$ seconds to allow adequate pre-burn time before extinction conditions are reached. The mass fraction of nitrogen is varied between the values specified

V_0 [m/s]	-0.5
Y_{N_2}	0.0-0.45
Y_{air}	0.55-1.0

in Table 4-4 for various simulations to find the extinction limit. All other walls are adiabatic, and the humidity is set to 0 %. The fuel source is JP-8, as outlined in section 4.1, with a modified MLRPUA of 0.015 kg/m²/s, an AIT of 310 °C, and a fuel surface temperature ramp used for ignition. The simulations are conducted in a 6 m x 3 m x 3 m

compartment with a grid size of 0.1 m to accurately capture the dynamics at the pool surface. An angular resolution of 100 angles is used to solve the radiation transport equation.

Figure 4-13 shows the combustion efficiency of the reaction as a function of incoming oxygen mole fraction from the vent surface. The combustion efficiency is defined as the average measured HRR in FDS divided by the expected HRR, 500 kW. When the incoming oxygen mole fraction decreases below 0.135, complete extinction rapidly occurs and the combustion efficiency reaches zero. When the incoming oxygen mole fraction is above 0.135 complete combustion occurs and the combustion efficiency reaches 100 %.

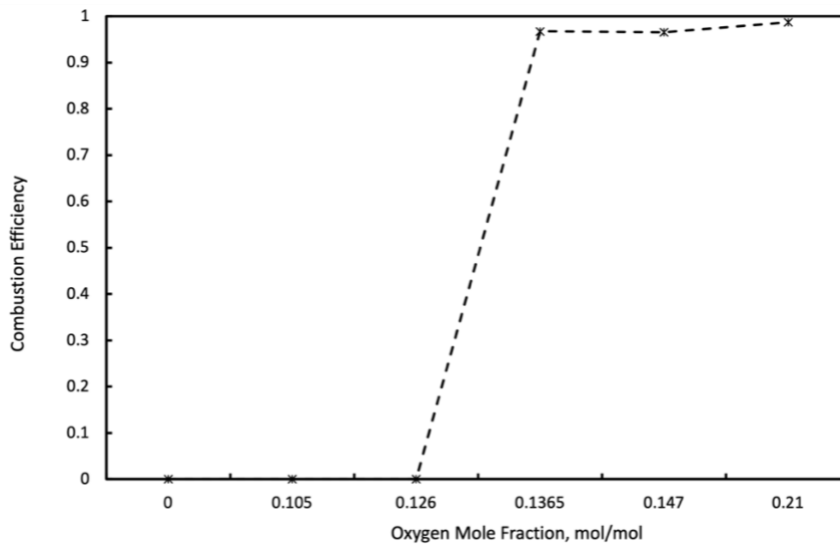


Figure 4-13 Combustion efficiency versus oxygen mole fraction in the incoming oxidizer stream

These simulations demonstrate that a limitation of the specified MLRPUA pyrolysis and mixing controlled combustion model is that extinction in FDS is modeled as a binary process. When conditions in the space are viable complete combustion occurs and when conditions in the space are unviable complete extinction occurs.

4.3.4 Evaporation Model Description

The evaporation model in FDS solves a series of equations to determine the droplets in a grid cell that evaporate and form the gas species α during a given time step. The mass and energy transfer between the gas and liquid particle are described by

$$\frac{dm_p}{dt} = -A_{p,s} h_m \rho_f (Y_{\alpha,l} - Y_{\alpha,g}) \quad \text{Eq. 12}$$

$$\rho_g V \frac{dY_{\alpha,g}}{dt} = -(1 - Y_{\alpha,g}) * \frac{dm_p}{dt} \quad \text{Eq. 13}$$

$$\frac{dT_p}{dt} = \frac{1}{m_p c_p} \left[\dot{q}_r + A_{p,s} h_g (T_g - T_p) + A_{p,s} h_w (T_w - T_p) + \frac{dm_p}{dt} h_v \right] \quad \text{Eq. 14}$$

$$\frac{dT_g}{dt} = \frac{1}{m_g c_g} \left[A_{p,s} h_s (T_p - T_g) - \frac{dm_p}{dt} (h_{\alpha,p} - h_{\alpha,g}) \right] \quad \text{Eq. 15}$$

where m , A , h , h_m , T , ρ , and c represent the mass, surface area, heat transfer coefficient, mass heat transfer coefficient, temperature, density, and specific heat respectively. The subscript ‘g’ represents the average gas quantity in the cell occupied by the droplet, the subscript ‘p’ represents the particle quantity, the subscript ‘f’ represents the particle film quantity, and the subscript ‘ α ’ represents the gas species formed from evaporation.

The evaporation model in FDS solves the set of equations describing mass and energy transfer between the gas and liquid as a set of coupled implicit equations over the course of the gas phase time step. The liquid equilibrium water vapor mass fraction is obtained from the Clausius-Clapeyron equation and the mass transfer coefficient is described by a series of empirical relationships based on the Spalding mass transfer number, the low mass flux Sherwood number, and the binary diffusion coefficient. A full description of the evaporation model and equations for the liquid equilibrium water vapor mass fraction and mass transfer coefficient can be found in the FDS technical reference guide [4].

The evaporation rate is determined as a function of the liquid equilibrium vapor mass fraction, the local gas phase vapor mass fraction, the (assumed uniform) droplet temperature, and the local gas temperature. When the temperature of the surrounding gas is sufficiently high, the evaporation rate is limited by the mass of liquid droplets entering the space. Conversely, when the temperature of the surrounding gas is low the evaporation rate is limited by the saturated water-vapor mass fraction.

4.3.5 Evaporation Verification Simulations

A series of verification simulations were conducted by modifying the input conditions of `water_evaporation_4` from the FDS library of examples. The simulations are conducted with the default configuration, 3 m x 1 m x 1 m domain with a grid size of 0.1 m. The radiation solver is turned off. A hot air vent is located at XMIN and an open vent source located at XMAX, all other walls are considered adiabatic. The hot air vent has varying conditions for each simulation, which are described below. A constant mass flow rate of 0.05 kg/s of particles with uniform 20 micron diameter are introduced into the domain 1 m away from the hot air source. The particles are considered static in the space and the number of particles representing the flow was modified from the default options to 100 particles every 0.01 seconds.

The hot air vent temperature and mass flow rate of air were varied to verify the energy transfer and mass fraction of water vapor predicted in FDS to expected results based on hand calculations. The expected mass fraction of water vapor is predicted by

$$Y_{H_2O} = \frac{\dot{m}_{evap}}{\dot{m}_{evap} + \dot{m}_{air}} \quad Eq. 16$$

where the evaporation rate is taken from the HRR output file and the mass flow rate of air can be determined based on the specified initial velocity at the vent source. The expected

energy transfer can be predicted based on the steady state temperature in FDS and the mass flow of air

$$\dot{\Delta Q} = \dot{m}_{air} * c_p * \Delta T \quad Eq. 17$$

where \dot{m}_{air} is situation dependent, c_p is assumed to constant at 1 kJ/kg-K and ΔT is the temperature difference measured in FDS. Then energy difference between the enthalpy of the gas before water droplets enter the domain and the steady state value after droplets evaporate can be compared to the energy consumed through the temperature change in Equation 13 to give the estimated heat flow.

Figures 4-14 and 4-15 show the results with a hot air temperature of 200 °C and incoming air mass flow rate of 0.742 kg/s, corresponding to an initial velocity of 1 m/s. The droplets evaporate from the space at roughly the same rate as they enter the space. The water vapor mass fraction is estimated as 0.063 by Equation 12. The equilibrium gas temperature in the space is measured as 47 °C. The heat flow at equilibrium conditions is estimated to be 26 kW, by subtracting the value obtained with Equation 13 from the heat flow without water droplets present. The results show that values measured in FDS match hand calculation estimates.

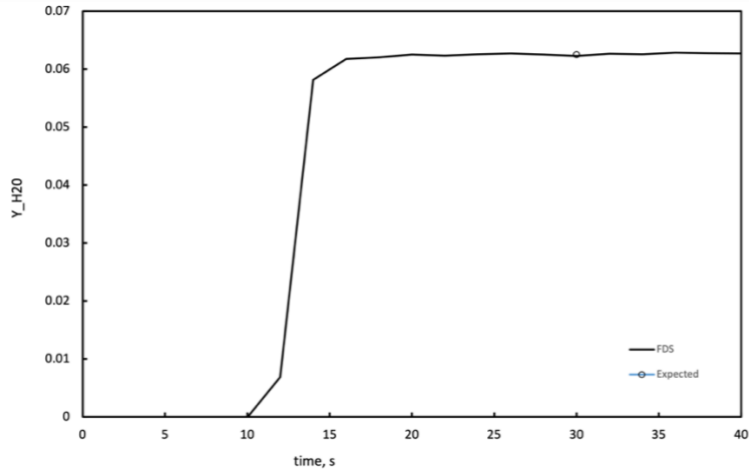


Figure 4-14 Mass Fraction of Water Vapor in air flow versus time for simulation with mass flow rate of air 0.742 kg/s and incoming air temperature of 200 °C

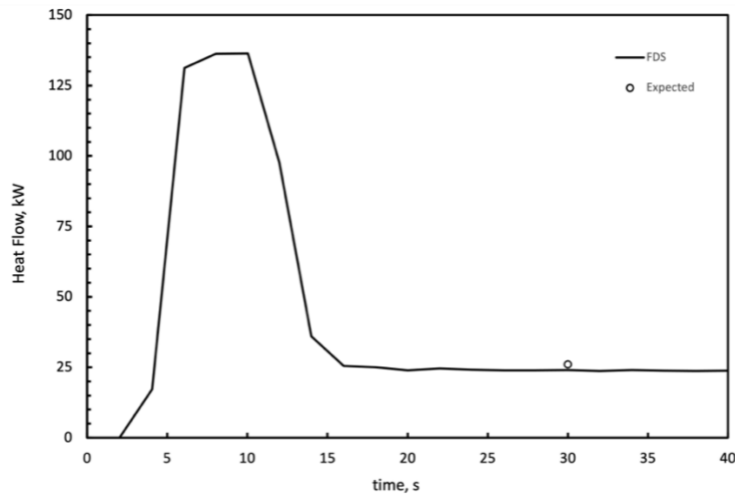


Figure 4-15 Heat flow of air versus time for simulation with mass flow rate of air 0.742 kg/s and incoming air temperature of 200 °C

Figures 4-16 and 4-17 show the results of the simulations with an incoming gas temperature of 500 °C and incoming air mass flow rate of 0.23 kg/s, corresponding to an initial velocity of 0.5 m/s. The droplets evaporate from the space at roughly the same rate as they enter the space. The water vapor mass fraction is estimated as 0.185 by Equation 12. The equilibrium gas temperature in the space is measured as 85 °C. The heat flow at equilibrium conditions is estimated to be 18 kW, by subtracting the value obtained from

Equation 13 from the heat flow without water droplets present. These results show that with varying temperatures FDS is able to predict evaporation and heat transfer between water droplets and air. Small discrepancies in the estimated values and FDS predicted values can be decreased with a larger number of particles representing the flow.

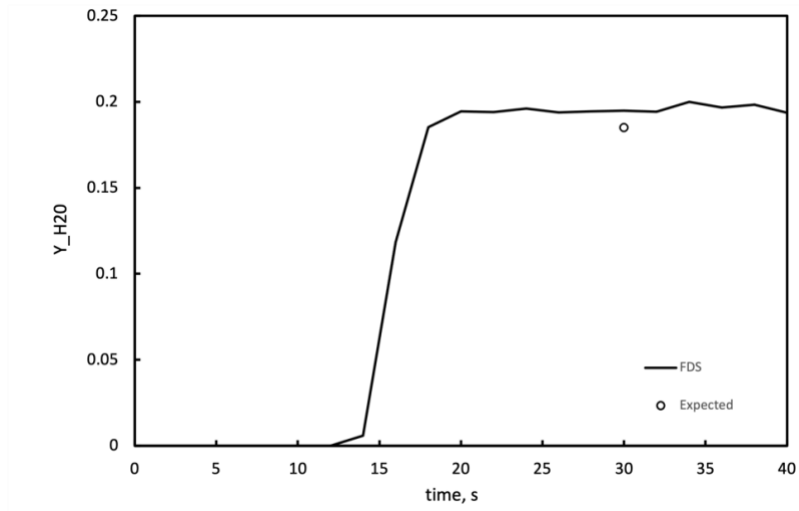


Figure 4-16 Mass Fraction of Water Vapor in air flow versus time for simulation with mass flow rate of air 0.23 kg/s and incoming air temperature of 500 °C

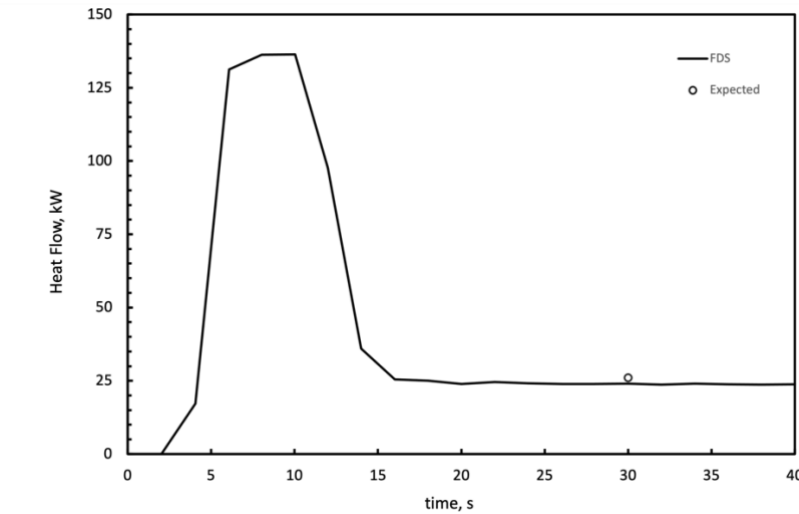


Figure 4-17 Heat flow of air versus time for simulation with mass flow rate of air 0.23 kg/s and incoming air temperature of 500 °C

Chapter 5 Model Inputs

The final simulations conducted in this research project assess the impact of each water mist nozzle on a full-scale JP-8 pool fire in a mock DoD hangar of interest. This chapter outlines the combination of inputs for each of the final engineering configuration simulations based on the analysis in Chapter 4. The final configurations assess the impact of activation time on the performance of each water mist system and compare high pressure versus low pressure ceiling nozzle and ceiling level discharge versus floor level discharge for protection of an aircraft hangar.

5.1 Compartment Geometry

The engineering configuration of interest is an F-35 aircraft maintenance hangar. The hangar dimensions are 26 m x 26 m x 12 m with a 24 m x 7 m door opening on one side. The full dimensions of the sample hangar can be found in Appendix E. The FDS model includes an additional outdoor mesh of 26 m x 6 m x 12 m to correctly account for the air entrainment through the hangar door. The hangar is constructed with a concrete floor and corrugated metal panel walls, the thermal properties used to model these materials in FDS are shown in Table 5-1.

Table 5-1 Hangar Construction & Obstruction Thermal Properties [15-19]

	Conductivity [W/m/K]	Density [kg/m ³]	Specific Heat [kJ/kg/K]	Thickness [m]
Concrete	1.8	2200	1.04	0.1
Metal Panels	52.0	7800	0.47	0.2
Composite (IM7/RM3002)	1.2	1514	2.2	0.0032
Carbon Steel	36	7753	0.48	0.05
Steel SN400	53	7851	0.52	0.006

Inside the hangar is a mock-up F-35, fighter aircraft. The purpose of this obstruction is to assess the incident heat flux to the surface of the plane throughout the duration of the simulation. The dimensions are approximated based on an F-35 aircraft; however, the plane is created with Cartesian grid cells and lacks the curvature of a real aircraft. The simulated model has a wingspan of 11 m, a length of 16 m, a fuselage height of 2 m, and a tail height of 4 m. Fighter aircraft are composed of multiple materials but one of the major compositions that has the most stringent thermal exposure criteria is a composite. For the purposes of this simulation the plane is assumed to be composed solely of a composite material. The thermal properties of the selected composite material are shown in Table 5-1.

Four electrical boxes are arbitrarily placed on various walls of the domain to measure the heat flux to representative wall targets in the hangar during a fire event. The electrical boxes are assumed to be 0.4 m x 0.8 m x 0.8 m in size and are composed of carbon steel. Thermal properties of carbon steel used in the simulations are shown in Table 5-1.

Three representative structural steel members are strategically placed along the ceiling and walls of the hangar to capture the impact of the fire on the most sensitive components of the structural steel members. The most fragile component was taken to be the thinnest dimension of an ASTM A572 steel channel member, which is 6 mm. Thermal properties of structural steel used in this simulation are shown in Table 5-1 and are assumed equal to steel SN400.

Figures 5-1 and 5-2 show the Smokeview animation of the hangar compartment from various viewpoints.

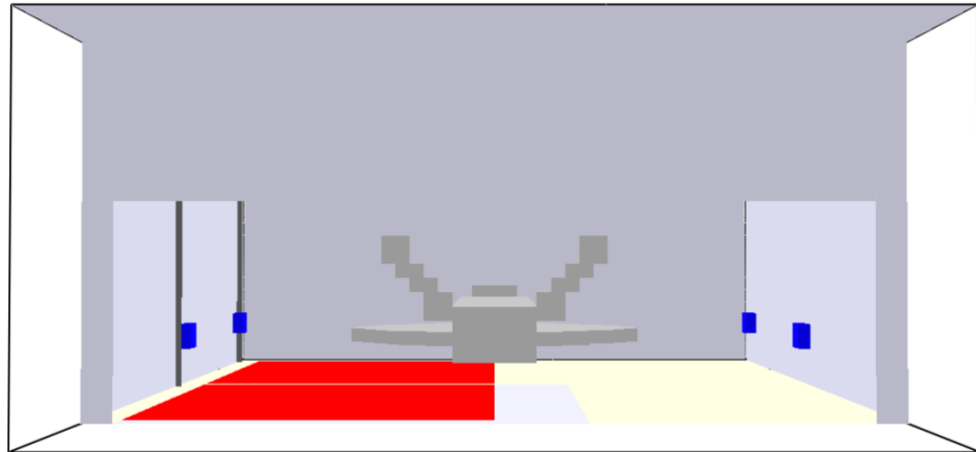


Figure 5-1 Smokeview animation of hangar configuration, view from YMIN

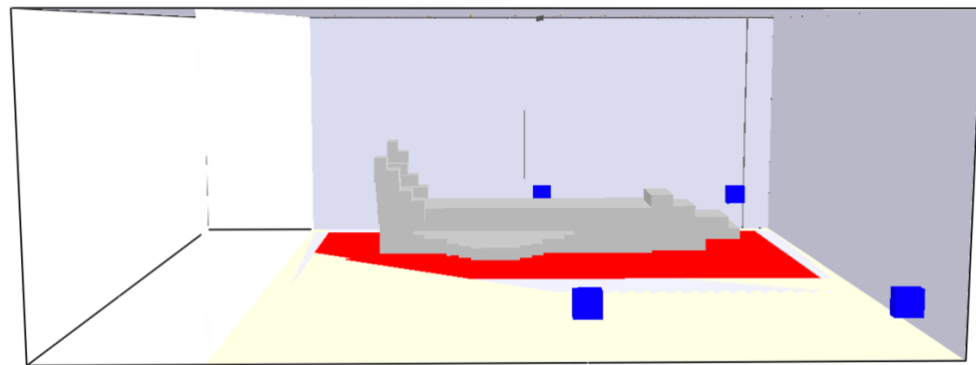


Figure 5-2 Smokeview animation of hangar configuration, view from XMAX

5.2 Design Fire

The design fire scenario for this analysis assumes a full F-35 fuel tank (10,900 L) that is ruptured during maintenance and produces a fuel spill originating underneath the left wing of the aircraft. The spill size is confined to 12 m x 24 m by assuming the Navy's standard trench system is installed on the floor. Because of the large volume of fuel and the one-minute extinction criteria imposed by the Air Force, the fuel spill is assumed to be constant in size and of uniform depth for the duration of interest. No additional

combustible items in the hangar are assumed to catch fire due to the minimal impact of small combustible objects on the fire intensity.

The fuel is modelled with the final input parameters as determined in section 4.1, with the inclusion of an AIT and surface temperature ramp for ignition as described in section 4.2. The fire spreads radially from the center of the pool fire (except for simulation 1b for Nozzle B). The final fuel input conditions are summarized in Table 5-2 for reference.

Table 5-2 Fuel FDS Input Values for Final Simulations in the Hangar Configuration

FDS Input Statement	Value
MLRPUA [kg/s/m ²]	0.06
FORMULA	C ₁₁ H ₂₁
RADIATIVE_FRACTION	0.1
SOOT_YIELD	0.03
SPREAD_RATE [m/s]	0.03
HEAT_OF_COMBUSTION [kJ/kg]	42,800
OPTICALLY_THIN	.TRUE.
AUTO_IGNITION_TEMPERATURE [°C]	300-330 ^a
CRITICAL_FLAME_TEMPERATURE [°C]	1527
TMP_FRONT ^a [°C]	700 → 36 ^b

^a AIT varies based on the grid resolution in each final simulation, 300 °C corresponds to dx = 0.2 m, 310 °C corresponds to dx = 0.1m, 330 °C corresponds to dx = 0.05 m

^b Surface temp starts at 700 °C and ramps down to 36 °C after 9 seconds

5.4 Nozzle Inputs and Spacing

The nozzle inputs for each simulation are based on the validation simulations outlined in Chapter 4. One parameter not thoroughly resolved in this report is DROPLETS_PER_SECOND. A small analysis on the effect of droplets per second was conducted using small scale extinction simulations with Nozzle B. The results of these simulations showed large variations in results with less than 20,000 droplets per second representing the flow and convergence of results with more than 20,000 droplets per second representing the flow. These results conclude that Nozzle B must be represented by a minimum of 20,000 droplets per second. Full results of this analysis are given in Appendix F. This number presents a challenge in large scale simulations with many water mist nozzles activating and the associated large number of particles that must be tracked. Simulations with the floor level nozzle can utilize a high number of particles representing the flow because the particles fall to the ground very quickly and do not accumulate in the space. Simulations using ceiling level nozzles use a modified number of droplets due to long run times and increasingly small-time steps required to solve equations with 20,000 particles per second as mist accumulates over the duration of the simulation. The impact of using a reduced number of particles to represent the flow is not quantified in this report and should be considered an area of further research.

The final inputs for each nozzle are derived from chapter 4 and are repeated in Table 5-3 for convenience. The inputs for Nozzle A and B represent the entire multi-orifice nozzle and the various orifices are modelled through a spray pattern table. Nozzle C inputs represents a single micro-nozzle where the multi-orifice nozzle is constructed from 9 individual micro-nozzles at the same location with varying orientation.

Table 5-3 Summary of final FDS input parameters for Nozzle A, B, & C

Nozzle	k-factor [L/min/bar ^{1/2}]	Operating pressure [bar]	V ₀ [m/s]	φ [degrees]	Number of Perimeter Micronozzles & Orientation	Droplet Size Distribution ^a			r ₀ [m]	Droplets per Second
						D _{v50} [um]	γ	σ		
A	5.6	16	10	80	6 45°	See figure 4-7			0.3	10,000 ^d
B	10	8	35 ^b 20 ^c	60	3 45°	200	2	0.58	0.1	20,000
C	0.433	70	118	24	8 30 °	79	2.26	0.5	0.1	5,000

^a default Rosin Rammler Lognormal distribution

^b center nozzle

^c perimeter nozzles

^d 30 sec activation uses 10,000 PPS and 50 second activation uses 20,000 PPS

The spacing and location of the nozzles in the hangar are based on manufacturer recommended spacing. Both ceiling nozzles, A and C, are equally spaced 3 m x 3 m throughout the entire hangar with 1 m distance from each wall. The floor nozzle, B, is spaced 2 m x 5.75 m throughout the entire hangar, corresponding to a nozzle coverage area of 2 m x 2.8 m. In the center of the hangar where nozzles must be installed back-to-back the extra set of nozzles is placed overlapping the original nozzle by 0.5 m and shifting 1 m, per manufacturer recommendations [20]. All three systems are deluge systems and are assumed to utilize zoned activation. Through this assumption only half of the water mist nozzles in the hangar activate to protect the fire.

Through preliminary simulations the fire with Nozzle C traveled underneath of the aircraft to the side of the hangar with no water mist nozzles activating. In an effort to prevent this type of behavior one additional row of nozzles on the far side of the plane activates for simulations with Nozzle C.

5.4 Instrumentation Devices

The simulated hangar is equipped with thermocouples and incident heat flux gauges to measure critical temperatures and heat fluxes at the aircraft surface, structural steel members, and electrical boxes. Thermocouple trees and slice file outputs are used to monitor the temperature in the compartment for the duration of the simulation. An FDS input file including all devices used in the final simulations is given in Annex F.

The output values of the thermocouples and incident heat flux gauges are used to assess the performance of each mist system based on critical temperatures and heat fluxes of relevant materials.

5.4.1 Performance Criteria

The performance of each water mist systems will be analyzed based on control of the fire based on HRR reduction and temperature and incident heat flux measurements at critical locations of interest. For the purpose of this analysis representative critical heat flux and temperature values for composite and structural steel are used to assess the performance of each water mist system.

Critical heat flux values for the selected composite material are based on the time to delamination from an analysis by the Air Force and are shown in Table 5-4 [17]. The critical temperature for structural steel components ranges from 450 °C to 550

Table 5-4 Composite Performance Criteria

Heat Flux [kW]	Time until Delamination [s]
15	129
25	74
35	51

°C, for the purpose of this analysis a conservative value of 450 °C will be used to assess the performance of each system.

An acceptable level of protection will ultimately be determined by the Air Force based on incident heat flux to the aircraft, temperature of critical structural steel members, and control of the fire.

5.5 Simulated Scenarios

All of the simulations completed in this analysis use the same fuel source and compartment geometry. The simulations look at the impact of activation time on the effectiveness of each water mist system. The two activation times analyzed in this research are 30 seconds and 50 seconds, see Appendix B for justification of activation

times. Nozzle B includes an additional simulation looking at the impact of the ignition source location. The simulated scenarios are summarized as

Nozzle A

1. Water mist activation at 30 seconds
2. Water mist activation at 50 seconds

Nozzle B

1. Water mist activation at 30 seconds
 - a. Center of pool ignition source
 - b. Side of pool ignition source
2. Water mist activation at 50 seconds

Nozzle C

1. Water mist activation at 30 seconds
2. Water mist activation at 30 seconds

5.6. FDS Grid Analysis and Selection

5.6.1 Critical Length Scales Analysis

The grid size in FDS is a fundamental parameter that determines which length scales are resolved in the LES framework. The rule of thumb in FDS modelling is each critical length scale should be resolved by at least 10 grid cells. The critical length scales of interest in this problem are the pool fire surface and turbulent eddies, the air velocity boundary layer created through water mist activation, and the hangar door for ventilation. The Lagrangian particles representing the water mist are not included as a critical length scale because Lagrangian particles do not take up any space in the Eulerian frame of reference. However, the air entrainment pattern into the nozzle and the induced flow created through the discharge of water mist must be correctly resolved through the grid.

For each simulation the fire size ranges from 0 m diameter to 7.2 m diameter over the course of the simulation. Because the goal of this research is to analyze extinction with water mist the growth phase of the fire before mist activation is not of interest and does not need to be completely resolved. The two water mist activation times of interest are 30 seconds and 50 seconds, which corresponds to a pool diameter of 1.8 m and 3 m respectively. At the time of mist activation, the pool surface and large turbulent eddies should be resolved for accurate water mist and flame sheet interactions. Resolving each of these fire sizes corresponds to a grid size of 0.18 m and 0.3 m in the fire region.

The hangar door is 7 m high which must be resolved with grid cells less than 0.7 m. This is much larger than the other critical length scales and does not pose any additional constraints on the grid selection.

The following three sections analyze critical length scales for each individual water mist nozzle. Each water mist nozzle must be analyzed to check convergence of the velocity field of the droplets and velocity field of the gas to ensure an accurate representation of the spray.

5.6.1.1 Nozzle A critical length scales

From a previous grid analysis provided in Appendix D, Nozzle A can be adequately resolved with a 0.1 m grid resolution. This analysis expands upon those results to look at the effect of increasing the grid size downstream of the nozzle on the velocity flow field. Simulations were conducted with a grid size of 0.1 m within 1 m of the nozzle and 0.2 m greater than 1 m from the nozzle. The results of this simulation are compared to the results of the simulation with a 0.1 m grid size in Appendix D.

Figure 5-3 and 5-4 plot the particle diameter and particle velocity, measured with the PDPA device in FDS, versus height for the two mesh selections.

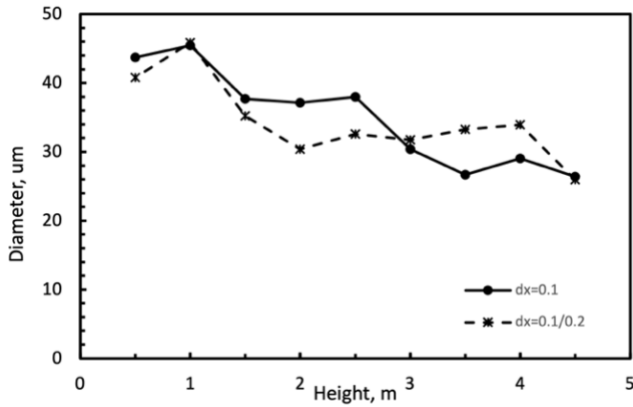


Figure 5-3 Diameter (D_{10}) vs vertical distance from nozzle for small mesh and hybrid mesh with Nozzle A. Nozzle located at $z = 5$ m.

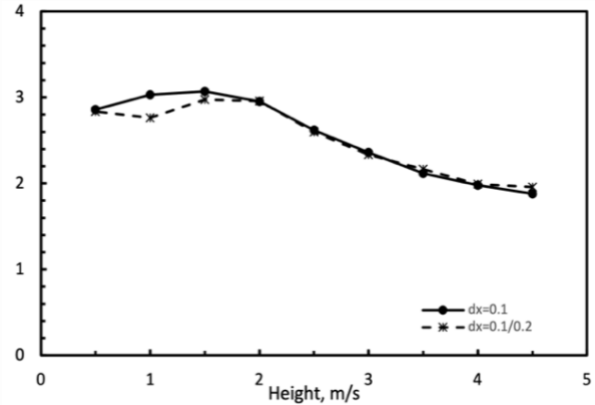


Figure 5-4 Velocity vs vertical distance from nozzle for small mesh and hybrid mesh with Nozzle A. Nozzle located at $z = 5$ m.

Figures 5-5 and 5-6 plot the particle diameter and velocity as a function of radial distance 3.5 m below the nozzle for the two grid resolutions.

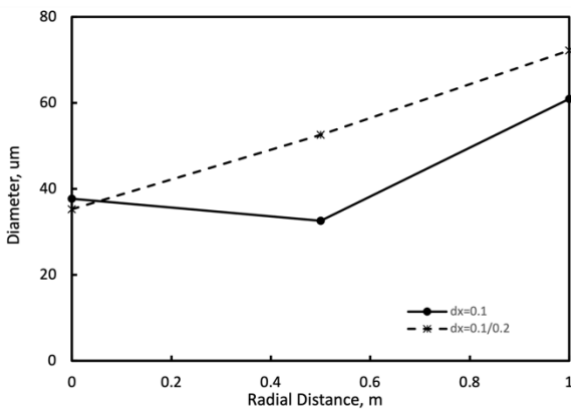


Figure 5-5 Diameter (D_{10}) vs radial distance for small mesh and hybrid mesh with Nozzle A. Measurements at $z = 3.5$ m below nozzle

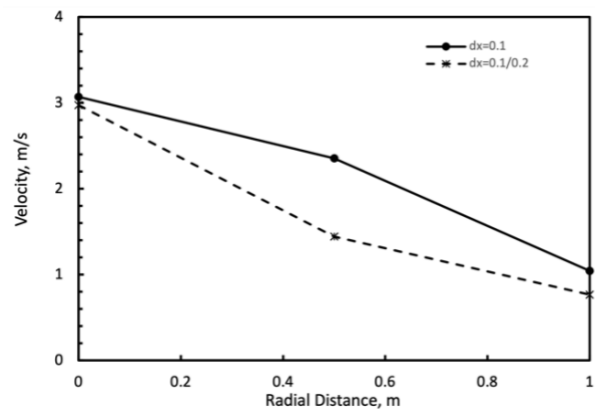


Figure 5-6 Velocity vs radial distance for small mesh and hybrid mesh with Nozzle A. Measurements at $z = 3.5$ m below nozzle

Figures 5-7 and 5-8 show the vector gas velocity flow field downstream of the nozzle for each simulation.

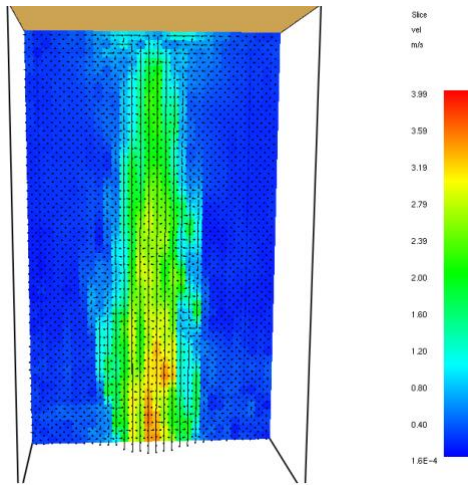


Figure 5-7 Gas velocity vector SLCF through center of spray for Nozzle A, $dx = 0.1$ m

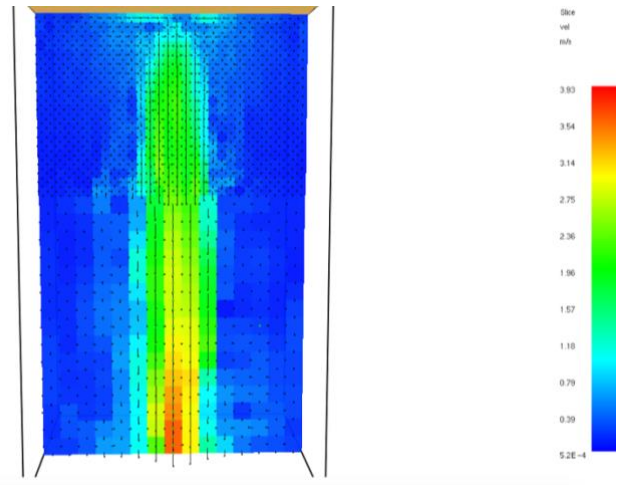


Figure 5-8 Gas velocity vector SLCF through center of spray for Nozzle A, hybrid mesh

These results show that Nozzle A forms a gas velocity boundary layer that can be sufficiently captured with a grid size of 0.1 m. Increasing the grid size downstream loses some accuracy and under predicts the velocity in the radial direction of the mist spray. To sufficiently resolve all length scales associated with Nozzle A, a grid size of 0.1 m is needed throughout the entire spray pattern discharge of the nozzle.

5.6.1.2 Nozzle B critical length scales

Through small scale extinction simulations, it has been determined the floor nozzle performance is very dependent on the resolution of both the nozzle and the flame sheet in areas where the particles interact with the flame. Two identical scenarios where only the location of the grid size increase varies, affects whether or not the nozzle is able to extinguish the fire. When the transition to a 0.1 m grid occurs 2 m above the fire source no extinction occurs, but when the transition to a 0.1 m grid occurs 3 m above the fire

source extinction occurs. Different grid requirements were found for simulations with larger spacing from the fire source to the nozzles. These small simulations demonstrate the large dependency on the grid size with Nozzle B. Full results of the small scale simulations can be found in Appendix F.

A series of simulations were conducted looking at only the nozzle discharge and flow patterns with increasing grid size downstream of the nozzle and increasing grid size vertically above the nozzle. The simulations were conducted in a 4 m x 2 m x 3 m domain with all walls considered open vents and the nozzle placed 0.2 m above the floor centered at the XMIN plane. Figures 5-9 and 5-10 plot the diameter and velocity of the droplets, measured with a PDPA device in FDS, for each grid size versus horizontal distance from the center of the nozzle.

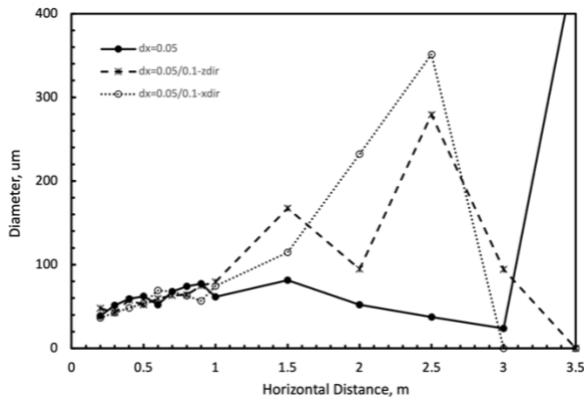


Figure 5-9 Diameter (D_{10}) vs horizontal distance from nozzle for small mesh and hybrid meshes with Nozzle B. Nozzle located at $x = 0$ m

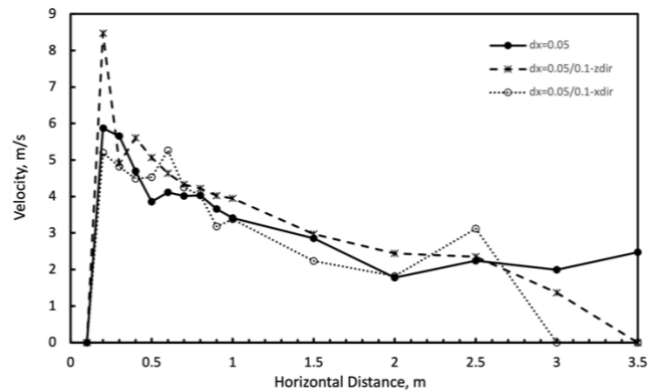


Figure 5-10 Velocity vs horizontal distance from nozzle for small mesh and hybrid meshes with Nozzle B. Nozzle located at $x = 0$ m

Figure 5-11 to 5-13 show the gas phase velocity flow in Smokeview with varying hybrid mesh selections.

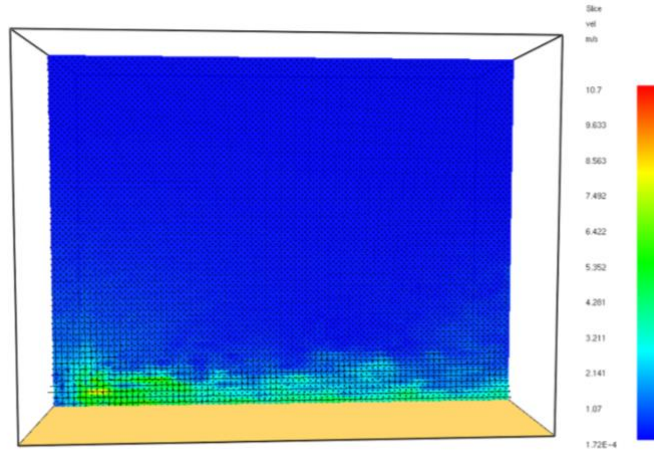


Figure 5-11 Gas velocity vector SLCF through center of spray for Nozzle B, $dx = 0.05$ m

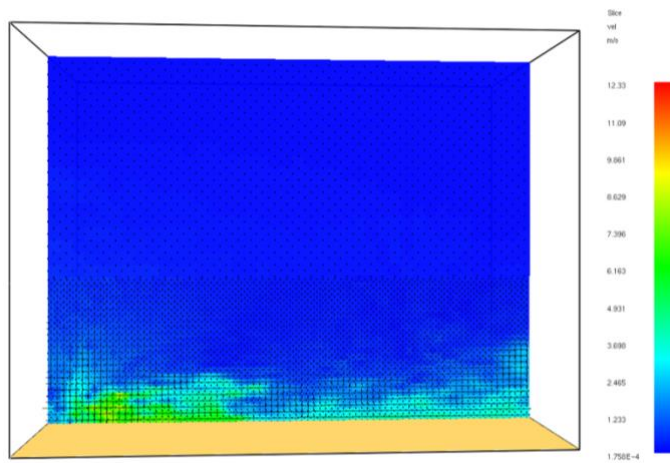


Figure 5-12 Gas velocity vector SLCF through center of spray for Nozzle B, hybrid mesh with grid size 0.05 m close to nozzle and 0.1 m above nozzle

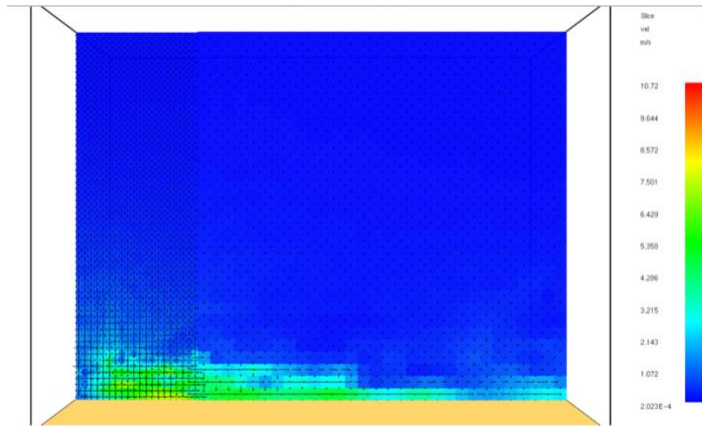


Figure 5-13 Gas velocity vector SLCF through center of spray for Nozzle B, hybrid mesh with grid size 0.05 m close to nozzle and 0.1 m downstream

These results show that the gas phase boundary layer for the floor nozzle is greatly impacted with increasing grid size. When the grid size increases downstream from the nozzle the air velocity is unresolved and consequently droplets fall prematurely and are not able to travel the entire nozzle coverage area distance. When the grid size increases vertically above the nozzle there is no visual impact on the velocity field in Smokeview but the droplet velocity shows a significant decrease from the 0.05 m grid simulations demonstrating a grid dependence above the nozzle. To sufficiently resolve the length scales associated with Nozzle B a 0.05 m grid resolution is needed throughout the entire spray pattern area, both vertically above the nozzle discharge and throughout the flame region. The grid size can be increased a sufficient distance above the nozzle that does not impact the flow; due to time constraints this height is not directly resolved.

This nozzle might be improved with a smaller grid size; however, smaller grid sizes are not evaluated in this analysis because they are not feasible for large scale engineering configuration simulations.

5.6.1.3 Nozzle C critical length scales

This analysis expands upon the grid analysis completed in section 4.2.2.3 which determined a large grid dependency and required resolution of 0.02 m in the near field of the nozzle. Simulations were completed with the same inputs in section 4.2.2.3 with increasing grid sizes downstream from the nozzle.

Figure 5-14 and 5-15 plot the particle diameter and velocity versus height for each mesh selection.

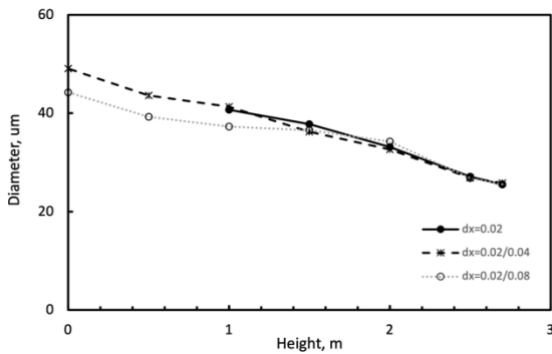


Figure 5-14 Diameter (D10) vs vertical distance from nozzle for small mesh and hybrid meshes with Nozzle C. Nozzle located at $z = 3$ m.

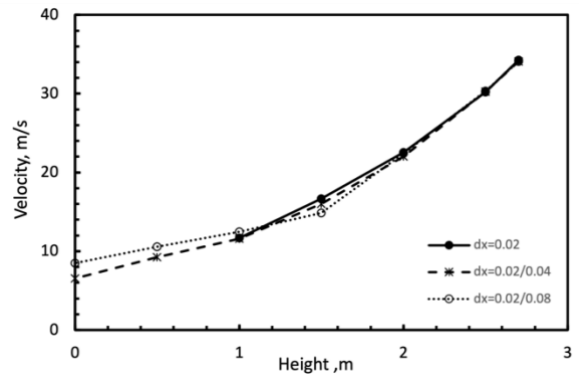


Figure 5-15 Velocity vs vertical distance from nozzle for small mesh and hybrid meshes with Nozzle C. Nozzle located at $z = 3$ m.

Figure 5-16 and 5-17 plot the particle diameter and velocity versus radial position for each mesh selection.

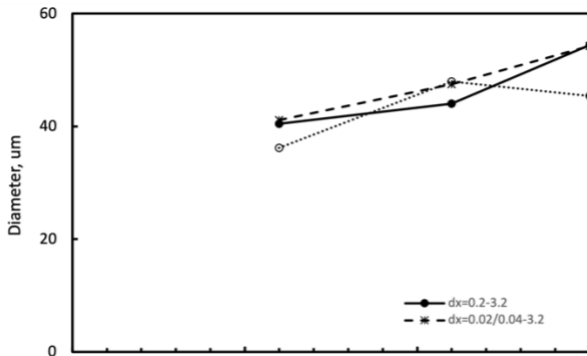


Figure 5-16 Diameter (D10) vs radial distance for small mesh and hybrid meshes with Nozzle C. Measurements at $Z = 3.2$ m below nozzle.

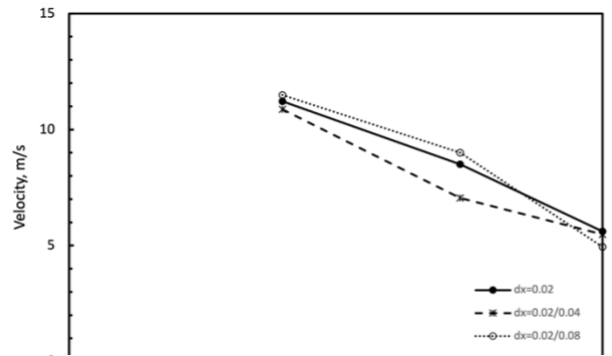


Figure 5-17 Velocity vs radial distance for small mesh and hybrid meshes with Nozzle C. Measurements at $z = 3.2$ m below nozzle.

Figure 5-18 to 5-20 show the gas velocity flow field downstream of the nozzle for each simulation.

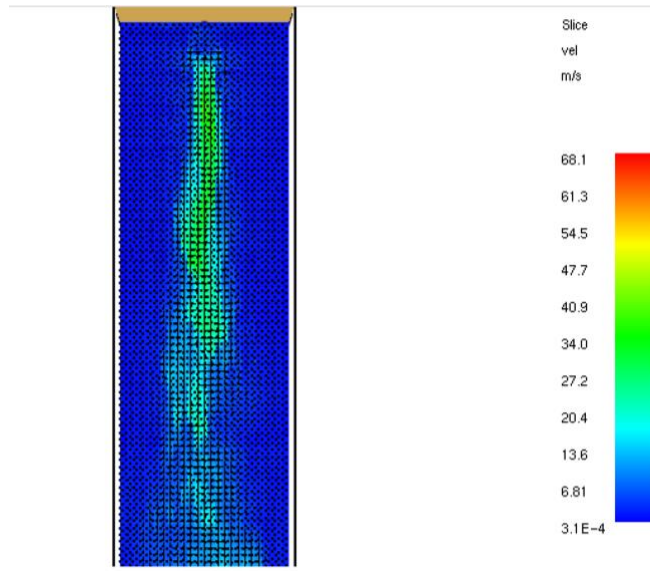


Figure 5-18 Gas velocity vector SLCF through center of spray for Nozzle C, $dx = 0.02\text{ m}$

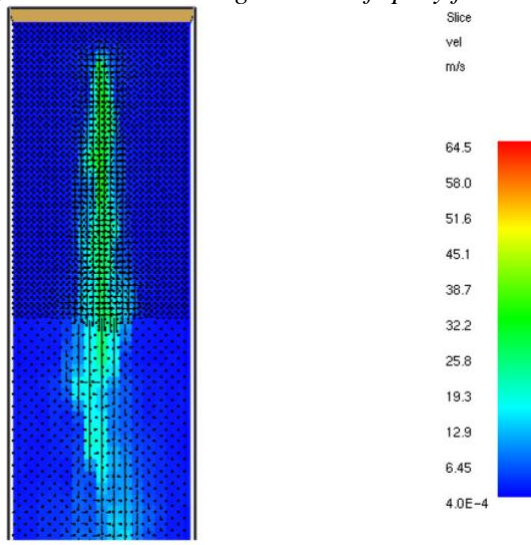


Figure 5-19 Gas velocity vector SLCF through center of spray for Nozzle C, hybrid mesh with $dx = 0.02\text{ m}$ to 0.04 m

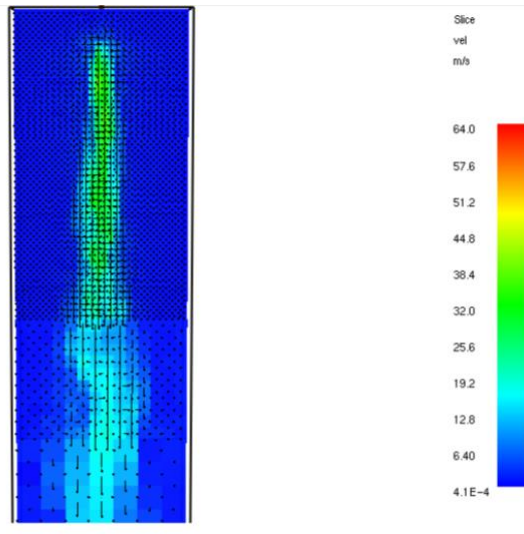


Figure 5-20 Gas velocity vector SLCF through center of spray for Nozzle C, hybrid mesh with $dx = 0.02\text{ m to }0.08\text{ m}$

The results show that downstream of the nozzle, once the flow is fully turbulent, the grid size can be increased up to a factor of 4 times the initial grid requirement. Despite the large increase, this still corresponds to a grid resolution less than 0.1 m downstream, which is not feasible for large scale engineering problems. To adequately resolve Nozzle B the grid size must be 0.02 m up to 1 m away from the nozzle and can be systematically increased up to 0.08 m for the remainder of the spray pattern.

5.6.2 Final Grid Selection

Following the analysis of critical length scales in section 5.5.1 the final grid resolution was determined taking into consideration all critical length scales, required CPU, available CPU, and project timeline. All simulations utilize a hybrid mesh for fine resolution in areas of interest and coarse resolution in less important areas based on the given research problem. All simulations started at a large grid size, 0.5 m, and were systematically decreased to the final grid resolutions given below.

The simulations with Nozzle A use 0.1 m resolution in the near field of the nozzles (up to 1 m downstream of the nozzles) and in the near field of the flame sheet. The grid size is increased between the nozzles and the near field flame region to 0.2 m on the fire side of the hangar. The non-fire side of the hangar and the outdoor mesh use 0.4 m grid resolution. The complete mesh selection for simulations using Nozzle A is given in Appendix G.1.

Simulations with Nozzle B use 0.05 m resolution in the near field of the nozzles in the flame region and in the near field of the flame sheet. Due to the nature of the location of the floor nozzles the fire origin is varied between the center of the pool, where there is a 0.5 m ‘unprotected’ gap between 2 rows of nozzles, and the edge of the pool, where the fire remains completely centered between two rows of nozzles. Each of these simulations utilize a 0.05 m resolution in the fire region, including all applicable water mist nozzles in the area. The grid size selection does not change based on the fire location but the number of nozzles that need to be resolved does change. The side nozzle only requires fine resolution for the two rows of nozzles directly around the fire, whereas the center fire source requires all 4 rows of nozzles in the fire region have fine resolution. The grid size is increased to 0.1 m at 4 m above the flame and is increased again to 0.2 m at 6 m above the flame sheet. The grid size is increased to 0.2 m around the flame region on the fire side of the hangar. The non-fire side of the hangar and the outdoor mesh use 0.4 m grid resolution. The complete mesh selection for simulations using Nozzle B with ignition location are given in Appendix G.2.1 and G.2.2 respectively.

Simulations with Nozzle C use a 0.2 m resolution for the half of the hangar with the fuel source and increase to 0.4 m resolution on the non-fire size and for the outdoor

mesh. The constraint imposed by `PARTICLE_CFL = .TRUE.` significantly increases the run time for simulations with this nozzle which limited the grid size and number of particles used in this simulation. The complete mesh selection for simulations using Nozzle C is given in Appendix G.3.

5.7 Model Limitations

There are many inherent model limitations with LES modeling in FDS; however, there are additional limitations imposed on these simulations based on the selection of various models' and level of analysis completed. The most important user-imposed limitations are summarized below.

1. The MLRPUA is not a function of pool surface temperature and thermal feedback, consequently the extinction model does not account for any fuel surface cooling or MLRPUA reduction due to reduced thermal feedback.
2. All critical length scales are not fully resolved and critical length scales that are fully resolved are only resolved in small areas, there is some loss of accuracy through increased grid cell size with a hybrid grid.
3. The impact of particles per second on the extinction results with respect to varying grid size is not well understood.

Chapter 6 Results

This chapter analyzes the results of each simulation based on the input conditions described in chapter 5. Performance of each water mist system is evaluated based on the criteria in section 5.4.1. Representative FDS Input Files are attached in Appendix G. All final simulations were run on the UMD High-Performance Computing cluster,

Deethought2, using 1 node and up to 20 processors. The run times for each simulation varied between 46 hours and 72 hours for completion. Exact run times are specified for each simulation in the following sections.

For the purpose of this analysis each representative structural steel beam, electrical box, and portion of the plane will be referenced for analysis based on the designations shown in Figure 6-1. Heat flux measurements along the bottom of the plane will be referenced with designations depicted in Figure 6-2 based on relative location.

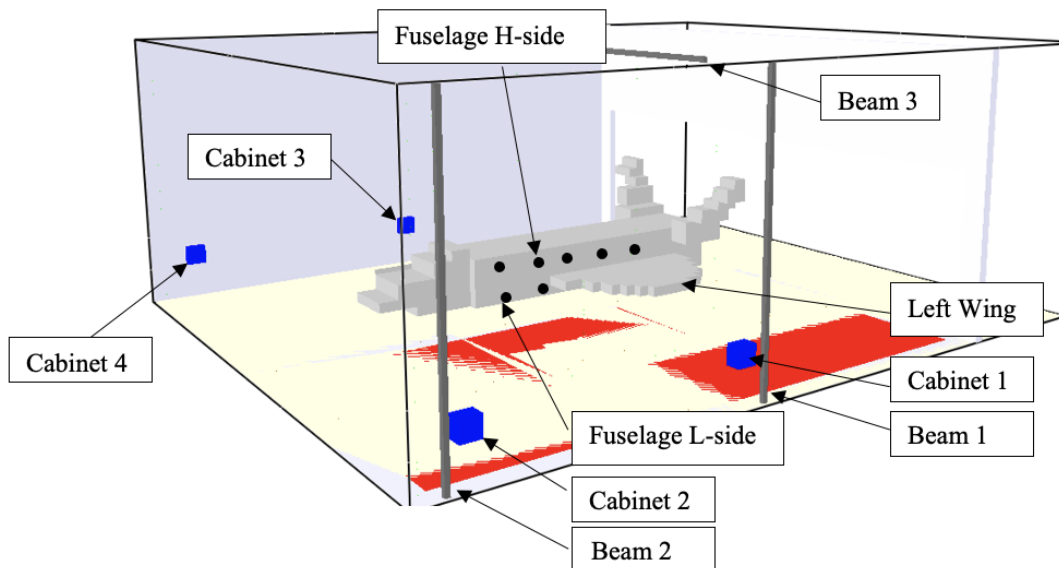


Figure 6-1 Designations of various 'targets' in hangar compartment for results and analysis

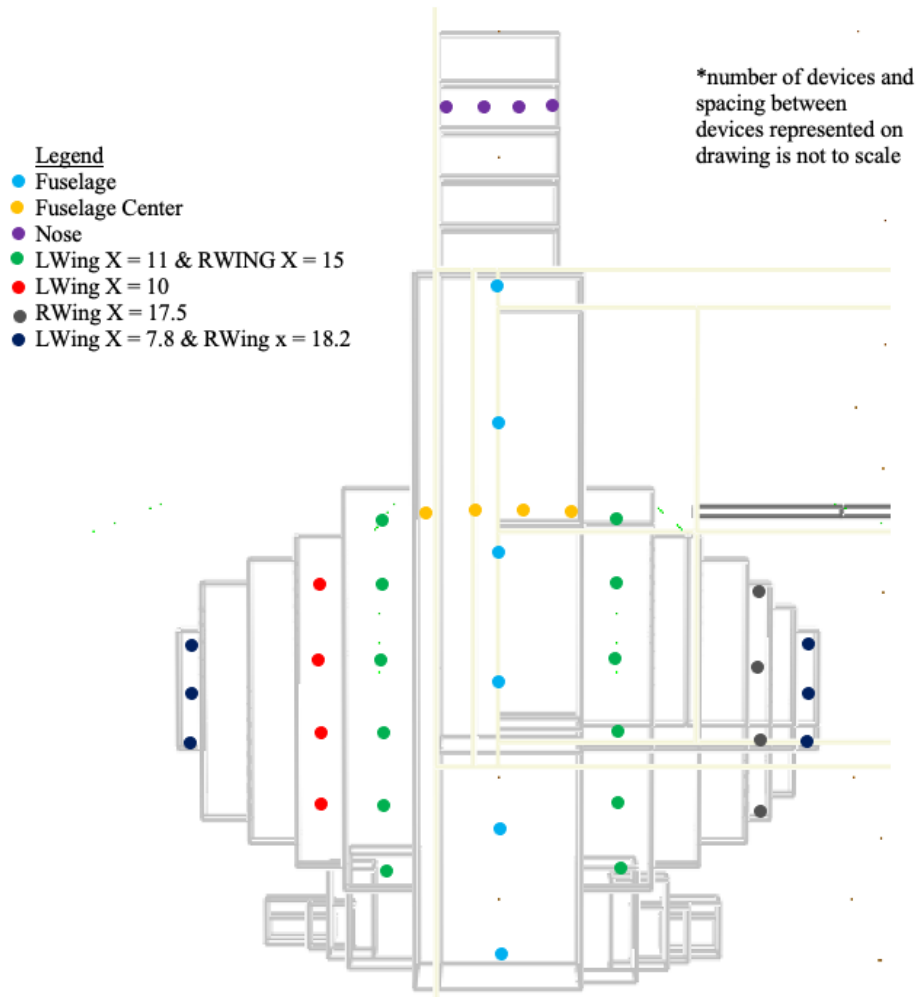


Figure 6-2 Visual representation of incident heat flux device locations for results and analysis

6.1 Nozzle A Final Simulations

6.1.1 Simulation A.1: 30 second activation time

Simulation A.1 investigated Nozzle A for protection against a JP-8 jet fuel pool fire with an assumed ignition source in the center of the pool and a 30 second water mist activation time. The nozzle characteristics, nozzle spacing, room configuration, fire characteristics, and grid size are outlined in chapter 5 of this report. Simulation A.1 was run on 1 node using 18 MPI processes and completed in approximately 32 hours.

The results of this simulation are compiled below. Figure 6-3 plots the measured HRR in FDS and the expected HRR versus time. Figure 6-4 plots the MLR of fuel and evaporation rate of water mist versus time.

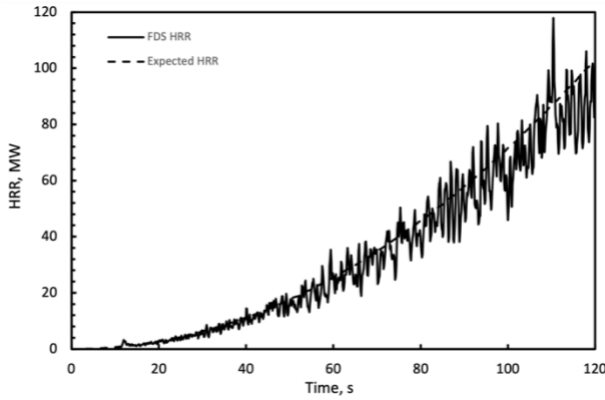


Figure 6-3 FDS measured and expected HRR versus time for simulation A.1

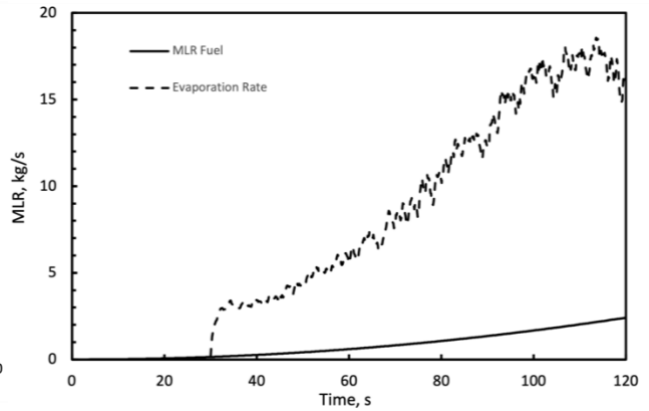


Figure 6-4 MLR fuel and evaporation rate of water mist versus time for simulation A.1

Figures 6-5 to 6-8 plot selected incident heat flux measurements versus time for various locations according to Figures 6 -1 and 6-2. The locations with the highest heat fluxes are shown here and additional graphs showing all incident heat flux measurements are provided in Appendix H.

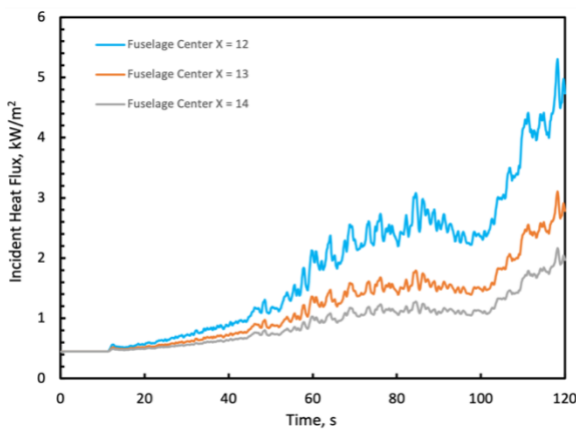


Figure 6-5 Incident Heat Flux versus time across the center of the fuselage (Y = 13) for simulation A.1

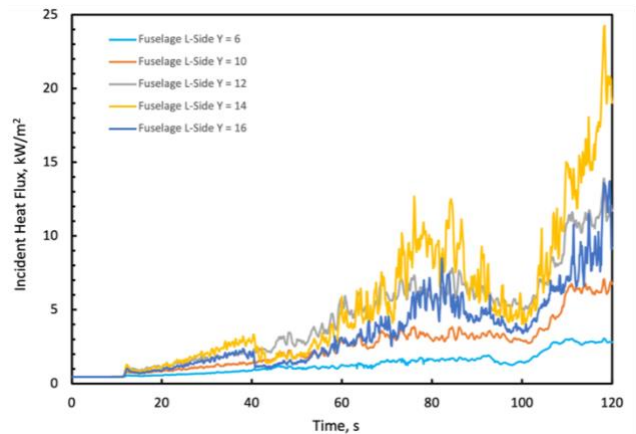


Figure 6-6 Incident Heat Flux versus time low on the side of the fuselage for simulation A.1

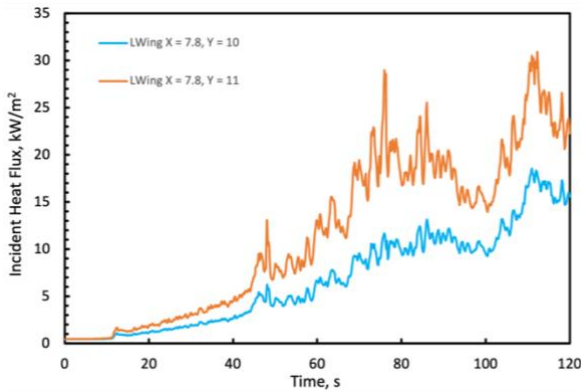


Figure 6-7 Incident Heat Flux versus time to the left wing ($X = 7.8$) for simulation A.1

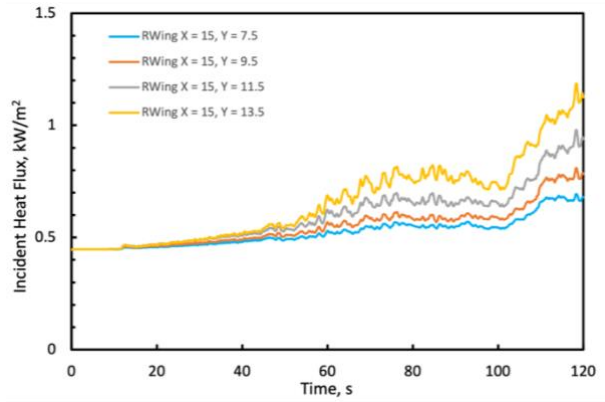


Figure 6-8 Incident Heat Flux versus time to the right wing ($X = 15$) for simulation A.1

Figures 6-9 to 6-11 plot the temperature versus time for various locations on each structural steel beam.

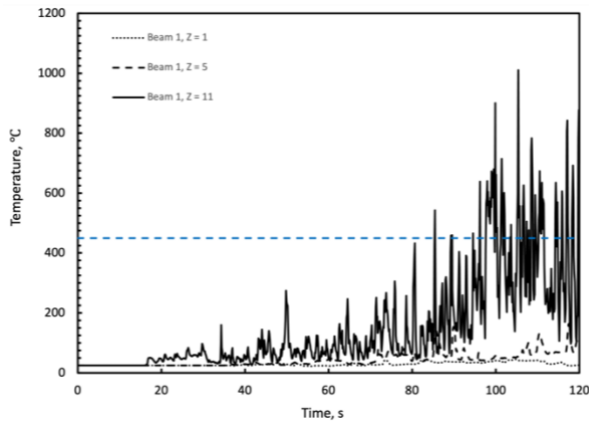


Figure 6-4 Temperature versus time at various heights on Beam 1 for simulation A.1

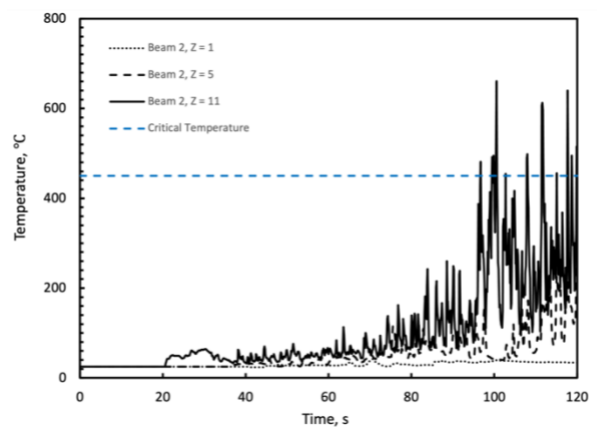


Figure 6-3 Temperature versus time at various heights on Beam 2 for simulation A.1

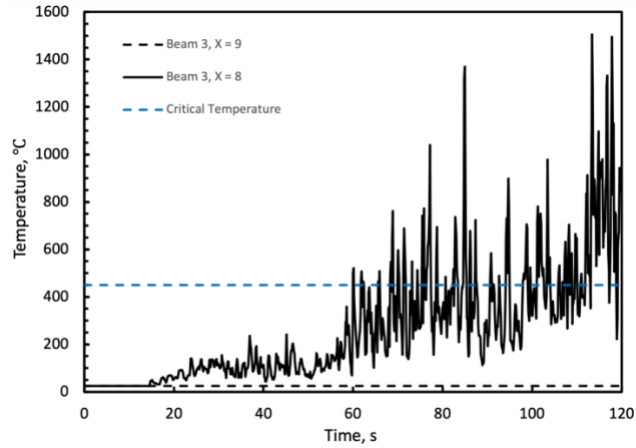


Figure 6-5 Temperature versus time for various horizontal locations on Beam 3 for simulation A.1

Figure 6-12 plots the incident heat flux measurements versus time for each of the electrical cabinets. The variation in incident heat flux versus location are negligible for each of the cabinets consequently, the values in the graph are representative of the maximum and minimum heat flux to each cabinet.

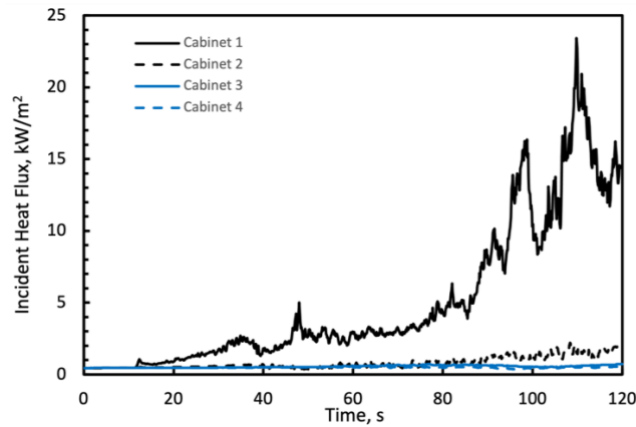


Figure 6-6 Incident heat flux versus time at each electrical box for simulation A.1

Figures 6-13 to 6-15 show SLCF's in Smokeview of temperature, sprinkler water vapor mass fraction, and oxygen volume fraction 0.5 seconds, 10 seconds, 30 seconds, 60 seconds, and 90 seconds after the water mist system activates.

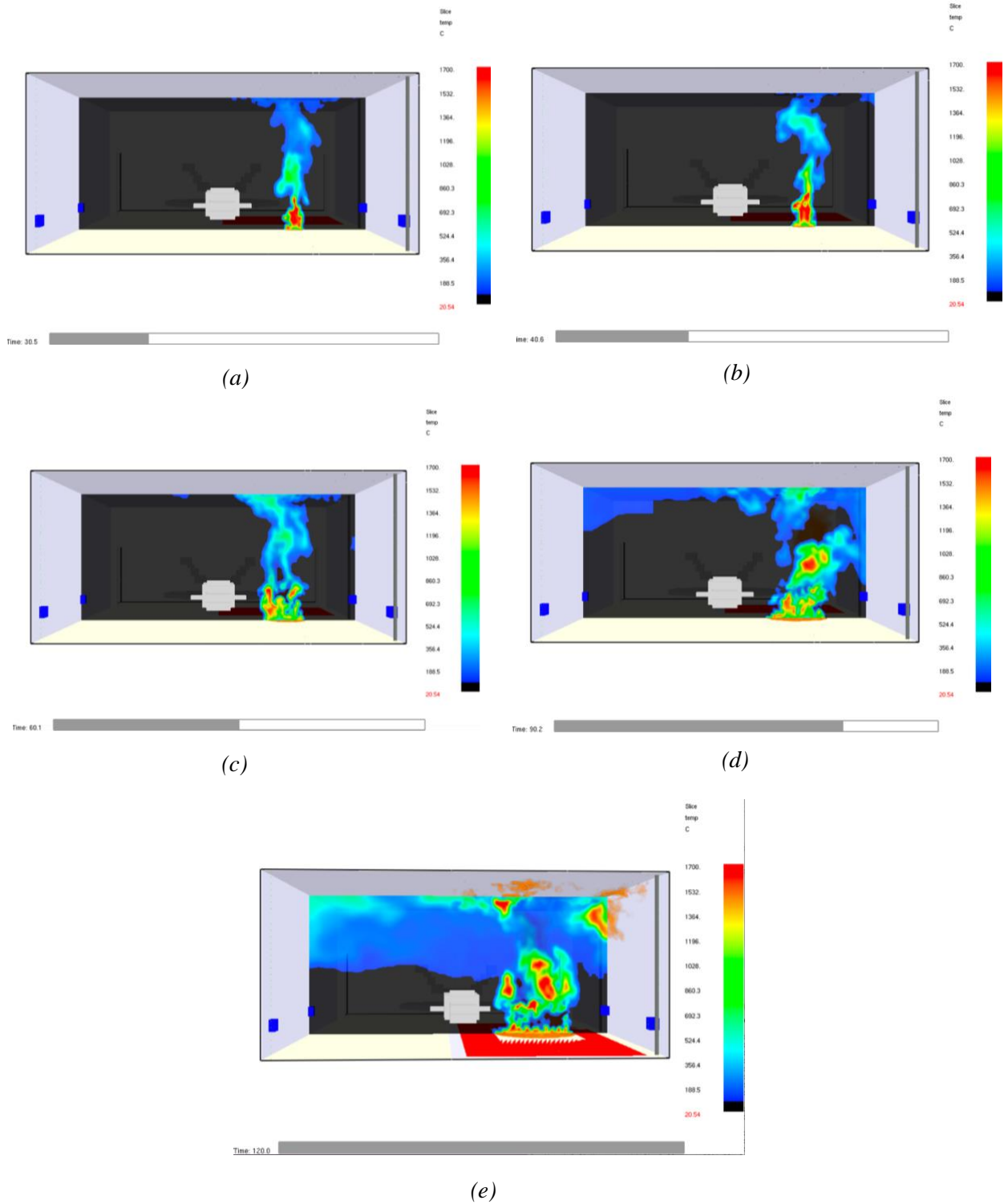


Figure 6-7 Temperature SLCF at (a) $t = 30.5$ seconds, (b) $t = 40$ seconds, (c) $t = 60$ seconds, (d) $t = 90$ seconds, (e) $t = 120$ seconds for simulation A.1

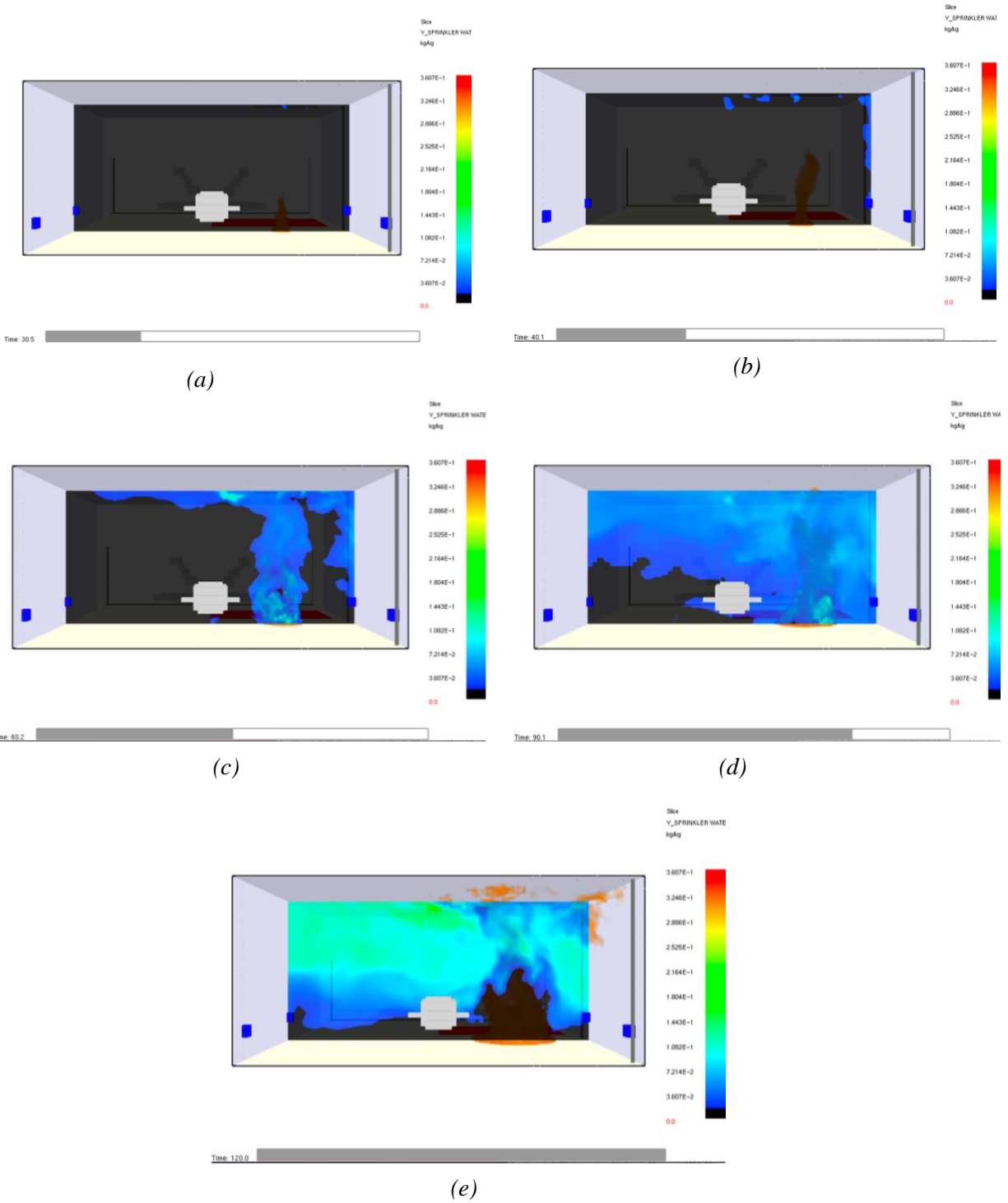


Figure 6-8 Sprinkler Water Vapor Mass Fraction SLCF at (a) $t = 30.5$ seconds, (b) $t = 40$ seconds, (c) $t = 60$ seconds, (d) $t = 90$ seconds, (e) $t = 120$ seconds for simulation A.1

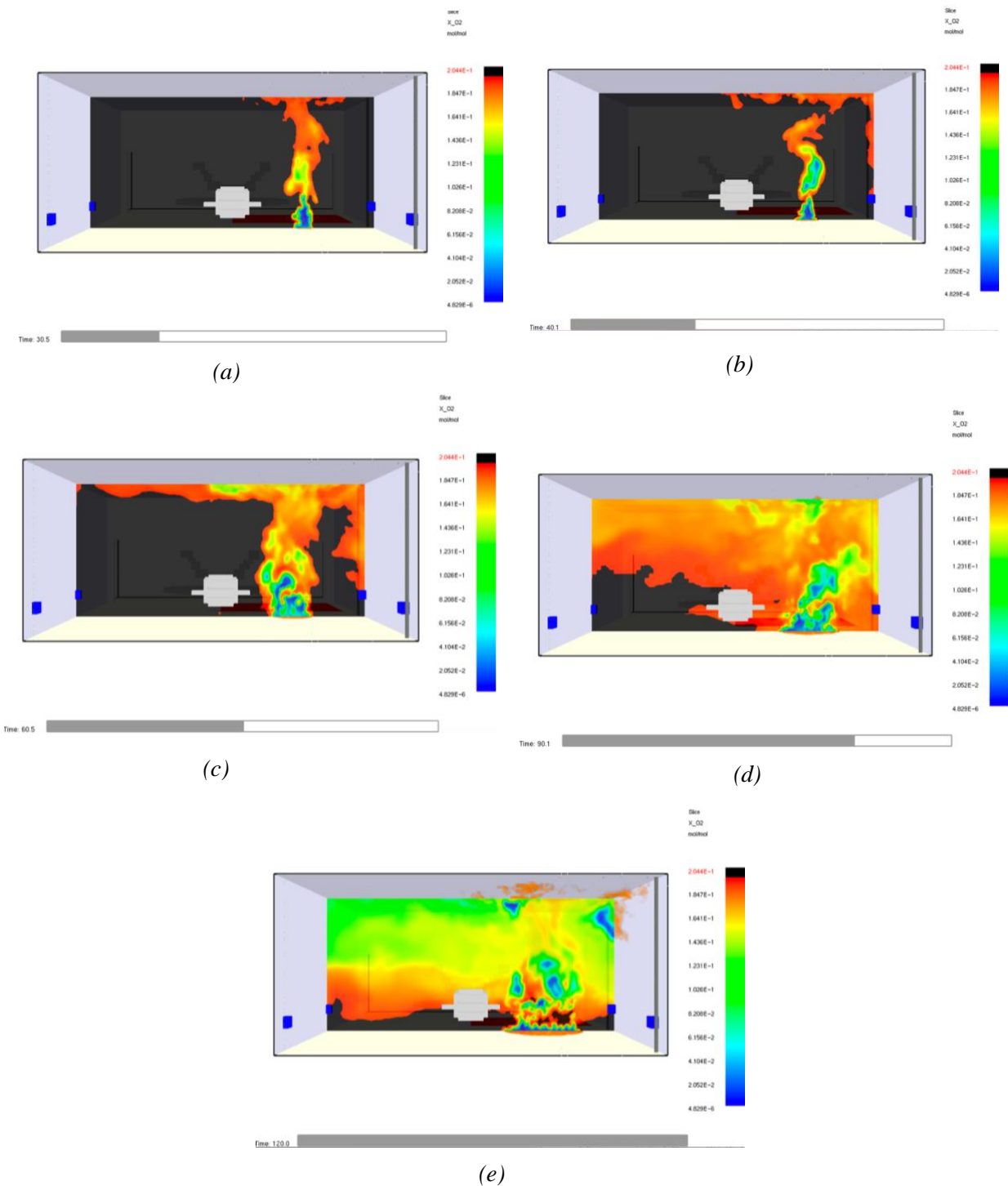


Figure 6-9 Oxygen Volume Fraction SLCF at (a) $t = 30.5$ seconds, (b) $t = 40$ seconds, (c) $t = 60$ seconds, (d) $t = 90$ seconds, (e) $t = 120$ seconds for simulation A.1

The results show that activation of Nozzle A is not able to extinguish the fire. Nozzle A does not have a significant impact on the HRR; the predicted HRR is approximately equal to the measured HRR, as shown in Figure 6-3. The maximum cooling power of the nozzles corresponds to 37.9 MW, by 63 seconds into the simulation the fire power exceeds the cooling power of the water mist nozzles. It takes 10-15 seconds for the water mist to cool and penetrate the ceiling jet and reach the flame sheet. Once the water mist reaches the flame the evaporation rate increases with the increased particles entering the hot flame zone. At this point the flame is weaker and there is a reduction in incident heat flux to electrical boxes and a decrease in temperature of the structural steel members.

The water mist is not able to remove enough heat from the flame to prevent growth and soon the fire power overpowers the water mist system. When the fire overpowers the mist system, water from the mist nozzles evaporate at roughly the same rate as which they enter the space, meaning all of the evaporation occurs quickly in the ceiling jet and the flame is unaffected. These effects can be seen through the high evaporation rate in Figure 6-4, and the lack of water vapor present in the flame region at the end of the simulation in Figure 6-14.

Within 60 seconds the flame height is close enough to the ceiling to increase the temperature of the structural steel and reach failure limits. Within 80 seconds the temperature of the top portion of Beam 1 reaches failure limits.

The left wing of the plane, closest to the fire, may experience delamination during this fire scenario. The left wing endures a heat flux between 15 and 30 kW/m² for 60 seconds. From previous research it has been found that the composite can endure a heat

flux of 35 kW/m² for up to 50 seconds. Due to the longer exposure time with combined lower heat flux it is difficult to conclude whether or not delamination will occur.

6.1.2 Simulation A.2: 50 second activation time

Simulation A.2 investigated Nozzle A for protection against a JP-8 jet fuel pool fire with an assumed ignition source in the center of the pool and a 50 second water mist activation time. The nozzle characteristics, nozzle spacing, room configuration, fire characteristics, and grid size are outlined in chapter 5 of this report. Simulation A.2 was run on 1 node using 18 MPI processes and completed in approximately 46.5 hours.

The results of this simulation are compiled below. Figure 6-16 plots the measured HRR in FDS and the expected HRR versus time. Figure 6-17 plots the MLR of fuel and evaporation rate of water mist versus time.

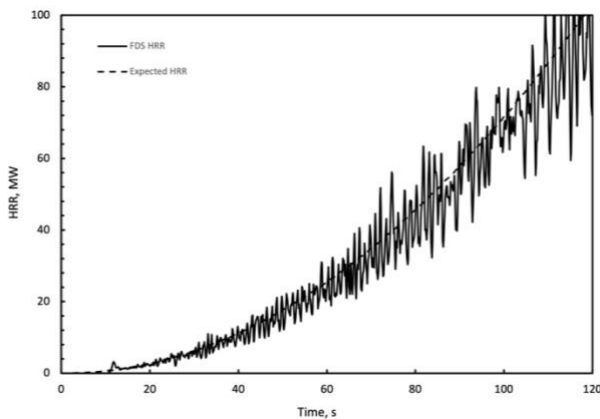


Figure 6-11 FDS measured and expected HRR versus time for simulation A.2

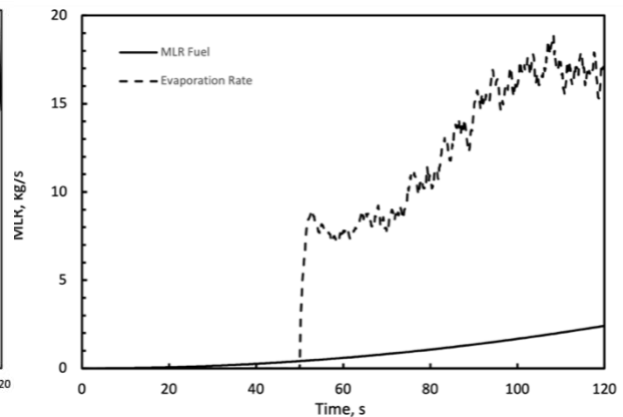


Figure 6-10 MLR fuel and evaporation rate of water mist versus time for simulation A.2

Figures 6-18 to 6-20 plot selected incident heat flux measurements versus time for various locations according to Figures 6 -1 and 6-2. The locations with the highest heat fluxes are shown here and additional graphs showing all incident heat flux measurements are provided in Appendix H. This simulation was run without side of fuselage heat flux

measurements consequently, no analysis of the incident heat flux to the side of the aircraft is conducted.

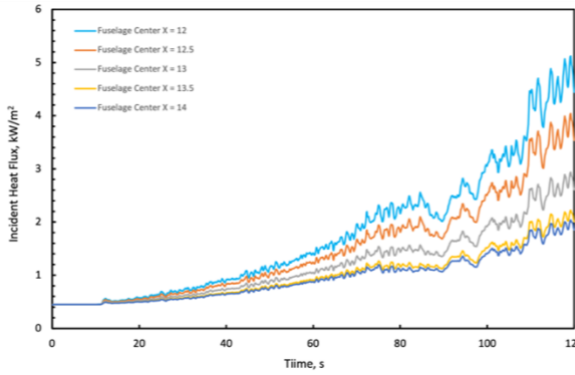


Figure 6-12 Incident heat flux versus time for various locations across the center of the fuselage (Y=13) for simulation A.2

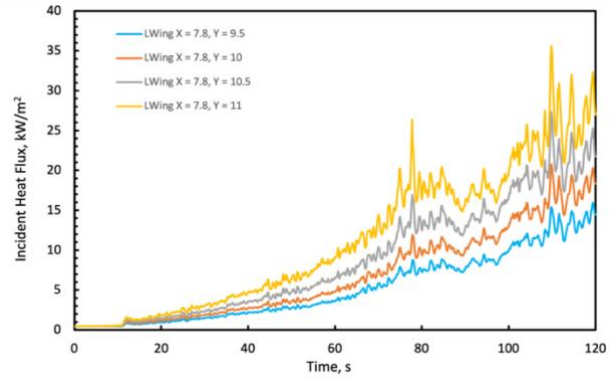


Figure 6-13 Incident heat flux versus time for various location along the bottom of the left wing (X = 7.8) for simulation A.2

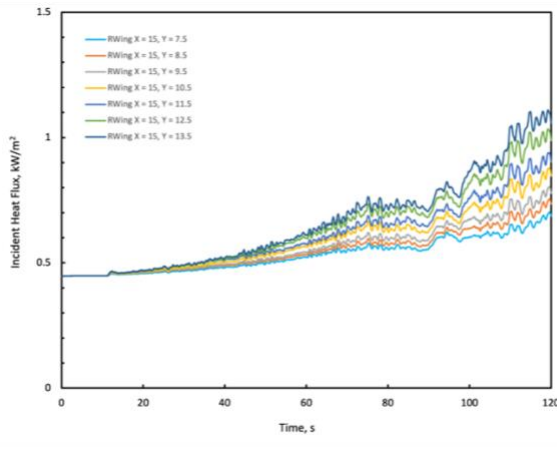


Figure 6-14 Incident Heat flux versus time for various locations along the bottom of the right wing (X = 15) for simulation A.2

Figures 6-21 to 6-23 plot the temperature versus time for various locations on each structural steel beam.

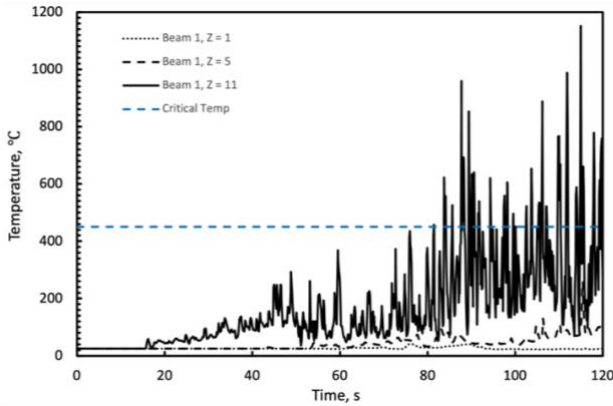


Figure 6-16 Temperature versus time at various heights on Beam 1 for simulation A.2

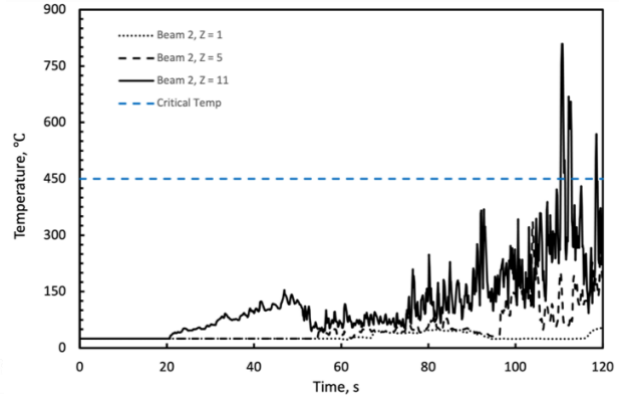


Figure 6-15 Temperature versus time at various heights on Beam 2 for simulation A.2.

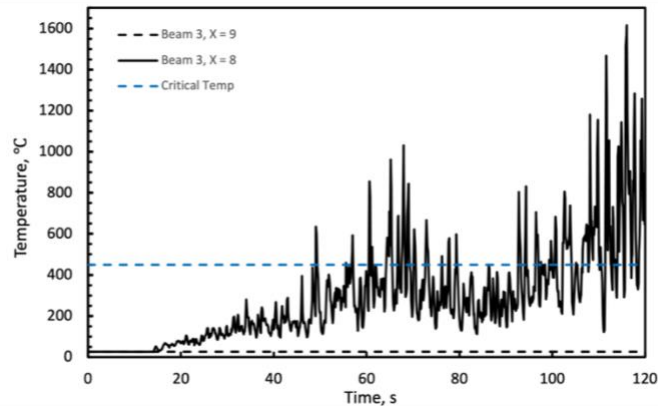


Figure 6-17 Temperature versus time for various horizontal locations on Beam 3 for simulation A.2

Figure 6-24 plots the incident heat flux measurements versus time for each of the electrical cabinets. The variation in incident heat flux versus location are negligible for each of the cabinets consequently, the values in the graph are representative of the maximum and minimum heat flux to each cabinet.

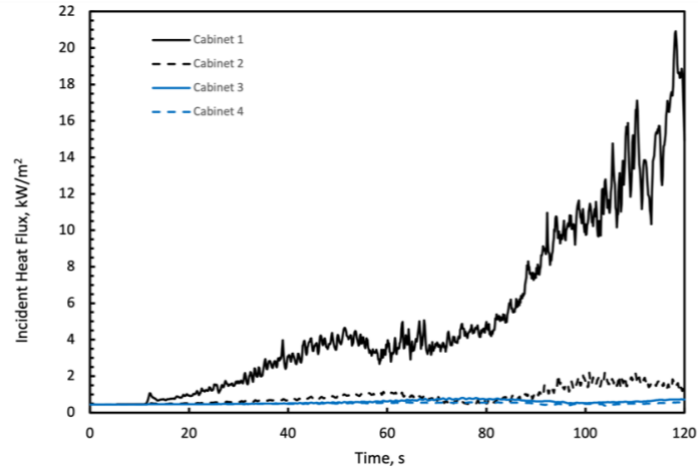
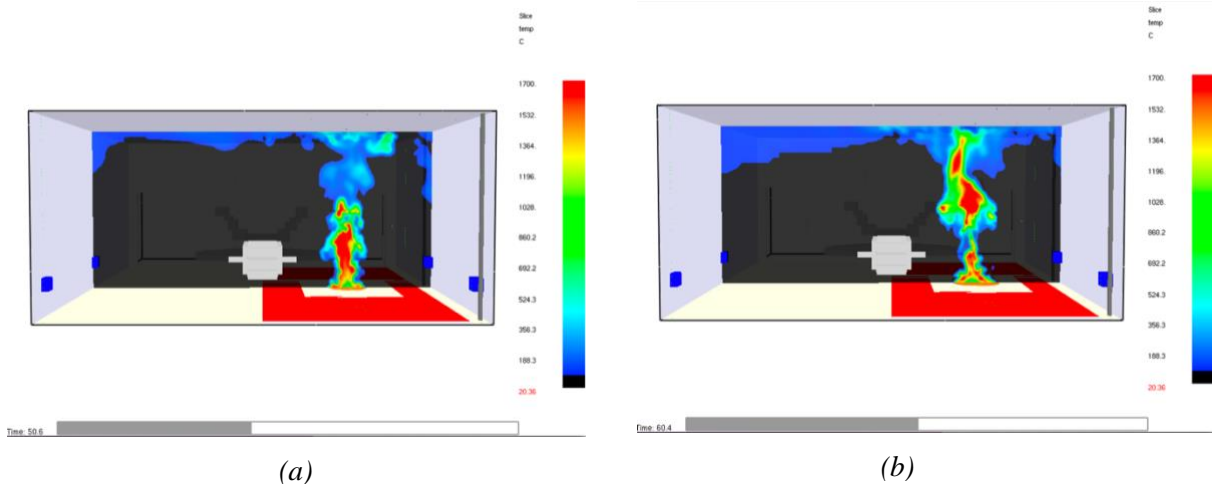


Figure 6-18 Incident heat flux versus time at each electrical box for simulation A.2

Figures 6-25 to 6-27 show SLCF's in Smokeview of temperature, sprinkler water vapor mass fraction, and oxygen volume fraction 0.5 seconds, 10 seconds, 30 seconds, and 70 seconds after the water mist system activates. Portions of the space-colored black correspond to roughly ambient conditions.



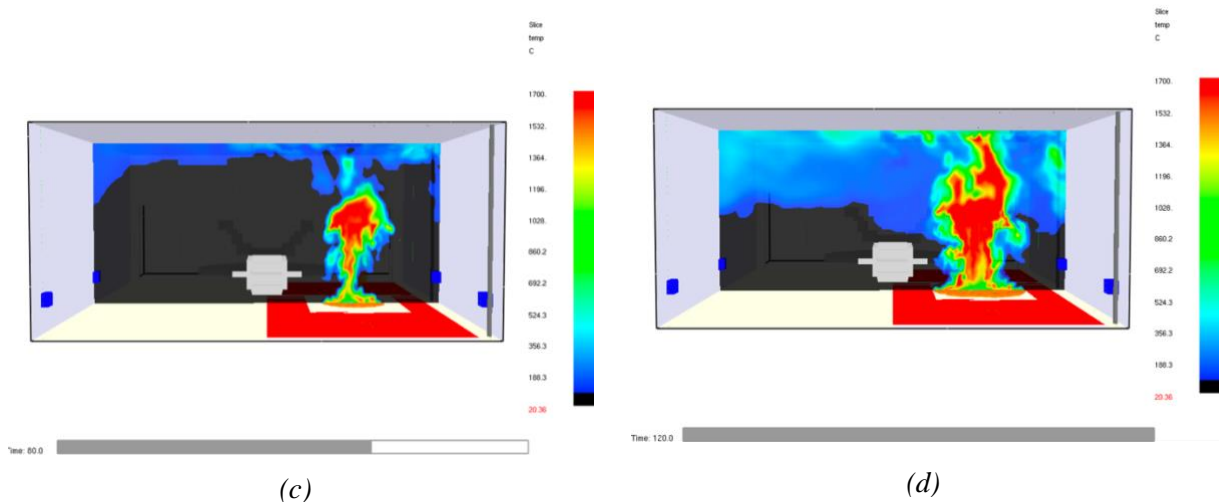
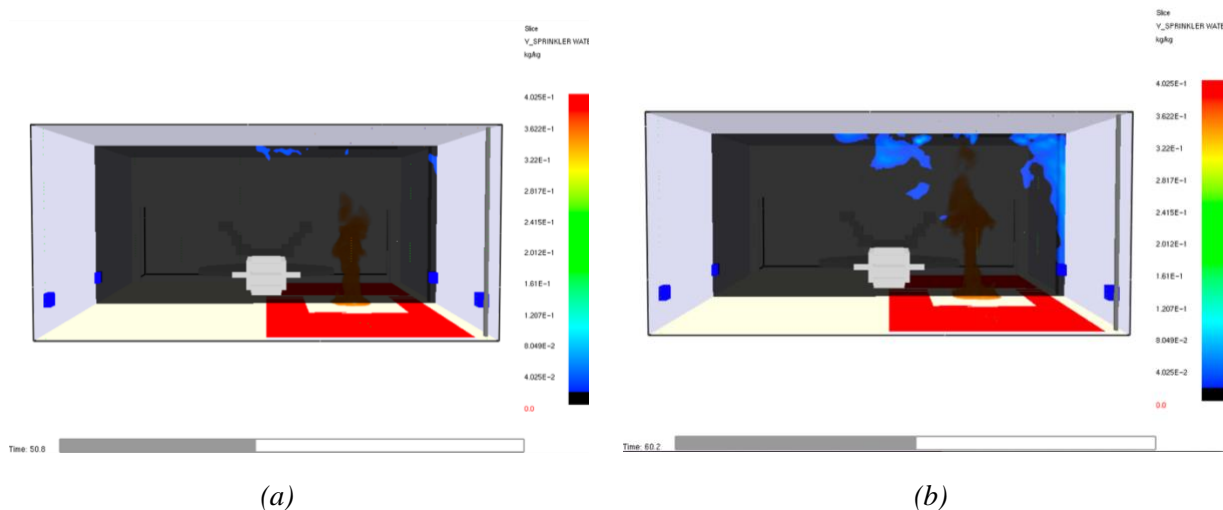


Figure 6-19 Temperature SLCF at (a) $t = 50.5$ seconds, (b) $t = 60$ seconds, (c) $t = 80$ seconds, (d) $t = 120$ seconds for simulation A.2



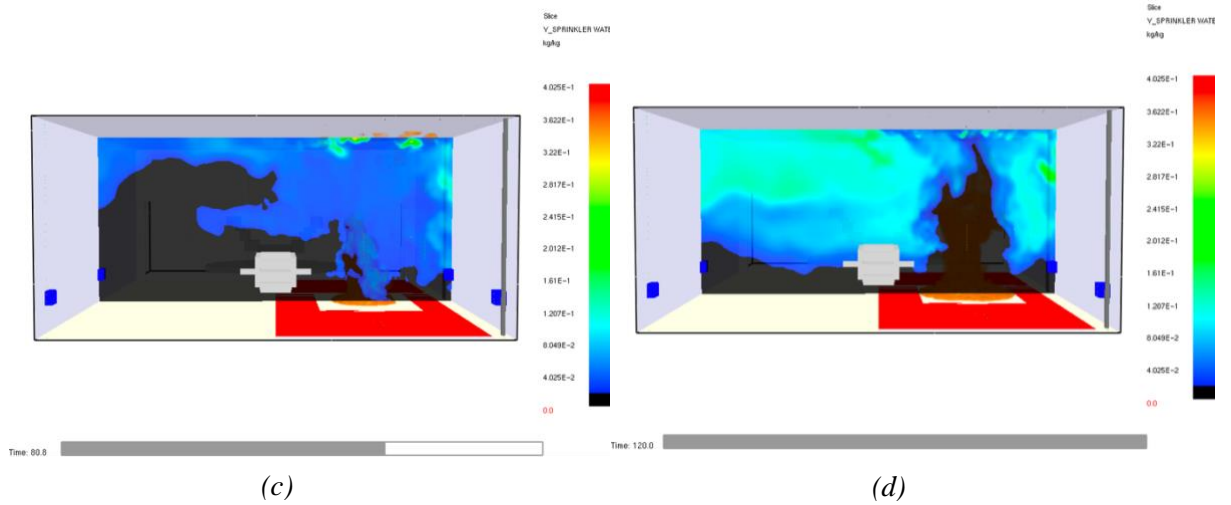
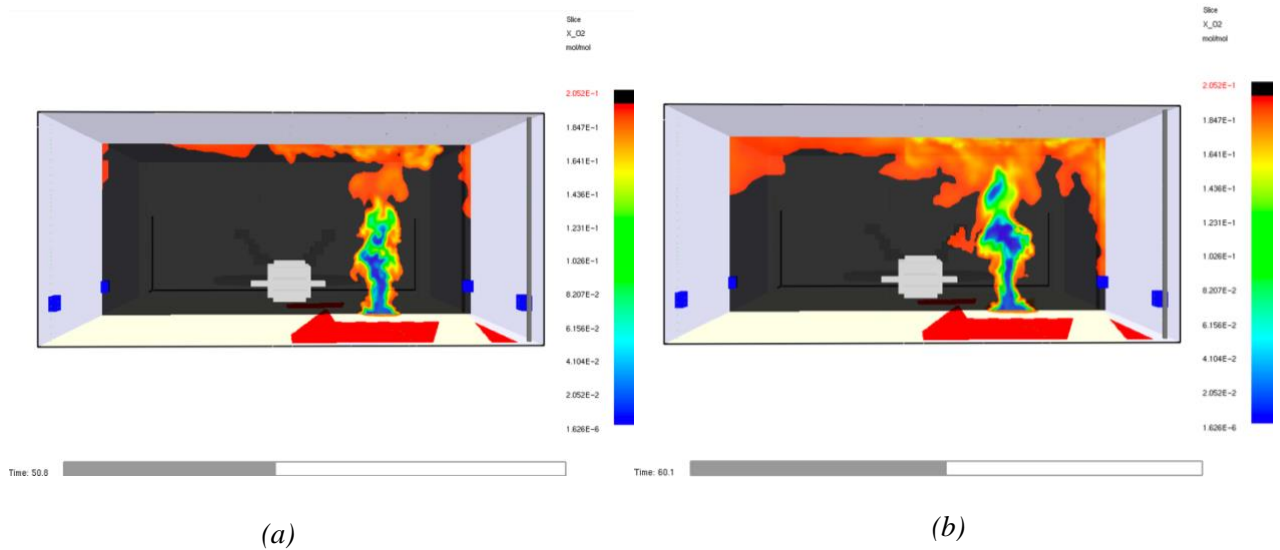


Figure 6-20 Sprinkler Water Vapor Mass Fraction SLCF at (a) $t = 50.5$ seconds, (b) $t = 60$ seconds, (c) $t = 80$ seconds, (d) $t = 120$ seconds for simulation A.2



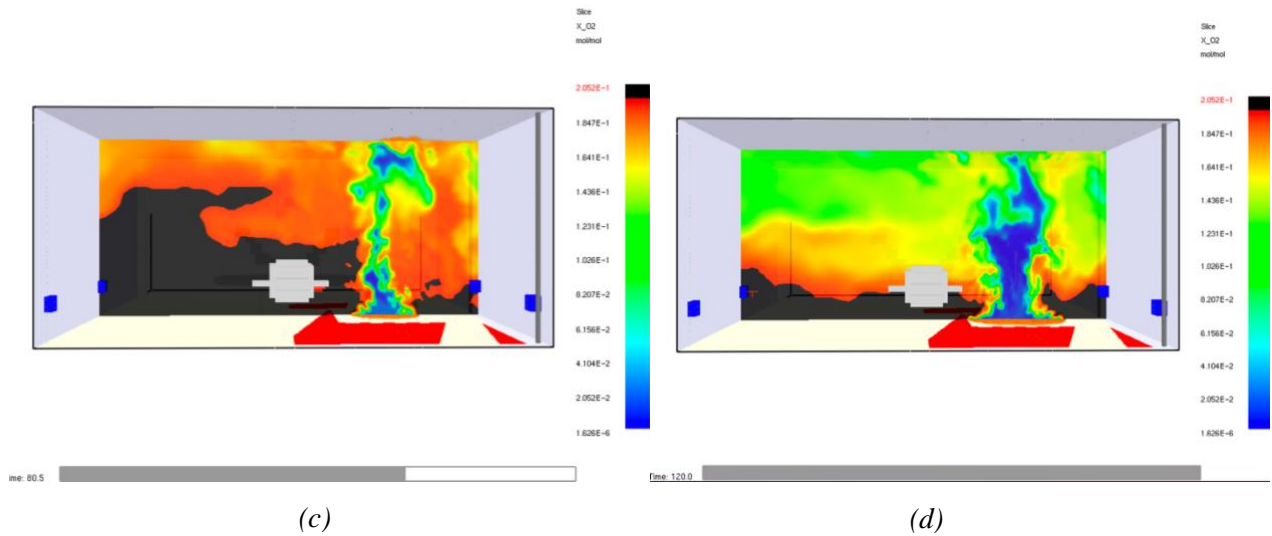


Figure 6-21 Oxygen Volume Fraction SLCF at (a) $t = 50.5$ seconds, (b) $t = 60$ seconds, (c) $t = 80$ seconds, (d) $t = 120$ seconds for simulation A.2

The results of this simulation show that Nozzle A with a 50 second activation time is not able to suppress the pool fire. The results of this simulation are very similar to simulation A.1 and will not be repeated here. The main differences due to the longer activation time are beam 3 reaches $450\text{ }^{\circ}\text{C}$ about 20 seconds sooner in this simulation. This is because with an earlier activation the flame structure is significantly impacted and the flame height does not reach the ceiling as quickly as with the delayed activation time.

The maximum incident heat flux to the left wing increases by approximately 5 kW/m^2 but the duration of high incident heat flux decreases with the delayed activation time. The plane is subject to an incident heat flux between 15 and 30 kW/m^2 for less than 60 seconds.

6.2 Nozzle B Final Simulations

6.2.1 Simulations B.1: 30 second activation time

6.2.1.1 Simulation B.1.a: side of pool ignition source

Simulation B.1.a investigated Nozzle B for protection against a JP-8 jet fuel pool fire with an assumed ignition source at the center of the edge of the pool under the aircraft and a 30 second water mist activation time. The nozzle characteristics, nozzle spacing, room configuration, fire characteristics, and grid size are outlined in chapter 5 of this report. Simulation B.1.a was run on 1 node using 14 MPI processes and completed in approximately 60 hours.

The results of this simulation are compiled below. Figure 6-28 plots the measured HRR in FDS and the expected HRR versus time. Figure 6-29 plots the MLR of fuel and evaporation rate of water mist versus time.

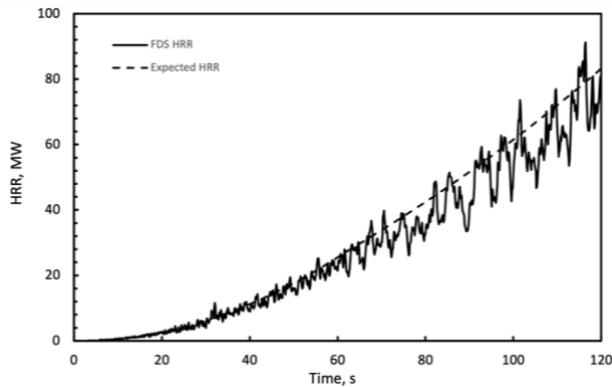


Figure 6-28 FDS measured and expected HRR versus time for simulation B.1.a

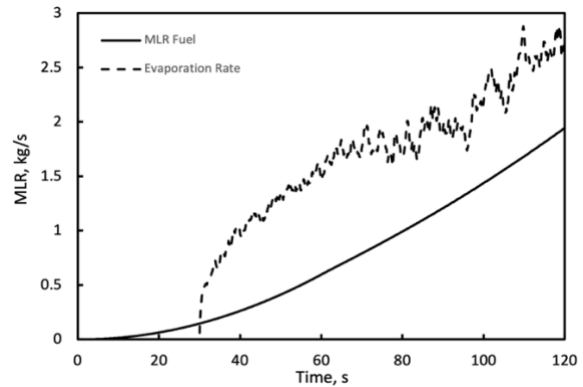


Figure 6-29 MLR fuel and evaporation rate of water mist versus time for simulation B.1.a

Figures 6-30 to 6-33 plot selected incident heat flux measurements versus time for various locations according to Figures 6 -1 and 6-2. The locations with the greatest heat

fluxes are shown here and additional graphs showing all incident heat flux measurements are provided in Appendix H.

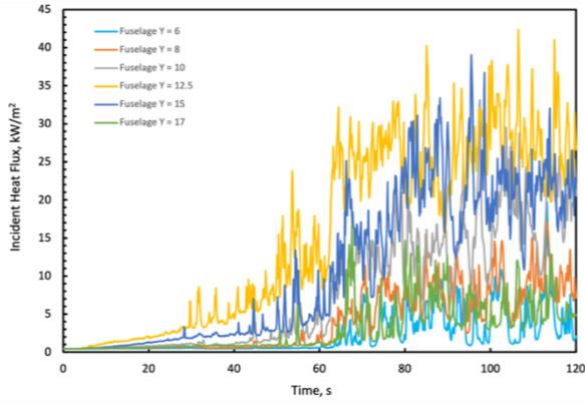


Figure 6-24 Incident Heat Flux versus time at various locations along the low side of the fuselage for simulation B.1.a

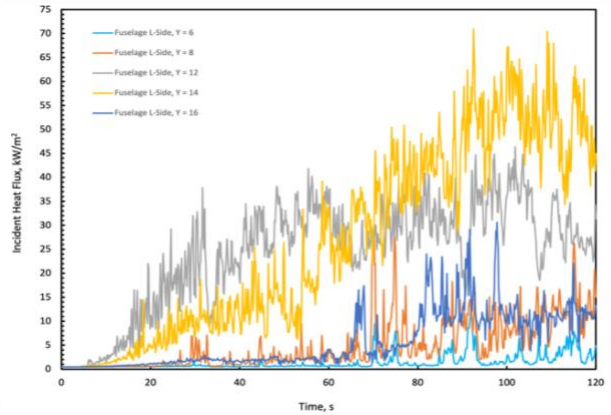


Figure 6-25 Incident Heat Flux versus time at various locations on the right wing ($X=15$) for simulation B.1.a

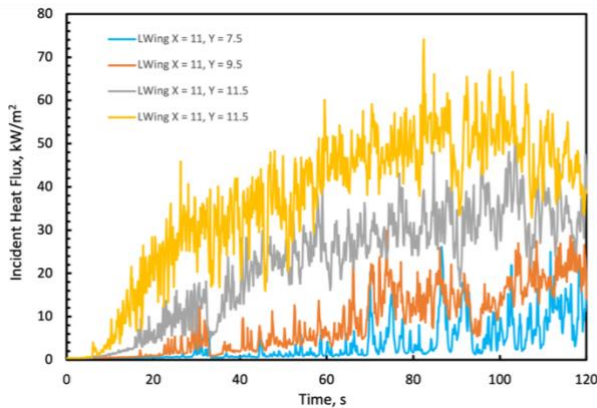


Figure 6-22 Incident Heat Flux versus time at various locations along fuselage ($X = 13$) for simulation B.1.a

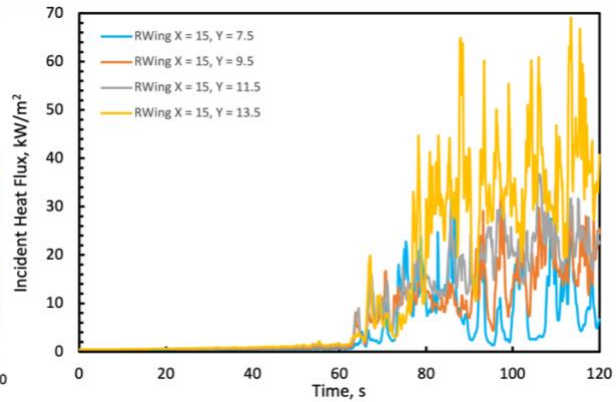


Figure 6-23 Incident Heat Flux versus time at various locations on the left wing ($X=11$) for simulation B.1.a

Figures 6-34 to 6-36 plot the temperature versus time for various locations on each structural steel beam.

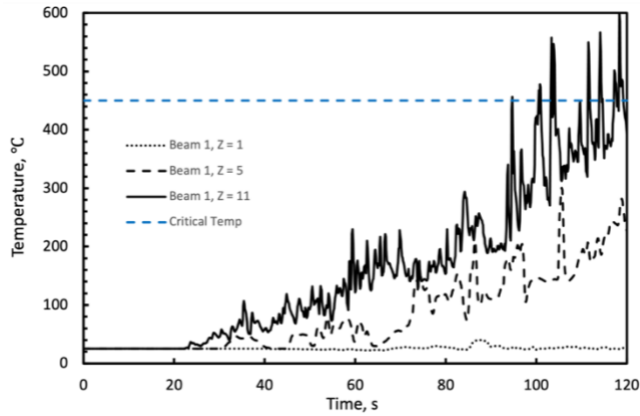


Figure 6-26 Temperature versus time at various heights on Beam 1 for simulation B.1.a

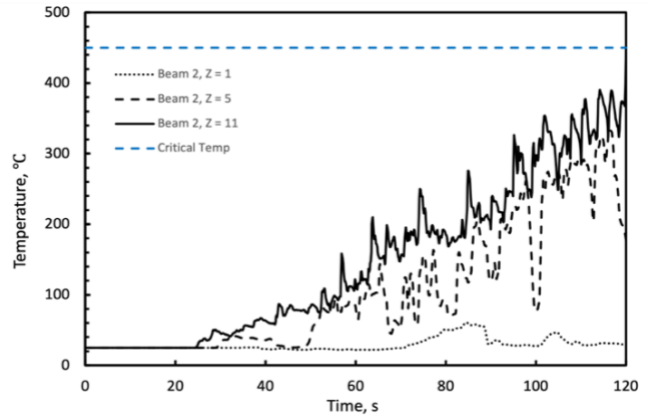


Figure 6-27 Temperature versus time at various heights on Beam 2 for simulation B.1.a

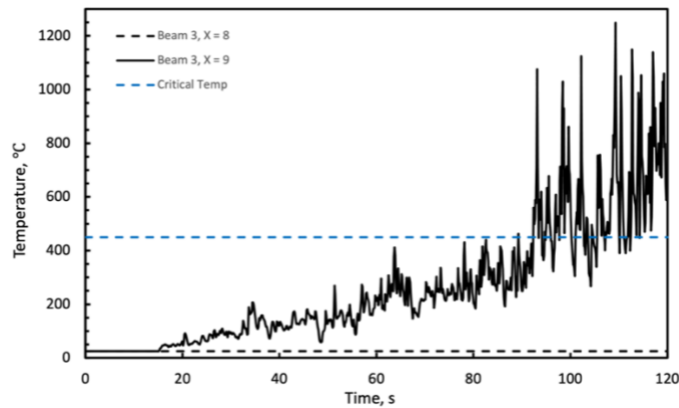


Figure 6-28 Temperature versus time at various horizontal locations on Beam 3 for simulation B.1.a

Figure 6-37 plots the incident heat flux measurements versus time for each of the electrical cabinets. The variation in incident heat flux versus location are negligible for each of the cabinets consequently, the values in the graph are representative of the maximum and minimum heat flux to each cabinet.

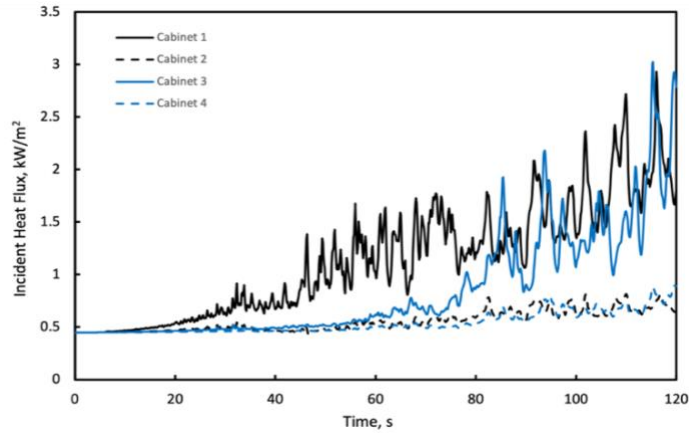


Figure 6-29 Incident heat flux versus time at each electrical box for simulation B.1.a

Figures 6-38 to 6-40 show SLCF's in Smokeview of temperature, sprinkler water vapor mass fraction, and oxygen volume fraction, 0.5 seconds, 10 seconds, 30 seconds, 60 seconds, and 90 seconds after the water mist system activates. Portions of the space-colored black correspond to roughly ambient conditions.

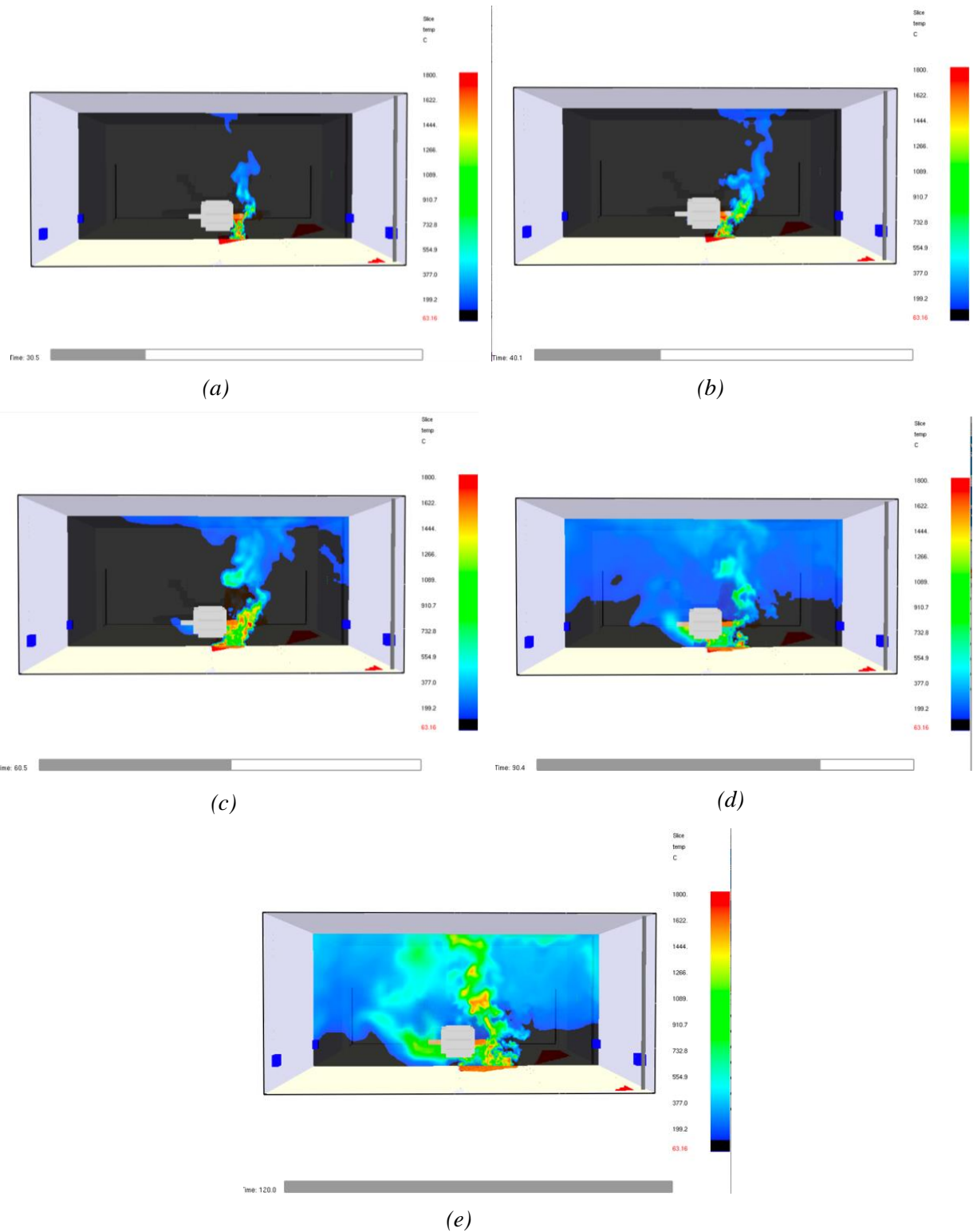
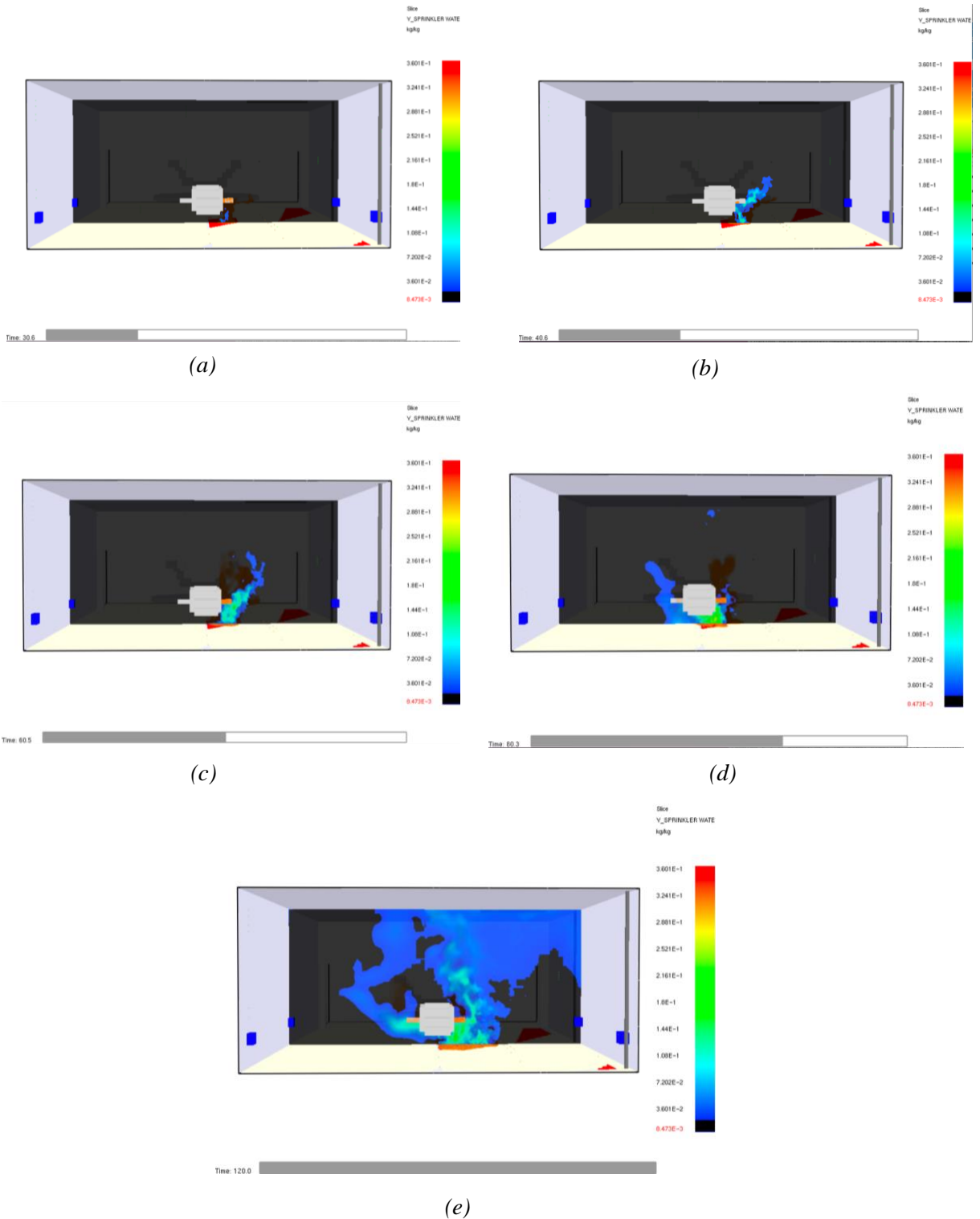


Figure 6-30 Temperature SLCF at (a) $t = 30.5$ seconds, (b) $t = 40$ seconds, (c) $t = 60$ seconds, (d) $t = 90$ seconds, (e) $t = 120$ seconds for simulation B.1.a



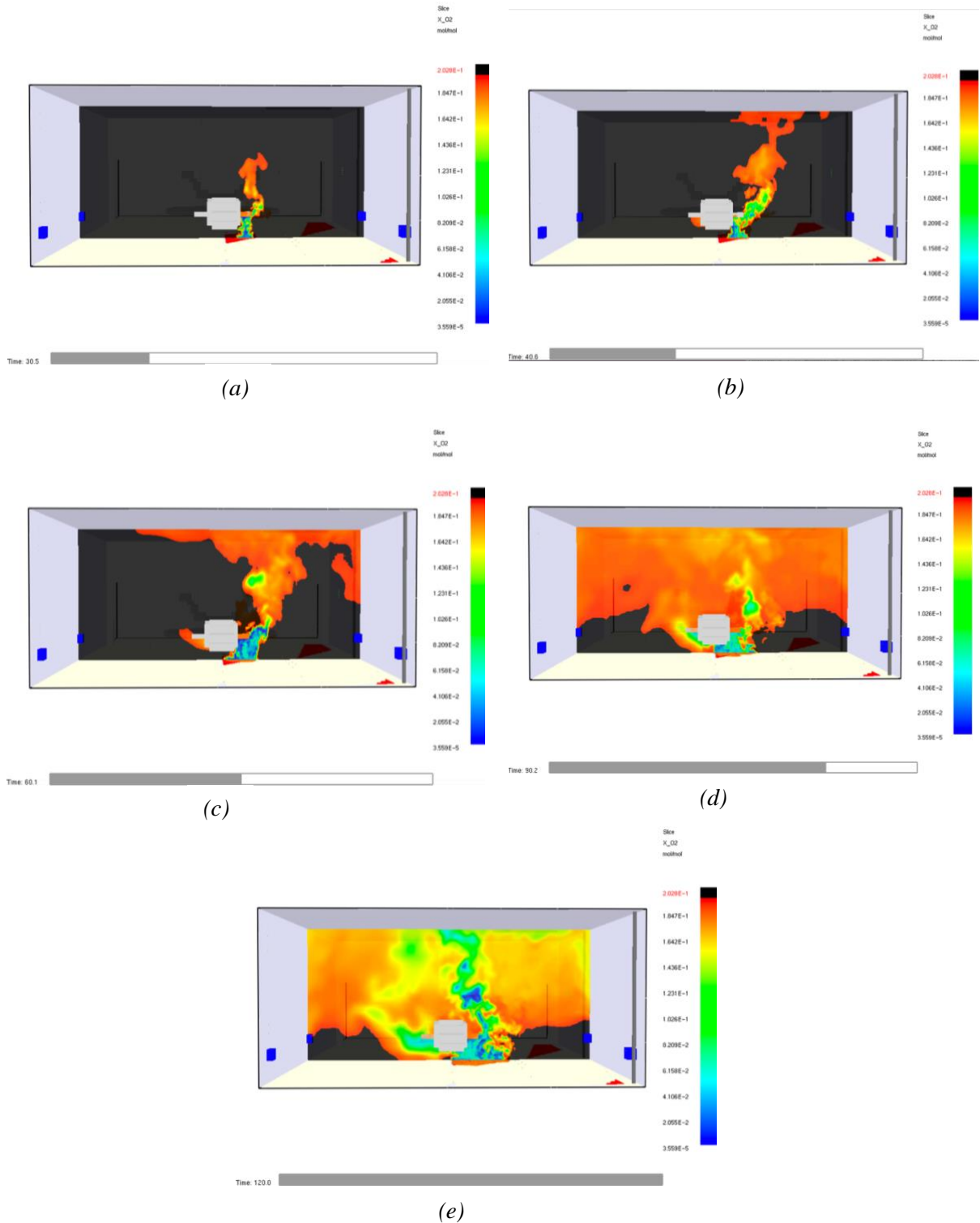


Figure 6-32 Oxygen Volume Fraction SLCF at (a) $t = 30.5$ seconds, (b) $t = 40$ seconds, (c) $t = 60$ seconds, (d) $t = 90$ seconds, (e) $t = 120$ seconds for simulation B.1.a

The results of this simulation show that Nozzle B with a 30 second activation time is not able to suppress the fire. However, Nozzle B prevents the fire from growing at its predicted rate, which is shown Figure 6-28. The nozzles significantly impact the flame and reduce the temperature at the base of the flame region.

Due to the assumed side ignition source the flame is in direct contact with the fuselage, left wing, and right wing for the duration of the simulation resulting in high incident heat fluxes to the aircraft and correspondingly delamination.

Both the top portion of beam 1 and beam 3 reach critical temperatures around 90 seconds into the simulation. Beam 2 does not reach critical temperatures in this scenario. As the fire continues to grow temperatures in the ceiling jet and plume increase without limit and temperatures low in the space where the water mist reaches, remain cool.

These results are based upon the assumptions stated throughout this paper and do not account for fuel surface cooling effects. Due to the orientation of Nozzle B, surface cooling effects are likely much more important for this nozzle than the ceiling nozzles.

6.2.1.2 Simulation B.1.b: center of pool ignition source

Simulation B.1.b investigated Nozzle B for protection against a JP-8 jet fuel pool fire with an assumed ignition source in the center of the pool and a 30 second water mist activation time. The nozzle characteristics, nozzle spacing, room configuration, fire characteristics, and grid size are outlined in chapter 5 of this report. Simulation B.1.b was run on 1 node using 20 MPI processes and completed 114 of 120 seconds in 72 hours.

The results of this simulation are compiled below. Figure 6-41 plots the measured HRR in FDS and the expected HRR versus time. Figure 6-42 plots the MLR of fuel and evaporation rate of water mist versus time.

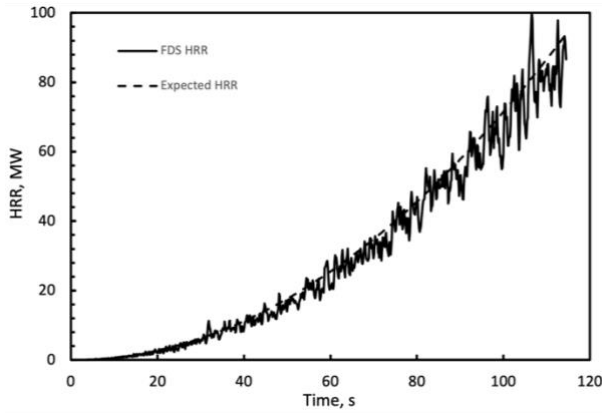


Figure 6-41 FDS measured and expected HRR versus time for simulation B.1.b

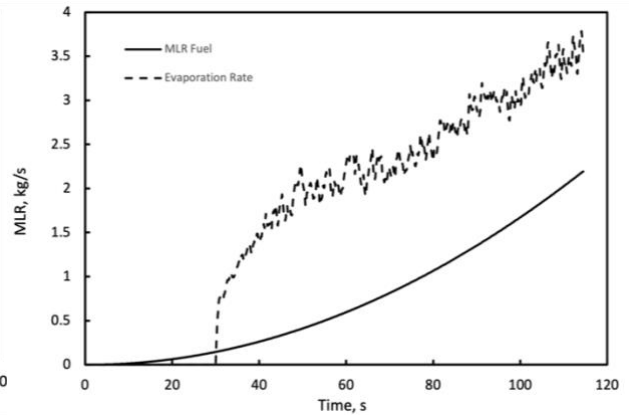


Figure 6-42 MLR Fuel and evaporation rate versus time for simulation B.1.b

Figures 6-43 to 6-46 plot selected incident heat flux measurements versus time for various locations according to Figures 6-1 and 6-2. The locations with the highest heat fluxes are shown here and additional graphs showing all incident heat flux measurements are provided in Appendix H.

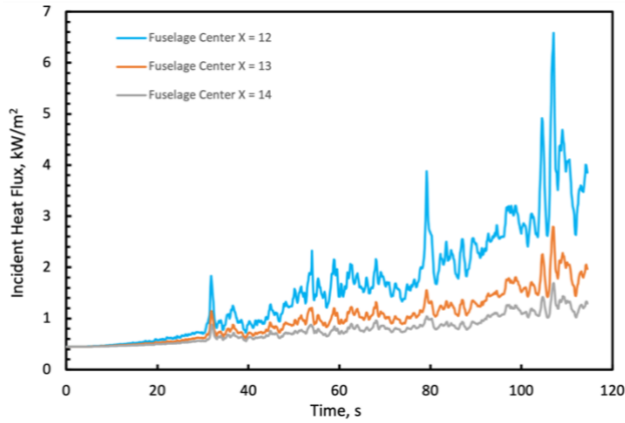


Figure 6-43 Incident Heat Flux versus time to center of fuselage ($Y = 13$) for simulation B.1.b

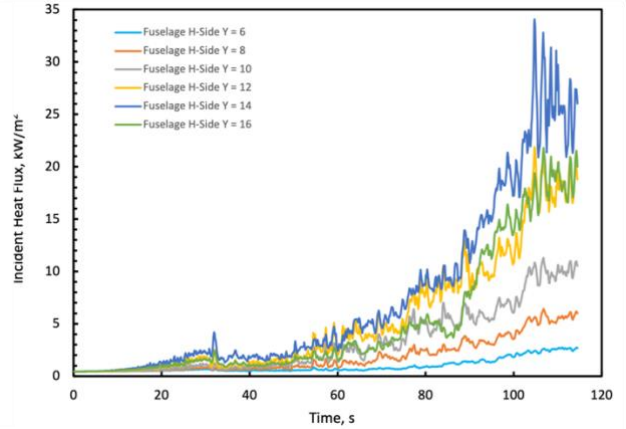


Figure 6-44 Incident Heat Flux versus time to high side of fuselage for simulation B.1.b

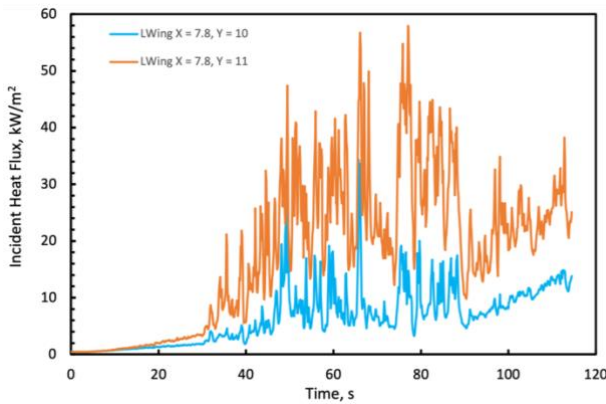


Figure 6-45 Incident Heat Flux versus time to various locations on the left wing ($X = 7.8$) for simulation B.1.b

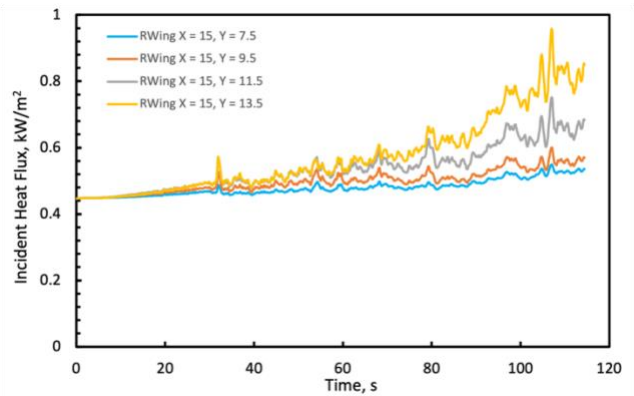


Figure 6-46 Incident Heat Flux versus time to various locations on the right wing ($X = 15$) for simulation B.1.b

Figures 6-47 to 6-49 plot the temperature versus time for various locations on each structural steel beam.

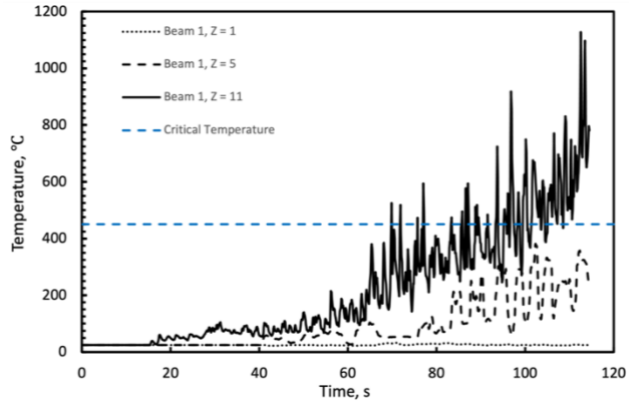


Figure 6-47 Temperature versus time at various heights on Beam 1 for simulation B.1.b

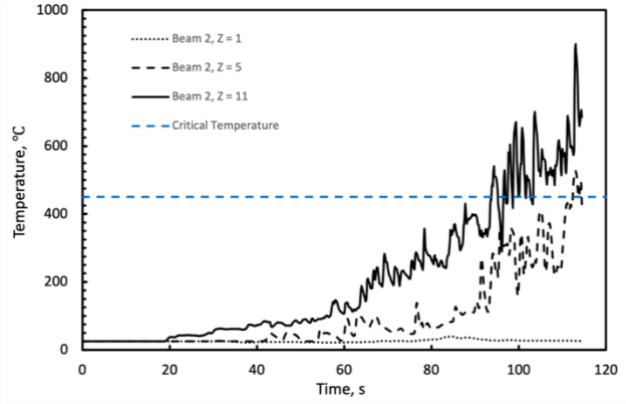


Figure 6-48 Temperature versus time at various heights on Beam 2 for simulation B.1.b

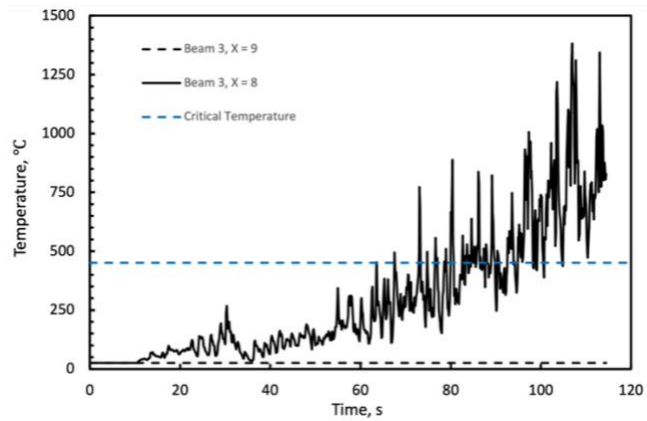


Figure 6-33 Temperature versus time at various horizontal locations on Beam 3 for simulation B.1.b

Figure 6-50 plots the incident heat flux measurements versus time for each of the electrical cabinets. The variation in incident heat flux versus location are negligible for each of the cabinets consequently, the values in the graph are representative of the maximum and minimum heat flux to each cabinet.

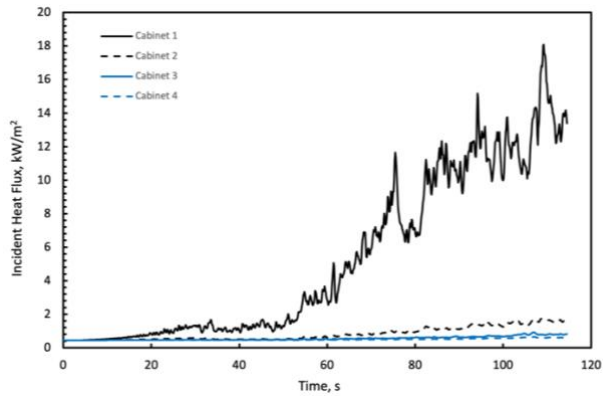


Figure 6-34 Incident heat flux versus time at each electrical box for simulation B.1.b

Figures 6-51 to 6-53 show SLCF's in Smokeview of temperature, sprinkler water vapor mass fraction, and oxygen volume fraction, 0.5 seconds, 10 seconds, 30 seconds, 60 seconds, and 84 seconds after the water mist system activates. Portions of the space-colored black correspond to roughly ambient conditions.

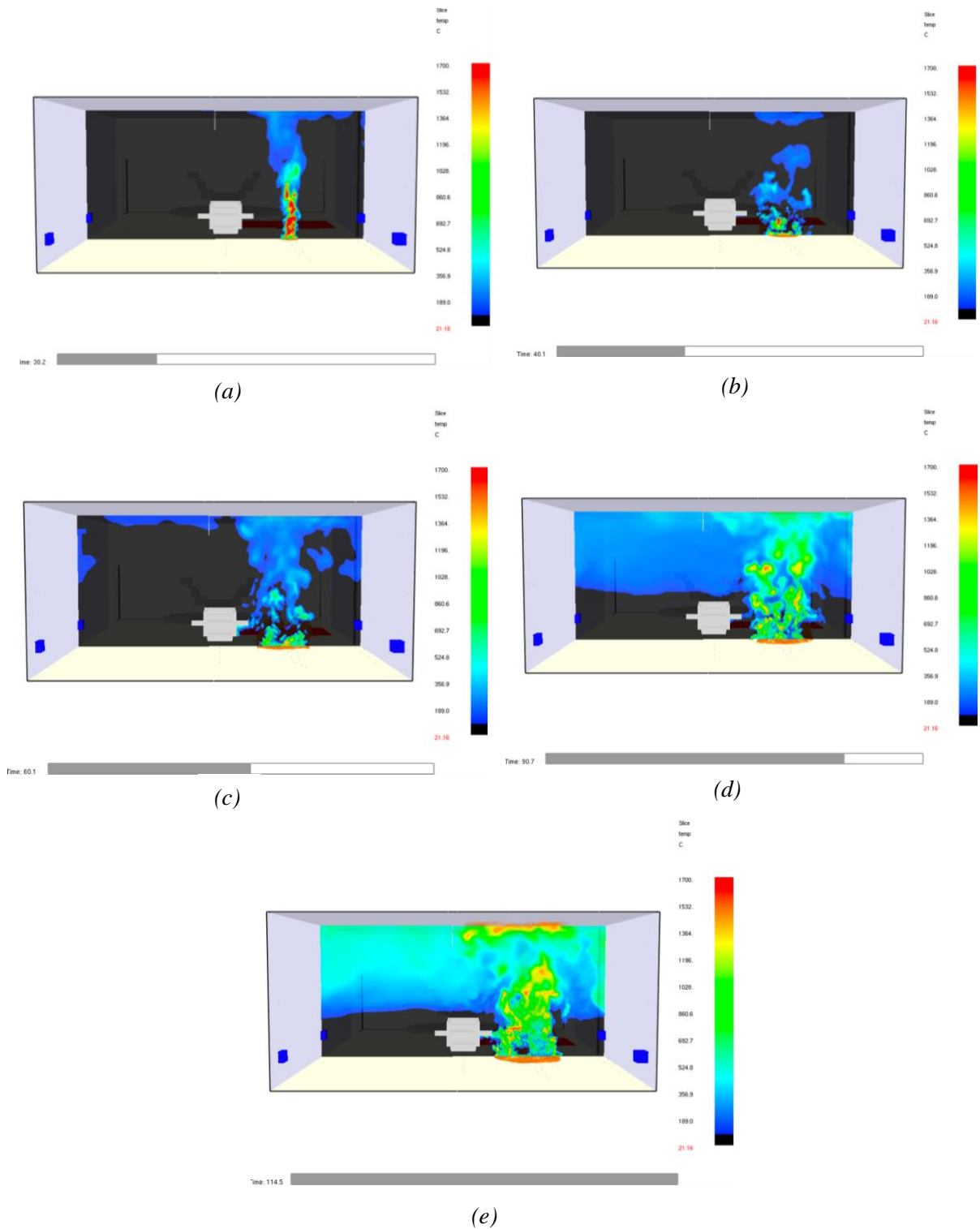


Figure 6-35 Temperature SLCF at (a) $t = 30.5$ seconds, (b) $t = 40$ seconds, (c) $t = 60$ seconds, (d) $t = 90$ seconds, (e) $t = 114$ seconds for simulation B.1.b

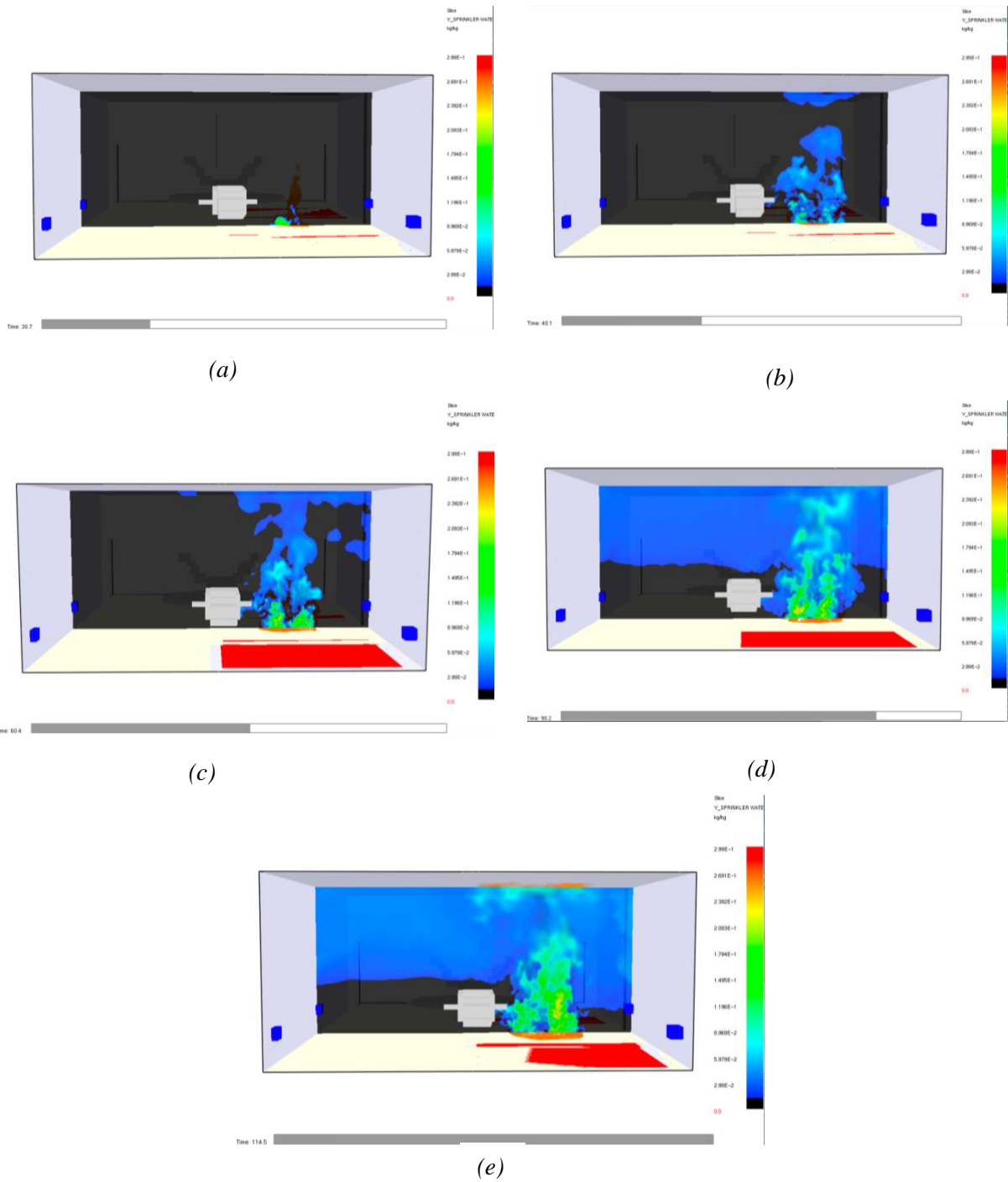


Figure 6-36 Sprinkler Water Vapor Mass Fraction SLCF at (a) $t = 30.5$ seconds, (b) $t = 40$ seconds, (c) $t = 60$ seconds, (d) $t = 90$ seconds, (e) $t = 114$ seconds for simulation B.1.b

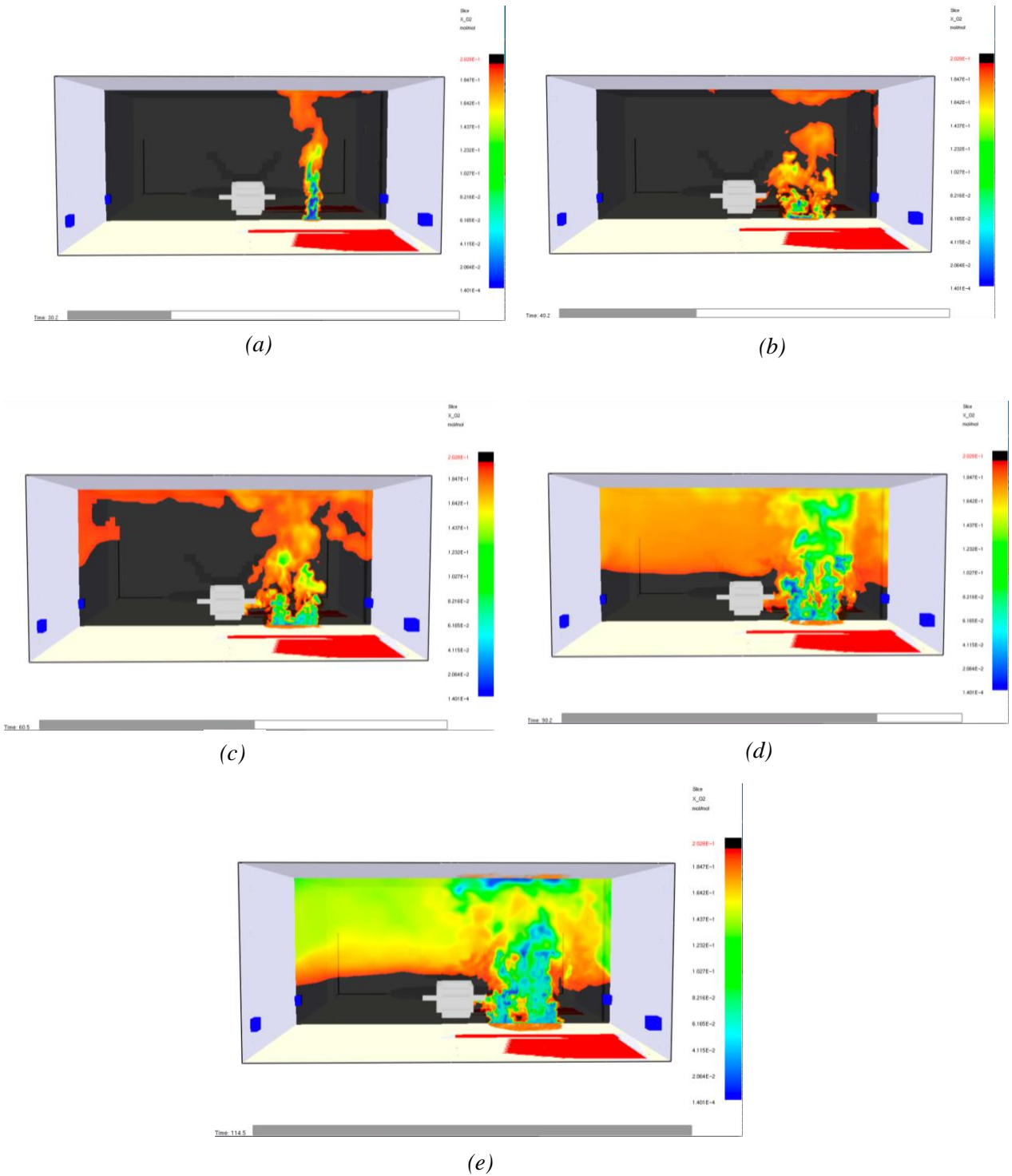


Figure 6-37 Oxygen Volume Fraction SLCF at (a) $t = 30.5$ seconds, (b) $t = 40$ seconds, (c) $t = 60$ seconds, (d) $t = 90$ seconds, (e) $t = 114$ seconds for simulation B.1.b

The results of this simulation show Nozzle B with a 30 second activation time is not able to suppress a fire originating in the center of the fuel source. The measured HRR in FDS is virtually the same as the expected HRR, as shown in Figure 6-41. The floor nozzles significantly impact the structure of the flame and weaken the flame through a reduction in the temperature. Lower mass fractions of water vapor are present in the flame region for the center originating fire, between two rows of nozzles, than in the fire originating from the side of the pool.

All three representative structural steel beams reach the critical temperature in this simulation as opposed to only two of the beams in simulation B.1.a. Beam 1 and 3 reach 450 °C around 70 seconds into the simulation and beam 2 increases to failure limits 20 seconds later.

The incident heat flux to portions of the left wing is sufficient to sustain delamination. No other part of the aircraft reaches high sustained heat fluxes to cause delamination as with the fire scenario originating underneath of the aircraft.

As mentioned previously these conclusions are based on the assumptions stated throughout this paper and do not account for fuel surface cooling effects which may be important for floor level discharge.

6.2.2 Simulation B.2: 50 second water mist activation

Simulation B.2 investigated Nozzle B for protection against a JP-8 jet fuel pool fire with an assumed ignition source at the center of the edge of the pool under the aircraft and a 30 second water mist activation time. The nozzle characteristics, nozzle spacing, room configuration, fire characteristics, and grid size are outlined in chapter 5 of this report.

Simulation B.2 was run on 1 node using 14 MPI processes and completed in approximately 57 hours.

The results of this simulation are compiled below. Figure 6-54 plots the measured HRR in FDS and the expected HRR versus time. Figure 6-55 plots the MLR of fuel and evaporation rate of water mist versus time.

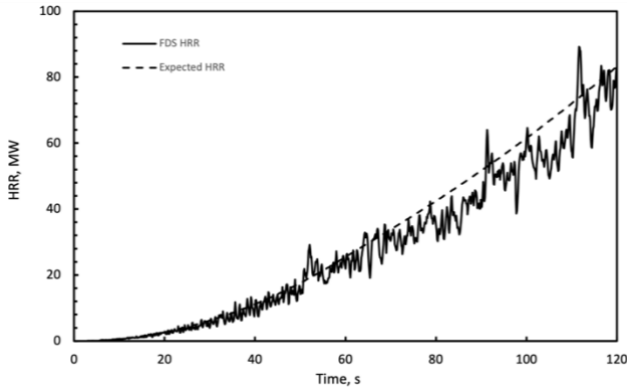


Figure 6-54 FDS measured and expected HRR versus time for simulation B.2

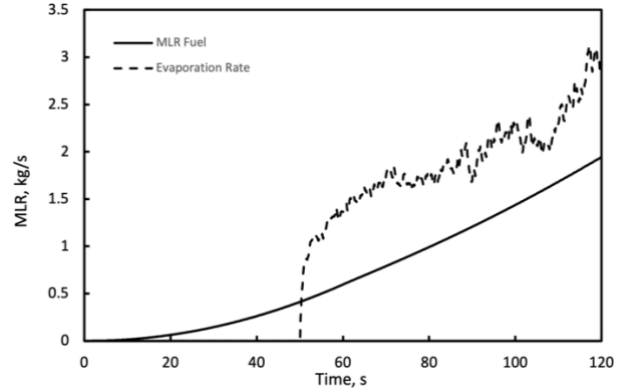


Figure 6-55 MLR Fuel and evaporation rate versus time for simulation B.2

Figures 6-56 to 6-59 plot selected incident heat flux measurements versus time for various locations according to Figures 6 -1 and 6-2. The locations with the highest heat fluxes are shown here and additional graphs showing all incident heat flux measurements are provided in Appendix H.

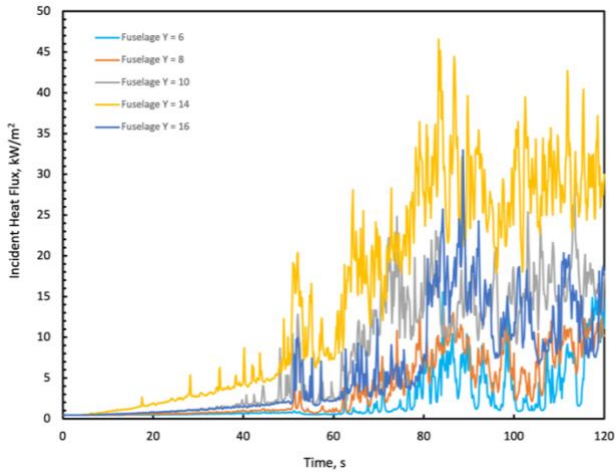


Figure 6-39 Incident Heat Flux versus time to various down the center of the fuselage ($X=13$) for simulation B.2

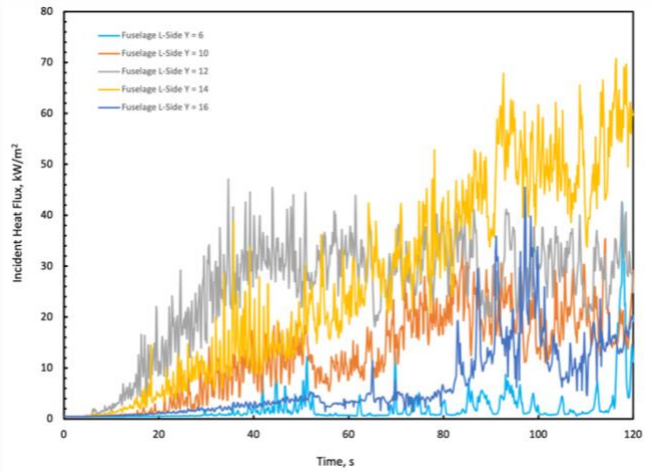


Figure 6-57 Incident Heat Flux versus time to various locations on the low side of the fuselage for simulation B.2

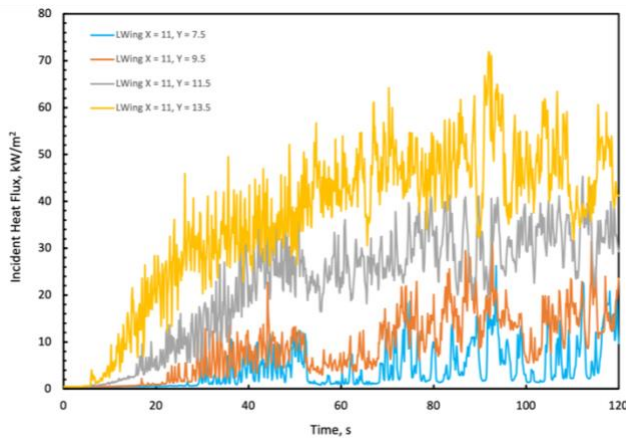


Figure 6-38 Incident Heat Flux versus time to various locations on the left wing ($X = 11$) for simulation B.2

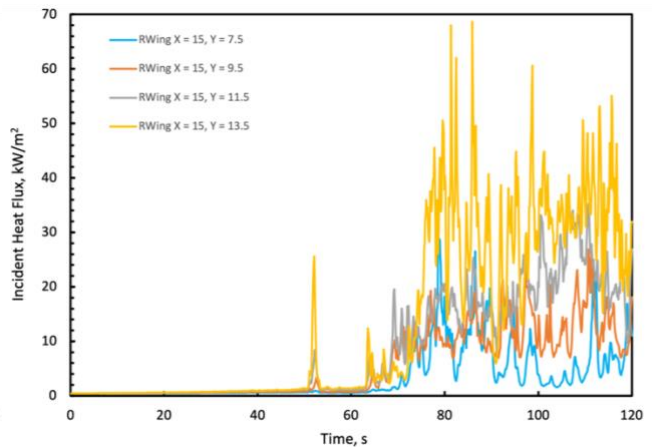


Figure 6-59 Incident Heat Flux versus time to various locations on the right wing ($X = 15$) for simulation B.2

Figures 6-60 to 6-62 plot the temperature versus time for various locations on each structural steel beam.

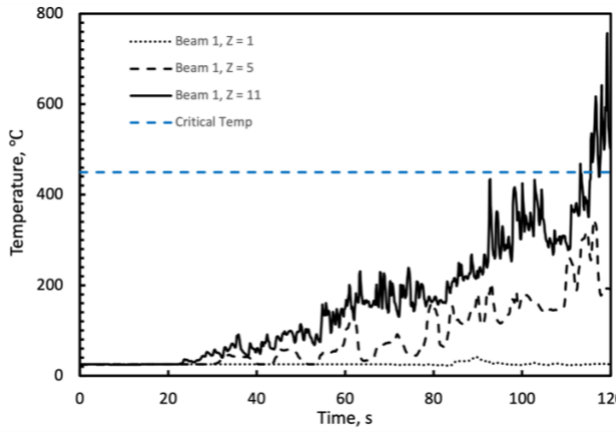


Figure 6-40 Temperature versus time at various heights on Beam 1 for simulation B.2

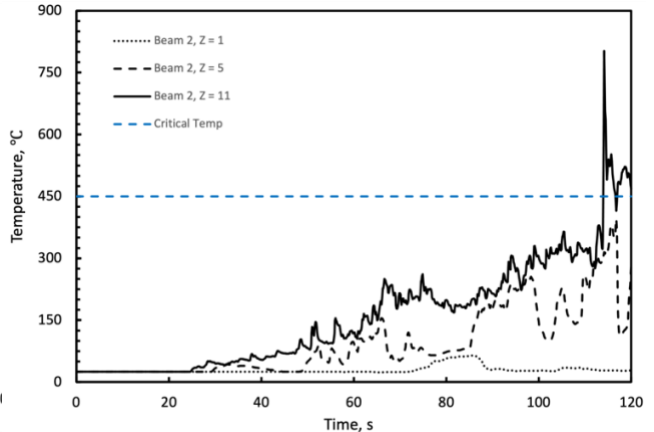


Figure 6-41 Temperature versus time at various heights on Beam 2 for simulation B.2

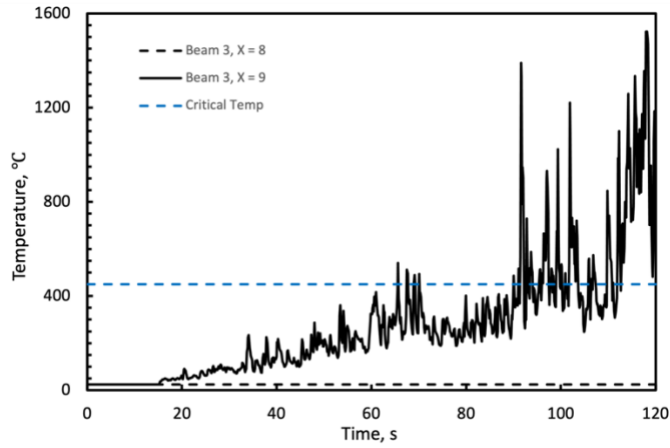


Figure 6-42 Temperature versus time at various horizontal locations on Beam 3 for simulation B.2

Figure 6-63 plots the incident heat flux measurements versus time for each of the electrical cabinets. The variation in incident heat flux versus location are negligible for each of the cabinets, consequently the values in the graph are representative of the maximum and minimum heat flux to each cabinet.

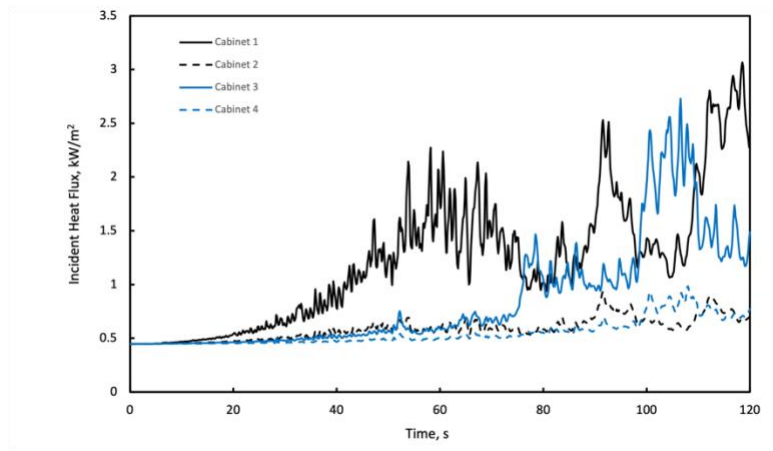
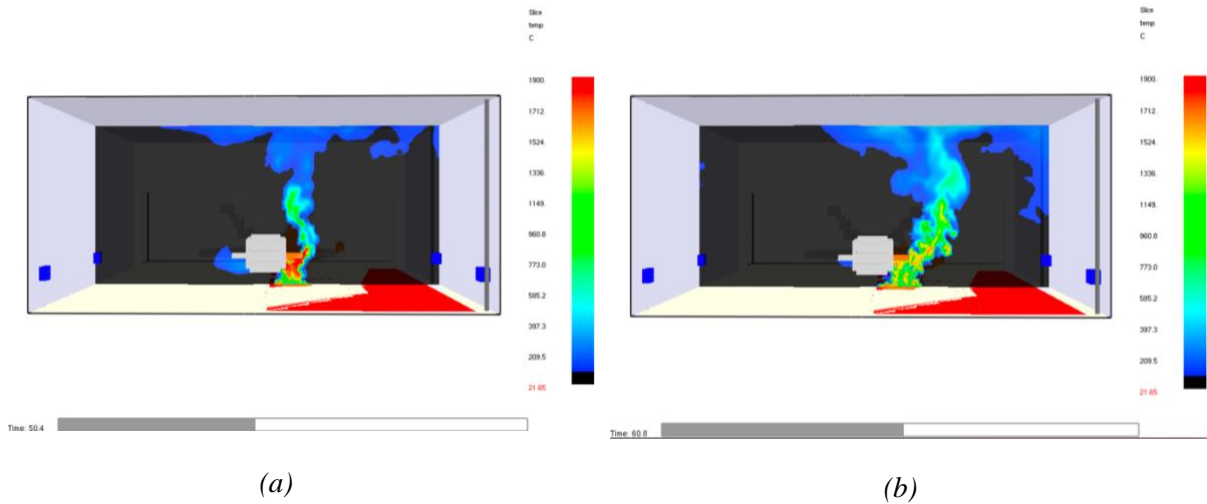


Figure 6-43 Incident heat flux versus time at each electrical box for simulation B.2

Figures 6-64 to 6-66 show SLCF's in Smokeview of temperature, sprinkler water vapor mass fraction, and oxygen volume fraction, 0.5 seconds, 10 seconds, 30 seconds, and 70 seconds after the water mist system activates. Portions of the space-colored black correspond to roughly ambient conditions.



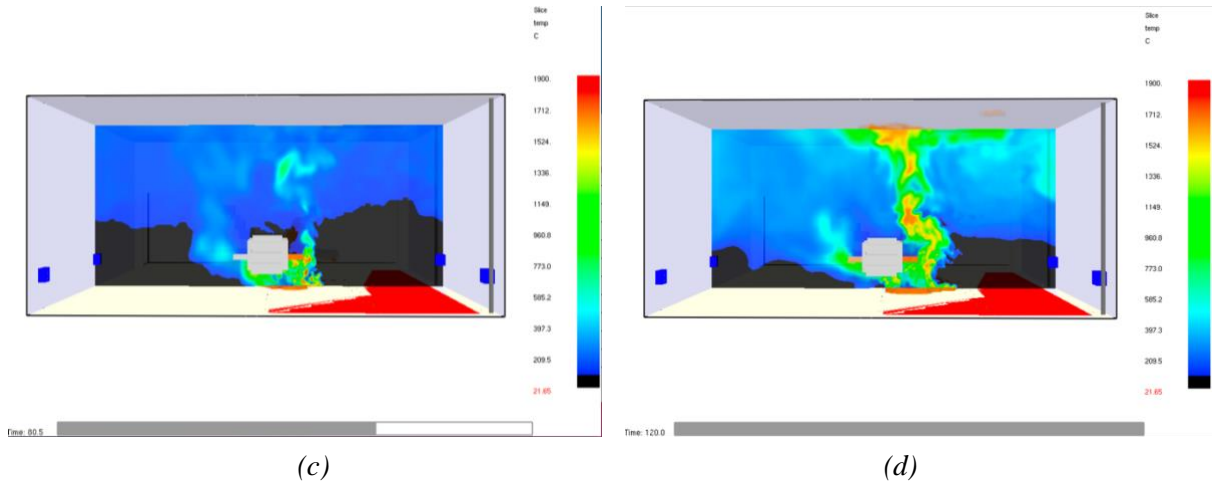
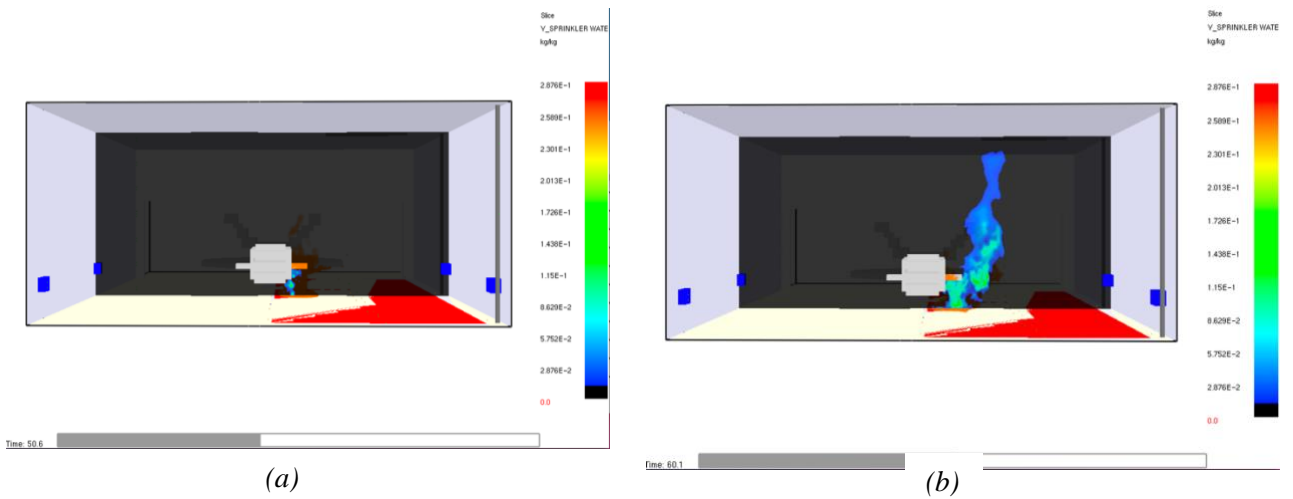


Figure 6-44 Temperature SLCF at (a) $t = 50.5$ seconds, (b) $t = 60$ seconds, (c) $t = 80$ seconds, (d) $t = 120$ seconds for simulation B.2



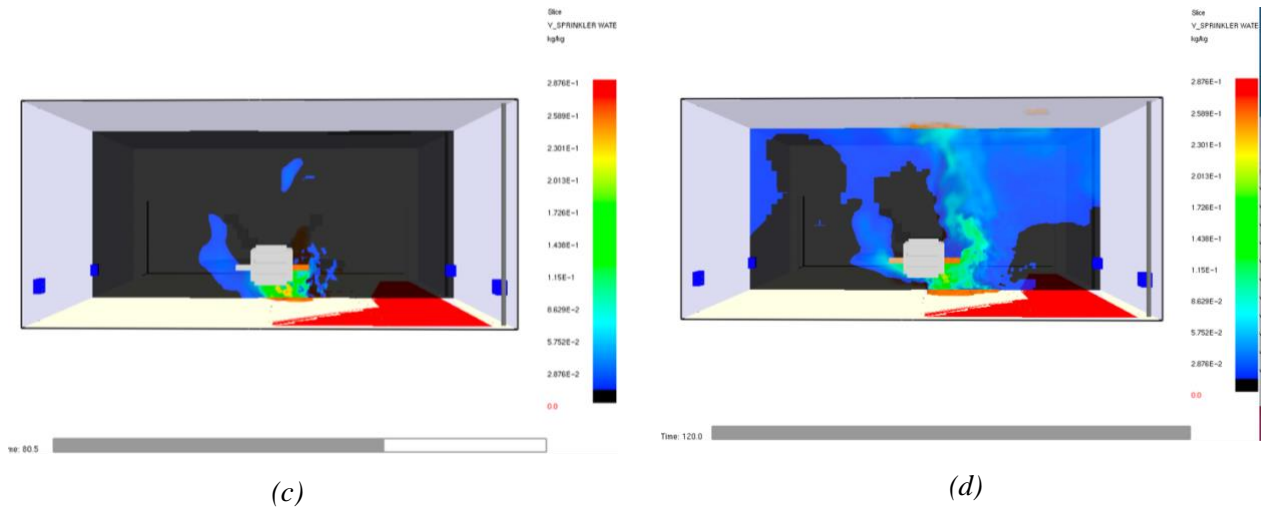
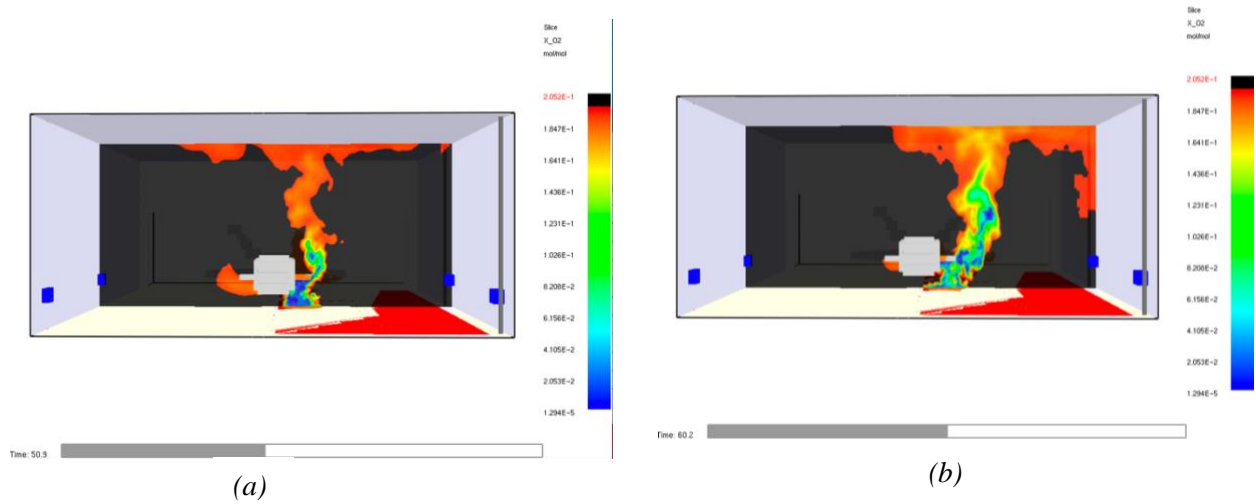


Figure 6-45 Sprinkler Water Vapor Mass Fraction SLCF at (a) $t = 50.5$ seconds, (b) $t = 60$ seconds, (c) $t = 80$ seconds, (d) $t = 120$ seconds for simulation B.2



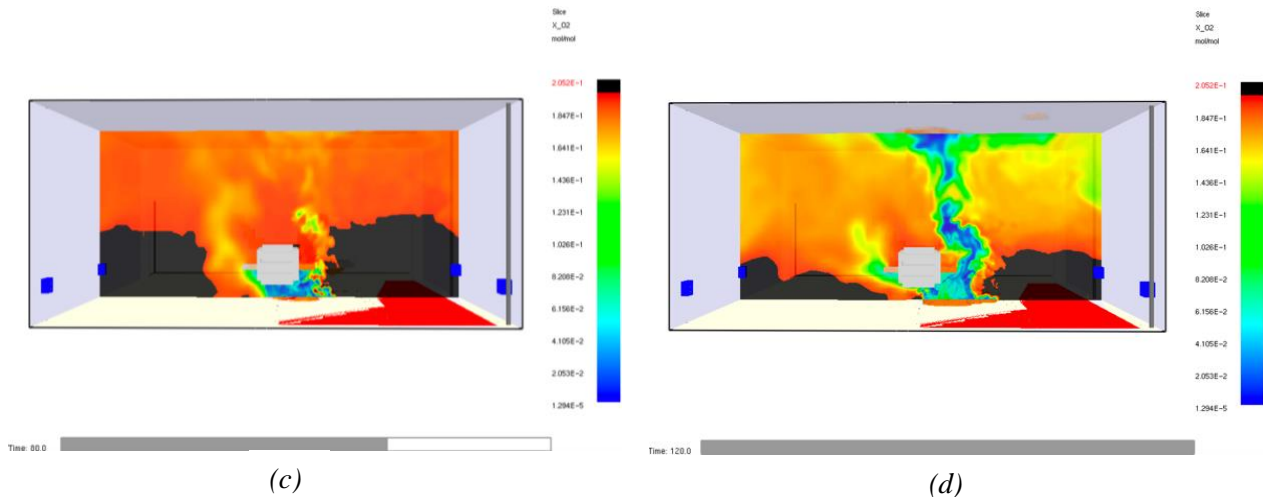


Figure 6-46 Oxygen Volume Fraction SLCF at (a) $t = 50.5$ seconds, (b) $t = 60$ seconds, (c) $t = 80$ seconds, (d) $t = 120$ seconds for simulation B.2

The results of this simulation show Nozzle B with a 50 second activation time and side ignition source is not able to extinguish the fire. The results of this simulation are similar to simulation B.1.a and will not be repeated here. The main differences are because the fire is larger at the time of mist activation there is a larger decrease in incident heat flux to the plane surface at the time of activation. The portions of the plane that do not see a decrease in incident heat flux are in direct contact with the flame.

All three beams reach critical temperatures by the end of the simulation and the entire bottom side of the fuselage and wings is exposed to high incident heat fluxes for 60 seconds corresponding to delamination.

6.3 Nozzle C Final Simulations

6.3.1 Simulation C.1: 30 second activation time

Simulation C.1 investigated Nozzle C for protection against a JP-8 jet fuel pool fire with an assumed ignition source in the center of the pool and a 30 second water mist activation

time. The nozzle characteristics, nozzle spacing, room configuration, fire characteristics, and grid size are outlined in chapter 5 of this report. Simulation C.1 was run on 1 node using 18 MPI processes and completed 95 of 120 seconds in 72 hours.

The results of this simulation are compiled below. Figure 6-67 plots the measured HRR in FDS and the expected HRR versus time. Figure 6-68 plots the MLR of fuel and evaporation rate of water mist versus time.

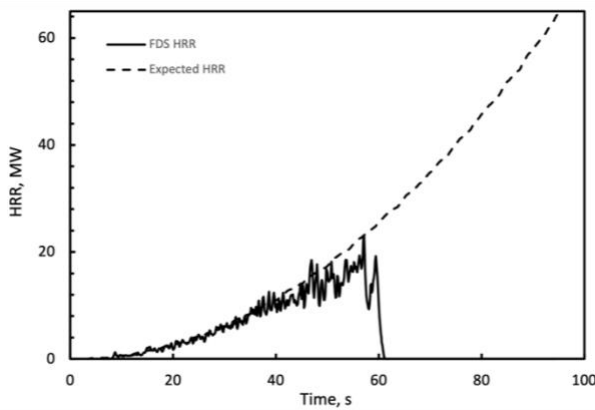


Figure 6-47 FDS measured and expected HRR versus time for simulation C.1

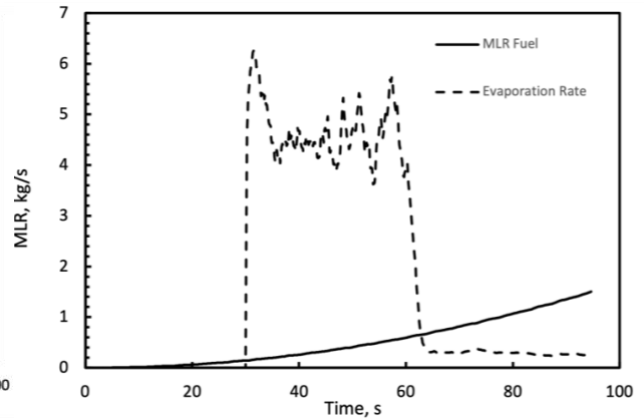


Figure 6-48 MLR fuel and evaporation rate of water mist versus time for simulation C.1

Figures 6-69 to 6-72 plot selected incident heat flux measurements versus time for various locations according to Figures 6 -1 and 6-2. The locations with the highest heat fluxes are shown here and additional graphs showing all incident heat flux measurements are provided in Appendix H.

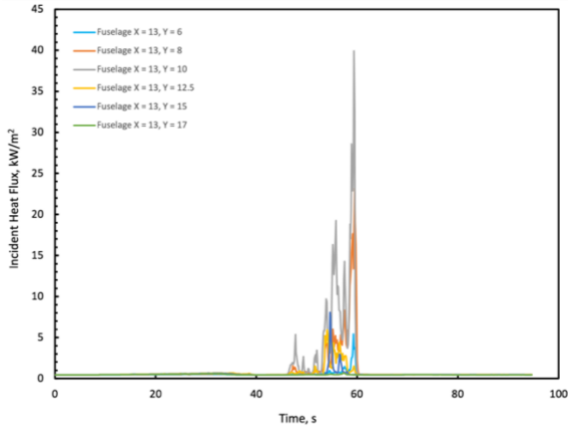


Figure 6-69 Incident Heat Flux versus time to various locations down the center of the fuselage (X=13) for simulation C.1

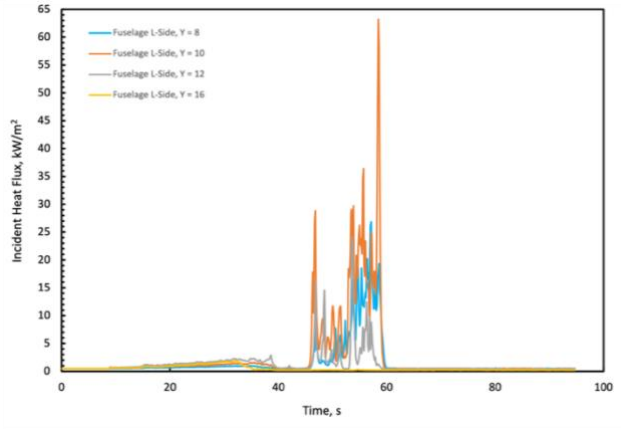


Figure 6-70 Incident Heat Flux versus time to various locations on the low side of the fuselage for simulation C.1

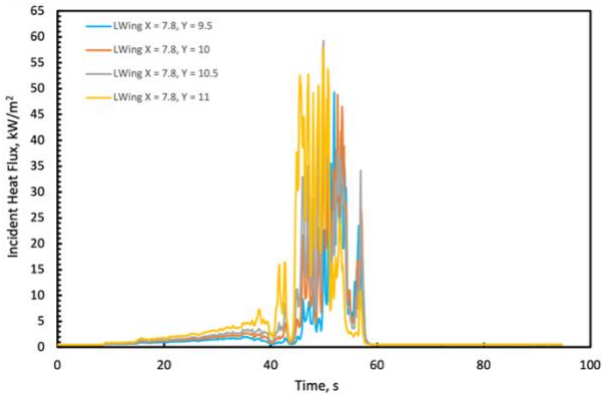


Figure 6-50 Incident Heat Flux versus time to various locations on the left wing (X = 7.8) for simulation C.1

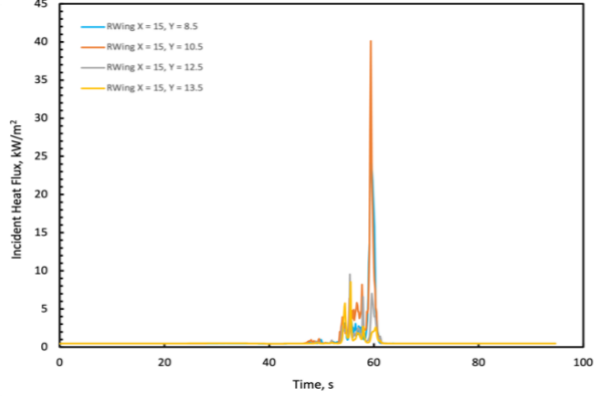


Figure 6-49 Incident Heat Flux versus time to various locations on the right wing (X = 15) for simulation C.1

Figures 6-73 to 6-75 plot the temperature versus time for various locations on each structural steel beam.

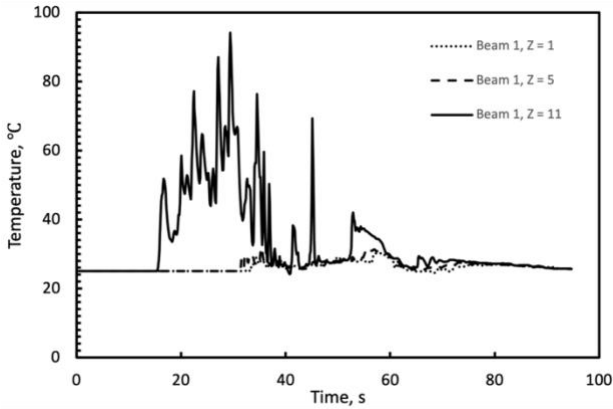


Figure 6-51 Temperature versus time at various heights on Beam 1 for simulation C.1

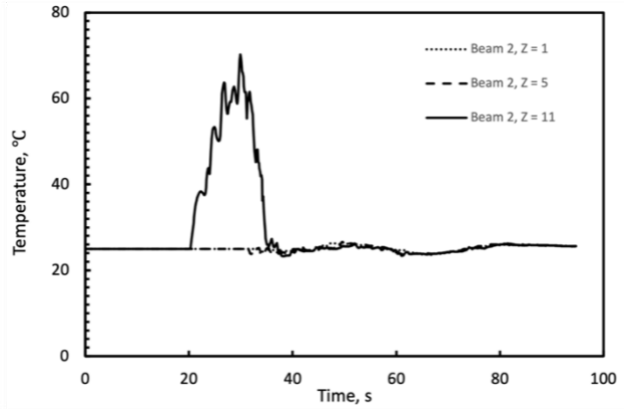


Figure 6-52 Temperature versus time at various heights on Beam 2 for simulation C.1

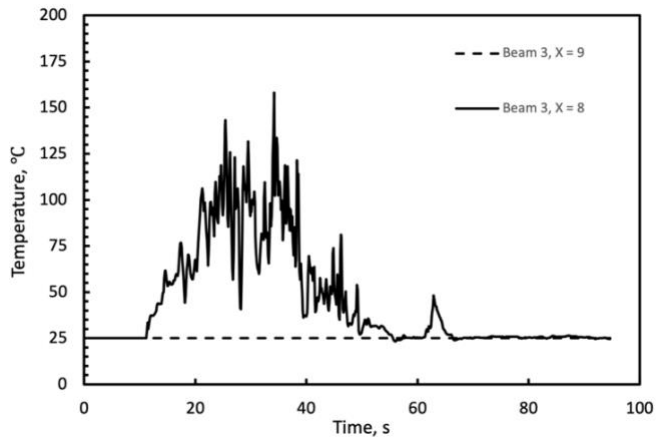


Figure 6-53 Temperature versus time at various horizontal locations on Beam 3 for simulation C.1

Figure 6-76 plots the incident heat flux measurements versus time for each of the electrical cabinets. The variation in incident heat flux versus location are negligible for each of the cabinets consequently, the values in the graph are representative of the maximum and minimum heat flux to each cabinet.

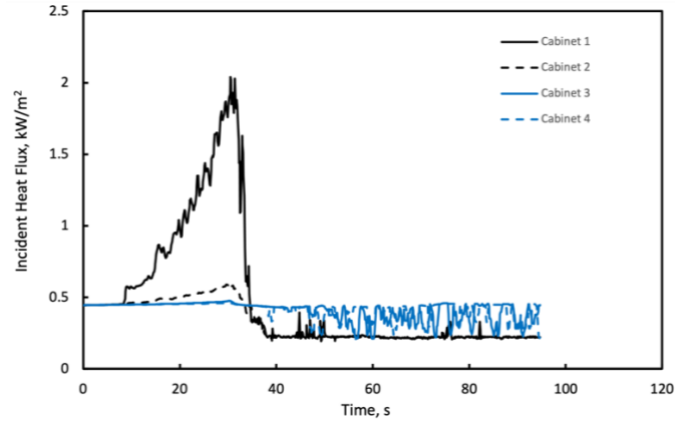


Figure 6-54 Incident heat flux versus time at each electrical box for simulation C.1

Figures 6-77 to 6-79 show SLCF's in Smokeview of temperature, sprinkler water vapor mass fraction, and oxygen volume fraction 0.5 seconds, 10 seconds, 30 seconds and 40 seconds after the water mist system activates. Portions of the space-colored black correspond to roughly ambient conditions.

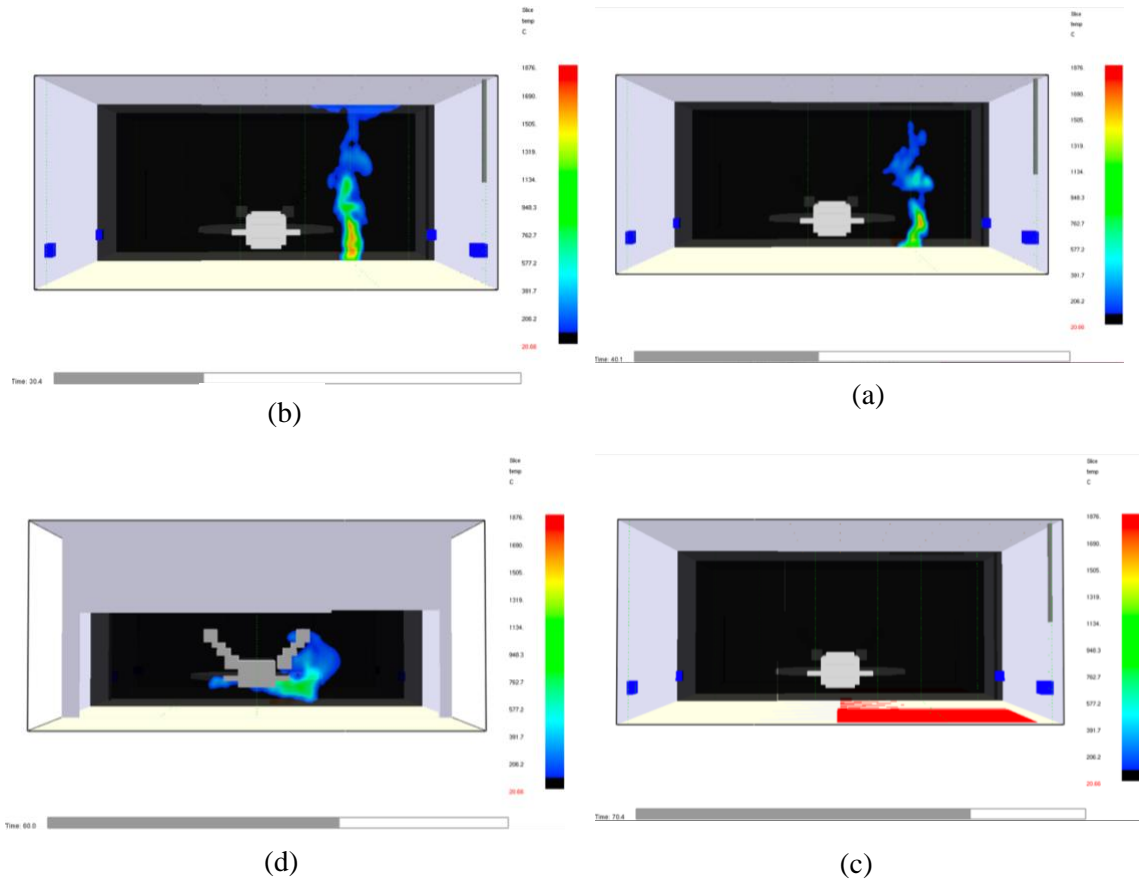
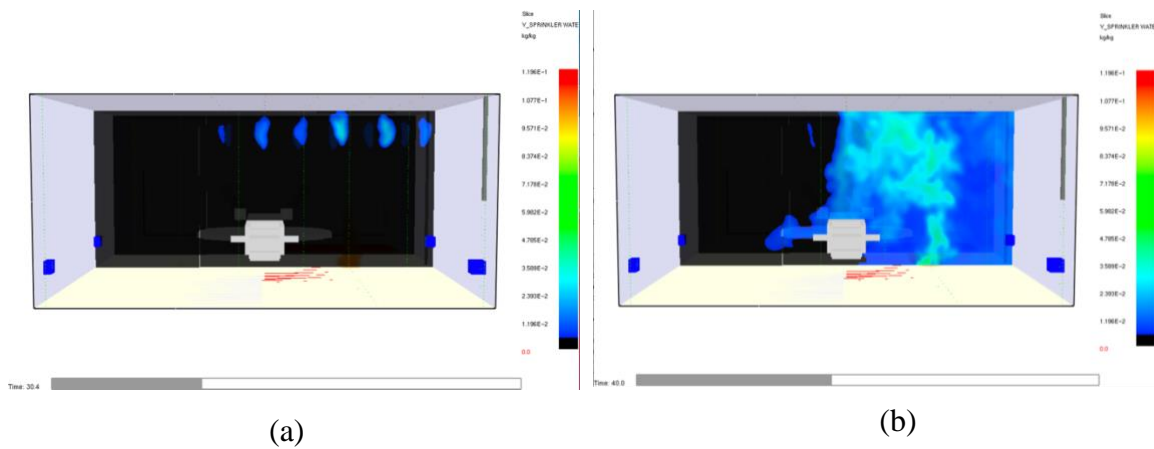


Figure 6-55 Temperature SLCF at (a) $t = 30.5$ seconds, (b) $t = 40$ seconds, (c) $t = 60$ seconds, (d) $t = 70$ seconds for simulation C.1



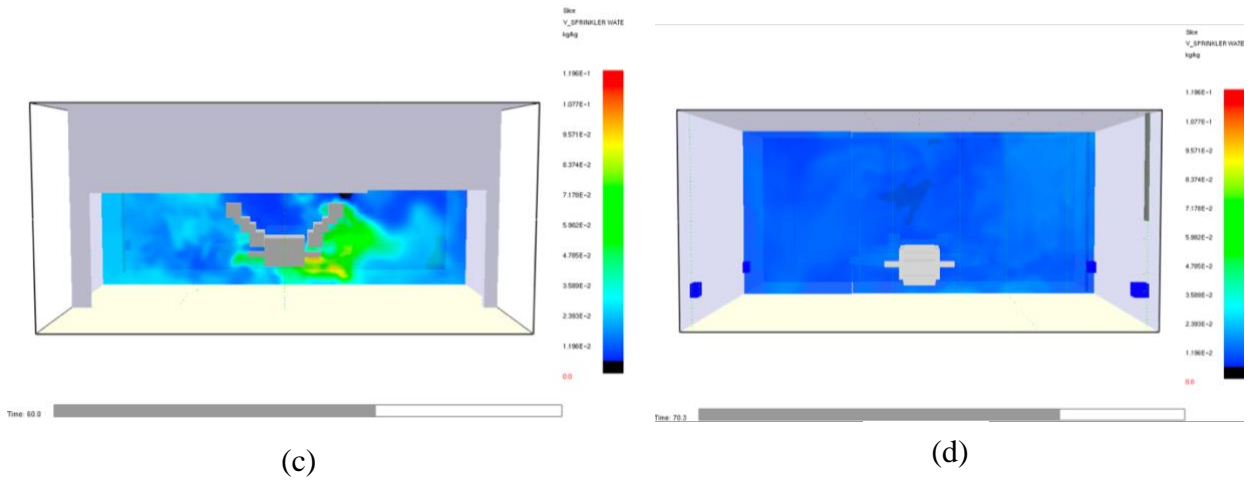


Figure 6-56 Sprinkler Water Vapor Mass Fraction SLCF at (a) $t = 30.5$ seconds, (b) $t = 40$ seconds, (c) $t = 60$ seconds, (d) $t = 70$ seconds for simulation C.1

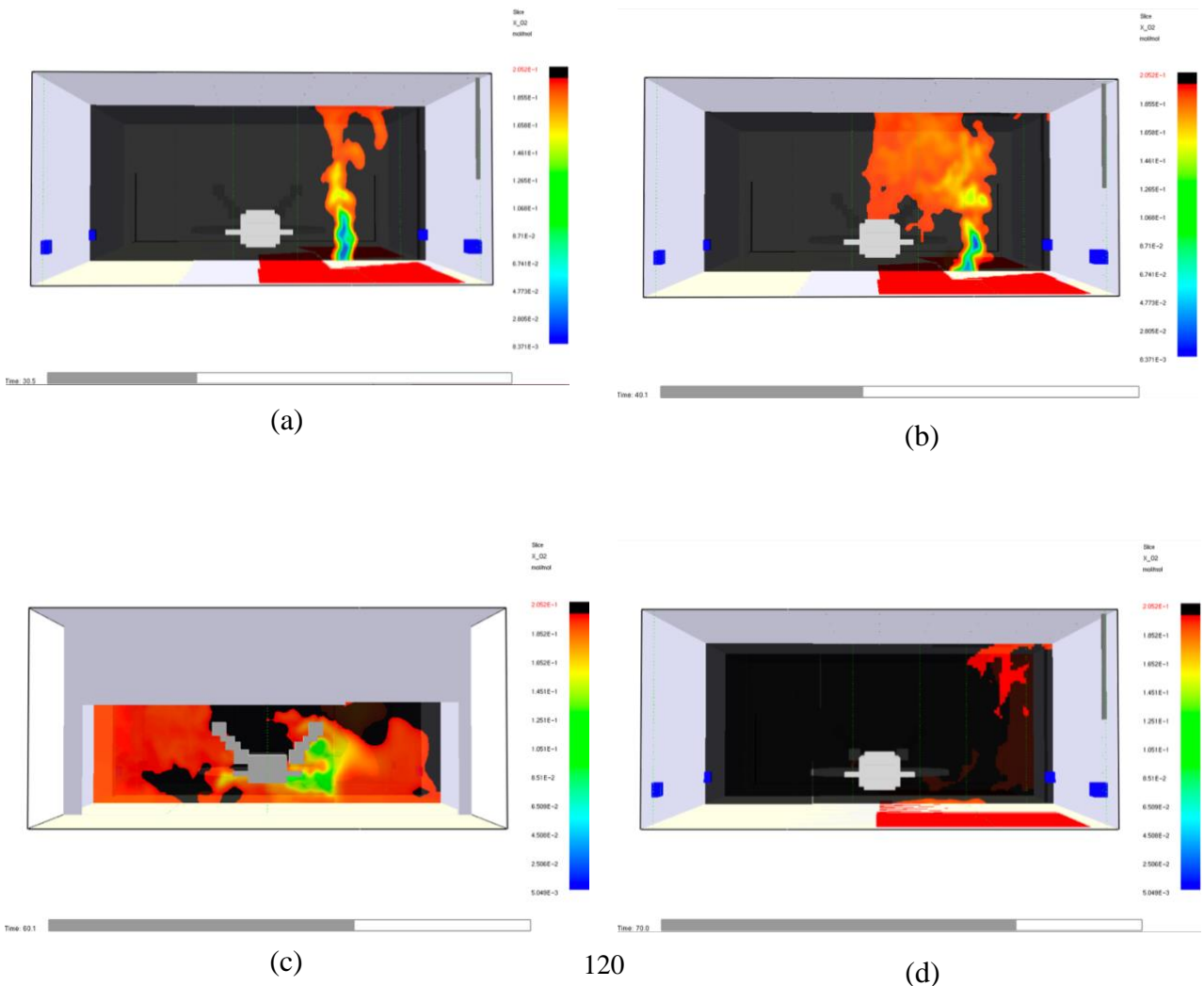


Figure 6-57 Oxygen Volume Fraction SLCF at (a) t = 30.5 seconds, (b) t = 40 seconds, (c) t = 60 seconds, (d) t = 70 seconds for simulation C.1

The results show that Nozzle C with a 30 second activation time is able to extinguish the fire. As previously mentioned, extinction with a prescribed MLRPUA is a binary process in FDS, consequently extinction occurs very rapidly, as shown in Figure 6-67. Similar to Nozzle A it takes about 10 to 15 seconds for the ceiling water mist to penetrate the ceiling jet and plume and reach the fire source. Once the water mist reaches the flame region the flame structure is significantly impacted and the flame retreats underneath of the aircraft and extinguishes. Extinction occurs within 30 seconds of water mist activation.

Due to quick extinction of the flame and cooling effects of the water mist all of the structural steel members remain at temperatures well below the critical temperature. All of the beams reach their maximum temperature at 30 seconds and then continually decrease back to ambient temperature after water mist activation.

The fuselage, left wing, and right wing all experience high incident heat fluxes due to the flame travelling underneath of the aircraft during the extinction process. It is likely the plane will suffer from damage due to direct flame impingement; however, each portion of the plane is only subject to high heat fluxes for 5 to 20 seconds.

These results are based on the assumptions as stated throughout this report. The grid size in the near field of the nozzle is too large to resolve the nozzle dynamics and increased grid resolution is recommended for future analysis. This simulation was run with and without the parameter `PARTICLE_CFL=.TRUE.` and extinction does not occur within 120 seconds without this diagnostic. These results prove that `PARTICLE_CFL =`

.TRUE. is important for both near field resolution and for large scale simulations using this nozzle.

6.3.2 Simulation C.2: 50 second activation time

Simulation C.2 investigated Nozzle C for protection against a JP-8 jet fuel pool fire with an assumed ignition source in the center of the pool and a 50 second water mist activation time. The nozzle characteristics, nozzle spacing, room configuration, fire characteristics, and grid size are outlined in chapter 5 of this report. Simulation C.2 was run on 1 node using 18 MPI processes and completed 110 of 120 seconds in 72 hours

The results of this simulation are compiled below. Figure 6-80 plots the measured HRR in FDS and the expected HRR versus time. Figure 6-81 plots the MLR of fuel and evaporation rate of water mist versus time.

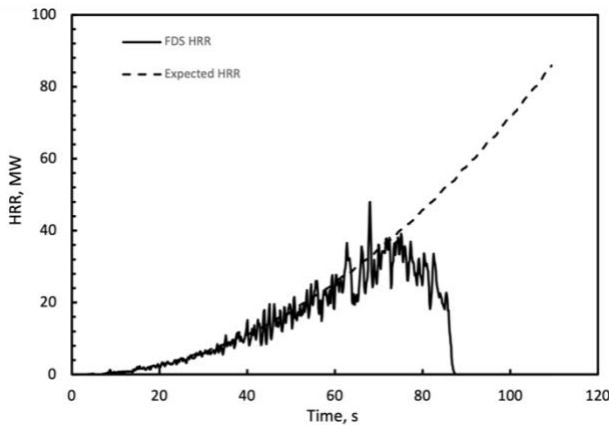


Figure 6-58 FDS measured and expected HRR versus time for simulation C.2

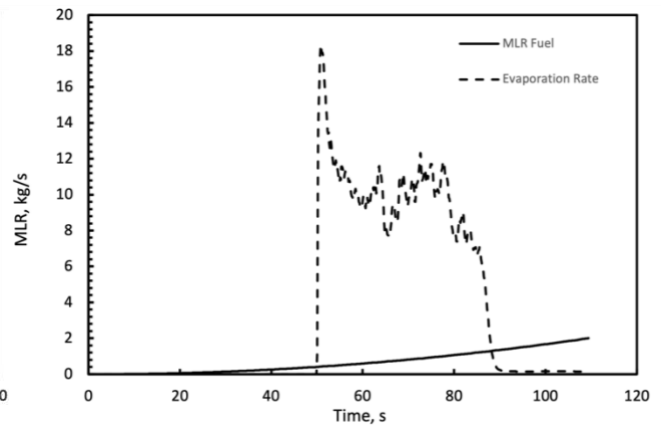


Figure 6-59 MLR fuel and evaporation rate of water mist versus time for simulation C.2

Figures 6-82 to 6-85 plot selected incident heat flux measurements versus time for various locations according to Figures 6 -1 and 6-2. The locations with the highest heat

fluxes are shown here and additional graphs showing all incident heat flux measurements are provided in Appendix H.

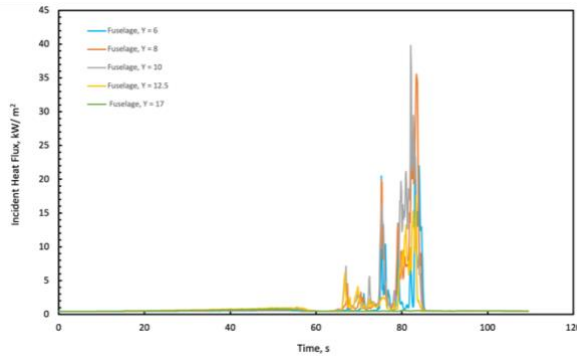


Figure 6-60 Incident Heat Flux versus time to various locations down the center of the fuselage ($X=13$) for simulation C.2

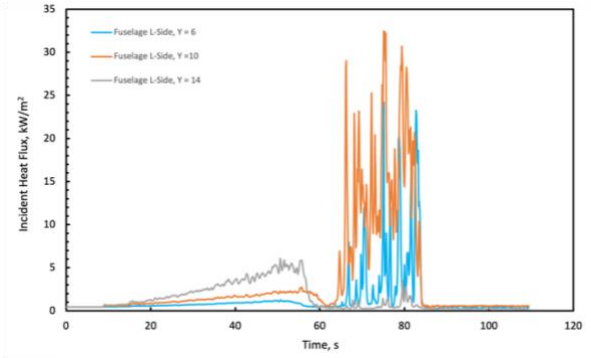


Figure 6-61 Incident Heat Flux versus time to various locations on the low side of the fuselage for simulation C.2

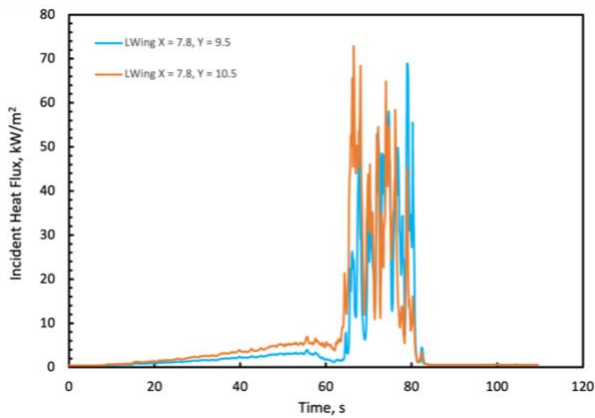


Figure 6-63 Incident Heat Flux versus time to various locations on the left wing ($X = 7.8$) for simulation C.2

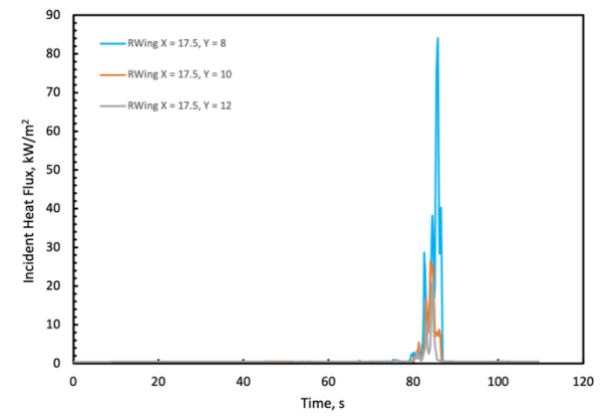


Figure 6-62 Incident Heat Flux versus time to various locations on the right wing ($X = 17.5$) for simulation C.2

Figures 6-86 to 6-88 plot the temperature versus time for various locations on each structural steel beam.

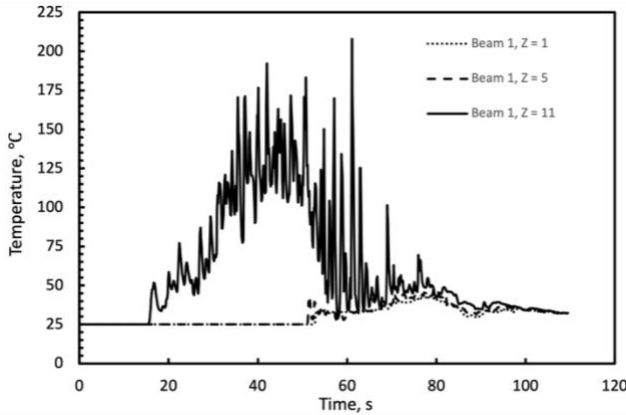


Figure 6-65 Temperature versus time at various heights on Beam 1 for simulation C.2

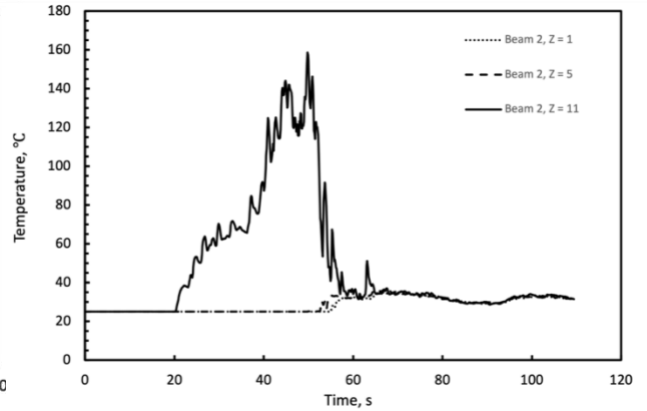


Figure 6-64 Temperature versus time at various heights on Beam 2 for simulation C.2

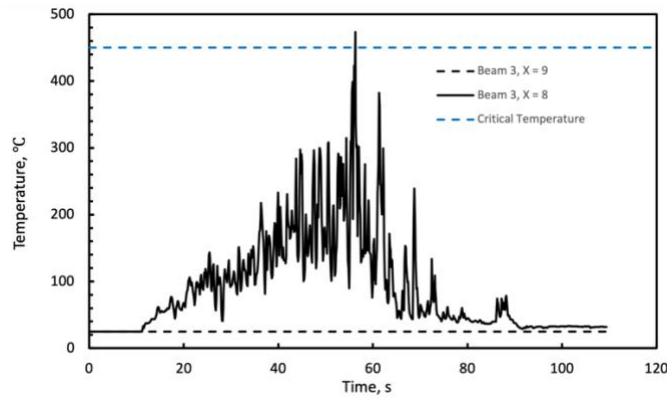


Figure 6-66 Temperature versus time at various horizontal locations on Beam 3 for simulation C.2

Figure 6-89 plots the incident heat flux measurements versus time for each of the electrical cabinets. The variation in incident heat flux versus location are negligible for each of the cabinets consequently, the values in the graph are representative of the maximum and minimum heat flux to each cabinet.

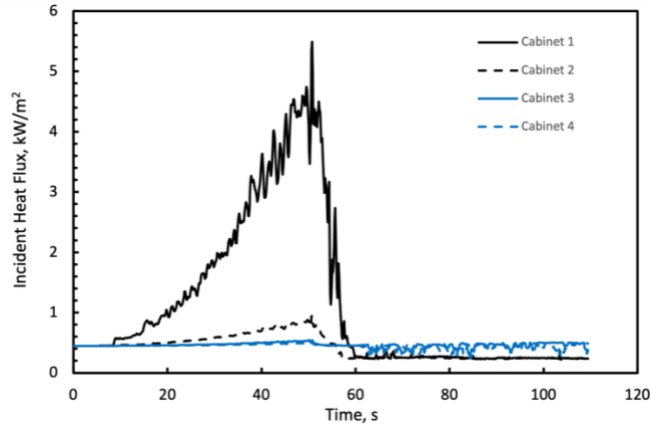
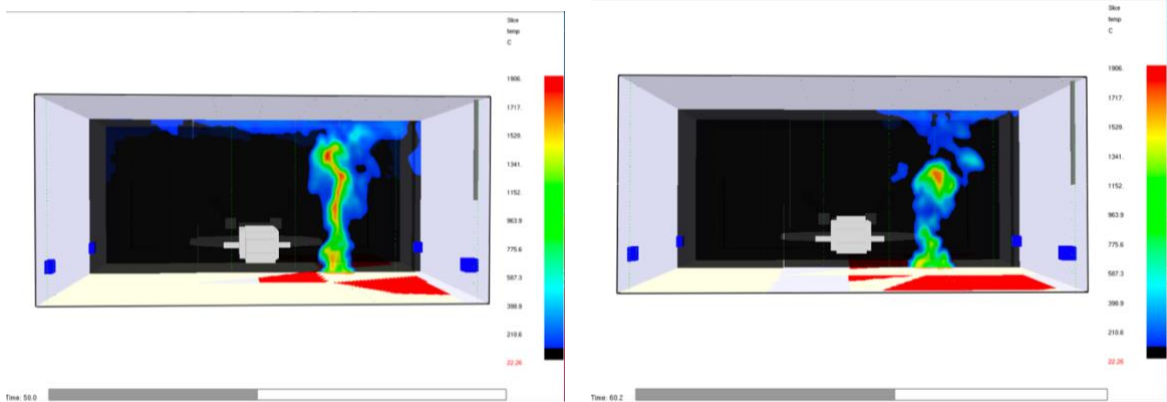


Figure 6-67 Incident heat flux versus time at each electrical box for simulation C.2

Figures 6-90 to 6-92 show SLCF's in Smokeview of temperature, sprinkler water vapor mass fraction, and oxygen volume fraction 0.5 seconds, 10 seconds, 30 seconds and 40 seconds after the water mist system activates. Portions of the space-colored black correspond to roughly ambient conditions.



(a)

(b)

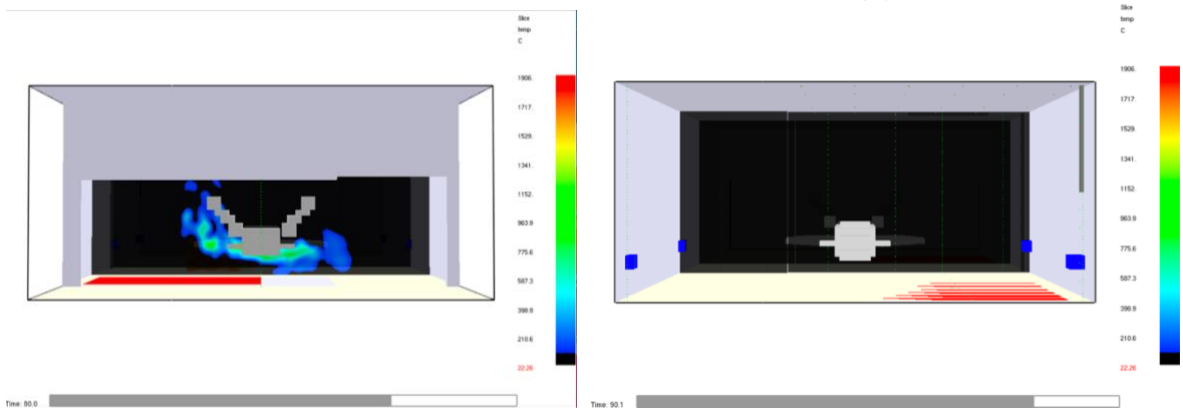


Figure 6-68 Temperature SLCF at (a) $t = 50.5$ seconds, (b) $t = 60$ seconds, (c) $t = 80$ seconds, (d) $t = 90$ seconds for simulation C.2

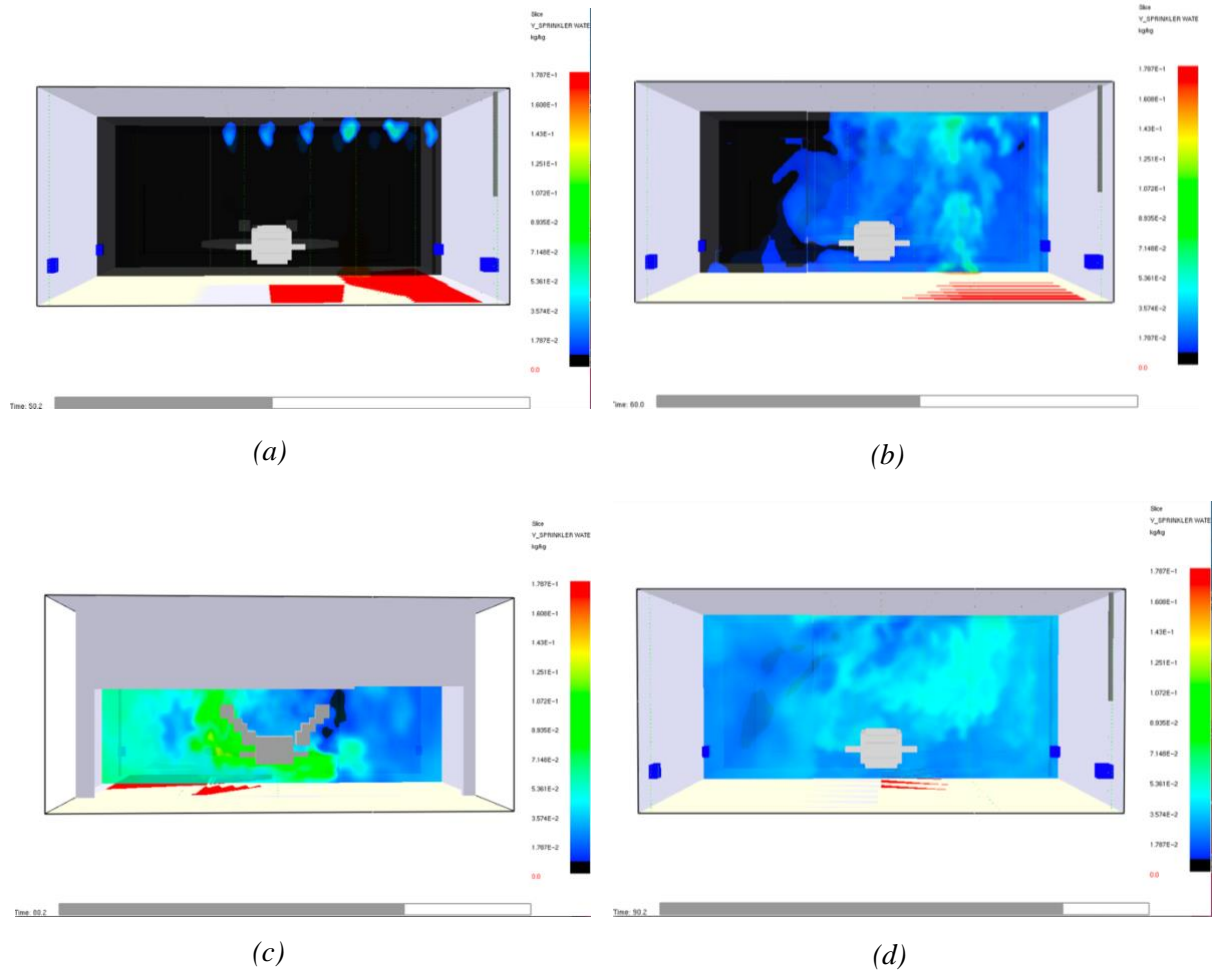


Figure 6-69 Sprinkler Water Vapor Mass Fraction SLCF at (a) $t = 50.5$ seconds, (b) $t = 60$ seconds, (c) $t = 80$ seconds, (d) $t = 90$ seconds for simulation C.2

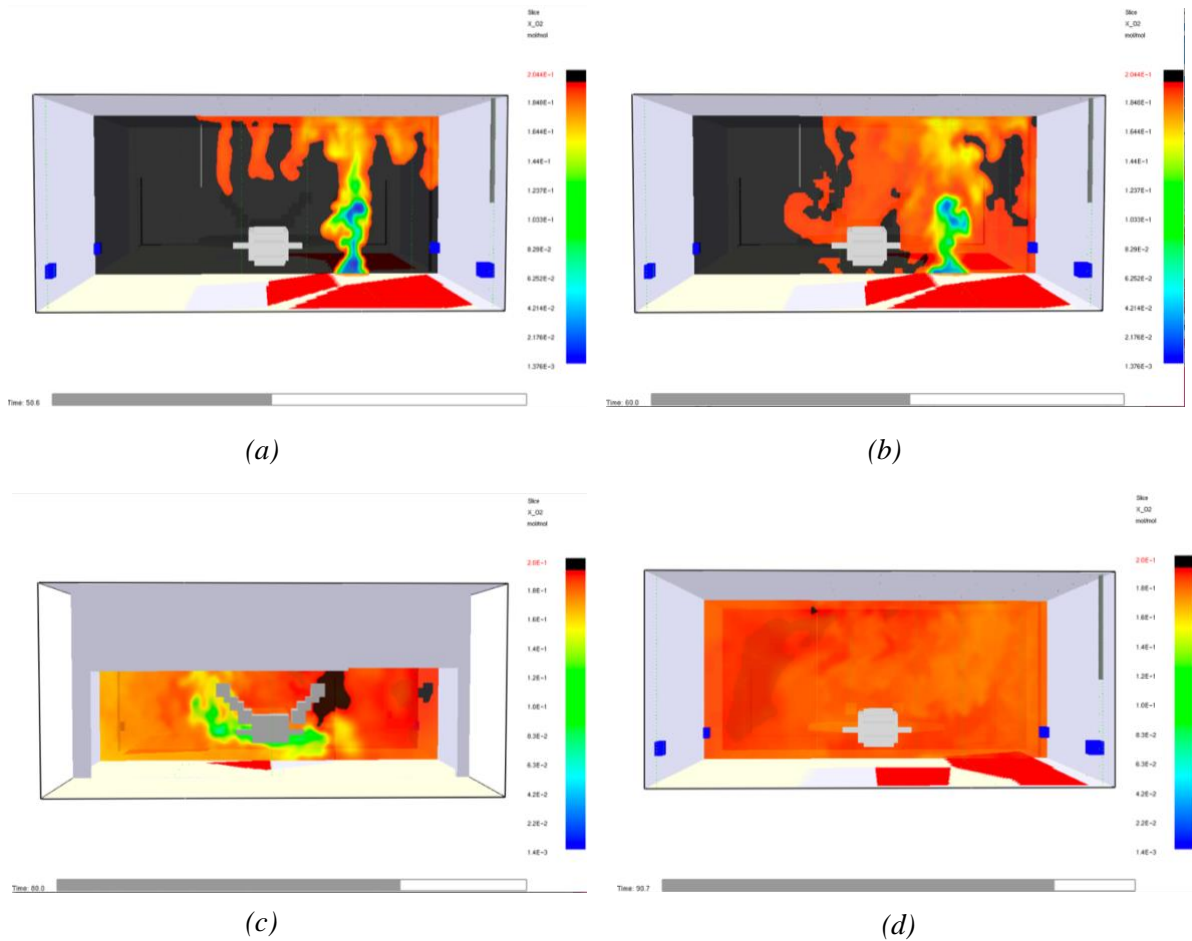


Figure 6-70 Oxygen Volume Fraction SLCF at (a) $t = 50.5$ seconds, (b) $t = 60$ seconds, (c) $t = 80$ seconds, (d) $t = 90$ seconds for simulation C.2

The results show that Nozzle C with a 50 second water mist activation time can extinguish the fire. The results of this simulation are similar to simulation C.1 and will not be repeated here. The main differences are due to the larger fire size at the time of activation. The plane endures higher incident heat fluxes as the flame travels underneath of the aircraft and the structural steel members reach a higher peak temperature value, which is still below the critical temperature. Additionally, the extinction process takes approximately 10 seconds longer due to the delayed activation.

Chapter 7 Conclusion

7.1 Summary

Through this two-phase feasibility analysis, water mist was explored as an alternative to foam fire suppression systems for protection of JP-8 jet fuel pool fires in aircraft hangars.

Phase I assessed the feasibility of COTS water mist systems through literature and previous research efforts. A total of 27 water mist manufacturers were evaluated; eight water mist systems were initially dismissed due to lack of published data, dissimilar applications, or lack of approvals. Nineteen were further evaluated based on manufacturer specifications, literature, previous test results, and relevant approvals.

Phase I identified seven manufacturers with ten combined water mist systems as being potential candidates to provide successful protection from pool fires in aircraft hangars.

These systems were selected from the initial systems due to their success in large unenclosed environments, success in extinguishing class B fires, success from high ceiling heights, or their applicability for the protection of hangars.

Phase II conducted CFD modeling of three water mist systems identified in phase I using FDS. Two low pressure nozzles from VID Fire-Kill, Nozzle A and B, and one high pressure nozzle from Marioff, Nozzle C, were evaluated in phase II. Nozzle A and C are ceiling mounted nozzles and Nozzle B is a floor pop up nozzle. Each nozzle endured a series of preliminary simulations to validate the FDS input parameters. Through these simulations it was determined water mist nozzles are highly grid dependent and high-pressure water mist nozzles must use the parameter `PARTICLE_CFL=.TRUE.` to accurately model the near field of the nozzle. Although Lagrangian particles themselves

are not grid dependent the water mist nozzle is grid dependent due to the induced air flow from activation of the water mist nozzle. If the grid is not sufficiently small to capture this air flow pattern, then the radial velocities and droplet diameters can be incorrectly predicted.

Following characterization of each water mist nozzle small scale simulations were completed to verify the extinction and evaporation models. These simulations verified that when using the default single step infinitely fast chemistry model with a user prescribed MLRPUA, extinction occurs as a binary process. The evaporation model was verified and determined evaporation is either limited by the mass of water entering the space or by the saturation values at low temperatures.

The final simulations completed in this research effort evaluated the impact of each water mist nozzle in a mock aircraft hangar for protection against a JP-8 jet fuel pool fire. The simulations found, based on the modelling assumptions, only the high pressure water mist nozzle, Nozzle C, was able to extinguish this fire. The simulations found that for each nozzle an earlier activation time decreases the incident heat flux to the plane, decreases the temperature of structural steel members, and generally decreases thermal impact on the hangar because of cooling and radiation attenuation effects of water mist .

Overall, the full scale engineering configurations utilize significant assumptions and could be improved with additional research into the Lagrangian particle model, extinction model, and combustion model. The main takeaways from this research are through the background modeling phases which verify the evaporation and Lagrangian

particle model for small scale simulations and detail various methods used to characterize water mist nozzles in FDS.

7.2 Future Work

Through the course of this research the following topics were identified as areas of further research:

1. Quantify the effect of `PARTICLE_CFL=.TRUE.` on extinction
2. Develop a tangible relationship between the parameter `DROPLETS_PER_SECOND` and extinction accuracy.
3. Investigate the effect of using an increased grid size for modeling water mist nozzles in FDS to use practical grid sizes for engineering configurations.
4. Develop pyrolysis model for JP-8 to incorporate fuel cooling effects and reduction in MLR during extinction with water mist.
5. Create a data base of experimental water mist nozzle droplet size and velocity characteristics for validation of FDS models.
6. Expand data of medium to large scale extinction experiments using water mist.

The final simulations presented in this report could be improved with additional knowledge in each of these areas.

Appendix A: Additional Manufacturer Information

A.1 Danfoss Fire Safety

Danfoss is a developer of fixed fire suppression systems based in Denmark. Danfoss manufactures a high pressure water mist system, SEM-SAFE, which is FM approved for

the protection of machinery spaces up to 800 cubic meters and less than 8 m tall. Danfoss is one of the leading manufacturers for the marine industry but also develops land-based solutions. Marketed land-based applications include industrial buildings, transportation tunnels, healthcare facilities, hotels, and offices. There is limited nozzle and testing data for land-based applications and most installed uses fall under an HC-1 category. Danfoss has installed water mist systems for multiple machinery spaces on ships; one system was proven effective in a real fire scenario. In 2012, the SEM-SAFE system onboard the Esvagt Aurora, a standby safety vessel, extinguished a fire in a machinery space in less than 2 minutes.

A.2 Fike

Fike is a manufacturer of industrial safety equipment based in Missouri. Fike manufactures a low-pressure water mist system, duraquench, and an intermediate pressure system, micromist. The micromist system is powered by compressed Nitrogen and innately has smaller volume protection limitations due to this powering source. Micromist is FM approved to protect machinery and turbine enclosures up to 4.9 m tall. The duraquench system is powered through a centrifugal water pump and is FM approved to protect machinery and turbine enclosures up to 12 m tall. Although not yet FM approved for local application, the representative said they had performed successful full-scale tests for local application of class B fires in their testing facility. Fike representatives provided a video of the K6 water mist nozzle, at ceiling height, extinguishing a shielded heptane fire in a large open space. In a recent webinar, Fike extrapolated data from large volume tests to show potential success in aircraft hangars

with ceiling only protection or paired with VID Fire-Kill floor nozzles for protection. To this date ceiling only nozzles for this use have not been full scale tested.

Date Completed: 7/21/2020

A.3 Fogtec

Fogtec is a developer and manufacturer of fixed and mobile fire detection and suppression systems based in Germany. Fogtec was established in 1997 and is one of the industry leaders in tunnel water mist fire suppression and testing. Fogtec has participated in SOLIT and UPTUN, research projects in tunnels proving the capability of Fogtec systems to control class A and class B fires up to 150 MW. The system has only been tested up to maximum tunnel heights of 9 m and cannot suppress obstructed class B pool fires from those heights. Fogtec has one FM approved system for combustion and steam turbine enclosures less than 270 cubic meters with no height limit specification. Due to limited published information and no responsive company representative, we are unsure of any potential floor nozzles or hangar applications currently being investigated.

Date Completed: 8/11/2020

A.4 GW Sprinklers A/S

GW Sprinklers is a water-based fire suppression manufacturer based in Denmark, established over 60 years. GW Sprinklers manufactures two low pressure water mist system nozzles, but only the M5 nozzle applies to combustible liquid fires. The M5 mist system nozzle is marketed for protection of turbine and machinery enclosures, paint booths, and similar applications where flammable liquid pool and spray fires are the main hazard. Their website features a local application fire test for the protection of a 6 MW light diesel oil spray fire, which is extinguished within 10 seconds of ignition in a 10 m x

10 m x 4 m space. Additional information for the M5 nozzle states the maximum obstruction for a single nozzle is 20 degrees of the spray obstructed. Obstructions that block more than 20 degrees of the nozzle spray can have supplementary nozzles installed under the obstruction or wall installations to cover the obstructed area. The nozzle has been FM tested for protection of combustion and turbine enclosures; however, GW does not supply a complete water mist system and is therefore unable to attain an FM approval. The nozzle has approvals from multiple third-party testing laboratories for IMO MSC.1/CIRC 1387; however, this testing only requires extinguishment of two spray fires for ship spaces and is not comprehensive of land-based applications.

Date Completed: 8/26/2020

A.5 Hydrocore

Hydrocore is a developer and manufacturer of high pressure water mist systems established in the UK in 2012. Hydrocore develops solutions for machine rooms, local application of combustible liquids, and transportation tunnels. Hydrocore has FM approved systems for the protection of machinery and turbine enclosures less than 260 cubic meters, and local application protection of combustible liquids. The machinery and turbine FM approvals have a low ceiling height limitation compared to other high pressure water mist systems, 5 meters, and has no published information on height limitations for local application nozzles. Hydrocore has been involved in tunnel applications in the UK, but due to limited published materials and data, performance outcomes are unknown. Hydrocore is a small company and is one of the newest manufacturers in the water mist industry.

A.6 Johnson Control International

Johnson Controls International is a conglomerate that designs fire protection, HVAC, and security for buildings. JCI manufactures Aquamist ULF, a low-pressure water mist system, and has acquired high pressure and hybrid water mist systems through mergers. All three systems are FM approved for machinery spaces and turbine enclosures to protect spaces with varying heights and volumes. The low-pressure system has various open and closed nozzles that are FM approved for a wide range of applications. By speaking with a water mist specialist at JCI, they have not previously done any testing in aircraft hangars or with floor nozzles. The representative also confirmed they have done little testing with the high pressure and hybrid system and are most knowledgeable about the low-pressure system. The Aquamist ULF open AM4 nozzle is FM approved for heights up to 8 m and creates large water droplets to penetrate the fire plume. Aquamist fog, the high pressure system, is advertised as applicable for the protection of paint spray booths; however, the representative was unaware of any actual testing or installation of this application. The representatives are responsive and willing to provide preliminary nozzles for testing at UMD if requested.

Date Completed: 7/21/2020

A.7 Marioff

Marioff is a manufacturer of high pressure water mist fire suppression based in Finland. Marioff is a leading global developer of high pressure water mist, produces over one-hundred nozzles for protection of various hazards, and manufactures six different power sources. The GPU and MT4 pumps are FM approved for machinery and turbine enclosures less than 11 m and 1,376 cubic meters. Marioff has performed over 7,000 full-

scale tests for all mist applications, including aircraft hangar testing with floor nozzles. The Marioff YouTube page features videos of a flammable liquid pool fire test with ceiling only protection and a flammable liquid spray fire test with local protection nozzles.

Marioff provided summary sheets for full-scale tests in aircraft hangars; the summary proved water mist to be as effective as foam systems for extinguishing and preventing damage to aircraft in hangars. The representative mentioned working with safe spill for the protection of flowing fires and integrating nozzles to the diversion storage tank for collected liquid. No current efforts have been made to integrate Marioff nozzles into a floor drainage system, but this integration seems very feasible.

Date Completed: 8/6/2020

A.8 Minimax

Minimax is a developer and manufacturer of fire protection solutions based in Germany. Minimax began manufacturing water mist in 1993 and currently manufactures low pressure and high pressure water mist systems. Minimax produces four separate water mist technologies but only the low pressure water mist system, ProCon, and high pressure water mist system, ProCon XP, are relevant to the protection of Class B fires on land. The ProCon system is not FM approved but is marketed for use in enclosed and non-enclosed industrial environments. The ProCon XP is FM approved for protection of turbine and machinery spaces less than 13.5 meters and 2,430 cubic meters and is marketed for use in protecting machinery using combustible liquids in confined spaces. This high pressure system has also been tested and certified by VDS for engine rooms

and turbine enclosures. Representatives have been unresponsive; additional mist nozzle specifications are necessary before moving forward with these systems.

Date Completed: 9/25/2020

A.9 Phirex Australia

Phirex Australia, established in 1993, is a designer and manufacturer of water mist systems based in Australia. Phirex Australia manufactures a low pressure water mist system, MISTEX, and high pressure water mist system, FOGEX. FOGEX is FM approved for protection of machinery enclosures less than 500 cubic meters with no height limit specified and turbine enclosures less than 500 cubic meters and 5 meters high. MISTEX has no FM approvals. FOGEX produces water droplets between 1 and 100 microns creating a fog-like distribution to reach recessed areas. According to the manufacturer's testing information page, local application and total flooding testing have successfully been completed and witnessed by multiple third-party authorities. Local application testing has been completed up to 11 meters above the hazard, and total flooding testing has been completed in enclosures up to 10 meters tall.

The FOGEX system is marketed as applicable for aircraft hangars. Through email correspondence with a representative, FOGEX is installed at ceiling level, 11- 12 meters high, in multiple military aircraft hangars. The representative stated that Phirex has "not developed a floor mounted nozzle for obvious reasons, i.e., they face the prospect of getting damaged or stolen on the floor level and rendered ineffective if a heavy object or plane parks on top of them. If necessity required floor mounted nozzles, then Phirex can easily develop them for a specific application."

Date Completed: 8/31/2020

A.10 RG Systems

RG Systems is a fire protection developer with a focus on sustainable and ecological water mist systems, based in Brazil. RG systems develop high pressure water mist systems for the protection of various building types, industrial hazards, and transportation industries. They have developed one FM approved water mist system for the protection of turbine and machinery enclosures that is powered by compressed air and discharges with decreasing pressure. The electric and diesel powered pump systems are not FM approved. The nozzle for protection of turbine spaces has successfully completed SINTEF's testing protocol involving 16 different turbine enclosure fire scenarios. RG systems also develop a water mist system for cable and highway tunnels where VTT, VdS, and Sintef have tested all components. No published information about nozzle characteristics or test results is available on the website, and company representatives have been unresponsive.

A.11 Securiplex

Securiplex is a manufacturer of fire suppression and detection systems based in Alabama. Securiplex has a low pressure system, fire scope 2000, and a high pressure system, fire scope 5000. The fire scope 2000 system is powered by compressed air and FM approved for protection of 260 cubic meters and 5 meters tall. The fire scope 5000 system is powered by an electric pump or compressed nitrogen and FM approved for both delivery methods to protect turbine and machinery enclosures up to 1225 cubic meters and 11 meters tall. The low pressure system was involved in full-scale machinery tests by the U.S. Airforce and Navy in the 1990s. These tests showed the mist system was unable to extinguish small concealed pan fires in the enclosure. It appears that recently, the fire

scope 5000 is the more popular system and is marketed for protection of various hazards. One of these marketed hazards includes aircraft hangars. A representative mentioned Securiplex has worked with a military agency to develop a movable local water mist system for protection in an aircraft hangar. The protection involved local application nozzles surrounding the plane at an elevated height; however, for undisclosed reasons this system has not been installed in an industry hangar.

Date Completed: 8/28/2020

A.12 Ultra Fog

Ultra fog, established in 1990, is a manufacturer of high pressure water mist systems based in Sweden. Ultra fog began by developing water mist solutions for marine applications and quickly expanded to land based applications. Land-based applications include turbine and machinery enclosures, aircraft hangars, energy and industry hazards, tunnels, and HC-1 buildings. Ultra fog is FM approved for protection of turbine and machinery enclosure less than 1320 cubic meters and 12 meters tall. This water mist system is also tested to IMO standards for machinery spaces and local applications. As of August 2020, the Ultra fog water mist tunnel solution has successfully controlled a full scale 30 MW class A tunnel fire, and additional verification experiments are scheduled in the upcoming months. Ultra fog is marketed for protection of aircraft hangars. The aircraft hangar brochure features pop-up floor nozzles in conjunction with ceiling nozzles for the protection of aircraft hangars. A general installation is completed on military bases in Sweden; however, no full-scale testing results or nozzle characteristics are publicly available.

Date Completed: 9/4/2020

A.13 Victaulic

Victaulic is a global manufacturer of mechanical pipe, flow control, and fire protection systems based in Pennsylvania. Victaulic manufactures a twin fluid hybrid mist system called Vortex. Victaulic Vortex is a dual agent fire extinguishing system designed for use in water-sensitive facilities. Vortex is FM approved for machinery and turbine enclosures less than 7.5 meters tall and 3610 cubic meters. This hybrid system uses a uniform blend of water and nitrogen to extinguish hazards via a combination of heat absorption and oxygen deprivation with minimal water presence. Representatives from Victaulic expressed that large quantities of nitrogen would be needed for the protection of an aircraft hangar, and the system would not be successful in total flooding of the space. The representatives recommended local application for the protection of a fuel spill to utilize the nitrogen to inert the atmosphere near the flame. Victaulic is currently conducting experiments to determine Vortex's performance in large open spaces in Australia and with running fuel fires in Europe. Preliminary test results show success in extinguishing running fuel fires.

Date Completed: 7/23/2020

A.14 VID Fire-Kill

VID Fire-Kill is a water-based fire suppression manufacturer in Denmark. VID has FM approved water mist applications for enclosed machinery spaces, turbine enclosures, data centers, non-storage HC-1 occupancies, and local application (i.e. flammable liquid hazards and conveyor openings). VID has also been involved in full-scale water mist system tests for aircraft hangars and tunnel applications. Through discussions with the CEO of VID Fire-Kill, they have successfully completed full-scale testing and currently

protect multiple military aircraft hangars. For hangar applications, they can use a zoned system to minimize water usage and water damage from accidental discharge of a system. Water discharge from the ground also minimizes water consumption for plume penetration. Currently, only fuel spill fire scenarios have been tested; however, preliminary tests for flowing fuel fires show success, and additional testing is underway. Hangar floor nozzles can be integrated into the floor construction or retrofitted on top of the floor for existing construction.

Date Completed: 7/28/2020

Appendix B: Flame Detector Response and Water Mist Activation Time

To estimate the response time of flame detectors in the hangar the critical heat flux to the flame detector was calculated based on the manufacturers test fire (assuming General Motors model FL400H). The manufacturer's fire test used a 0.3 m x 0.3 m methane fire source. The representative diameter of the burner is 0.34 m, found using

$$D = \sqrt{\frac{4 \cdot A_s}{\pi}},$$

where $A_s = 0.09 \text{ m}^2$. The HRR from the fire source is found using Zabetakis and Burgess' correlation from the SFPE handbook,

$$Q = \dot{m}'' \Delta H_c * A_s * (1 - \exp(-k\beta D))$$

where $\dot{m}'' = 0.066 \text{ kg/m}^2 \cdot \text{s}$, $\Delta H_c = 42,200 \text{ kJ/kg}$, $k\beta = 1.1$, and all other values are previously defined [8]. Using a simple point source model,

$$\dot{q}'' = \chi_r * \frac{Q}{4\pi r^2}$$

the critical heat flux at the flame detector, 70 m away, is 0.24 W/m^2 .

By running an FDS simulation with a heat flux device on the far side of the hangar, the heat flux device reached the critical heat flux for detection within 2 seconds of ignition. Adding a safety factor of 5 the assumed detection response time is 10 seconds. Assuming once detection occurs, there is a 20 second delay for water to reach the water mist nozzles, the lower bound activation time of the nozzles is 30 seconds.

From hand calculated estimates the detection time can be under 30 seconds; however, practical detection times with flame detectors can be significantly longer than theoretical detection times as calculated above. The Airforce requires all flame detectors to activate within 30 seconds of ignition. Using this requirement and assuming a 20 second delay for water to reach the water mist nozzles, the upper bound activation time of the nozzles is 50 seconds.

Appendix C: Air Entrainment Verification Simulations

A series of simulations were conducted with monodisperse droplets, 80 microns, and varying user prescribed drag coefficient, 0 to 5, to compare the expected terminal velocity of the Lagrangian particles to the predicted particle velocity in FDS with entrained air. The simulations were conducted in a 3 m x 3 m x 3 m compartment with a grid size of 0.1 m and 5×10^4 particles per second. The compartment is open to the environment on all sides and the ceiling and floor are composed of concrete. The humidity in the space is set to 100 % to prevent evaporation of small water droplets and ensure monodisperse droplets for the duration of the simulation. The nozzle characteristics used in this simulation are identical to Nozzle A in 4.2.2.2, except with an initial velocity of 1 m/s and monodisperse droplets of 80 microns.

The results of the simulation in Figure 11-1 show that with a drag coefficient of 0 the particle velocity versus height in FDS matches the predicted particle velocity versus height from hand calculations. The predicted particle velocity is calculated based on simple particle motion equations,

$$w_p = \frac{(\rho_{liq} - \rho_{gas})}{\rho_{gas}} * g_z * t + w_{p,0},$$

assuming no drag and quiescent gas. This verifies that FDS can correctly predict the position and velocity of a particle given no drag effects in quiescent air; however, water mist nozzles entrain air into the spray and the entrained gas carries the water particles at their terminal velocity.

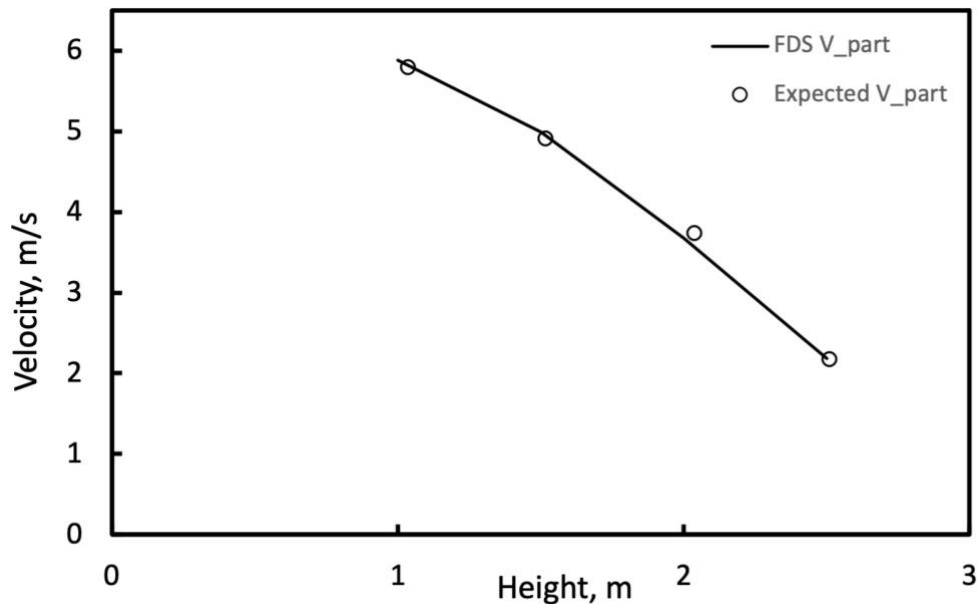


Figure 0-1 FDS particle velocity and expected particle velocity with $C_d = 0$

To check that FDS accurately predicts the particle terminal velocity given a non-quiescent gas environment, simulations were conducted with increasing specified drag coefficients to compare to hand calculations. The particle velocity measured in FDS is compared to the expected particle terminal velocity,

$$w_{liq,inf} = w_{gas} - \left(\left(\frac{4d_{liq}}{3C_d} \right) * \frac{(\rho_{liq} - \rho_{gas})}{\rho_{gas}} * g_z \right)^{0.5},$$

where u_{gas} is taken from device measurements in FDS, ρ_{liq} is 1000 kg/m³, ρ_{gas} is 1.2 kg/m³, g_z is the gravitational constant, d_{liq} is 80 um, and C_d changes for each simulation.

The results in Figures 11-2 and 11-3 show that FDS is able to correctly predict the particle terminal velocity with drag coefficients of 0.8 and 5 respectively in non-quiescent air.

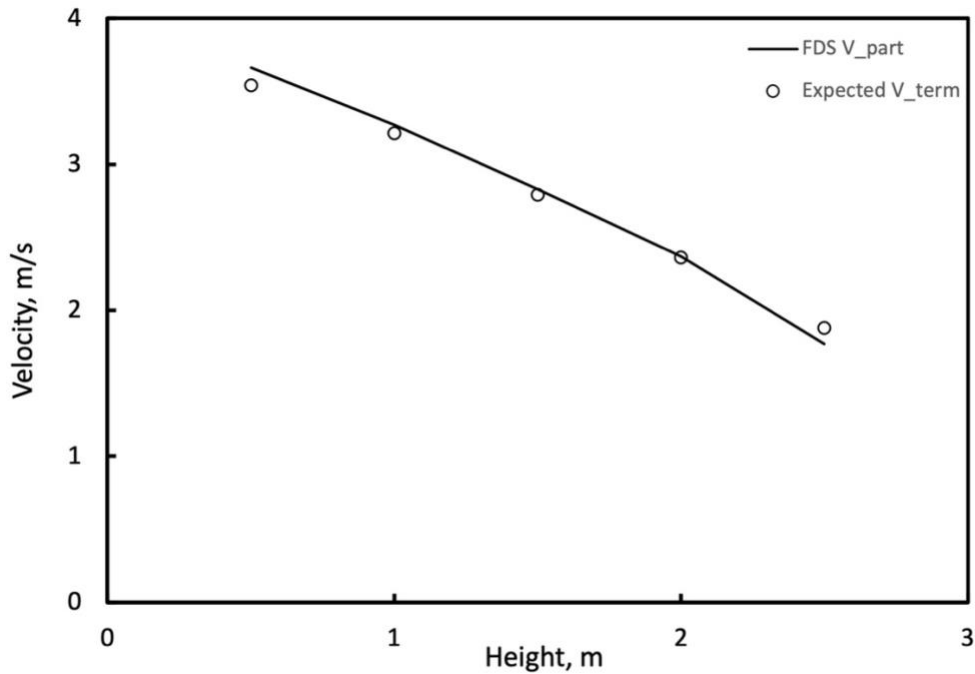


Figure 0-2 FDS particle velocity and expected terminal velocity versus height with $C_d = 0.8$

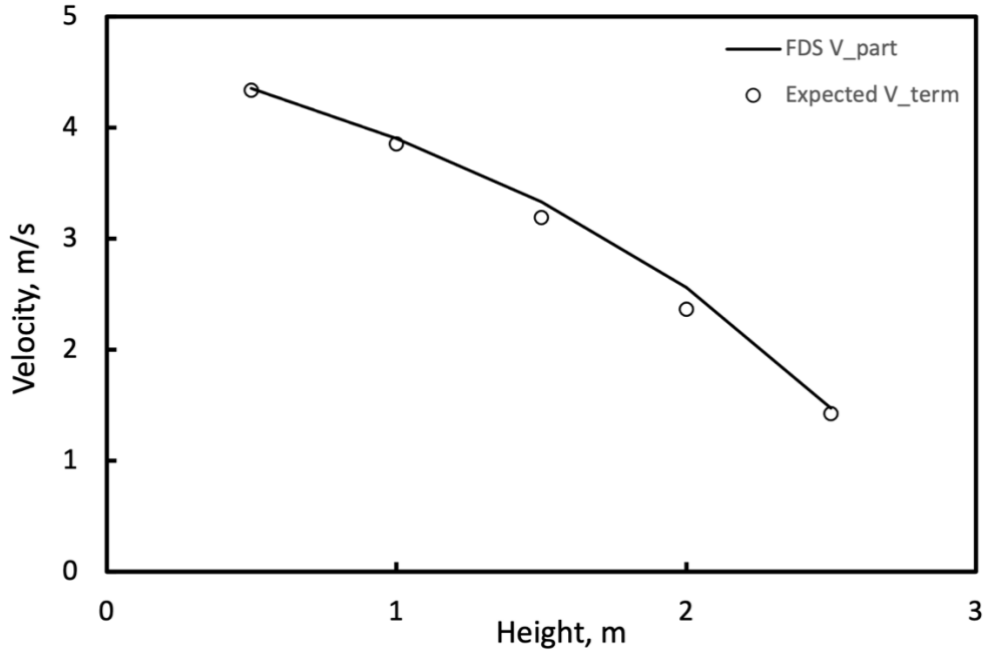


Figure 0-3 FDS particle velocity and expected terminal velocity versus height with $C_d = 5$

Appendix D: Nozzle A & B Grid Sensitivity Analysis

D.1 Nozzle A Grid Sensitivity

A grid sensitivity analysis was performed for Nozzle A. The simulations were conducted in a 3 m x 3 m x 2 m compartment with all domain boundaries open, except for ZMAX. The nozzle is located in the center of the domain 0.1 m from the ceiling. The nozzle characteristics are the final characteristics as given in Table 4-3.

The results in Figure 12-1 and 12-2 reveal less than a 10 % discrepancy at any given measurement between a grid size of 5 cm and 10 cm. The increased computational time for the smaller grid is not worth the small increased accuracy.

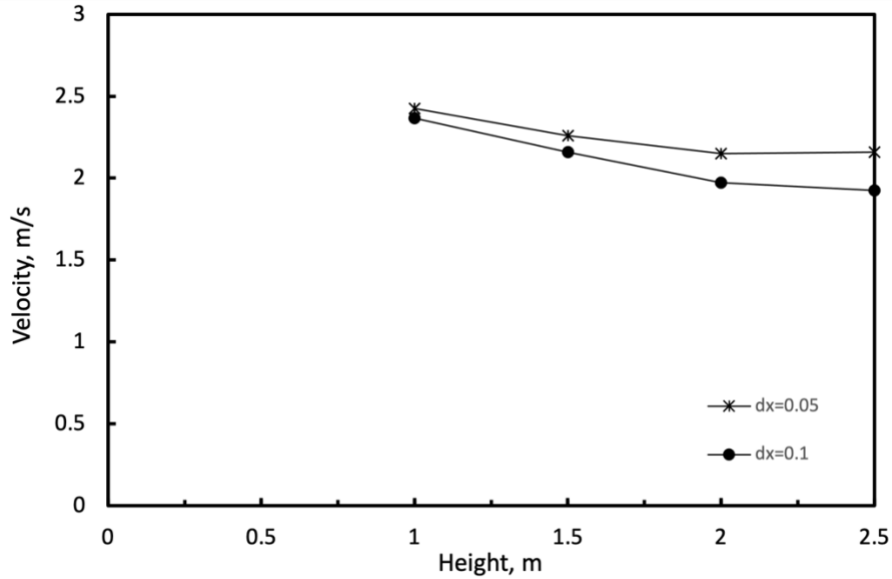


Figure 0-1 Velocity versus vertical height for Nozzle A with varying grid size and final droplet size distribution and nozzle characteristics

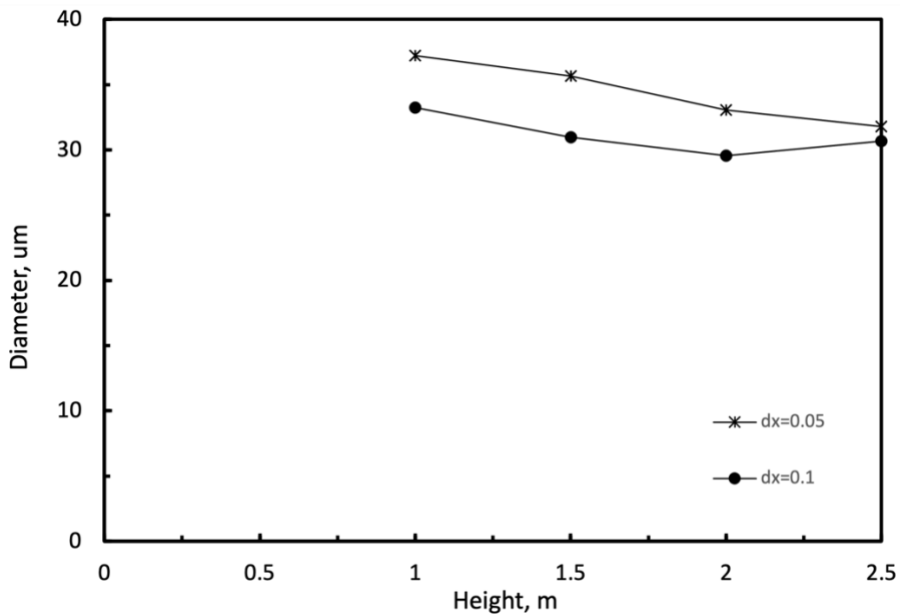


Figure 0-2 Diameter versus vertical height for Nozzle A with varying grid size and final droplet size distribution and nozzle characteristics

D.2. Nozzle B Grid Sensitivity Analysis

A grid sensitivity analysis was performed for Nozzle B. Two sets of simulations were conducted looking at the sensitivity of the nozzle with monodisperse droplets and with a droplet distribution. Both sets of simulations were conducted in a 3 m x 3 m x 1.5

m compartment with all domain boundaries, except for ZMIN, constructed of open vents. The nozzle is centered 0.2 m above the ground, 0.1 m from the XMIN direction, and oriented in the positive x direction. All PDDA measurement devices were located in a straight line horizontally from the center nozzle.

The first set of simulations analyzed Nozzle B with k-factor, pressure, offset, and angles as described in section 4.2 and with monodisperse droplets of 80 μm and uniform initial velocity of 20 m/s. Figures 12-3 and 12-4 compare the velocity and diameter versus horizontal distance from the center of the nozzle for each grid size. The results show small discrepancies between the two grid sizes and the increased accuracy is not worth the increased computation time in these scenarios.

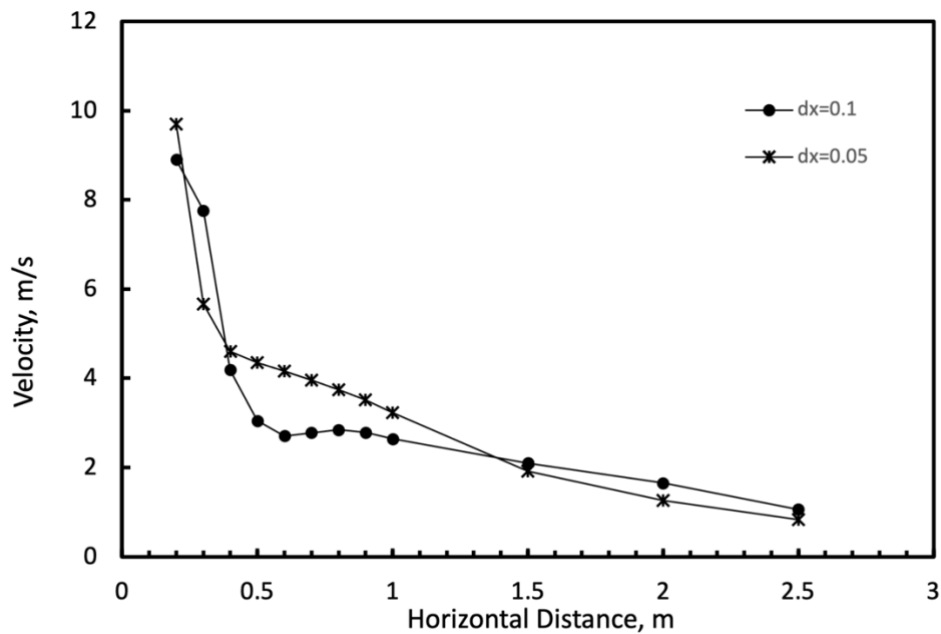


Figure 0-3 Velocity versus horizontal distance from the center of Nozzle B for varying grid size with uniform velocity and droplet size.

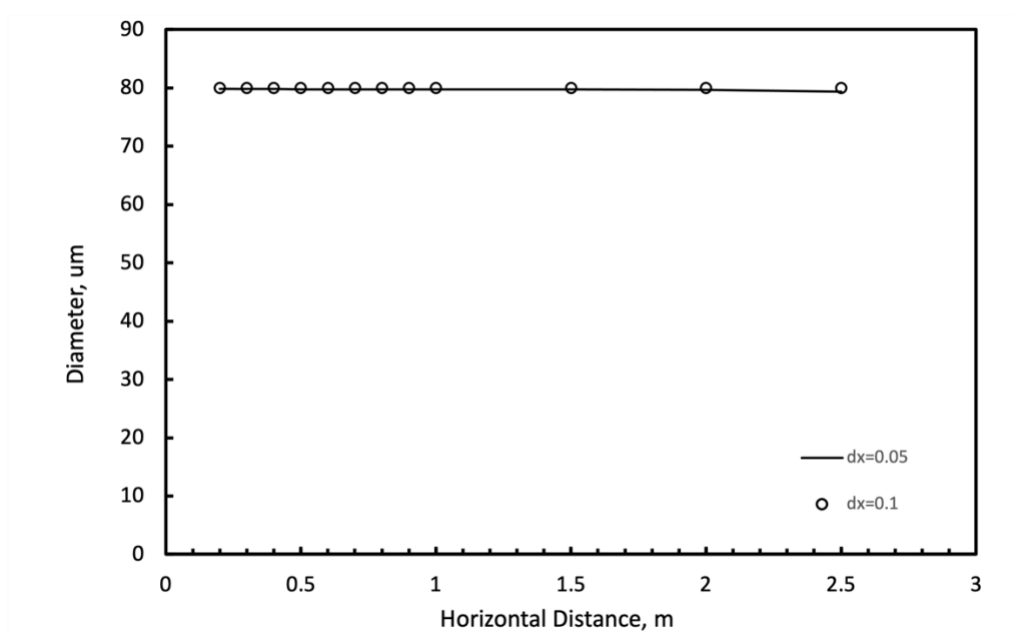


Figure 0-4 Diameter versus horizontal distance from the center of Nozzle B for varying grid size with uniform velocity and droplet size.

The second set of simulations analyzed Nozzle B with all of the final input parameters and droplet size distribution as described in Table 4-4. Figures 12-5 and 12-6 compare the velocity and diameter versus horizontal distance from the center of the nozzle for each grid size. The results reveal a large discrepancy, by up to 400 % at some locations in the flow, for the varying grid sizes. The smaller grid size can better predict the transport of large droplets further in the space; whereas the larger grid over predicts the number of droplets that fall to the ground close to the nozzle.

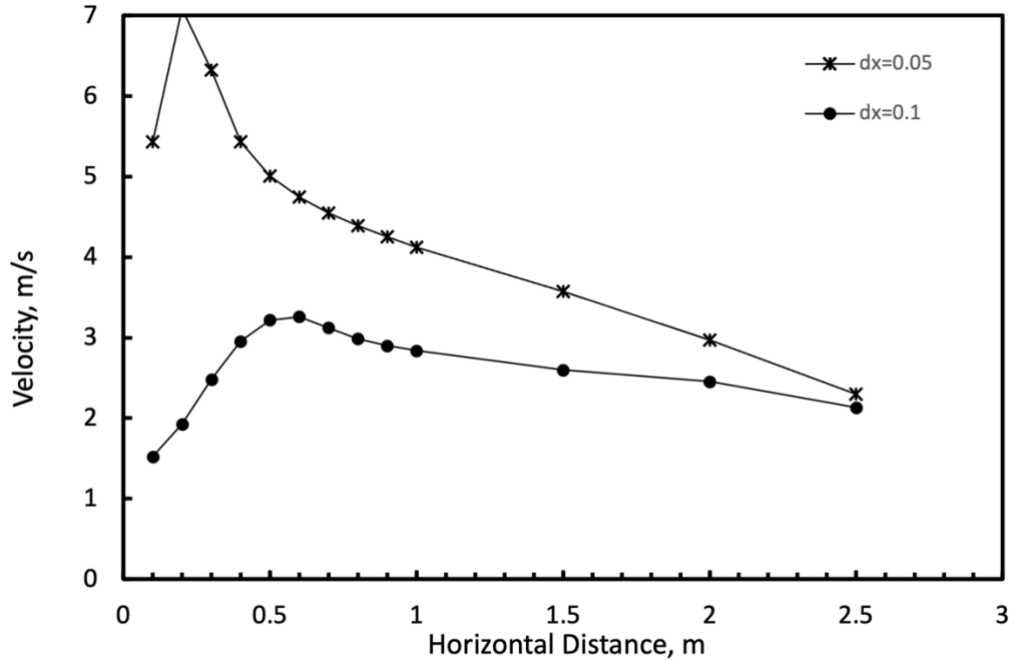


Figure 0-5 Velocity versus horizontal distance from the center of Nozzle B for varying grid size with final droplet size distribution and input characteristics

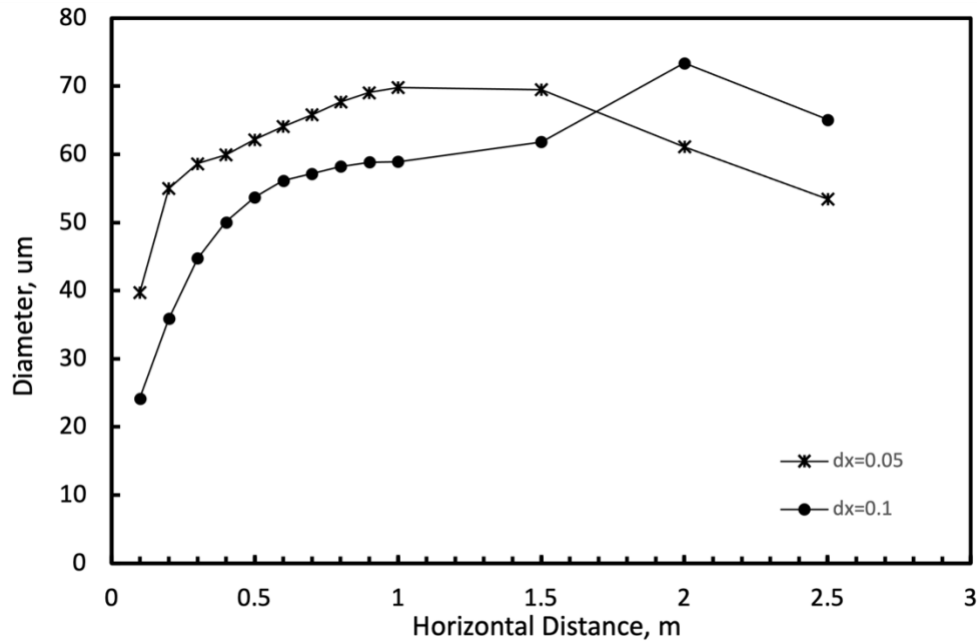


Figure 0-6 Velocity versus horizontal distance from the center of Nozzle B for varying grid size with final droplet size distribution and input characteristics

Appendix E: Hangar Drawings

Retracted for Public Distribution

Appendix F: Nozzle B Small Scale Extinction Simulations

Experimental results were provided by VID Fire-Kill which prove extinction with Nozzle B using four nozzles surrounding a 1 m² JP-8 fire source in a large un-enclosed space.

Small-scale extinction simulations were conducted in a 5 m x 5 m x 4 m open domain with varying grid sizes as specified below. A 1 m diameter JP-8 fire source, with characteristics as outlined in section 4.1, is located in the center of the room and four floor nozzles are equally spaced around the fire at 2 m x 2 m spacing. The spray is represented by varying droplet sizes as specified below. The extinction model for these simulations use the default LOI of 0.135, a CFT of 1527 °C, an AIT of 330 °C everywhere in the domain, and a fuel surface temperature ramp for ignition.

This configuration analyzes the main features of the extinction experiments conducted by VID Aps and results of these simulations are compared to the experimental results.

F.1 Droplets per second Analysis

Using the configuration described above with a grid size of 0.05 m below 3 m in the space and 0.1 m above 3 m in the space, simulations were conducted varying the parameter DROPLETS_PER_SECOND. Three simulations were performed using 1×10^4 , 2×10^4 , and 5×10^4 droplets per second to represent the flow.

Figure 14-1 and 14-2 plot the HRR and evaporation rates versus time for each simulation with varying number of particles.

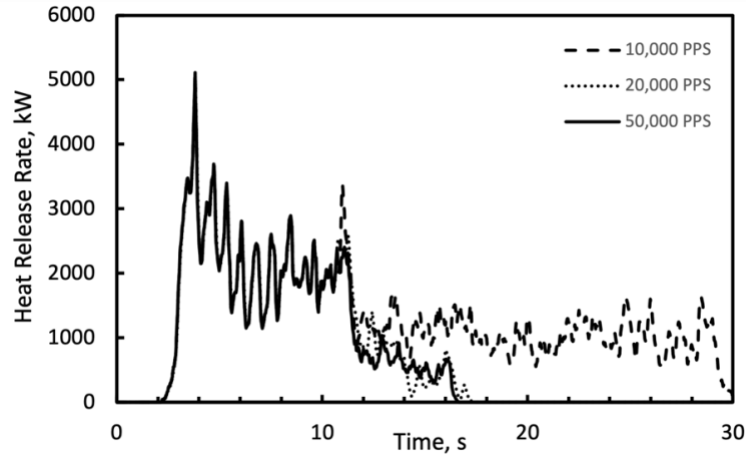


Figure 0-1 HRR versus time for small scale extinction simulations using Nozzle B and varying the number of droplets representing the flow

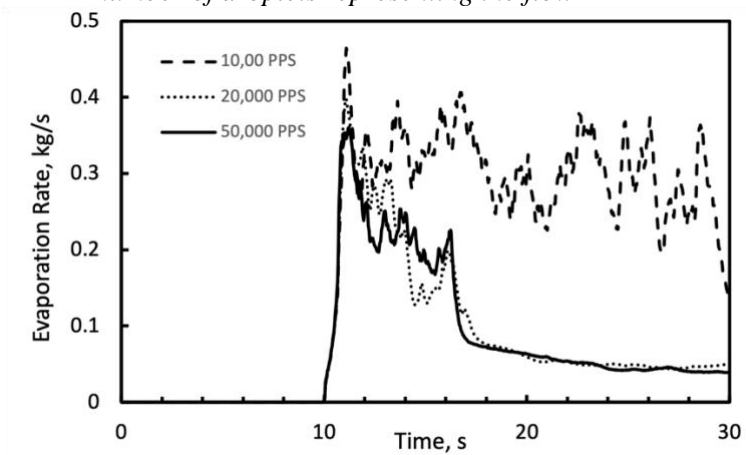


Figure 0-2 Evaporation rate versus time for small scale extinction simulations using Nozzle B and varying the number of droplets representing the flow

The results of these simulations demonstrate that evaporation and extinction are dependent on the value of droplets used to represent the flow. Simulations using more than 2×10^4 droplets per second show small differences in the evaporation rate over time but converge on the time to extinction. Simulations using less than 2×10^4 droplets per second do not demonstrate extinction within 20 seconds of activation. Using a lower number of particles to represent the spray corresponds to over a 4 x increase in the time to extinction. Although increased particles improves the accuracy of the simulation it also

increases the computation time for each simulation. For this reason, 2×10^4 droplets per second is used to accurately represent the flow with the lowest CPU requirement.

F.2 Grid Size Analysis

Using the configuration described above with 2×10^4 particles per second representing the flow, simulations were conducted varying the height at which the grid size increases from 0.05 m to 0.1 m. Two simulations were conducted varying the height, from 2 m to 3 m, at which the grid size increases.

Figures 14-3 and 14-4 plot the HRR and evaporation rate versus time for the varying vertical location of grid size increase.

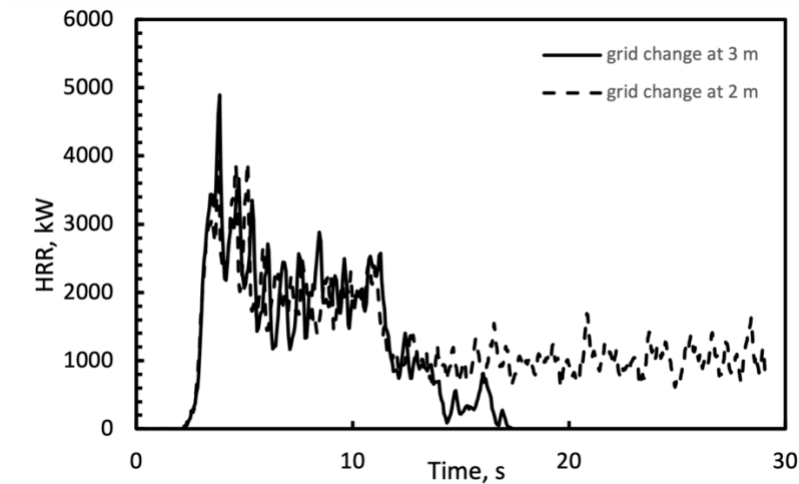


Figure 0-3 HRR versus time for small scale extinction simulations using Nozzle B and varying the vertical location of grid size increase

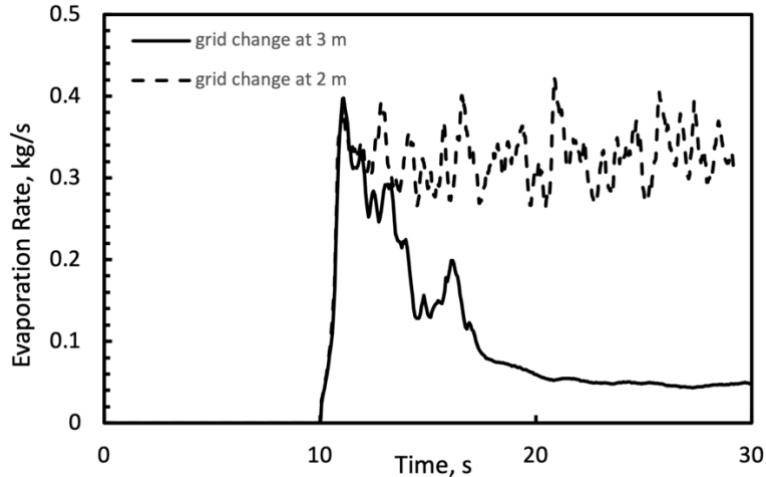


Figure 0-4 Evaporation rate versus time for small scale extinction simulations using Nozzle B and varying the vertical location of grid size increase
 The results of these simulations demonstrate a grid dependency in the flame region for extinction with Nozzle B.

Appendix G: FDS Input File

/FDS input file for hangar configuration and diagnostics

&DUMP MAXIMUM_PARTICLES = 500000 /

&RADI OPTICALLY_THIN = .TRUE. /

&TIME T_END=120/

&MISC TMPA = 25, HUMIDITY = 65 /

&MATL ID = 'CONCRETE',
 DENSITY = 2200,
 SPECIFIC_HEAT = 1.04,
 CONDUCTIVITY = 1.8 /

&SURF ID = 'FLOOR',
 MATL_ID = 'CONCRETE'
 THICKNESS = 0.1
 COLOR ='BEIGE' /

&MATL ID = 'CORRUGATED METAL',
 CONDUCTIVITY = 52,

SPECIFIC_HEAT = 0.47,
DENSITY = 7800 /

&SURF ID = 'WALL',
THICKNESS = 0.2,
DEFAULT = .TRUE.,
MATL_ID = 'CORRUGATED METAL'
COLOR='LAVENDER'/

&MATL ID = 'Carbon Steel',
FYI = '1.5 % carbon steel from NCFS database',
CONDUCTIVITY = 36,
SPECIFIC_HEAT = 0.486,
DENSITY = 7753 /

&SURF ID = 'ELECTRICAL PANEL',
THICKNESS = 0.05,
MATL_ID = 'Carbon Steel'
COLOR='MELON'/

/ create hangar space

&OBST XB = 0,26,0,26,0,0, SURF_ID = 'FLOOR' / main floor
&OBST XB = 0,26,0,0.4,0,12, SURF_ID = 'WALL' / front wall

&HOLE XB = 1,25,-0.4,0.8,0,7/ hangar door

/open outdoor space

&VENT XB = 0,26,-6,-6,0,12, SURF_ID = 'OPEN' /
&VENT XB = 26,26,-6,0,0,12, SURF_ID = 'OPEN' /
&VENT XB = 0,0,-6,0,0,12, SURF_ID = 'OPEN' /
&VENT XB = 0,26,-6,0,0,0, SURF_ID = 'FLOOR' /

&MATL ID = 'STEEL SN400',
FYI = 'SN400 International Journal of Steel Structures',
CONDUCTIVITY_RAMP = 'k',
SPECIFIC_HEAT_RAMP = 'c',
DENSITY = 7851 /

&RAMP ID = 'c' , T = 20, F = 0.52/
&RAMP ID = 'c' , T = 200, F = 0.535/
&RAMP ID = 'c' , T = 500, F = 0.709/

&RAMP ID = 'k' , T = 20, F = 53.7/

&RAMP ID = 'k' , T = 200, F = 48.3/
&RAMP ID = 'k' , T = 500, F = 42.1/

&SURF ID = 'Structural Steel',
THICKNESS = 0.006,
MATL_ID = 'STEEL SN400'
COLOR='DIM GRAY'/

/ Structural Steel Representatives - smallest steel structure members being represented

&OBST XB = 0.2,0.4,12,12.2,0,12, SURF_ID = 'Structural Steel'/
&OBST XB = 0.2,0.4,24.6,24.8,0,12, SURF_ID = 'Structural Steel'/
&OBST XB = 3,9,12.6,12.8,11.8,12, SURF_ID = 'Structural Steel'/

/temperature measurements of structural steel - only analyze the maximum temperature for the given beam

&DEVC XYZ = 0.4,12.1,1, ID = 'beam1-1', QUANTITY = 'TEMPERATURE', IOR = 1
/
&DEVC XYZ = 0.4,12.1,2, ID = 'beam1-2', QUANTITY = 'TEMPERATURE', IOR = 1
/
&DEVC XYZ = 0.4,12.1,3, ID = 'beam1-3', QUANTITY = 'TEMPERATURE', IOR = 1
/
&DEVC XYZ = 0.4,12.1,4, ID = 'beam1-4', QUANTITY = 'TEMPERATURE', IOR = 1
/
&DEVC XYZ = 0.4,12.1,5, ID = 'beam1-5', QUANTITY = 'TEMPERATURE', IOR = 1
/
&DEVC XYZ = 0.4,12.1,6, ID = 'beam1-6', QUANTITY = 'TEMPERATURE', IOR = 1
/
&DEVC XYZ = 0.4,12.1,7, ID = 'beam1-7', QUANTITY = 'TEMPERATURE', IOR = 1
/
&DEVC XYZ = 0.4,12.1,8, ID = 'beam1-8', QUANTITY = 'TEMPERATURE', IOR = 1
/
&DEVC XYZ = 0.4,12.1,9, ID = 'beam1-9', QUANTITY = 'TEMPERATURE', IOR = 1
/
&DEVC XYZ = 0.4,12.1,10, ID = 'beam1-10', QUANTITY = 'TEMPERATURE', IOR = 1
1 /
&DEVC XYZ = 0.4,12.1,11, ID = 'beam1-11', QUANTITY = 'TEMPERATURE', IOR = 1
1 /

&DEVC XYZ = 0.4,24.7,1, ID = 'beam2-1', QUANTITY = 'TEMPERATURE', IOR = 1
/
&DEVC XYZ = 0.4,24.7,2, ID = 'beam2-2', QUANTITY = 'TEMPERATURE', IOR = 1
/

THICKNESS = 0.0032,
COLOR = 'SILVER'/

&OBST XB = 11.6,14.4,5.2,17.2,1.6,3.6, SURF_ID = 'PLANE' / FUSALAGE
&OBST XB = 12,14,17.2,18,1.6,4, SURF_ID = 'PLANE' / NOSE
&OBST XB = 12,14,18,18.8,1.6,3.6, SURF_ID = 'PLANE' / NOSE
&OBST XB = 12,14,18.8,19.6,1.6,3, SURF_ID = 'PLANE' / NOSE
&OBST XB = 12,14,19.6,20.4,2,3, SURF_ID = 'PLANE' /NOSE
&OBST XB = 12,14,20.4,21.2,2,2.4, SURF_ID = 'PLANE' / NOSE

&OBST XB =10.4,11.6,6.8,13.6,2,2.4 , SURF_ID = 'PLANE' / LHS WING
&OBST XB = 9.6,10.4,7.2,12.8,2,2.4, SURF_ID = 'PLANE'/ LHS WING
&OBST XB = 8.8,9.6,7.6,12.4,2,2.4, SURF_ID = 'PLANE'/ LHS WING
&OBST XB = 8.4,8.8,8,12,2,2.4, SURF_ID = 'PLANE'/ LHS WING
&OBST XB = 8,8.4,8.4,11.6,2,2.4, SURF_ID = 'PLANE'/ LHS WING
&OBST XB = 7.6,8,9.2,11.2,2,2.4, SURF_ID = 'PLANE'/ LHS WING

&OBST XB =14.4,15.6,6.8,13.6,2,2.4 , SURF_ID = 'PLANE' / RHS WING
&OBST XB = 15.6,16.4,7.2,12.8,2,2.4, SURF_ID = 'PLANE'/ RHS WING
&OBST XB = 16.4,17.2,7.6,12.4,2,2.4, SURF_ID = 'PLANE'/ RHS WING
&OBST XB = 17.2,17.8,8,12,2,2.4, SURF_ID = 'PLANE'/ RHS WING
&OBST XB = 17.8,18,8.4,11.6,2,2.4, SURF_ID = 'PLANE'/ RHS WING
&OBST XB = 18,18.4,9.2,11.2,2,2.4, SURF_ID = 'PLANE'/ RHS WING

&OBST XB = 10.6,11.6,5,7,3,4, SURF_ID ='PLANE' / LHS TAIL
&OBST XB = 10,11,5,6.6,4,4.6, SURF_ID = 'PLANE'/LHS TAIL
&OBST XB = 9.6,10.6,5,6,4.6,5, SURF_ID = 'PLANE'/LHS TAIL
&OBST XB = 9,10,5,6,5,5.6, SURF_ID = 'PLANE' / LHS TAIL
&OBST XB = 9,10,5,5.6,5.6,6, SURF_ID = 'PLANE' /LHS TAIL

&OBST XB = 14.6,15.6,5,7,3,4, SURF_ID ='PLANE' / RHS TAIL
&OBST XB = 15,16,5,6.6,4,4.6, SURF_ID = 'PLANE'/RHS TAIL
&OBST XB = 15.6,16.5,5,6,4.6,5, SURF_ID = 'PLANE'/RHS TAIL
&OBST XB = 16,17,5,6,5,5.6, SURF_ID = 'PLANE' / RHS TAIL
&OBST XB = 16,17,5,5.6,5.6,6, SURF_ID = 'PLANE' /RHS TAIL

/ fire

&REAC FUEL= 'JP-8',
FORMULA = 'C11H21',
HEAT_OF_COMBUSTION = 42800,
RADIATIVE_FRACTION = 0.1,
SOOT_YIELD= 0.03,
CO_YIELD= 0.01
CRITICAL_FLAME_TEMPERATURE=1527

AUTO_IGNITION_TEMPERATURE = 310/

&SURF ID='FIRE',
FYI='JP-8',
MLRPUA = 0.06
TMP_FRONT = 700
RAMP_T='Fuel Temp' /

&RAMP ID = 'Fuel Temp', T = 0.0, F = 0.0 /
&RAMP ID = 'Fuel Temp', T = 1.0, F = 1.0 /
&RAMP ID = 'Fuel Temp', T = 9.0, F = 1.0 /
&RAMP ID = 'Fuel Temp', T = 10.0, F = 0.05 /

&VENT XB = 1,13,1,25,0,0, XYZ = 6.5,13,0, COLOR ='RED', SURF_ID =
'FIRE',SPREAD_RATE=0.03/

/WATER MIST NOZZLES

&SPEC ID='SPRINKLER WATER VAPOR', SPEC_ID='WATER VAPOR'/

/ electrical cabinet(s)

&OBST XB = 0,0.6,12.8,13.6,1.6,2.4, SURF_ID = 'ELECTRICAL PANEL',
COLOR='BLUE'/
&OBST XB = 0,0.6,23.6,24.4,1.6,2.4, SURF_ID = 'ELECTRICAL PANEL',
COLOR='BLUE'/

&OBST XB = 25.6,26,12.8,13.6,1.6,2.4, SURF_ID = 'ELECTRICAL PANEL',
COLOR='BLUE'/
&OBST XB = 25.6,26,23.6,24.4,1.6,2.4, SURF_ID = 'ELECTRICAL PANEL',
COLOR='BLUE'/

/heat flux at electrical cabinets

&DEVC ID='I cabinet1 z=1.6', XYZ=0.6,13,1.6, IOR = +1, QUANTITY ='INCIDENT
HEAT FLUX'/
&DEVC ID='I cabinet1 z=1.7', XYZ=0.6,13,1.7, IOR = +1, QUANTITY ='INCIDENT
HEAT FLUX'/
&DEVC ID='I cabinet1 z=1.8', XYZ=0.6,13,1.8, IOR = +1, QUANTITY ='INCIDENT
HEAT FLUX'/
&DEVC ID='I cabinet1 z=1.9', XYZ=0.6,13,1.9, IOR = +1, QUANTITY ='INCIDENT
HEAT FLUX'/
&DEVC ID='I cabinet1 z=2.0', XYZ=0.6,13,2.0, IOR = +1, QUANTITY ='INCIDENT
HEAT FLUX'/

&DEVC ID='I cabinet1 z=2.1', XYZ=0.6,13,2.1, IOR = +1, QUANTITY ='INCIDENT HEAT FLUX'
&DEVC ID='I cabinet1 z=2.2', XYZ=0.6,13,2.2, IOR = +1, QUANTITY ='INCIDENT HEAT FLUX'
&DEVC ID='I cabinet1 z=2.3', XYZ=0.6,13,2.3, IOR = +1, QUANTITY ='INCIDENT HEAT FLUX'
/&DEVC ID='I cabinet1 z=2.4', XYZ=0.6,13,2.4, IOR = +1, QUANTITY ='INCIDENT HEAT FLUX'

&DEVC ID='I cabinet2 z=1.6', XYZ=0.6,24,1.6, IOR = +1, QUANTITY ='INCIDENT HEAT FLUX'
&DEVC ID='I cabinet2 z=1.7', XYZ=0.6,24,1.7, IOR = +1, QUANTITY ='INCIDENT HEAT FLUX'
&DEVC ID='I cabinet2 z=1.8', XYZ=0.6,24,1.8, IOR = +1, QUANTITY ='INCIDENT HEAT FLUX'
&DEVC ID='I cabinet2 z=1.9', XYZ=0.6,24,1.9, IOR = +1, QUANTITY ='INCIDENT HEAT FLUX'
&DEVC ID='I cabinet2 z=2', XYZ=0.6,24,2.0, IOR = +1, QUANTITY ='INCIDENT HEAT FLUX'
&DEVC ID='I cabinet2 z=2.1', XYZ=0.6,24,2.1, IOR = +1, QUANTITY ='INCIDENT HEAT FLUX'
&DEVC ID='I cabinet2 z=2.2', XYZ=0.6,24,2.2, IOR = +1, QUANTITY ='INCIDENT HEAT FLUX'
&DEVC ID='I cabinet2 z=2.3', XYZ=0.6,24,2.3, IOR = +1, QUANTITY ='INCIDENT HEAT FLUX'

&DEVC ID='I cabinet3 z=1.6', XYZ=25.6,13,1.6, IOR = -1, QUANTITY ='INCIDENT HEAT FLUX'
&DEVC ID='I cabinet3 z=1.7', XYZ=25.6,13,1.7, IOR = -1, QUANTITY ='INCIDENT HEAT FLUX'
&DEVC ID='I cabinet3 z=1.8', XYZ=25.6,13,1.8, IOR = -1, QUANTITY ='INCIDENT HEAT FLUX'
&DEVC ID='I cabinet3 z=1.9', XYZ=25.6,13,1.9, IOR = -1, QUANTITY ='INCIDENT HEAT FLUX'
&DEVC ID='I cabinet3 z=2.0', XYZ=25.6,13,2.0, IOR = -1, QUANTITY ='INCIDENT HEAT FLUX'
&DEVC ID='I cabinet3 z=2.1', XYZ=25.6,13,2.1, IOR = -1, QUANTITY ='INCIDENT HEAT FLUX'
&DEVC ID='I cabinet3 z=2.2', XYZ=25.6,13,2.2, IOR = -1, QUANTITY ='INCIDENT HEAT FLUX'
&DEVC ID='I cabinet3 z=2.3', XYZ=25.6,13,2.3, IOR = -1, QUANTITY ='INCIDENT HEAT FLUX'

&DEVC ID='I cabinet4 z=1.6', XYZ=25.6,24,1.6, IOR = -1, QUANTITY ='INCIDENT HEAT FLUX'

&DEVC ID='I cabinet4 z=1.7', XYZ=25.6,24,1.7, IOR = -1, QUANTITY = 'INCIDENT HEAT FLUX'
&DEVC ID='I cabinet4 z=1.8', XYZ=25.6,24,1.8, IOR = -1, QUANTITY = 'INCIDENT HEAT FLUX'
&DEVC ID='I cabinet4 z=1.9', XYZ=25.6,24,1.9, IOR = -1, QUANTITY = 'INCIDENT HEAT FLUX'
&DEVC ID='I cabinet4 z=2', XYZ=25.6,24,2.0, IOR = -1, QUANTITY = 'INCIDENT HEAT FLUX'
&DEVC ID='I cabinet4 z=2.1', XYZ=25.6,24,2.1, IOR = -1, QUANTITY = 'INCIDENT HEAT FLUX'
&DEVC ID='I cabinet4 z=2.2', XYZ=25.6,24,2.2, IOR = -1, QUANTITY = 'INCIDENT HEAT FLUX'
&DEVC ID='I cabinet4 z=2.3', XYZ=25.6,24,2.3, IOR = -1, QUANTITY = 'INCIDENT HEAT FLUX'

/HEAT FLUXES FOR AIRPLANE

&DEVC ID = 'I Plane back1', XYZ = 11.6,6,1.6 , IOR = -3, QUANTITY = 'INCIDENT HEAT FLUX' /
&DEVC ID = 'I Plane back2', XYZ = 12,6,1.6 , IOR = -3, QUANTITY = 'INCIDENT HEAT FLUX' /
&DEVC ID = 'I Plane back3', XYZ = 12.5,6,1.6 , IOR = -3, QUANTITY = 'INCIDENT HEAT FLUX' /
&DEVC ID = 'I Plane back4', XYZ = 13,6,1.6 , IOR = -3, QUANTITY = 'INCIDENT HEAT FLUX' /
&DEVC ID = 'I Plane back5', XYZ = 13.5,6,1.6 , IOR = -3, QUANTITY = 'INCIDENT HEAT FLUX' /
&DEVC ID = 'I Plane back6', XYZ = 14.0,6,1.6 , IOR = -3, QUANTITY = 'INCIDENT HEAT FLUX' /

&DEVC ID = 'Fuselage 2', XYZ=13,5.6,1.6, QUANTITY = 'INCIDENT HEAT FLUX',IOR = -3/
&DEVC ID = 'Fuselage 3', XYZ=13,6,1.6, QUANTITY = 'INCIDENT HEAT FLUX',IOR = -3/
&DEVC ID = 'Fuselage 4', XYZ=13,6.6,1.6, QUANTITY = 'INCIDENT HEAT FLUX',IOR = -3/
&DEVC ID = 'Fuselage 5', XYZ=13,7,1.6, QUANTITY = 'INCIDENT HEAT FLUX',IOR = -3/
&DEVC ID = 'Fuselage 6', XYZ=13,7.6,1.6, QUANTITY = 'INCIDENT HEAT FLUX',IOR = -3/
&DEVC ID = 'Fuselage 7', XYZ=13,8,1.6, QUANTITY = 'INCIDENT HEAT FLUX',IOR = -3/
&DEVC ID = 'Fuselage 8', XYZ=13,8.6,1.6, QUANTITY = 'INCIDENT HEAT FLUX',IOR = -3/

&DEVC ID = 'Fuselage 9', XYZ=13,9,1.6, QUANTITY = 'INCIDENT HEAT
FLUX',IOR = -3/
&DEVC ID = 'Fuselage 10', XYZ=13,9.6,1.6, QUANTITY = 'INCIDENT HEAT
FLUX',IOR = -3/
&DEVC ID = 'Fuselage 11', XYZ=13,10,1.6, QUANTITY = 'INCIDENT HEAT
FLUX',IOR = -3/
&DEVC ID = 'Fuselage 12', XYZ=13,10.6,1.6, QUANTITY = 'INCIDENT HEAT
FLUX',IOR = -3/
&DEVC ID = 'Fuselage 13', XYZ=13,11,1.6, QUANTITY = 'INCIDENT HEAT
FLUX',IOR = -3/
&DEVC ID = 'Fuselage 14', XYZ=13,11.6,1.6, QUANTITY = 'INCIDENT HEAT
FLUX',IOR = -3/
&DEVC ID = 'Fuselage 15', XYZ=13,12.6,1.6, QUANTITY = 'INCIDENT HEAT
FLUX',IOR = -3/
&DEVC ID = 'Fuselage 16', XYZ=13,13,1.6, QUANTITY = 'INCIDENT HEAT
FLUX',IOR = -3/
&DEVC ID = 'Fuselage 17', XYZ=13,14,1.6, QUANTITY = 'INCIDENT HEAT
FLUX',IOR = -3/
&DEVC ID = 'Fuselage 18', XYZ=13,14.6,1.6, QUANTITY = 'INCIDENT HEAT
FLUX',IOR = -3/
&DEVC ID = 'Fuselage 19', XYZ=13,15,1.6, QUANTITY = 'INCIDENT HEAT
FLUX',IOR = -3/
&DEVC ID = 'Fuselage 20', XYZ=13,15.6,1.6, QUANTITY = 'INCIDENT HEAT
FLUX',IOR = -3/
&DEVC ID = 'Fuselage 21', XYZ=13,16,1.6, QUANTITY = 'INCIDENT HEAT
FLUX',IOR = -3/
&DEVC ID = 'Fuselage 22', XYZ=13,16.6,1.6, QUANTITY = 'INCIDENT HEAT
FLUX',IOR = -3/
&DEVC ID = 'Fuselage 23', XYZ=13,17,1.6, QUANTITY = 'INCIDENT HEAT
FLUX',IOR = -3/

&DEVC ID = 'Fuselage Lside1', XYZ=11.6,5.3,1.7, QUANTITY = 'INCIDENT HEAT
FLUX',IOR = -1/
&DEVC ID = 'Fuselage Lside2', XYZ=11.6,6.3,1.7, QUANTITY = 'INCIDENT HEAT
FLUX',IOR = -1/
&DEVC ID = 'Fuselage Lside3', XYZ=11.6,7.3,1.7, QUANTITY = 'INCIDENT HEAT
FLUX',IOR = -1/
&DEVC ID = 'Fuselage Lside4', XYZ=11.6,8.3,1.7, QUANTITY = 'INCIDENT HEAT
FLUX',IOR = -1/
&DEVC ID = 'Fuselage Lside5', XYZ=11.6,9.3,1.7, QUANTITY = 'INCIDENT HEAT
FLUX',IOR = -1/
&DEVC ID = 'Fuselage Lside6', XYZ=11.6,10.3,1.7, QUANTITY = 'INCIDENT HEAT
FLUX',IOR = -1/
&DEVC ID = 'Fuselage Lside7', XYZ=11.6,11.3,1.7, QUANTITY = 'INCIDENT HEAT
FLUX',IOR = -1/

&DEVC ID = 'Fuselage Lside8', XYZ=11.6,12.3,1.7, QUANTITY = 'INCIDENT HEAT FLUX',IOR = -1/
&DEVC ID = 'Fuselage Lside9', XYZ=11.6,13.3,1.7, QUANTITY = 'INCIDENT HEAT FLUX',IOR = -1/
&DEVC ID = 'Fuselage Lside10', XYZ=11.6,14.3,1.7, QUANTITY = 'INCIDENT HEAT FLUX',IOR = -1/
&DEVC ID = 'Fuselage Lside11', XYZ=11.6,15.3,1.7, QUANTITY = 'INCIDENT HEAT FLUX',IOR = -1/
&DEVC ID = 'Fuselage Lside12', XYZ=11.6,16.3,1.7, QUANTITY = 'INCIDENT HEAT FLUX',IOR = -1/

&DEVC ID = 'Fuselage Hside1', XYZ=11.6,5.3,2.7, QUANTITY = 'INCIDENT HEAT FLUX',IOR = -1/
&DEVC ID = 'Fuselage Hside2', XYZ=11.6,6.3,2.7, QUANTITY = 'INCIDENT HEAT FLUX',IOR = -1/
&DEVC ID = 'Fuselage Hside3', XYZ=11.6,7.3,2.7, QUANTITY = 'INCIDENT HEAT FLUX',IOR = -1/
&DEVC ID = 'Fuselage Hside4', XYZ=11.6,8.3,2.7, QUANTITY = 'INCIDENT HEAT FLUX',IOR = -1/
&DEVC ID = 'Fuselage Hside5', XYZ=11.6,9.3,2.7, QUANTITY = 'INCIDENT HEAT FLUX',IOR = -1/
&DEVC ID = 'Fuselage Hside6', XYZ=11.6,10.3,2.7, QUANTITY = 'INCIDENT HEAT FLUX',IOR = -1/
&DEVC ID = 'Fuselage Hside7', XYZ=11.6,11.3,2.7, QUANTITY = 'INCIDENT HEAT FLUX',IOR = -1/
&DEVC ID = 'Fuselage Hside8', XYZ=11.6,12.3,2.7, QUANTITY = 'INCIDENT HEAT FLUX',IOR = -1/
&DEVC ID = 'Fuselage Hside9', XYZ=11.6,13.3,2.7, QUANTITY = 'INCIDENT HEAT FLUX',IOR = -1/
&DEVC ID = 'Fuselage Hside10', XYZ=11.6,14.3,2.7, QUANTITY = 'INCIDENT HEAT FLUX',IOR = -1/
&DEVC ID = 'Fuselage Hside11', XYZ=11.6,15.3,2.7, QUANTITY = 'INCIDENT HEAT FLUX',IOR = -1/
&DEVC ID = 'Fuselage Hside12', XYZ=11.6,16.3,2.7, QUANTITY = 'INCIDENT HEAT FLUX',IOR = -1/

&DEVC ID = 'I Plane center2', XYZ =12,13,1.6 , IOR = -3, QUANTITY = 'INCIDENT HEAT FLUX' /
&DEVC ID = 'I Plane center3', XYZ =12.6,13,1.6 , IOR = -3, QUANTITY = 'INCIDENT HEAT FLUX' /
&DEVC ID = 'I Plane center4', XYZ =13,13,1.6 , IOR = -3, QUANTITY = 'INCIDENT HEAT FLUX' /
&DEVC ID = 'I Plane center5', XYZ =13.6,13,1.6 , IOR = -3, QUANTITY = 'INCIDENT HEAT FLUX' /

&DEVC ID = 'I Plane center6', XYZ = 14,13,1.6 , IOR = -3, QUANTITY = 'INCIDENT HEAT FLUX' /

&DEVC ID = 'I Plane nose2', XYZ = 12,20,2 , IOR = -3, QUANTITY = 'INCIDENT HEAT FLUX' /

&DEVC ID = 'I Plane nose3', XYZ = 12.5,20,2 , IOR = -3, QUANTITY = 'INCIDENT HEAT FLUX' /

&DEVC ID = 'I Plane nose4', XYZ = 13,20,2 , IOR = -3, QUANTITY = 'INCIDENT HEAT FLUX' /

&DEVC ID = 'I Plane nose5', XYZ = 13.5,20,2 , IOR = -3, QUANTITY = 'INCIDENT HEAT FLUX' /

&DEVC ID = 'LWing Sside1', XYZ=7.6,10,2.2 QUANTITY = 'INCIDENT HEAT FLUX', IOR = -1/

&DEVC ID = 'LWing X-11-2', XYZ=11,7,2 QUANTITY = 'INCIDENT HEAT FLUX', IOR = -3/

&DEVC ID = 'LWing X-11-3', XYZ=11,7.5,2 QUANTITY = 'INCIDENT HEAT FLUX', IOR = -3/

&DEVC ID = 'LWing X-11-4', XYZ=11,8,2 QUANTITY = 'INCIDENT HEAT FLUX', IOR = -3/

&DEVC ID = 'LWing X-11-5', XYZ=11,8.5,2 QUANTITY = 'INCIDENT HEAT FLUX', IOR = -3/

&DEVC ID = 'LWing X-11-6', XYZ=11,9,2 QUANTITY = 'INCIDENT HEAT FLUX', IOR = -3/

&DEVC ID = 'LWing X-11-7', XYZ=11,9.5,2 QUANTITY = 'INCIDENT HEAT FLUX', IOR = -3/

&DEVC ID = 'LWing X-11-8', XYZ=11,10,2 QUANTITY = 'INCIDENT HEAT FLUX', IOR = -3/

&DEVC ID = 'LWing X-11-9', XYZ=11,10.5,2 QUANTITY = 'INCIDENT HEAT FLUX', IOR = -3/

&DEVC ID = 'LWing X-11-10', XYZ=11,11,2 QUANTITY = 'INCIDENT HEAT FLUX', IOR = -3/

&DEVC ID = 'LWing X-11-11', XYZ=11,11.5,2 QUANTITY = 'INCIDENT HEAT FLUX', IOR = -3/

&DEVC ID = 'LWing X-11-12', XYZ=11,12,2 QUANTITY = 'INCIDENT HEAT FLUX', IOR = -3/

&DEVC ID = 'LWing X-11-13', XYZ=11,12.5,2 QUANTITY = 'INCIDENT HEAT FLUX', IOR = -3/

&DEVC ID = 'LWing X-11-14', XYZ=11,13,2 QUANTITY = 'INCIDENT HEAT FLUX', IOR = -3/

&DEVC ID = 'LWing X-11-15', XYZ=11,13.5,2 QUANTITY = 'INCIDENT HEAT FLUX', IOR = -3/

&DEVC ID = 'LWing X-10-1', XYZ=10,7.5,2 QUANTITY = 'INCIDENT HEAT FLUX', IOR = -3/
&DEVC ID = 'LWing X-10-2', XYZ=10,8,2 QUANTITY = 'INCIDENT HEAT FLUX', IOR = -3/
&DEVC ID = 'LWing X-10-3', XYZ=10,8.5,2 QUANTITY = 'INCIDENT HEAT FLUX', IOR = -3/
&DEVC ID = 'LWing X-10-4', XYZ=10,9,2 QUANTITY = 'INCIDENT HEAT FLUX', IOR = -3/
&DEVC ID = 'LWing X-10-5', XYZ=10,9.5,2 QUANTITY = 'INCIDENT HEAT FLUX', IOR = -3/
&DEVC ID = 'LWing X-10-6', XYZ=10,10,2 QUANTITY = 'INCIDENT HEAT FLUX', IOR = -3/
&DEVC ID = 'LWing X-10-7', XYZ=10,10.5,2 QUANTITY = 'INCIDENT HEAT FLUX', IOR = -3/
&DEVC ID = 'LWing X-10-8', XYZ=10,11,2 QUANTITY = 'INCIDENT HEAT FLUX', IOR = -3/
&DEVC ID = 'LWing X-10-9', XYZ=10,11.5,2 QUANTITY = 'INCIDENT HEAT FLUX', IOR = -3/
&DEVC ID = 'LWing X-10-10', XYZ=10,12,2 QUANTITY = 'INCIDENT HEAT FLUX', IOR = -3/
&DEVC ID = 'LWing X-10-11', XYZ=10,12.5,2 QUANTITY = 'INCIDENT HEAT FLUX', IOR = -3/

&DEVC ID = 'LWing X-7.8-2', XYZ=7.8,9.5,2 QUANTITY = 'INCIDENT HEAT FLUX', IOR = -3/
&DEVC ID = 'LWing X-7.8-3', XYZ=7.8,10,2 QUANTITY = 'INCIDENT HEAT FLUX', IOR = -3/
&DEVC ID = 'LWing X-7.8-4', XYZ=7.8,10.5,2 QUANTITY = 'INCIDENT HEAT FLUX', IOR = -3/
&DEVC ID = 'LWing X-7.8-5', XYZ=7.8,11,2 QUANTITY = 'INCIDENT HEAT FLUX', IOR = -3/

&DEVC ID ='I Plane LWing2', XYZ =7.7,10,2 , IOR = -3, QUANTITY = 'INCIDENT HEAT FLUX' /
&DEVC ID ='I Plane LWing3', XYZ =8,10,2 , IOR = -3, QUANTITY = 'INCIDENT HEAT FLUX' /
&DEVC ID ='I Plane LWing4', XYZ =8.5,10,2 , IOR = -3, QUANTITY = 'INCIDENT HEAT FLUX' /
&DEVC ID ='I Plane LWing5', XYZ =9,10,2 , IOR = -3, QUANTITY = 'INCIDENT HEAT FLUX' /
&DEVC ID ='I Plane LWing6', XYZ =9.5,10,2 , IOR = -3, QUANTITY = 'INCIDENT HEAT FLUX' /
&DEVC ID ='I Plane LWing7', XYZ =10,10,2 , IOR = -3, QUANTITY = 'INCIDENT HEAT FLUX' /

&DEVC ID = 'I Plane LWing8', XYZ = 10.5, 10, 2, IOR = -3, QUANTITY = 'INCIDENT HEAT FLUX' /

&DEVC ID = 'I Plane LWing9', XYZ = 11, 10, 2, IOR = -3, QUANTITY = 'INCIDENT HEAT FLUX' /

&DEVC ID = 'I Plane LWing9', XYZ = 11.5, 10, 2, IOR = -3, QUANTITY = 'INCIDENT HEAT FLUX' /

&DEVC ID = 'RWing X-15-2', XYZ = 15, 7.1, 2 QUANTITY = 'INCIDENT HEAT FLUX', IOR = -3/

&DEVC ID = 'RWing X-15-3', XYZ = 15, 7.5, 2 QUANTITY = 'INCIDENT HEAT FLUX', IOR = -3/

&DEVC ID = 'RWing X-15-4', XYZ = 15, 8, 2 QUANTITY = 'INCIDENT HEAT FLUX', IOR = -3/

&DEVC ID = 'RWing X-15-5', XYZ = 15, 8.5, 2 QUANTITY = 'INCIDENT HEAT FLUX', IOR = -3/

&DEVC ID = 'RWing X-15-6', XYZ = 15, 9, 2 QUANTITY = 'INCIDENT HEAT FLUX', IOR = -3/

&DEVC ID = 'RWing X-15-7', XYZ = 15, 9.5, 2 QUANTITY = 'INCIDENT HEAT FLUX', IOR = -3/

&DEVC ID = 'RWing X-15-8', XYZ = 15, 10, 2 QUANTITY = 'INCIDENT HEAT FLUX', IOR = -3/

&DEVC ID = 'RWing X-15-9', XYZ = 15, 10.5, 2 QUANTITY = 'INCIDENT HEAT FLUX', IOR = -3/

&DEVC ID = 'RWing X-15-10', XYZ = 15, 11, 2 QUANTITY = 'INCIDENT HEAT FLUX', IOR = -3/

&DEVC ID = 'RWing X-15-11', XYZ = 15, 11.5, 2 QUANTITY = 'INCIDENT HEAT FLUX', IOR = -3/

&DEVC ID = 'RWing X-15-12', XYZ = 15, 12, 2 QUANTITY = 'INCIDENT HEAT FLUX', IOR = -3/

&DEVC ID = 'RWing X-15-13', XYZ = 15, 12.5, 2 QUANTITY = 'INCIDENT HEAT FLUX', IOR = -3/

&DEVC ID = 'RWing X-15-14', XYZ = 15, 13, 2 QUANTITY = 'INCIDENT HEAT FLUX', IOR = -3/

&DEVC ID = 'RWing X-15-15', XYZ = 15, 13.5, 2 QUANTITY = 'INCIDENT HEAT FLUX', IOR = -3/

&DEVC ID = 'RWing X-17.5-2', XYZ = 17.5, 8.1, 2 QUANTITY = 'INCIDENT HEAT FLUX', IOR = -3/

&DEVC ID = 'RWing X-17.5-3', XYZ = 17.5, 8.5, 2 QUANTITY = 'INCIDENT HEAT FLUX', IOR = -3/

&DEVC ID = 'RWing X-17.5-4', XYZ = 17.5, 9, 2 QUANTITY = 'INCIDENT HEAT FLUX', IOR = -3/

&DEVC ID = 'RWing X-17.5-5', XYZ = 17.5, 9.5, 2 QUANTITY = 'INCIDENT HEAT FLUX', IOR = -3/

&DEVC ID = 'RWing X-17.5-6', XYZ=17.5,10,2 QUANTITY = 'INCIDENT HEAT FLUX',IOR = -3/
&DEVC ID = 'RWing X-17.5-7', XYZ=17.5,10.5,2 QUANTITY = 'INCIDENT HEAT FLUX',IOR = -3/
&DEVC ID = 'RWing X-17.5-8', XYZ=17.5,11,2 QUANTITY = 'INCIDENT HEAT FLUX',IOR = -3/
&DEVC ID = 'RWing X-17.5-9', XYZ=17.5,11.5,2 QUANTITY = 'INCIDENT HEAT FLUX',IOR = -3/
&DEVC ID = 'RWing X-17.5-10', XYZ=17.5,11.9,2 QUANTITY = 'INCIDENT HEAT FLUX',IOR = -3/

&DEVC ID = 'RWing X-18.2-2', XYZ=18.2,9.5,2 QUANTITY = 'INCIDENT HEAT FLUX',IOR = -3/
&DEVC ID = 'RWing X-18.2-3', XYZ=18.2,10,2 QUANTITY = 'INCIDENT HEAT FLUX',IOR = -3/
&DEVC ID = 'RWing X-18.2-4', XYZ=18.2,10.5,2 QUANTITY = 'INCIDENT HEAT FLUX',IOR = -3/
&DEVC ID = 'RWing X-18.2-5', XYZ=18.2,11,2 QUANTITY = 'INCIDENT HEAT FLUX',IOR = -3/

&DEVC ID ='I Plane RWing2', XYZ =14.5,10,2 , IOR = -3, QUANTITY = 'INCIDENT HEAT FLUX' /
&DEVC ID ='I Plane RWing3', XYZ =15,10,2 , IOR = -3, QUANTITY = 'INCIDENT HEAT FLUX' /
&DEVC ID ='I Plane RWing4', XYZ =15.5,10,2 , IOR = -3, QUANTITY = 'INCIDENT HEAT FLUX' /
&DEVC ID ='I Plane RWing5', XYZ =16,10,2 , IOR = -3, QUANTITY = 'INCIDENT HEAT FLUX' /
&DEVC ID ='I Plane RWing6', XYZ =16.5,10,2 , IOR = -3, QUANTITY = 'INCIDENT HEAT FLUX' /
&DEVC ID ='I Plane RWing7', XYZ =17,10,2 , IOR = -3, QUANTITY = 'INCIDENT HEAT FLUX' /
&DEVC ID ='I Plane RWing8', XYZ =17.5,10,2 , IOR = -3, QUANTITY = 'INCIDENT HEAT FLUX' /
&DEVC ID ='I Plane RWing9', XYZ =18,10,2, IOR = -3, QUANTITY = 'INCIDENT HEAT FLUX' /

/HEAT FLUXES AT SURFACE OF POOL

&DEVC ID='I Pool1', XYZ=6.5,1,0, IOR = +3, QUANTITY ='INCIDENT HEAT FLUX'/
&DEVC ID='I Pool2', XYZ=6.5,2,0, IOR = +3, QUANTITY ='INCIDENT HEAT FLUX'/

&DEVC ID='I Pool3', XYZ=6.5,3,0, IOR = +3, QUANTITY ='INCIDENT HEAT FLUX'/
&DEVC ID='I Pool4', XYZ=6.5,4,0, IOR = +3, QUANTITY ='INCIDENT HEAT FLUX'/
&DEVC ID='I Pool5', XYZ=6.5,5,0, IOR = +3, QUANTITY ='INCIDENT HEAT FLUX'/
&DEVC ID='I Pool6', XYZ=6.5,6,0, IOR = +3, QUANTITY ='INCIDENT HEAT FLUX'/
&DEVC ID='I Pool7', XYZ=6.5,7,0, IOR = +3, QUANTITY ='INCIDENT HEAT FLUX'/
&DEVC ID='I Pool8', XYZ=6.5,8,0, IOR = +3, QUANTITY ='INCIDENT HEAT FLUX'/
&DEVC ID='I Pool9', XYZ=6.5,9,0, IOR = +3, QUANTITY ='INCIDENT HEAT FLUX'/
&DEVC ID='I Pool10', XYZ=6.5,10,0, IOR = +3, QUANTITY ='INCIDENT HEAT FLUX'/
&DEVC ID='I Pool11', XYZ=6.5,11,0, IOR = +3, QUANTITY ='INCIDENT HEAT FLUX'/
&DEVC ID='I Pool12', XYZ=6.5,12,0, IOR = +3, QUANTITY ='INCIDENT HEAT FLUX'/
&DEVC ID='I Pool13', XYZ=6.5,13,0, IOR = +3, QUANTITY ='INCIDENT HEAT FLUX'/
&DEVC ID='I Pool14', XYZ=6.5,14,0, IOR = +3, QUANTITY ='INCIDENT HEAT FLUX'/
&DEVC ID='I Pool15', XYZ=6.5,15,0, IOR = +3, QUANTITY ='INCIDENT HEAT FLUX'/
&DEVC ID='I Pool16', XYZ=6.5,16,0, IOR = +3, QUANTITY ='INCIDENT HEAT FLUX'/
&DEVC ID='I Pool17', XYZ=6.5,17,0, IOR = +3, QUANTITY ='INCIDENT HEAT FLUX'/
&DEVC ID='I Pool18', XYZ=6.5,18,0, IOR = +3, QUANTITY ='INCIDENT HEAT FLUX'/
&DEVC ID='I Pool19', XYZ=6.5,19,0, IOR = +3, QUANTITY ='INCIDENT HEAT FLUX'/
&DEVC ID='I Pool20', XYZ=6.5,20,0, IOR = +3, QUANTITY ='INCIDENT HEAT FLUX'/
&DEVC ID='I Pool21', XYZ=6.5,21,0, IOR = +3, QUANTITY ='INCIDENT HEAT FLUX'/
&DEVC ID='I Pool22', XYZ=6.5,22,0, IOR = +3, QUANTITY ='INCIDENT HEAT FLUX'/
&DEVC ID='I Pool23', XYZ=6.5,23,0, IOR = +3, QUANTITY ='INCIDENT HEAT FLUX'/
&DEVC ID='I Pool24', XYZ=6.5,24,0, IOR = +3, QUANTITY ='INCIDENT HEAT FLUX'/

&DEVC ID='I Pool25', XYZ=6.5,25,0, IOR = +3, QUANTITY = 'INCIDENT HEAT FLUX'/

&DEVC ID='N Pool1', XYZ=6.5,1,0, IOR = +3, QUANTITY = 'NET HEAT FLUX'/
&DEVC ID='N Pool2', XYZ=6.5,2,0, IOR = +3, QUANTITY = 'NET HEAT FLUX'/
&DEVC ID='N Pool3', XYZ=6.5,3,0, IOR = +3, QUANTITY = 'NET HEAT FLUX'/
&DEVC ID='N Pool4', XYZ=6.5,4,0, IOR = +3, QUANTITY = 'NET HEAT FLUX'/
&DEVC ID='N Pool5', XYZ=6.5,5,0, IOR = +3, QUANTITY = 'NET HEAT FLUX'/
&DEVC ID='N Pool6', XYZ=6.5,6,0, IOR = +3, QUANTITY = 'NET HEAT FLUX'/
&DEVC ID='N Pool7', XYZ=6.5,7,0, IOR = +3, QUANTITY = 'NET HEAT FLUX'/
&DEVC ID='N Pool8', XYZ=6.5,8,0, IOR = +3, QUANTITY = 'NET HEAT FLUX'/
&DEVC ID='N Pool9', XYZ=6.5,9,0, IOR = +3, QUANTITY = 'NET HEAT FLUX'/
&DEVC ID='N Pool10', XYZ=6.5,10,0, IOR = +3, QUANTITY = 'NET HEAT FLUX'/
&DEVC ID='N Pool11', XYZ=6.5,11,0, IOR = +3, QUANTITY = 'NET HEAT FLUX'/
&DEVC ID='N Pool12', XYZ=6.5,12,0, IOR = +3, QUANTITY = 'NET HEAT FLUX'/
&DEVC ID='N Pool13', XYZ=6.5,13,0, IOR = +3, QUANTITY = 'NET HEAT FLUX'/
&DEVC ID='N Pool14', XYZ=6.5,14,0, IOR = +3, QUANTITY = 'NET HEAT FLUX'/
&DEVC ID='N Pool15', XYZ=6.5,15,0, IOR = +3, QUANTITY = 'NET HEAT FLUX'/
&DEVC ID='N Pool16', XYZ=6.5,16,0, IOR = +3, QUANTITY = 'NET HEAT FLUX'/
&DEVC ID='N Pool17', XYZ=6.5,17,0, IOR = +3, QUANTITY = 'NET HEAT FLUX'/
&DEVC ID='N Pool18', XYZ=6.5,18,0, IOR = +3, QUANTITY = 'NET HEAT FLUX'/
&DEVC ID='N Pool19', XYZ=6.5,19,0, IOR = +3, QUANTITY = 'NET HEAT FLUX'/
&DEVC ID='N Pool20', XYZ=6.5,20,0, IOR = +3, QUANTITY = 'NET HEAT FLUX'/
&DEVC ID='N Pool21', XYZ=6.5,21,0, IOR = +3, QUANTITY = 'NET HEAT FLUX'/
&DEVC ID='N Pool22', XYZ=6.5,22,0, IOR = +3, QUANTITY = 'NET HEAT FLUX'/
&DEVC ID='N Pool23', XYZ=6.5,23,0, IOR = +3, QUANTITY = 'NET HEAT FLUX'/
&DEVC ID='N Pool24', XYZ=6.5,24,0, IOR = +3, QUANTITY = 'NET HEAT FLUX'/
&DEVC ID='N Pool25', XYZ=6.5,25,0, IOR = +3, QUANTITY = 'NET HEAT FLUX'/

/ temperature measurements throughout the room

/FIRE TEMPERATURES

&DEVC ID = 'XY=6.5,13', XB=6.5,6.5,13,13,0,12 QUANTITY = 'TEMPERATURE',
POINTS = 61, TIME_HISTORY = .TRUE/

&DEVC ID = 'XY=2,13', XB=2,2,13,13,0,12 QUANTITY = 'TEMPERATURE',
POINTS = 61, TIME_HISTORY = .TRUE/

&DEVC ID = 'XY=10,13', XB=10,10,13,13,0,12 QUANTITY = 'TEMPERATURE',
POINTS = 61, TIME_HISTORY = .TRUE/

/CENTER OF ROOM AWAY FROM FIRE

&DEVC ID = 'XY=19.5,13', XB=19.5,19.5,13,13,0,12 QUANTITY =
'TEMPERATURE', POINTS = 61, TIME_HISTORY = .TRUE/

&DEVC ID = 'XY=15,13', XB=15,15,13,13,0,12 QUANTITY = 'TEMPERATURE',
POINTS = 61, TIME_HISTORY = .TRUE/

&DEVC ID = 'XY=23,13', XB=23,23,13,13,0,12 QUANTITY = 'TEMPERATURE',
POINTS = 61, TIME_HISTORY = .TRUE/

/CORNER ROOM TEMPERATURES

&DEVC ID = 'XY=0.5,25.5', XB=0.5,0.5,25.5,25.5,0,12 QUANTITY =
'TEMPERATURE', POINTS = 61, TIME_HISTORY = .TRUE/

&DEVC ID = 'XY=25.5,25.5', XB=25.5,25.5,25.5,25.5,0,12 QUANTITY =
'TEMPERATURE', POINTS = 61, TIME_HISTORY = .TRUE/

/Center of door opening temperature

&DEVC ID = 'XY=13,0', XB=13,13,0,0,0,7 QUANTITY = 'TEMPERATURE', POINTS
= 36, TIME_HISTORY = .TRUE/

/SLICE FILES

&SLCF PBX=0, QUANTITY='TEMPERATURE' /

&SLCF PBX=7, QUANTITY='TEMPERATURE' /

&SLCF PBX=13, QUANTITY='TEMPERATURE' /

&SLCF PBX=19, QUANTITY='TEMPERATURE' /

&SLCF PBX=6.5, QUANTITY='TEMPERATURE' /

&SLCF PBX=13, QUANTITY='TEMPERATURE' /

&SLCF PBX=20, QUANTITY='TEMPERATURE' /

&SLCF PBX=0, QUANTITY='MASS FRACTION', SPEC_ID='SPRINKLER WATER
VAPOR' /

&SLCF PBX=7, QUANTITY='MASS FRACTION', SPEC_ID='SPRINKLER WATER
VAPOR' /

&SLCF PBX=13, QUANTITY='MASS FRACTION', SPEC_ID='SPRINKLER WATER
VAPOR' /

&SLCF PBX=19, QUANTITY='MASS FRACTION', SPEC_ID='SPRINKLER WATER
VAPOR' /

&SLCF PBX=6.5, QUANTITY='MASS FRACTION', SPEC_ID='SPRINKLER
WATER VAPOR' /

&SLCF PBX=13, QUANTITY='MASS FRACTION', SPEC_ID='SPRINKLER WATER
VAPOR' /

&SLCF PBX=20, QUANTITY='MASS FRACTION', SPEC_ID='SPRINKLER WATER
VAPOR' /

&SLCF PBX=0, QUANTITY='VOLUME FRACTION', SPEC_ID='OXYGEN' /

&SLCF PBX=7, QUANTITY='VOLUME FRACTION', SPEC_ID='OXYGEN' /

&SLCF PBX=13, QUANTITY='VOLUME FRACTION', SPEC_ID='OXYGEN' /

&SLCF PBX=19, QUANTITY='VOLUME FRACTION', SPEC_ID='OXYGEN' /

&SLCF PBX=6.5, QUANTITY='VOLUME FRACTION', SPEC_ID='OXYGEN' /

&SLCF PBX=13, QUANTITY='VOLUME FRACTION', SPEC_ID='OXYGEN' /

&SLCF PBX=20, QUANTITY='VOLUME FRACTION', SPEC_ID='OXYGEN' /

```

/ACCUMULATED MASS OF WATER IN FIRE REGIONS
&DEVC ID='Mass Front Fire', XB=1.0,13.0,1.0,9.0,0.0,0.1, QUANTITY='AMPUA',
PART_ID='WaterK6', STATISTICS='SURFACE INTEGRAL' /
&DEVC ID='Mass Middle Fire', XB=1,13,9,17,0.0,0.1, QUANTITY='AMPUA',
PART_ID='WaterK6', STATISTICS='SURFACE INTEGRAL' /
&DEVC ID='Mass Back Fire', XB=1,13,17,25,0.0,0.1, QUANTITY='AMPUA',
PART_ID='WaterK6', STATISTICS='SURFACE INTEGRAL' /
&DEVC ID='Non-Fire Region', XB=13,26,0,26,0.0,0.1, QUANTITY='AMPUA',
PART_ID='WaterK6', STATISTICS='SURFACE INTEGRAL' /

```

&TAIL/

F.1 Nozzle A FDS Inputs

/GRID SELECTION dx = 0.1 in fire region and near field of nozzles

```

&MESH ID='Nozzle Mesh1', IJK=70,52,8,XB=0,7,0.8,6,11.2,12.0, MPI_PROCESS = 0/
dx = 0.1
&MESH ID='Nozzle Mesh2', IJK=70,70,8,XB=0,7,6,13,11.2,12.0, MPI_PROCESS = 1/
dx = 0.1
&MESH ID='Nozzle Mesh3', IJK=60,122,8,XB=7,13,0.8,13,11.2,12.0, MPI_PROCESS
= 2/ dx = 0.1
&MESH ID='Nozzle Mesh4', IJK=70,60,8,XB=0,7,13,19,11.2,12.0, MPI_PROCESS =
3/ dx = 0.1
&MESH ID='Nozzle Mesh5', IJK=70,70,8,XB=0,7,19,26,11.2,12.0, MPI_PROCESS =
4/ dx = 0.1
&MESH ID='Nozzle Mesh6', IJK=60,130,8,XB=7,13,13,26,11.2,12.0, MPI_PROCESS =
5/ dx = 0.1
&MESH ID='Bridge to non-fire side', IJK=5,126,4,XB=13,14,0.8,26,11.2,12.0,
MPI_PROCESS = 6/ dx = 0.2

&MESH ID='bridge to outdoor mesh', IJK=70,4,4,XB=0,14,0,0.8,11.2,12.0,
MPI_PROCESS = 6/ dx = 0.2
&MESH ID='fire mesh', IJK=35,38,15,XB=3,10,9.2,16.8,3.0,6.0, MPI_PROCESS = 6/
dx = 0.2
&MESH ID='Outdoors1', IJK=65,15,30,XB=0,26,-6,0,0.0,12.0, MPI_PROCESS = 6/ dx
= 0.4

&MESH ID='fire mesh', IJK=36,76,30,XB=3,6.6,9.2,16.8,0.0,3.0, MPI_PROCESS = 7/
dx = 0.1
&MESH ID='fire mesh', IJK=34,76,30,XB=6.6,10,9.2,16.8,0.0,3.0, MPI_PROCESS = 8/
dx = 0.1

```

&MESH ID='Mesh01', IJK=15,84,30,XB=0,3,9.2,26,0.0,6.0, MPI_PROCESS = 9/ dx = 0.2
&MESH ID='Mesh01', IJK=20,84,30,XB=10,14,9.2,26,0.0,6.0, MPI_PROCESS = 10/ dx = 0.2
&MESH ID='Mesh01', IJK=70,46,30,XB=0,14,0,9.2,0.0,6.0, MPI_PROCESS = 11/ dx = 0.2
&MESH ID='Mesh01', IJK=35,46,30,XB=3,10,16.8,26,0.0,6.0, MPI_PROCESS = 12/ dx = 0.2

&MESH ID='Mesh05', IJK=70,30,26,XB=0,14,0,6,6.0,11.2, MPI_PROCESS = 13/ dx = 0.2
&MESH ID='Mesh06', IJK=70,30,26,XB=0,14,6,12,6.0,11.2, MPI_PROCESS = 14/ dx = 0.2
&MESH ID='Mesh07', IJK=70,30,26,XB=0,14,12,18,6.0,11.2, MPI_PROCESS = 15/ dx = 0.2
&MESH ID='Mesh08', IJK=70,40,26,XB=0,14,18,26,6.0,11.2, MPI_PROCESS = 16/ dx = 0.2

&MESH ID='non-fire side1', IJK=30,65,30,XB=14,26,0,26,0.0,12.0, MPI_PROCESS = 17/ dx = 0.4

/WATER MIST NOZZLE

&PART ID='WaterK6',
SPEC_ID='SPRINKLER WATER VAPOR'
CNF_RAMP_ID='distribution',
MINIMUM_DIAMETER = 10,
MAXIMUM_DIAMETER = 250,
CHECK_DISTRIBUTION = .TRUE.
SAMPLING_FACTOR=800,
QUANTITIES(1:3) = 'PARTICLE TEMPERATURE', 'PARTICLE DIAMETER',
'PARTICLE AGE'/

&RAMP ID = 'distribution', T = 0
F = 0 /
&RAMP ID = 'distribution', T = 2.06706
F = 6.33e-05 /
&RAMP ID = 'distribution', T = 10.3376
F = 0.00126 /
&RAMP ID = 'distribution', T = 11.792
F = 0.0106/
&RAMP ID = 'distribution', T = 13.861
F = 0.0414 /
&RAMP ID = 'distribution', T = 15.9342

F = 0.0974 /
&RAMP ID = 'distribution', T = 18.8254
F = 0.209 /
&RAMP ID = 'distribution', T = 21.1427
F = 0.289 /
&RAMP ID = 'distribution', T = 24.2363
F = 0.362 /
&RAMP ID = 'distribution', T = 29.0541
F = 0.437 /
&RAMP ID = 'distribution', T = 35.4338
F = 0.512 /
&RAMP ID = 'distribution', T = 40.9248
F = 0.566 /
&RAMP ID = 'distribution', T = 48.1933
F = 0.631 /
&RAMP ID = 'distribution', T = 52.9636
F = 0.67 /
&RAMP ID = 'distribution', T = 60.1774
F = 0.72 /
&RAMP ID = 'distribution', T = 66.6121
F = 0.761 /
&RAMP ID = 'distribution', T = 73.2706
F = 0.793 /
&RAMP ID = 'distribution', T = 80.4283
F = 0.826 /
&RAMP ID = 'distribution', T = 85.6987
F = 0.847 /
&RAMP ID = 'distribution', T = 91.4687
F = 0.869 /
&RAMP ID = 'distribution', T = 95.6302
F = 0.882 /
&RAMP ID = 'distribution', T = 101.845
F = 0.897 /
&RAMP ID = 'distribution', T = 107.172
F = 0.911 /
&RAMP ID = 'distribution', T = 114.107
F = 0.926 /
&RAMP ID = 'distribution', T = 121.82
F = 0.936 /
&RAMP ID = 'distribution', T = 129.866
F = 0.948 /
&RAMP ID = 'distribution', T = 137.08
F = 0.957 /
&RAMP ID = 'distribution', T = 144.127
F = 0.964 /

&RAMP ID = 'distribution', T = 150.675
F = 0.969/
&RAMP ID = 'distribution', T = 159.665
F = 0.977 /
&RAMP ID = 'distribution', T = 165.325
F = 0.981 /
&RAMP ID = 'distribution', T = 173.371
F = 0.987 /
&RAMP ID = 'distribution', T = 180.252
F = 0.991/
&RAMP ID = 'distribution',T = 187.188
F = 0.994 /
&RAMP ID = 'distribution', T = 194.014
F = 0.998 /
&RAMP ID = 'distribution', T = 200, F = 1/

&PROP ID='WaterMist',
PART_ID='WaterK6',
OFFSET=0.3,
PARTICLES_PER_SECOND=10000,
K_FACTOR=5.6,
OPERATING_PRESSURE=16.0,
SPRAY_PATTERN_TABLE='WaterMist SPRAY_PATTERN_TABLE'/

&TABL ID='WaterMist SPRAY_PATTERN_TABLE', TABLE_DATA=5.0,85.0,-
40.0,40.0,10.0,0.1428/
&TABL ID='WaterMist SPRAY_PATTERN_TABLE',
TABLE_DATA=5.0,85.0,20.0,100.0,10.0,0.1428/
&TABL ID='WaterMist SPRAY_PATTERN_TABLE',
TABLE_DATA=5.0,85.0,80.0,160.0,10.0,0.1428/
&TABL ID='WaterMist SPRAY_PATTERN_TABLE',
TABLE_DATA=5.0,85.0,140.0,220.0,10.0,0.1428/
&TABL ID='WaterMist SPRAY_PATTERN_TABLE',
TABLE_DATA=5.0,85.0,200.0,280.0,10.0,0.1428/
&TABL ID='WaterMist SPRAY_PATTERN_TABLE',
TABLE_DATA=5.0,85.0,260.0,340.0,10.0,0.1428/
&TABL ID='WaterMist SPRAY_PATTERN_TABLE',
TABLE_DATA=0.0,40.0,0.0,360.0,10.0,0.1428/

&DEVC ID='NOZZLE K6_1', PROP_ID='WaterMist', XYZ=1,1,11.9, IOR = -3,
QUANTITY='TIME', SETPOINT=30/
&DEVC ID='NOZZLE K6_1', PROP_ID='WaterMist', XYZ=1,4,11.9, IOR = -3,
QUANTITY='TIME', SETPOINT=30/

&DEVC ID='NOZZLE K6_1', PROP_ID='WaterMist', XYZ=1,7,11.9, IOR = -3,
QUANTITY='TIME', SETPOINT=30/
&DEVC ID='NOZZLE K6_1', PROP_ID='WaterMist', XYZ=1,10,11.9, IOR = -3,
QUANTITY='TIME', SETPOINT=30/
&DEVC ID='NOZZLE K6_1', PROP_ID='WaterMist', XYZ=1,13,11.9, IOR = -3,
QUANTITY='TIME', SETPOINT=30/
&DEVC ID='NOZZLE K6_1', PROP_ID='WaterMist', XYZ=1,16,11.9, IOR = -3,
QUANTITY='TIME', SETPOINT=30/
&DEVC ID='NOZZLE K6_1', PROP_ID='WaterMist', XYZ=1,19,11.9, IOR = -3,
QUANTITY='TIME', SETPOINT=30/
&DEVC ID='NOZZLE K6_1', PROP_ID='WaterMist', XYZ=1,22,11.9, IOR = -3,
QUANTITY='TIME', SETPOINT=30/
&DEVC ID='NOZZLE K6_1', PROP_ID='WaterMist', XYZ=1,25,11.9, IOR = -3,
QUANTITY='TIME', SETPOINT=30/

&DEVC ID='NOZZLE K6_1', PROP_ID='WaterMist', XYZ=4,1,11.9, IOR = -3,
QUANTITY='TIME', SETPOINT=30/
&DEVC ID='NOZZLE K6_1', PROP_ID='WaterMist', XYZ=4,4,11.9, IOR = -3,
QUANTITY='TIME', SETPOINT=30/
&DEVC ID='NOZZLE K6_1', PROP_ID='WaterMist', XYZ=4,7,11.9, IOR = -3,
QUANTITY='TIME', SETPOINT=30/
&DEVC ID='NOZZLE K6_1', PROP_ID='WaterMist', XYZ=4,10,11.9, IOR = -3,
QUANTITY='TIME', SETPOINT=30/
&DEVC ID='NOZZLE K6_1', PROP_ID='WaterMist', XYZ=4,13,11.9, IOR = -3,
QUANTITY='TIME', SETPOINT=30/
&DEVC ID='NOZZLE K6_1', PROP_ID='WaterMist', XYZ=4,16,11.9, IOR = -3,
QUANTITY='TIME', SETPOINT=30/
&DEVC ID='NOZZLE K6_1', PROP_ID='WaterMist', XYZ=4,19,11.9, IOR = -3,
QUANTITY='TIME', SETPOINT=30/
&DEVC ID='NOZZLE K6_1', PROP_ID='WaterMist', XYZ=4,22,11.9, IOR = -3,
QUANTITY='TIME', SETPOINT=30/
&DEVC ID='NOZZLE K6_1', PROP_ID='WaterMist', XYZ=4,25,11.9, IOR = -3,
QUANTITY='TIME', SETPOINT=30/

&DEVC ID='NOZZLE K6_1', PROP_ID='WaterMist', XYZ=7,1,11.9, IOR = -3,
QUANTITY='TIME', SETPOINT=30/
&DEVC ID='NOZZLE K6_1', PROP_ID='WaterMist', XYZ=7,4,11.9, IOR = -3,
QUANTITY='TIME', SETPOINT=30/
&DEVC ID='NOZZLE K6_1', PROP_ID='WaterMist', XYZ=7,7,11.9, IOR = -3,
QUANTITY='TIME', SETPOINT=30/
&DEVC ID='NOZZLE K6_1', PROP_ID='WaterMist', XYZ=7,10,11.9, IOR = -3,
QUANTITY='TIME', SETPOINT=30/
&DEVC ID='NOZZLE K6_1', PROP_ID='WaterMist', XYZ=7,13,11.9, IOR = -3,
QUANTITY='TIME', SETPOINT=30/

&DEVC ID='NOZZLE K6_1', PROP_ID='WaterMist', XYZ=7,16,11.9, IOR = -3,
QUANTITY='TIME', SETPOINT=30/
&DEVC ID='NOZZLE K6_1', PROP_ID='WaterMist', XYZ=7,19,11.9, IOR = -3,
QUANTITY='TIME', SETPOINT=30/
&DEVC ID='NOZZLE K6_1', PROP_ID='WaterMist', XYZ=7,22,11.9, IOR = -3,
QUANTITY='TIME', SETPOINT=30/
&DEVC ID='NOZZLE K6_1', PROP_ID='WaterMist', XYZ=7,25,11.9, IOR = -3,
QUANTITY='TIME', SETPOINT=30/

&DEVC ID='NOZZLE K6_1', PROP_ID='WaterMist', XYZ=10,1,11.9, IOR = -3,
QUANTITY='TIME', SETPOINT=30/
&DEVC ID='NOZZLE K6_1', PROP_ID='WaterMist', XYZ=10,4,11.9, IOR = -3,
QUANTITY='TIME', SETPOINT=30/
&DEVC ID='NOZZLE K6_1', PROP_ID='WaterMist', XYZ=10,7,11.9, IOR = -3,
QUANTITY='TIME', SETPOINT=30/
&DEVC ID='NOZZLE K6_1', PROP_ID='WaterMist', XYZ=10,10,11.9, IOR = -3,
QUANTITY='TIME', SETPOINT=30/
&DEVC ID='NOZZLE K6_1', PROP_ID='WaterMist', XYZ=10,13,11.9, IOR = -3,
QUANTITY='TIME', SETPOINT=30/
&DEVC ID='NOZZLE K6_1', PROP_ID='WaterMist', XYZ=10,16,11.9, IOR = -3,
QUANTITY='TIME', SETPOINT=30/
&DEVC ID='NOZZLE K6_1', PROP_ID='WaterMist', XYZ=10,19,11.9, IOR = -3,
QUANTITY='TIME', SETPOINT=30/
&DEVC ID='NOZZLE K6_1', PROP_ID='WaterMist', XYZ=10,22,11.9, IOR = -3,
QUANTITY='TIME', SETPOINT=30/
&DEVC ID='NOZZLE K6_1', PROP_ID='WaterMist', XYZ=10,25,11.9, IOR = -3,
QUANTITY='TIME', SETPOINT=30/

&DEVC ID='NOZZLE K6_1', PROP_ID='WaterMist', XYZ=13,1,11.9, IOR = -3,
QUANTITY='TIME', SETPOINT=30/
&DEVC ID='NOZZLE K6_1', PROP_ID='WaterMist', XYZ=13,4,11.9, IOR = -3,
QUANTITY='TIME', SETPOINT=30/
&DEVC ID='NOZZLE K6_1', PROP_ID='WaterMist', XYZ=13,7,11.9, IOR = -3,
QUANTITY='TIME', SETPOINT=30/
&DEVC ID='NOZZLE K6_1', PROP_ID='WaterMist', XYZ=13,10,11.9, IOR = -3,
QUANTITY='TIME', SETPOINT=30/
&DEVC ID='NOZZLE K6_1', PROP_ID='WaterMist', XYZ=13,13,11.9, IOR = -3,
QUANTITY='TIME', SETPOINT=30/
&DEVC ID='NOZZLE K6_1', PROP_ID='WaterMist', XYZ=13,16,11.9, IOR = -3,
QUANTITY='TIME', SETPOINT=30/
&DEVC ID='NOZZLE K6_1', PROP_ID='WaterMist', XYZ=13,19,11.9, IOR = -3,
QUANTITY='TIME', SETPOINT=30/
&DEVC ID='NOZZLE K6_1', PROP_ID='WaterMist', XYZ=13,22,11.9, IOR = -3,
QUANTITY='TIME', SETPOINT=30/

&DEVC ID='NOZZLE K6_1', PROP_ID='WaterMist', XYZ=13,25,11.9, IOR = -3,
QUANTITY='TIME', SETPOINT=30/

F.2 Nozzle B FDS Inputs

/WATER MIST NOZZLE

&PART ID = 'WATERF-104',
SPEC_ID='SPRINKLER WATER VAPOR',
DIAMETER = 200
GAMMA_D=2
CHECK_DISTRIBUTION=.TRUE.
SAMPLING_FACTOR=200,
QUANTITIES(1:3) = 'PARTICLE TEMPERATURE', 'PARTICLE DIAMETER',
'PARTICLE AGE'/

&PROP ID = 'F-104 Nozzle',
OFFSET = 0.1,
PART_ID = 'WATERF-104',
PARTICLES_PER_SECOND = 20000.,
K_FACTOR = 10,
OPERATING_PRESSURE = 8,
SPRAY_PATTERN_TABLE = 'F-104 Characteristics'
SMOKEVIEW_ID = 'nozzle'/

&TABL ID = 'F-104 Characteristics', TABLE_DATA = 0,30,0,360,35,0.25 /
&TABL ID = 'F-104 Characteristics', TABLE_DATA = 15,75,-30,30,20,0.25/
&TABL ID = 'F-104 Characteristics', TABLE_DATA = 15,75,90,150,20,0.25 /
&TABL ID = 'F-104 Characteristics', TABLE_DATA = 15,75,210,270,20,0.25 /

&DEVC ID = 'Floor Mist Nozzle', XYZ = 1,1,0.2, ORIENTATION = 1,0,0, QUANTITY
='TIME', SETPOINT = 30., PROP_ID = 'F-104 Nozzle' /
&DEVC ID = 'Floor Mist Nozzle', XYZ = 1,3,0.2, ORIENTATION = 1,0,0, QUANTITY
='TIME', SETPOINT = 30., PROP_ID = 'F-104 Nozzle' /
&DEVC ID = 'Floor Mist Nozzle', XYZ = 1,5,0.2, ORIENTATION = 1,0,0, QUANTITY
='TIME', SETPOINT = 30., PROP_ID = 'F-104 Nozzle' /
&DEVC ID = 'Floor Mist Nozzle', XYZ = 1,7,0.2, ORIENTATION = 1,0,0, QUANTITY
='TIME', SETPOINT = 30., PROP_ID = 'F-104 Nozzle' /
&DEVC ID = 'Floor Mist Nozzle', XYZ = 1,9,0.2, ORIENTATION = 1,0,0, QUANTITY
='TIME', SETPOINT = 30., PROP_ID = 'F-104 Nozzle' /
&DEVC ID = 'Floor Mist Nozzle', XYZ = 1,11,0.2, ORIENTATION = 1,0,0, QUANTITY
='TIME', SETPOINT = 30., PROP_ID = 'F-104 Nozzle' /
&DEVC ID = 'Floor Mist Nozzle', XYZ = 1,13,0.2, ORIENTATION = 1,0,0, QUANTITY
='TIME', SETPOINT = 30., PROP_ID = 'F-104 Nozzle' /

&DEVC ID ='Floor Mist Nozzle', XYZ = 1,15,0.2, ORIENTATION = 1,0,0,QUANTITY = 'TIME',SETPOINT =30.,PROP_ID = 'F-104 Nozzle' /
&DEVC ID ='Floor Mist Nozzle', XYZ = 1,17,0.2, ORIENTATION = 1,0,0,QUANTITY = 'TIME',SETPOINT =30.,PROP_ID = 'F-104 Nozzle' /
&DEVC ID ='Floor Mist Nozzle', XYZ = 1,19,0.2, ORIENTATION = 1,0,0,QUANTITY = 'TIME',SETPOINT =30.,PROP_ID = 'F-104 Nozzle' /
&DEVC ID ='Floor Mist Nozzle', XYZ = 1,21,0.2, ORIENTATION = 1,0,0,QUANTITY = 'TIME',SETPOINT =30.,PROP_ID = 'F-104 Nozzle' /
&DEVC ID ='Floor Mist Nozzle', XYZ = 1,23,0.2, ORIENTATION = 1,0,0,QUANTITY = 'TIME',SETPOINT =30.,PROP_ID = 'F-104 Nozzle' /
&DEVC ID ='Floor Mist Nozzle', XYZ = 1,25,0.2, ORIENTATION = 1,0,0,QUANTITY = 'TIME',SETPOINT =30.,PROP_ID = 'F-104 Nozzle' /

&DEVC ID ='Floor Mist Nozzle', XYZ = 6.75,2,0.2, ORIENTATION = -1,0,0,QUANTITY = 'TIME',SETPOINT =30.,PROP_ID = 'F-104 Nozzle' /
&DEVC ID ='Floor Mist Nozzle', XYZ = 6.75,4,0.2, ORIENTATION = -1,0,0,QUANTITY = 'TIME',SETPOINT =30.,PROP_ID = 'F-104 Nozzle' /
&DEVC ID ='Floor Mist Nozzle', XYZ = 6.75,6,0.2, ORIENTATION = -1,0,0,QUANTITY = 'TIME',SETPOINT =30.,PROP_ID = 'F-104 Nozzle' /
&DEVC ID ='Floor Mist Nozzle', XYZ = 6.75,8,0.2, ORIENTATION = -1,0,0,QUANTITY = 'TIME',SETPOINT =30.,PROP_ID = 'F-104 Nozzle' /
&DEVC ID ='Floor Mist Nozzle', XYZ = 6.75,10,0.2, ORIENTATION = -1,0,0,QUANTITY = 'TIME',SETPOINT =30.,PROP_ID = 'F-104 Nozzle' /
&DEVC ID ='Floor Mist Nozzle', XYZ = 6.75,12,0.2, ORIENTATION = -1,0,0,QUANTITY = 'TIME',SETPOINT =30.,PROP_ID = 'F-104 Nozzle' /
&DEVC ID ='Floor Mist Nozzle', XYZ = 6.75,14,0.2, ORIENTATION = -1,0,0,QUANTITY = 'TIME',SETPOINT =30.,PROP_ID = 'F-104 Nozzle' /
&DEVC ID ='Floor Mist Nozzle', XYZ = 6.75,16,0.2, ORIENTATION = -1,0,0,QUANTITY = 'TIME',SETPOINT =30.,PROP_ID = 'F-104 Nozzle' /
&DEVC ID ='Floor Mist Nozzle', XYZ = 6.75,18,0.2, ORIENTATION = -1,0,0,QUANTITY = 'TIME',SETPOINT =30.,PROP_ID = 'F-104 Nozzle' /
&DEVC ID ='Floor Mist Nozzle', XYZ = 6.75,20,0.2, ORIENTATION = -1,0,0,QUANTITY = 'TIME',SETPOINT =30.,PROP_ID = 'F-104 Nozzle' /
&DEVC ID ='Floor Mist Nozzle', XYZ = 6.75,22,0.2, ORIENTATION = -1,0,0,QUANTITY = 'TIME',SETPOINT =30.,PROP_ID = 'F-104 Nozzle' /
&DEVC ID ='Floor Mist Nozzle', XYZ = 6.75,24,0.2, ORIENTATION = -1,0,0,QUANTITY = 'TIME',SETPOINT =30.,PROP_ID = 'F-104 Nozzle' /

&DEVC ID ='Floor Mist Nozzle', XYZ = 7.25,1,0.2, ORIENTATION = 1,0,0,QUANTITY = 'TIME',SETPOINT =30.,PROP_ID = 'F-104 Nozzle' /
&DEVC ID ='Floor Mist Nozzle', XYZ = 7.25,3,0.2, ORIENTATION = 1,0,0,QUANTITY = 'TIME',SETPOINT =30.,PROP_ID = 'F-104 Nozzle' /
&DEVC ID ='Floor Mist Nozzle', XYZ = 7.25,5,0.2, ORIENTATION = 1,0,0,QUANTITY = 'TIME',SETPOINT =30.,PROP_ID = 'F-104 Nozzle' /

&DEVC ID ='Floor Mist Nozzle', XYZ = 7.25,7,0.2, ORIENTATION = 1,0,0,QUANTITY ='TIME',SETPOINT =30.,PROP_ID = 'F-104 Nozzle' /
&DEVC ID ='Floor Mist Nozzle', XYZ = 7.25,9,0.2, ORIENTATION = 1,0,0,QUANTITY ='TIME',SETPOINT =30.,PROP_ID = 'F-104 Nozzle' /
&DEVC ID ='Floor Mist Nozzle', XYZ = 7.25,11,0.2, ORIENTATION = 1,0,0,QUANTITY ='TIME',SETPOINT =30.,PROP_ID = 'F-104 Nozzle' /
&DEVC ID ='Floor Mist Nozzle', XYZ = 7.25,13,0.2, ORIENTATION = 1,0,0,QUANTITY ='TIME',SETPOINT =30.,PROP_ID = 'F-104 Nozzle' /
&DEVC ID ='Floor Mist Nozzle', XYZ = 7.25,15,0.2, ORIENTATION = 1,0,0,QUANTITY ='TIME',SETPOINT =30.,PROP_ID = 'F-104 Nozzle' /
&DEVC ID ='Floor Mist Nozzle', XYZ = 7.25,17,0.2, ORIENTATION = 1,0,0,QUANTITY ='TIME',SETPOINT =30.,PROP_ID = 'F-104 Nozzle' /
&DEVC ID ='Floor Mist Nozzle', XYZ = 7.25,19,0.2, ORIENTATION = 1,0,0,QUANTITY ='TIME',SETPOINT =30.,PROP_ID = 'F-104 Nozzle' /
&DEVC ID ='Floor Mist Nozzle', XYZ = 7.25,21,0.2, ORIENTATION = 1,0,0,QUANTITY ='TIME',SETPOINT =30.,PROP_ID = 'F-104 Nozzle' /
&DEVC ID ='Floor Mist Nozzle', XYZ = 7.25,23,0.2, ORIENTATION = 1,0,0,QUANTITY ='TIME',SETPOINT =30.,PROP_ID = 'F-104 Nozzle' /
&DEVC ID ='Floor Mist Nozzle', XYZ = 7.25,25,0.2, ORIENTATION = 1,0,0,QUANTITY ='TIME',SETPOINT =30.,PROP_ID = 'F-104 Nozzle' /

&DEVC ID ='Floor Mist Nozzle', XYZ = 12.95,1,0.2, ORIENTATION = -1,0,0,QUANTITY ='TIME',SETPOINT =30.,PROP_ID = 'F-104 Nozzle' /
&DEVC ID ='Floor Mist Nozzle', XYZ = 12.95,3,0.2, ORIENTATION = -1,0,0,QUANTITY ='TIME',SETPOINT =30.,PROP_ID = 'F-104 Nozzle' /
&DEVC ID ='Floor Mist Nozzle', XYZ = 12.95,5,0.2, ORIENTATION = -1,0,0,QUANTITY ='TIME',SETPOINT =30.,PROP_ID = 'F-104 Nozzle' /
&DEVC ID ='Floor Mist Nozzle', XYZ = 12.95,7,0.2, ORIENTATION = -1,0,0,QUANTITY ='TIME',SETPOINT =30.,PROP_ID = 'F-104 Nozzle' /
&DEVC ID ='Floor Mist Nozzle', XYZ = 12.95,9,0.2, ORIENTATION = -1,0,0,QUANTITY ='TIME',SETPOINT =30.,PROP_ID = 'F-104 Nozzle' /
&DEVC ID ='Floor Mist Nozzle', XYZ = 12.95,11,0.2, ORIENTATION = -1,0,0,QUANTITY ='TIME',SETPOINT =30.,PROP_ID = 'F-104 Nozzle' /
&DEVC ID ='Floor Mist Nozzle', XYZ = 12.95,13,0.2, ORIENTATION = -1,0,0,QUANTITY ='TIME',SETPOINT =30.,PROP_ID = 'F-104 Nozzle' /
&DEVC ID ='Floor Mist Nozzle', XYZ = 12.95,15,0.2, ORIENTATION = -1,0,0,QUANTITY ='TIME',SETPOINT =30.,PROP_ID = 'F-104 Nozzle' /
&DEVC ID ='Floor Mist Nozzle', XYZ = 12.95,17,0.2, ORIENTATION = -1,0,0,QUANTITY ='TIME',SETPOINT =30.,PROP_ID = 'F-104 Nozzle' /
&DEVC ID ='Floor Mist Nozzle', XYZ = 12.95,19,0.2, ORIENTATION = -1,0,0,QUANTITY ='TIME',SETPOINT =30.,PROP_ID = 'F-104 Nozzle' /
&DEVC ID ='Floor Mist Nozzle', XYZ = 12.95,21,0.2, ORIENTATION = -1,0,0,QUANTITY ='TIME',SETPOINT =30.,PROP_ID = 'F-104 Nozzle' /
&DEVC ID ='Floor Mist Nozzle', XYZ = 12.95,23,0.2, ORIENTATION = -1,0,0,QUANTITY ='TIME',SETPOINT =30.,PROP_ID = 'F-104 Nozzle' /

&DEVC ID='Floor Mist Nozzle', XYZ = 12.95,25,0.2, ORIENTATION = -
1,0,0,QUANTITY='TIME',SETPOINT=30.,PROP_ID='F-104 Nozzle' /

F.2.1 Side Ignition Source Grid

/dx=0.05 - 0.4 mesh - fire originating under aircraft/ at edge of pool

&MESH ID='Mesh01', IJK=68,68,30,XB=6.4,9.8,9.6,13,0.0,1.5, MPI_PROCESS = 0/ dx
= 0.05

&MESH ID='Mesh01', IJK=68,68,30,XB=6.4,9.8,9.6,13,1.5,3.0, MPI_PROCESS = 1/ dx
= 0.05

&MESH ID='Mesh01', IJK=64,68,30,XB=9.8,13,9.6,13,0.0,1.5, MPI_PROCESS = 2/ dx
= 0.05

&MESH ID='Mesh01', IJK=64,68,30,XB=9.8,13,9.6,13,1.5,3.0, MPI_PROCESS = 3/ dx
= 0.05

&MESH ID='Mesh01', IJK=68,72,30,XB=6.4,9.8,13,16.6,0.0,1.5, MPI_PROCESS = 4/
dx = 0.05

&MESH ID='Mesh01', IJK=68,72,30,XB=6.4,9.8,13,16.6,1.5,3.0, MPI_PROCESS = 5/
dx = 0.05

&MESH ID='Mesh01', IJK=64,72,30,XB=9.8,13,13,16.6,0.0,1.5, MPI_PROCESS = 6/
dx = 0.05

&MESH ID='Mesh01', IJK=64,72,30,XB=9.8,13,13,16.6,1.5,3.0, MPI_PROCESS = 7/
dx = 0.05

&MESH ID='Mesh01', IJK=4,80,60,XB=6,6.4,9.2,17.2,0.0,6, MPI_PROCESS = 8/ dx =
0.1

&MESH ID='Mesh01', IJK=66,6,60,XB=6.4,13,16.6,17.2,0.0,6, MPI_PROCESS = 8/ dx
= 0.1

&MESH ID='Mesh01', IJK=66,4,60,XB=6.4,13,9.2,9.6,0.0,6, MPI_PROCESS = 8/ dx =
0.1

&MESH ID='Mesh01', IJK=66,70,30,XB=6.4,13,9.6,16.6,3.0,6, MPI_PROCESS = 8/ dx
= 0.1

&MESH ID='Mesh01', IJK=4,80,60,XB=13,13.4,9.2,17.2,0.0,6, MPI_PROCESS = 8/ dx
= 0.1

&MESH ID='Mesh01', IJK=40,40,30,XB=6,14,9.2,17.2,6,12, MPI_PROCESS = 8/ dx =
0.2

&MESH ID='Mesh01', IJK=3,40,30,XB=13.4,14,9.2,17.2,0,6, MPI_PROCESS = 8/ dx =
0.2

&MESH ID='Outdoors1', IJK=65,15,30,XB=0,26,-6,0,0.0,12.0, MPI_PROCESS = 8/ dx
= 0.4

&MESH ID='Mesh01', IJK=30,65,60,XB=0,6,0,13,0.0,12, MPI_PROCESS = 9/ dx = 0.2

&MESH ID='Mesh01', IJK=30,65,60,XB=0,6,13,26,0.0,12, MPI_PROCESS = 10/ dx = 0.2
&MESH ID='Mesh01', IJK=40,46,60,XB=6,14,0,9.2,0.0,12, MPI_PROCESS = 11/ dx = 0.2
&MESH ID='Mesh01', IJK=40,44,60,XB=6,14,17.2,26,0.0,12, MPI_PROCESS = 12/ dx = 0.2

&MESH ID='non-fire side1', IJK=30,65,30,XB=14,26,0,26,0.0,12.0, MPI_PROCESS = 13/ dx = 0.4

F.2.2 Center ignition source Grid

/dx=0.05-0.4 - center originating fire

&MESH ID='non-fire side1', IJK=60,44,56, XB=1,4,8.8,11,0.0,2.8, MPI_PROCESS = 0/ dx = 0.05
&MESH ID='non-fire side1', IJK=60,44,56, XB=1,4,11,13.2,0.0,2.8, MPI_PROCESS = 1/ dx = 0.05
&MESH ID='non-fire side1', IJK=60,44,56, XB=4,7,8.8,11,0.0,2.8, MPI_PROCESS =2/ dx = 0.05
&MESH ID='non-fire side1', IJK=60,44,56, XB=4,7,11,13.2,0.0,2.8, MPI_PROCESS =3/ dx = 0.05
&MESH ID='non-fire side1', IJK=60,44,56, XB=1,4,13.2,15.4,0.0,2.8, MPI_PROCESS =4/ dx = 0.05
&MESH ID='non-fire side1', IJK=60,44,56, XB=1,4,15.4,17.6,0.0,2.8, MPI_PROCESS =5/ dx = 0.05
&MESH ID='non-fire side1', IJK=60,44,56, XB=4,7,13.2,15.4,0.0,2.8, MPI_PROCESS =6/ dx = 0.05
&MESH ID='non-fire side1', IJK=60,44,56, XB=4,7,15.4,17.6,0.0,2.8, MPI_PROCESS =7/ dx = 0.05
&MESH ID='non-fire side1', IJK=60,44,56, XB=7,10,8.8,11,0.0,2.8, MPI_PROCESS =8/ dx = 0.05
&MESH ID='non-fire side1', IJK=60,44,56, XB=7,10,11,13.2,0.0,2.8, MPI_PROCESS =9/ dx = 0.05
&MESH ID='non-fire side1', IJK=60,44,56, XB=10,13,8.8,11,0.0,2.8, MPI_PROCESS =10/ dx = 0.05
&MESH ID='non-fire side1', IJK=60,44,56, XB=10,13,11,13.2,0.0,2.8, MPI_PROCESS =11/ dx = 0.05
&MESH ID='non-fire side1', IJK=60,44,56, XB=7,10,13.2,15.4,0.0,2.8, MPI_PROCESS =12/ dx = 0.05
&MESH ID='non-fire side1', IJK=60,44,56, XB=7,10,15.4,17.6,0.0,2.8, MPI_PROCESS =13/ dx = 0.05
&MESH ID='non-fire side1', IJK=60,44,56, XB=10,13,13.2,15.4,0.0,2.8, MPI_PROCESS =14/ dx = 0.05

&MESH ID='non-fire side1', IJK=60,44,56, XB=10,13,15.4,17.6,0.0,2.8,
MPI_PROCESS =15/ dx = 0.05

&MESH ID='non-fire side1', IJK=10,88,28, XB=0,1,8.8,17.6,0.0,2.8, MPI_PROCESS
=16/ dx = 0.1

&MESH ID='non-fire side1', IJK=4,88,28, XB=13,13.4,8.8,17.6,0.0,2.8, MPI_PROCESS
=16/ dx = 0.1

&MESH ID='non-fire side1', IJK=3,52,28, XB=13.4,14,8,18.4,0.0,2.8, MPI_PROCESS
=16/ dx = 0.2

&MESH ID='non-fire side1', IJK=134,8,28, XB=0,13.4,8,8.8,0.0,2.8, MPI_PROCESS
=16/dx = 0.1

&MESH ID='non-fire side1', IJK=134,8,28, XB=0,13.4,17.6,18.4,0.0,2.8,
MPI_PROCESS =16/ dx = 0.1

&MESH ID='non-fire side1', IJK=5,44,16, XB=0,1,8.8,17.6,2.8,6.0, MPI_PROCESS
=16/ dx = 0.2

&MESH ID='non-fire side1', IJK=5,44,16, XB=13,14,8.8,17.6,2.8,6.0, MPI_PROCESS
=16/ dx = 0.2

&MESH ID='non-fire side1', IJK=70,4,16, XB=0,14,8,8.8,2.8,6.0, MPI_PROCESS =16/
dx = 0.2

&MESH ID='non-fire side1', IJK=70,4,16, XB=0,14,17.6,18.4,2.8,6.0, MPI_PROCESS
=16/ dx = 0.2

&MESH ID='non-fire side1', IJK=70,4,14, XB=0,14,7.2,8,0,2.8, MPI_PROCESS =16/
dx = 0.2

&MESH ID='non-fire side1', IJK=70,4,14, XB=0,14,18.4,19.2,0,2.8, MPI_PROCESS
=16/ dx = 0.2

&MESH ID='non-fire side1', IJK=35,18,7, XB=0,14,0,7.2,0,2.8, MPI_PROCESS =16/
dx = 0.4

&MESH ID='non-fire side1', IJK=35,17,7, XB=0,14,19.2,26,0,2.8, MPI_PROCESS =16/
dx = 0.4

&MESH ID='non-fire side1', IJK=35,20,23, XB=0,14,0,8,2.8,12, MPI_PROCESS =16/
dx = 0.4

&MESH ID='non-fire side1', IJK=35,19,23, XB=0,14,18.4,26,2.8,12, MPI_PROCESS
=16/ dx = 0.4

&MESH ID='non-fire side1', IJK=60,88,32, XB=1,7,8.8,17.6,2.8,6, MPI_PROCESS
=17/ dx = 0.1

&MESH ID='non-fire side1', IJK=60,88,32, XB=7,13,8.8,17.6,2.8,6, MPI_PROCESS
=18/ dx = 0.1

&MESH ID='non-fire side1', IJK=30,65,30,XB=14,26,0,26,0.0,12.0, MPI_PROCESS
=19/ dx = 0.4

&MESH ID='Outdoors1', IJK=65,15,30,XB=0,26,-6,0,0.0,12.0, MPI_PROCESS =19/ dx = 0.4

&MESH ID='non-fire side1', IJK=70,52,30, XB=0,14,8,18.4,6.0,12, MPI_PROCESS =19/ dx = 0.2

F.3 Nozzle C FDS Inputs

/GRID SELECTION - dx =0.2 - 0.4 mesh

&MESH ID='Mesh01', IJK=40,30,30,XB=0,8,0,6,0.0,6.0/ dx = 0.2

&MESH ID='Mesh02', IJK=40,30,30,XB=0,8,6,12,0.0,6.0/ dx = 0.2

&MESH ID='Mesh03', IJK=40,30,30,XB=0,8,12,18,0.0,6.0/ dx = 0.2

&MESH ID='Mesh01', IJK=50,30,30,XB=8,18,0,6,0.0,6.0/ dx = 0.2

&MESH ID='Mesh02', IJK=50,30,30,XB=8,18,6,12,0.0,6.0/ dx = 0.2

&MESH ID='Mesh03', IJK=50,30,30,XB=8,18,12,18,0.0,6.0/ dx = 0.2

&MESH ID='Mesh01', IJK=40,30,30,XB=0,8,0,6,6.0,12.0/ dx = 0.2

&MESH ID='Mesh02', IJK=40,30,30,XB=0,8,6,12,6.0,12.0/ dx = 0.2

&MESH ID='Mesh03', IJK=40,30,30,XB=0,8,12,18,6.0,12.0/ dx = 0.2

&MESH ID='Mesh04', IJK=40,40,30,XB=0,8,18,26,6.0,12.0/ dx = 0.2

&MESH ID='Mesh01', IJK=50,30,30,XB=8,18,0,6,6.0,12.0/ dx = 0.2

&MESH ID='Mesh02', IJK=50,30,30,XB=8,18,6,12,6.0,12.0/ dx = 0.2

&MESH ID='Mesh03', IJK=50,30,30,XB=8,18,12,18,6.0,12.0/ dx = 0.2

&MESH ID='Mesh04', IJK=50,40,30,XB=8,18,18,26,6.0,12.0/ dx = 0.2

&MESH ID='Mesh04', IJK=20,20,15,XB=0,8,18,26,0.0,6.0/ dx = 0.4

&MESH ID='Mesh04', IJK=25,20,15,XB=8,18,18,26,0.0,6.0/ dx = 0.4

&MESH ID='non-fire side1', IJK=20,65,30,XB=18,26,0,26,0.0,12.0/ dx = 0.4

&MESH ID='Outdoors1', IJK=65,15,30,XB=0,26,-6,0,0.0,12.0/ dx = 0.4

/WATER MIST NOZZLES

&PART ID = 'Marioff Water Droplets',

 SPEC_ID='SPRINKLER WATER VAPOR',

 DIAMETER = 79

 GAMMA_D = 2.26

 MINIMUM_DIAMETER = 1

 MAXIMUM_DIAMETER = 250

 CHECK_DISTRIBUTION = .TRUE.

 SAMPLING_FACTOR=800,

 QUANTITIES(1:3) = 'PARTICLE TEMPERATURE', 'PARTICLE DIAMETER',

'PARTICLE AGE'/

&PROP ID='Marioff Characteristics ',
PART_ID='Marioff Water Droplets',
OFFSET=0.1,
PARTICLES_PER_SECOND=2222,
K_FACTOR=0.433,
OPERATING_PRESSURE=70.0,
SPRAY_PATTERN_TABLE='Marioff table'
SMOKEVIEW_ID='nozzle'/

&TABL ID='Marioff table', TABLE_DATA = 0,12,0,360,118,1 /

/x = 1 row

/one single nozzle created from 9 micro nozzles

&DEVC ID='Mist Nozzle 1', XYZ = 1,1,11.9, ORIENTATION = 0,0,-1, PROP_ID =
'Marioff Characteristics', QUANTITY='TIME', SETPOINT =30. /
&DEVC ID='Mist Nozzle 2', XYZ = 1,1,11.9, ORIENTATION = 0.5,0,-.866, PROP_ID
= 'Marioff Characteristics', QUANTITY='TIME', SETPOINT =30. /
&DEVC ID='Mist Nozzle 3', XYZ = 1,1,11.9, ORIENTATION = -0.5,0,-.866,PROP_ID
= 'Marioff Characteristics', QUANTITY='TIME', SETPOINT =30. /
&DEVC ID='Mist Nozzle 4', XYZ = 1,1,11.9, ORIENTATION = 0.3536,0.3563,-
.866,PROP_ID = 'Marioff Characteristics', QUANTITY='TIME', SETPOINT =30. /
&DEVC ID='Mist Nozzle 5', XYZ = 1,1,11.9, ORIENTATION = -0.3536,0.3563,-.866,
PROP_ID = 'Marioff Characteristics', QUANTITY='TIME', SETPOINT =30./
&DEVC ID='Mist Nozzle 6', XYZ = 1,1,11.9, ORIENTATION = 0.3536,-0.3536,-.866,
PROP_ID = 'Marioff Characteristics', QUANTITY='TIME', SETPOINT =30./
&DEVC ID='Mist Nozzle 7', XYZ = 1,1,11.9, ORIENTATION = -0.3536,-0.3536,-
.866,PROP_ID = 'Marioff Characteristics', QUANTITY='TIME', SETPOINT =30. /
&DEVC ID='Mist Nozzle 8', XYZ = 1,1,11.9, ORIENTATION = 0,0.5,-.866, PROP_ID
= 'Marioff Characteristics', QUANTITY='TIME', SETPOINT =30. /
&DEVC ID='Mist Nozzle 9', XYZ = 1,1,11.9, ORIENTATION = 0,-0.5,-.866,
PROP_ID = 'Marioff Characteristics', QUANTITY='TIME', SETPOINT =30. /

&DEVC ID='Mist Nozzle 1', XYZ = 1,4,11.9, ORIENTATION = 0,0,-1, PROP_ID =
'Marioff Characteristics', QUANTITY='TIME', SETPOINT =30. /
&DEVC ID='Mist Nozzle 2', XYZ = 1,4,11.9, ORIENTATION = 0.5,0,-.866, PROP_ID
= 'Marioff Characteristics', QUANTITY='TIME', SETPOINT =30./
&DEVC ID='Mist Nozzle 3', XYZ = 1,4,11.9, ORIENTATION = -0.5,0,-.866,PROP_ID
= 'Marioff Characteristics', QUANTITY='TIME', SETPOINT =30. /
&DEVC ID='Mist Nozzle 4', XYZ = 1,4,11.9, ORIENTATION = 0.3536,0.3563,-
.866,PROP_ID = 'Marioff Characteristics', QUANTITY='TIME', SETPOINT =30. /
&DEVC ID='Mist Nozzle 5', XYZ = 1,4,11.9, ORIENTATION = -0.3536,0.3563,-.866,
PROP_ID = 'Marioff Characteristics', QUANTITY='TIME', SETPOINT =30./
&DEVC ID='Mist Nozzle 6', XYZ = 1,4,11.9, ORIENTATION = 0.3536,-0.3536,-.866,
PROP_ID = 'Marioff Characteristics', QUANTITY='TIME', SETPOINT =30./

&DEVC ID = 'Mist Nozzle 7', XYZ = 1,4,11.9, ORIENTATION = -0.3536,-0.3536,-.866,PROP_ID = 'Marioff Characteristics', QUANTITY = 'TIME', SETPOINT = 30. /
&DEVC ID = 'Mist Nozzle 8', XYZ = 1,4,11.9, ORIENTATION = 0,0.5,-.866, PROP_ID = 'Marioff Characteristics', QUANTITY = 'TIME', SETPOINT = 30. /
&DEVC ID = 'Mist Nozzle 9', XYZ = 1,4,11.9, ORIENTATION = 0,-0.5,-.866, PROP_ID = 'Marioff Characteristics', QUANTITY = 'TIME', SETPOINT = 30. /

&DEVC ID = 'Mist Nozzle 1', XYZ = 1,7,11.9, ORIENTATION = 0,0,-1, PROP_ID = 'Marioff Characteristics', QUANTITY = 'TIME', SETPOINT = 30. /
&DEVC ID = 'Mist Nozzle 2', XYZ = 1,7,11.9, ORIENTATION = 0.5,0,-.866, PROP_ID = 'Marioff Characteristics', QUANTITY = 'TIME', SETPOINT = 30. /
&DEVC ID = 'Mist Nozzle 3', XYZ = 1,7,11.9, ORIENTATION = -0.5,0,-.866,PROP_ID = 'Marioff Characteristics', QUANTITY = 'TIME', SETPOINT = 30. /
&DEVC ID = 'Mist Nozzle 4', XYZ = 1,7,11.9, ORIENTATION = 0.3536,0.3563,-.866,PROP_ID = 'Marioff Characteristics', QUANTITY = 'TIME', SETPOINT = 30. /
&DEVC ID = 'Mist Nozzle 5', XYZ = 1,7,11.9, ORIENTATION = -0.3536,0.3536,-.866, PROP_ID = 'Marioff Characteristics', QUANTITY = 'TIME', SETPOINT = 30./
&DEVC ID = 'Mist Nozzle 6', XYZ = 1,7,11.9, ORIENTATION = 0.3536,-0.3536,-.866, PROP_ID = 'Marioff Characteristics', QUANTITY = 'TIME', SETPOINT = 30./
&DEVC ID = 'Mist Nozzle 7', XYZ = 1,7,11.9, ORIENTATION = -0.3536,-0.3536,-.866,PROP_ID = 'Marioff Characteristics', QUANTITY = 'TIME', SETPOINT = 30. /
&DEVC ID = 'Mist Nozzle 8', XYZ = 1,7,11.9, ORIENTATION = 0,0.5,-.866, PROP_ID = 'Marioff Characteristics', QUANTITY = 'TIME', SETPOINT = 30. /
&DEVC ID = 'Mist Nozzle 9', XYZ = 1,7,11.9, ORIENTATION = 0,-0.5,-.866, PROP_ID = 'Marioff Characteristics', QUANTITY = 'TIME', SETPOINT = 30. /

&DEVC ID = 'Mist Nozzle 1', XYZ = 1,10,11.9, ORIENTATION = 0,0,-1, PROP_ID = 'Marioff Characteristics', QUANTITY = 'TIME', SETPOINT = 30. /
&DEVC ID = 'Mist Nozzle 2', XYZ = 1,10,11.9, ORIENTATION = 0.5,0,-.866, PROP_ID = 'Marioff Characteristics', QUANTITY = 'TIME', SETPOINT = 30. /
&DEVC ID = 'Mist Nozzle 3', XYZ = 1,10,11.9, ORIENTATION = -0.5,0,-.866,PROP_ID = 'Marioff Characteristics', QUANTITY = 'TIME', SETPOINT = 30. /
&DEVC ID = 'Mist Nozzle 4', XYZ = 1,10,11.9, ORIENTATION = 0.3536,0.3563,-.866,PROP_ID = 'Marioff Characteristics', QUANTITY = 'TIME', SETPOINT = 30. /
&DEVC ID = 'Mist Nozzle 5', XYZ = 1,10,11.9, ORIENTATION = -0.3536,0.3536,-.866, PROP_ID = 'Marioff Characteristics', QUANTITY = 'TIME', SETPOINT = 30./
&DEVC ID = 'Mist Nozzle 6', XYZ = 1,10,11.9, ORIENTATION = 0.3536,-0.3536,-.866, PROP_ID = 'Marioff Characteristics', QUANTITY = 'TIME', SETPOINT = 30./
&DEVC ID = 'Mist Nozzle 7', XYZ = 1,10,11.9, ORIENTATION = -0.3536,-0.3536,-.866,PROP_ID = 'Marioff Characteristics', QUANTITY = 'TIME', SETPOINT = 30. /
&DEVC ID = 'Mist Nozzle 8', XYZ = 1,10,11.9, ORIENTATION = 0,0.5,-.866, PROP_ID = 'Marioff Characteristics', QUANTITY = 'TIME', SETPOINT = 30. /
&DEVC ID = 'Mist Nozzle 9', XYZ = 1,10,11.9, ORIENTATION = 0,-0.5,-.866, PROP_ID = 'Marioff Characteristics', QUANTITY = 'TIME', SETPOINT = 30. /

&DEVC ID = 'Mist Nozzle 1', XYZ = 1,13,11.9, ORIENTATION = 0,0,-1, PROP_ID = 'Marioff Characteristics', QUANTITY = 'TIME', SETPOINT = 30. /
&DEVC ID = 'Mist Nozzle 2', XYZ = 1,13,11.9, ORIENTATION = 0.5,0,-.866, PROP_ID = 'Marioff Characteristics', QUANTITY = 'TIME', SETPOINT = 30. /
&DEVC ID = 'Mist Nozzle 3', XYZ = 1,13,11.9, ORIENTATION = -0.5,0,-.866, PROP_ID = 'Marioff Characteristics', QUANTITY = 'TIME', SETPOINT = 30. /
&DEVC ID = 'Mist Nozzle 4', XYZ = 1,13,11.9, ORIENTATION = 0.3536,0.3563,-.866, PROP_ID = 'Marioff Characteristics', QUANTITY = 'TIME', SETPOINT = 30. /
&DEVC ID = 'Mist Nozzle 5', XYZ = 1,13,11.9, ORIENTATION = -0.3536,0.3536,-.866, PROP_ID = 'Marioff Characteristics', QUANTITY = 'TIME', SETPOINT = 30. /
&DEVC ID = 'Mist Nozzle 6', XYZ = 1,13,11.9, ORIENTATION = 0.3536,-0.3536,-.866, PROP_ID = 'Marioff Characteristics', QUANTITY = 'TIME', SETPOINT = 30. /
&DEVC ID = 'Mist Nozzle 7', XYZ = 1,13,11.9, ORIENTATION = -0.3536,-0.3536,-.866, PROP_ID = 'Marioff Characteristics', QUANTITY = 'TIME', SETPOINT = 30. /
&DEVC ID = 'Mist Nozzle 8', XYZ = 1,13,11.9, ORIENTATION = 0,0.5,-.866, PROP_ID = 'Marioff Characteristics', QUANTITY = 'TIME', SETPOINT = 30. /
&DEVC ID = 'Mist Nozzle 9', XYZ = 1,13,11.9, ORIENTATION = 0,-0.5,-.866, PROP_ID = 'Marioff Characteristics', QUANTITY = 'TIME', SETPOINT = 30. /

&DEVC ID = 'Mist Nozzle 1', XYZ = 1,16,11.9, ORIENTATION = 0,0,-1, PROP_ID = 'Marioff Characteristics', QUANTITY = 'TIME', SETPOINT = 30. /
&DEVC ID = 'Mist Nozzle 2', XYZ = 1,16,11.9, ORIENTATION = 0.5,0,-.866, PROP_ID = 'Marioff Characteristics', QUANTITY = 'TIME', SETPOINT = 30. /
&DEVC ID = 'Mist Nozzle 3', XYZ = 1,16,11.9, ORIENTATION = -0.5,0,-.866, PROP_ID = 'Marioff Characteristics', QUANTITY = 'TIME', SETPOINT = 30. /
&DEVC ID = 'Mist Nozzle 4', XYZ = 1,16,11.9, ORIENTATION = 0.3536,0.3563,-.866, PROP_ID = 'Marioff Characteristics', QUANTITY = 'TIME', SETPOINT = 30. /
&DEVC ID = 'Mist Nozzle 5', XYZ = 1,16,11.9, ORIENTATION = -0.3536,0.3536,-.866, PROP_ID = 'Marioff Characteristics', QUANTITY = 'TIME', SETPOINT = 30. /
&DEVC ID = 'Mist Nozzle 6', XYZ = 1,16,11.9, ORIENTATION = 0.3536,-0.3536,-.866, PROP_ID = 'Marioff Characteristics', QUANTITY = 'TIME', SETPOINT = 30. /
&DEVC ID = 'Mist Nozzle 7', XYZ = 1,16,11.9, ORIENTATION = -0.3536,-0.3536,-.866, PROP_ID = 'Marioff Characteristics', QUANTITY = 'TIME', SETPOINT = 30. /
&DEVC ID = 'Mist Nozzle 8', XYZ = 1,16,11.9, ORIENTATION = 0,0.5,-.866, PROP_ID = 'Marioff Characteristics', QUANTITY = 'TIME', SETPOINT = 30. /
&DEVC ID = 'Mist Nozzle 9', XYZ = 1,16,11.9, ORIENTATION = 0,-0.5,-.866, PROP_ID = 'Marioff Characteristics', QUANTITY = 'TIME', SETPOINT = 30. /

&DEVC ID = 'Mist Nozzle 1', XYZ = 1,19,11.9, ORIENTATION = 0,0,-1, PROP_ID = 'Marioff Characteristics', QUANTITY = 'TIME', SETPOINT = 30. /
&DEVC ID = 'Mist Nozzle 2', XYZ = 1,19,11.9, ORIENTATION = 0.5,0,-.866, PROP_ID = 'Marioff Characteristics', QUANTITY = 'TIME', SETPOINT = 30. /
&DEVC ID = 'Mist Nozzle 3', XYZ = 1,19,11.9, ORIENTATION = -0.5,0,-.866, PROP_ID = 'Marioff Characteristics', QUANTITY = 'TIME', SETPOINT = 30. /

&DEVC ID = 'Mist Nozzle 4', XYZ = 1,19,11.9, ORIENTATION = 0.3536,0.3563,-.866,PROP_ID = 'Marioff Characteristics', QUANTITY = 'TIME', SETPOINT = 30. /
&DEVC ID = 'Mist Nozzle 5', XYZ = 1,19,11.9, ORIENTATION = -0.3536,0.3536,-.866, PROP_ID = 'Marioff Characteristics', QUANTITY = 'TIME', SETPOINT = 30. /
&DEVC ID = 'Mist Nozzle 6', XYZ = 1,19,11.9, ORIENTATION = 0.3536,-0.3536,-.866, PROP_ID = 'Marioff Characteristics', QUANTITY = 'TIME', SETPOINT = 30. /
&DEVC ID = 'Mist Nozzle 7', XYZ = 1,19,11.9, ORIENTATION = -0.3536,-0.3536,-.866,PROP_ID = 'Marioff Characteristics', QUANTITY = 'TIME', SETPOINT = 30. /
&DEVC ID = 'Mist Nozzle 8', XYZ = 1,19,11.9, ORIENTATION = 0,0.5,-.866, PROP_ID = 'Marioff Characteristics', QUANTITY = 'TIME', SETPOINT = 30. /
&DEVC ID = 'Mist Nozzle 9', XYZ = 1,19,11.9, ORIENTATION = 0,-0.5,-.866, PROP_ID = 'Marioff Characteristics', QUANTITY = 'TIME', SETPOINT = 30. /

&DEVC ID = 'Mist Nozzle 1', XYZ = 1,22,11.9, ORIENTATION = 0,0,-1, PROP_ID = 'Marioff Characteristics', QUANTITY = 'TIME', SETPOINT = 30. /
&DEVC ID = 'Mist Nozzle 2', XYZ = 1,22,11.9, ORIENTATION = 0.5,0,-.866, PROP_ID = 'Marioff Characteristics', QUANTITY = 'TIME', SETPOINT = 30. /
&DEVC ID = 'Mist Nozzle 3', XYZ = 1,22,11.9, ORIENTATION = -0.5,0,-.866,PROP_ID = 'Marioff Characteristics', QUANTITY = 'TIME', SETPOINT = 30. /
&DEVC ID = 'Mist Nozzle 4', XYZ = 1,22,11.9, ORIENTATION = 0.3536,0.3563,-.866,PROP_ID = 'Marioff Characteristics', QUANTITY = 'TIME', SETPOINT = 30. /
&DEVC ID = 'Mist Nozzle 5', XYZ = 1,22,11.9, ORIENTATION = -0.3536,0.3536,-.866, PROP_ID = 'Marioff Characteristics', QUANTITY = 'TIME', SETPOINT = 30. /
&DEVC ID = 'Mist Nozzle 6', XYZ = 1,22,11.9, ORIENTATION = 0.3536,-0.3536,-.866, PROP_ID = 'Marioff Characteristics', QUANTITY = 'TIME', SETPOINT = 30. /
&DEVC ID = 'Mist Nozzle 7', XYZ = 1,22,11.9, ORIENTATION = -0.3536,-0.3536,-.866,PROP_ID = 'Marioff Characteristics', QUANTITY = 'TIME', SETPOINT = 30. /
&DEVC ID = 'Mist Nozzle 8', XYZ = 1,22,11.9, ORIENTATION = 0,0.5,-.866, PROP_ID = 'Marioff Characteristics', QUANTITY = 'TIME', SETPOINT = 30. /
&DEVC ID = 'Mist Nozzle 9', XYZ = 1,22,11.9, ORIENTATION = 0,-0.5,-.866, PROP_ID = 'Marioff Characteristics', QUANTITY = 'TIME', SETPOINT = 30. /

&DEVC ID = 'Mist Nozzle 1', XYZ = 1,25,11.9, ORIENTATION = 0,0,-1, PROP_ID = 'Marioff Characteristics', QUANTITY = 'TIME', SETPOINT = 30. /
&DEVC ID = 'Mist Nozzle 2', XYZ = 1,25,11.9, ORIENTATION = 0.5,0,-.866, PROP_ID = 'Marioff Characteristics', QUANTITY = 'TIME', SETPOINT = 30. /
&DEVC ID = 'Mist Nozzle 3', XYZ = 1,25,11.9, ORIENTATION = -0.5,0,-.866,PROP_ID = 'Marioff Characteristics', QUANTITY = 'TIME', SETPOINT = 30. /
&DEVC ID = 'Mist Nozzle 4', XYZ = 1,25,11.9, ORIENTATION = 0.3536,0.3563,-.866,PROP_ID = 'Marioff Characteristics', QUANTITY = 'TIME', SETPOINT = 30. /
&DEVC ID = 'Mist Nozzle 5', XYZ = 1,25,11.9, ORIENTATION = -0.3536,0.3536,-.866, PROP_ID = 'Marioff Characteristics', QUANTITY = 'TIME', SETPOINT = 30. /
&DEVC ID = 'Mist Nozzle 6', XYZ = 1,25,11.9, ORIENTATION = 0.3536,-0.3536,-.866, PROP_ID = 'Marioff Characteristics', QUANTITY = 'TIME', SETPOINT = 30. /

&DEVC ID = 'Mist Nozzle 7', XYZ = 1,25,11.9, ORIENTATION = -0.3536,-0.3536,-.866,PROP_ID = 'Marioff Characteristics', QUANTITY = 'TIME', SETPOINT = 30. /
&DEVC ID = 'Mist Nozzle 8', XYZ = 1,25,11.9, ORIENTATION = 0,0.5,-.866, PROP_ID = 'Marioff Characteristics', QUANTITY = 'TIME', SETPOINT = 30. /
&DEVC ID = 'Mist Nozzle 9', XYZ = 1,25,11.9, ORIENTATION = 0,-0.5,-.866, PROP_ID = 'Marioff Characteristics', QUANTITY = 'TIME', SETPOINT = 30. /

/x = 4 row

&DEVC ID = 'Mist Nozzle 1', XYZ = 4,1,11.9, ORIENTATION = 0,0,-1, PROP_ID = 'Marioff Characteristics', QUANTITY = 'TIME', SETPOINT = 30. /
&DEVC ID = 'Mist Nozzle 2', XYZ = 4,1,11.9, ORIENTATION = 0.5,0,-.866, PROP_ID = 'Marioff Characteristics', QUANTITY = 'TIME', SETPOINT = 30. /
&DEVC ID = 'Mist Nozzle 3', XYZ = 4,1,11.9, ORIENTATION = -0.5,0,-.866,PROP_ID = 'Marioff Characteristics', QUANTITY = 'TIME', SETPOINT = 30. /
&DEVC ID = 'Mist Nozzle 4', XYZ = 4,1,11.9, ORIENTATION = 0.3536,0.3563,-.866,PROP_ID = 'Marioff Characteristics', QUANTITY = 'TIME', SETPOINT = 30. /
&DEVC ID = 'Mist Nozzle 5', XYZ = 4,1,11.9, ORIENTATION = -0.3536,0.3536,-.866, PROP_ID = 'Marioff Characteristics', QUANTITY = 'TIME', SETPOINT = 30./
&DEVC ID = 'Mist Nozzle 6', XYZ = 4,1,11.9, ORIENTATION = 0.3536,-0.3536,-.866, PROP_ID = 'Marioff Characteristics', QUANTITY = 'TIME', SETPOINT = 30./
&DEVC ID = 'Mist Nozzle 7', XYZ = 4,1,11.9, ORIENTATION = -0.3536,-0.3536,-.866,PROP_ID = 'Marioff Characteristics', QUANTITY = 'TIME', SETPOINT = 30. /
&DEVC ID = 'Mist Nozzle 8', XYZ = 4,1,11.9, ORIENTATION = 0,0.5,-.866, PROP_ID = 'Marioff Characteristics', QUANTITY = 'TIME', SETPOINT = 30. /
&DEVC ID = 'Mist Nozzle 9', XYZ = 4,1,11.9, ORIENTATION = 0,-0.5,-.866, PROP_ID = 'Marioff Characteristics', QUANTITY = 'TIME', SETPOINT = 30. /

&DEVC ID = 'Mist Nozzle 1', XYZ = 4,4,11.9, ORIENTATION = 0,0,-1, PROP_ID = 'Marioff Characteristics', QUANTITY = 'TIME', SETPOINT = 30. /
&DEVC ID = 'Mist Nozzle 2', XYZ = 4,4,11.9, ORIENTATION = 0.5,0,-.866, PROP_ID = 'Marioff Characteristics', QUANTITY = 'TIME', SETPOINT = 30./
&DEVC ID = 'Mist Nozzle 3', XYZ = 4,4,11.9, ORIENTATION = -0.5,0,-.866,PROP_ID = 'Marioff Characteristics', QUANTITY = 'TIME', SETPOINT = 30. /
&DEVC ID = 'Mist Nozzle 4', XYZ = 4,4,11.9, ORIENTATION = 0.3536,0.3563,-.866,PROP_ID = 'Marioff Characteristics', QUANTITY = 'TIME', SETPOINT = 30. /
&DEVC ID = 'Mist Nozzle 5', XYZ = 4,4,11.9, ORIENTATION = -0.3536,0.3536,-.866, PROP_ID = 'Marioff Characteristics', QUANTITY = 'TIME', SETPOINT = 30./
&DEVC ID = 'Mist Nozzle 6', XYZ = 4,4,11.9, ORIENTATION = 0.3536,-0.3536,-.866, PROP_ID = 'Marioff Characteristics', QUANTITY = 'TIME', SETPOINT = 30./
&DEVC ID = 'Mist Nozzle 7', XYZ = 4,4,11.9, ORIENTATION = -0.3536,-0.3536,-.866,PROP_ID = 'Marioff Characteristics', QUANTITY = 'TIME', SETPOINT = 30. /
&DEVC ID = 'Mist Nozzle 8', XYZ = 4,4,11.9, ORIENTATION = 0,0.5,-.866, PROP_ID = 'Marioff Characteristics', QUANTITY = 'TIME', SETPOINT = 30. /
&DEVC ID = 'Mist Nozzle 9', XYZ = 4,4,11.9, ORIENTATION = 0,-0.5,-.866, PROP_ID = 'Marioff Characteristics', QUANTITY = 'TIME', SETPOINT = 30. /

&DEVC ID = 'Mist Nozzle 1', XYZ = 4,7,11.9, ORIENTATION = 0,0,-1, PROP_ID = 'Marioff Characteristics', QUANTITY = 'TIME', SETPOINT = 30. /
&DEVC ID = 'Mist Nozzle 2', XYZ = 4,7,11.9, ORIENTATION = 0.5,0,-.866, PROP_ID = 'Marioff Characteristics', QUANTITY = 'TIME', SETPOINT = 30. /
&DEVC ID = 'Mist Nozzle 3', XYZ = 4,7,11.9, ORIENTATION = -0.5,0,-.866,PROP_ID = 'Marioff Characteristics', QUANTITY = 'TIME', SETPOINT = 30. /
&DEVC ID = 'Mist Nozzle 4', XYZ = 4,7,11.9, ORIENTATION = 0.3536,0.3563,-.866,PROP_ID = 'Marioff Characteristics', QUANTITY = 'TIME', SETPOINT = 30. /
&DEVC ID = 'Mist Nozzle 5', XYZ = 4,7,11.9, ORIENTATION = -0.3536,0.3536,-.866, PROP_ID = 'Marioff Characteristics', QUANTITY = 'TIME', SETPOINT = 30./
&DEVC ID = 'Mist Nozzle 6', XYZ = 4,7,11.9, ORIENTATION = 0.3536,-0.3536,-.866, PROP_ID = 'Marioff Characteristics', QUANTITY = 'TIME', SETPOINT = 30./
&DEVC ID = 'Mist Nozzle 7', XYZ = 4,7,11.9, ORIENTATION = -0.3536,-0.3536,-.866,PROP_ID = 'Marioff Characteristics', QUANTITY = 'TIME', SETPOINT = 30. /
&DEVC ID = 'Mist Nozzle 8', XYZ = 4,7,11.9, ORIENTATION = 0,0.5,-.866, PROP_ID = 'Marioff Characteristics', QUANTITY = 'TIME', SETPOINT = 30. /
&DEVC ID = 'Mist Nozzle 9', XYZ = 4,7,11.9, ORIENTATION = 0,-0.5,-.866, PROP_ID = 'Marioff Characteristics', QUANTITY = 'TIME', SETPOINT = 30. /

&DEVC ID = 'Mist Nozzle 1', XYZ = 4,10,11.9, ORIENTATION = 0,0,-1, PROP_ID = 'Marioff Characteristics', QUANTITY = 'TIME', SETPOINT = 30. /
&DEVC ID = 'Mist Nozzle 2', XYZ = 4,10,11.9, ORIENTATION = 0.5,0,-.866, PROP_ID = 'Marioff Characteristics', QUANTITY = 'TIME', SETPOINT = 30. /
&DEVC ID = 'Mist Nozzle 3', XYZ = 4,10,11.9, ORIENTATION = -0.5,0,-.866,PROP_ID = 'Marioff Characteristics', QUANTITY = 'TIME', SETPOINT = 30. /
&DEVC ID = 'Mist Nozzle 4', XYZ = 4,10,11.9, ORIENTATION = 0.3536,0.3563,-.866,PROP_ID = 'Marioff Characteristics', QUANTITY = 'TIME', SETPOINT = 30. /
&DEVC ID = 'Mist Nozzle 5', XYZ = 4,10,11.9, ORIENTATION = -0.3536,0.3536,-.866, PROP_ID = 'Marioff Characteristics', QUANTITY = 'TIME', SETPOINT = 30./
&DEVC ID = 'Mist Nozzle 6', XYZ = 4,10,11.9, ORIENTATION = 0.3536,-0.3536,-.866, PROP_ID = 'Marioff Characteristics', QUANTITY = 'TIME', SETPOINT = 30./
&DEVC ID = 'Mist Nozzle 7', XYZ = 4,10,11.9, ORIENTATION = -0.3536,-0.3536,-.866,PROP_ID = 'Marioff Characteristics', QUANTITY = 'TIME', SETPOINT = 30. /
&DEVC ID = 'Mist Nozzle 8', XYZ = 4,10,11.9, ORIENTATION = 0,0.5,-.866, PROP_ID = 'Marioff Characteristics', QUANTITY = 'TIME', SETPOINT = 30. /
&DEVC ID = 'Mist Nozzle 9', XYZ = 4,10,11.9, ORIENTATION = 0,-0.5,-.866, PROP_ID = 'Marioff Characteristics', QUANTITY = 'TIME', SETPOINT = 30. /

&DEVC ID = 'Mist Nozzle 1', XYZ = 4,13,11.9, ORIENTATION = 0,0,-1, PROP_ID = 'Marioff Characteristics', QUANTITY = 'TIME', SETPOINT = 30. /
&DEVC ID = 'Mist Nozzle 2', XYZ = 4,13,11.9, ORIENTATION = 0.5,0,-.866, PROP_ID = 'Marioff Characteristics', QUANTITY = 'TIME', SETPOINT = 30. /

&DEVC ID = 'Mist Nozzle 3', XYZ = 4,13,11.9, ORIENTATION = -0.5,0,-
.866,PROP_ID = 'Marioff Characteristics', QUANTITY = 'TIME', SETPOINT = 30. /
&DEVC ID = 'Mist Nozzle 4', XYZ = 4,13,11.9, ORIENTATION = 0.3536,0.3563,-
.866,PROP_ID = 'Marioff Characteristics', QUANTITY = 'TIME', SETPOINT = 30. /
&DEVC ID = 'Mist Nozzle 5', XYZ = 4,13,11.9, ORIENTATION = -0.3536,0.3536,-
.866, PROP_ID = 'Marioff Characteristics' , QUANTITY = 'TIME', SETPOINT = 30./
&DEVC ID = 'Mist Nozzle 6', XYZ = 4,13,11.9, ORIENTATION = 0.3536,-0.3536,-
.866, PROP_ID = 'Marioff Characteristics' , QUANTITY = 'TIME', SETPOINT = 30./
&DEVC ID = 'Mist Nozzle 7', XYZ = 4,13,11.9, ORIENTATION = -0.3536,-0.3536,-
.866,PROP_ID = 'Marioff Characteristics', QUANTITY = 'TIME', SETPOINT = 30. /
&DEVC ID = 'Mist Nozzle 8', XYZ = 4,13,11.9, ORIENTATION = 0,0.5,-.866,
PROP_ID = 'Marioff Characteristics', QUANTITY = 'TIME', SETPOINT = 30. /
&DEVC ID = 'Mist Nozzle 9', XYZ = 4,13,11.9, ORIENTATION = 0,-0.5,-.866,
PROP_ID = 'Marioff Characteristics', QUANTITY = 'TIME', SETPOINT = 30. /

&DEVC ID = 'Mist Nozzle 1', XYZ = 4,16,11.9, ORIENTATION = 0,0,-1, PROP_ID =
'Marioff Characteristics', QUANTITY = 'TIME', SETPOINT = 30. /
&DEVC ID = 'Mist Nozzle 2', XYZ = 4,16,11.9, ORIENTATION = 0.5,0,-.866,
PROP_ID = 'Marioff Characteristics', QUANTITY = 'TIME', SETPOINT = 30. /
&DEVC ID = 'Mist Nozzle 3', XYZ = 4,16,11.9, ORIENTATION = -0.5,0,-
.866,PROP_ID = 'Marioff Characteristics', QUANTITY = 'TIME', SETPOINT = 30. /
&DEVC ID = 'Mist Nozzle 4', XYZ = 4,16,11.9, ORIENTATION = 0.3536,0.3563,-
.866,PROP_ID = 'Marioff Characteristics', QUANTITY = 'TIME', SETPOINT = 30. /
&DEVC ID = 'Mist Nozzle 5', XYZ = 4,16,11.9, ORIENTATION = -0.3536,0.3536,-
.866, PROP_ID = 'Marioff Characteristics' , QUANTITY = 'TIME', SETPOINT = 30./
&DEVC ID = 'Mist Nozzle 6', XYZ = 4,16,11.9, ORIENTATION = 0.3536,-0.3536,-
.866, PROP_ID = 'Marioff Characteristics' , QUANTITY = 'TIME', SETPOINT = 30./
&DEVC ID = 'Mist Nozzle 7', XYZ = 4,16,11.9, ORIENTATION = -0.3536,-0.3536,-
.866,PROP_ID = 'Marioff Characteristics', QUANTITY = 'TIME', SETPOINT = 30. /
&DEVC ID = 'Mist Nozzle 8', XYZ = 4,16,11.9, ORIENTATION = 0,0.5,-.866,
PROP_ID = 'Marioff Characteristics', QUANTITY = 'TIME', SETPOINT = 30. /
&DEVC ID = 'Mist Nozzle 9', XYZ = 4,16,11.9, ORIENTATION = 0,-0.5,-.866,
PROP_ID = 'Marioff Characteristics', QUANTITY = 'TIME', SETPOINT = 30. /

&DEVC ID = 'Mist Nozzle 1', XYZ = 4,19,11.9, ORIENTATION = 0,0,-1, PROP_ID =
'Marioff Characteristics', QUANTITY = 'TIME', SETPOINT = 30. /
&DEVC ID = 'Mist Nozzle 2', XYZ = 4,19,11.9, ORIENTATION = 0.5,0,-.866,
PROP_ID = 'Marioff Characteristics', QUANTITY = 'TIME', SETPOINT = 30. /
&DEVC ID = 'Mist Nozzle 3', XYZ = 4,19,11.9, ORIENTATION = -0.5,0,-
.866,PROP_ID = 'Marioff Characteristics', QUANTITY = 'TIME', SETPOINT = 30. /
&DEVC ID = 'Mist Nozzle 4', XYZ = 4,19,11.9, ORIENTATION = 0.3536,0.3563,-
.866,PROP_ID = 'Marioff Characteristics', QUANTITY = 'TIME', SETPOINT = 30. /
&DEVC ID = 'Mist Nozzle 5', XYZ = 4,19,11.9, ORIENTATION = -0.3536,0.3536,-
.866, PROP_ID = 'Marioff Characteristics' , QUANTITY = 'TIME', SETPOINT = 30./

&DEVC ID = 'Mist Nozzle 6', XYZ = 4,19,11.9, ORIENTATION = 0.3536,-0.3536,-.866, PROP_ID = 'Marioff Characteristics', QUANTITY = 'TIME', SETPOINT = 30. /
&DEVC ID = 'Mist Nozzle 7', XYZ = 4,19,11.9, ORIENTATION = -0.3536,-0.3536,-.866, PROP_ID = 'Marioff Characteristics', QUANTITY = 'TIME', SETPOINT = 30. /
&DEVC ID = 'Mist Nozzle 8', XYZ = 4,19,11.9, ORIENTATION = 0,0.5,-.866, PROP_ID = 'Marioff Characteristics', QUANTITY = 'TIME', SETPOINT = 30. /
&DEVC ID = 'Mist Nozzle 9', XYZ = 4,19,11.9, ORIENTATION = 0,-0.5,-.866, PROP_ID = 'Marioff Characteristics', QUANTITY = 'TIME', SETPOINT = 30. /

&DEVC ID = 'Mist Nozzle 1', XYZ = 4,22,11.9, ORIENTATION = 0,0,-1, PROP_ID = 'Marioff Characteristics', QUANTITY = 'TIME', SETPOINT = 30. /
&DEVC ID = 'Mist Nozzle 2', XYZ = 4,22,11.9, ORIENTATION = 0.5,0,-.866, PROP_ID = 'Marioff Characteristics', QUANTITY = 'TIME', SETPOINT = 30. /
&DEVC ID = 'Mist Nozzle 3', XYZ = 4,22,11.9, ORIENTATION = -0.5,0,-.866, PROP_ID = 'Marioff Characteristics', QUANTITY = 'TIME', SETPOINT = 30. /
&DEVC ID = 'Mist Nozzle 4', XYZ = 4,22,11.9, ORIENTATION = 0.3536,0.3536,-.866, PROP_ID = 'Marioff Characteristics', QUANTITY = 'TIME', SETPOINT = 30. /
&DEVC ID = 'Mist Nozzle 5', XYZ = 4,22,11.9, ORIENTATION = -0.3536,0.3536,-.866, PROP_ID = 'Marioff Characteristics', QUANTITY = 'TIME', SETPOINT = 30. /
&DEVC ID = 'Mist Nozzle 6', XYZ = 4,22,11.9, ORIENTATION = 0.3536,-0.3536,-.866, PROP_ID = 'Marioff Characteristics', QUANTITY = 'TIME', SETPOINT = 30. /
&DEVC ID = 'Mist Nozzle 7', XYZ = 4,22,11.9, ORIENTATION = -0.3536,-0.3536,-.866, PROP_ID = 'Marioff Characteristics', QUANTITY = 'TIME', SETPOINT = 30. /
&DEVC ID = 'Mist Nozzle 8', XYZ = 4,22,11.9, ORIENTATION = 0,0.5,-.866, PROP_ID = 'Marioff Characteristics', QUANTITY = 'TIME', SETPOINT = 30. /
&DEVC ID = 'Mist Nozzle 9', XYZ = 4,22,11.9, ORIENTATION = 0,-0.5,-.866, PROP_ID = 'Marioff Characteristics', QUANTITY = 'TIME', SETPOINT = 30. /

&DEVC ID = 'Mist Nozzle 1', XYZ = 4,25,11.9, ORIENTATION = 0,0,-1, PROP_ID = 'Marioff Characteristics', QUANTITY = 'TIME', SETPOINT = 30. /
&DEVC ID = 'Mist Nozzle 2', XYZ = 4,25,11.9, ORIENTATION = 0.5,0,-.866, PROP_ID = 'Marioff Characteristics', QUANTITY = 'TIME', SETPOINT = 30. /
&DEVC ID = 'Mist Nozzle 3', XYZ = 4,25,11.9, ORIENTATION = -0.5,0,-.866, PROP_ID = 'Marioff Characteristics', QUANTITY = 'TIME', SETPOINT = 30. /
&DEVC ID = 'Mist Nozzle 4', XYZ = 4,25,11.9, ORIENTATION = 0.3536,0.3536,-.866, PROP_ID = 'Marioff Characteristics', QUANTITY = 'TIME', SETPOINT = 30. /
&DEVC ID = 'Mist Nozzle 5', XYZ = 4,25,11.9, ORIENTATION = -0.3536,0.3536,-.866, PROP_ID = 'Marioff Characteristics', QUANTITY = 'TIME', SETPOINT = 30. /
&DEVC ID = 'Mist Nozzle 6', XYZ = 4,25,11.9, ORIENTATION = 0.3536,-0.3536,-.866, PROP_ID = 'Marioff Characteristics', QUANTITY = 'TIME', SETPOINT = 30. /
&DEVC ID = 'Mist Nozzle 7', XYZ = 4,25,11.9, ORIENTATION = -0.3536,-0.3536,-.866, PROP_ID = 'Marioff Characteristics', QUANTITY = 'TIME', SETPOINT = 30. /
&DEVC ID = 'Mist Nozzle 8', XYZ = 4,25,11.9, ORIENTATION = 0,0.5,-.866, PROP_ID = 'Marioff Characteristics', QUANTITY = 'TIME', SETPOINT = 30. /

&DEVC ID ='Mist Nozzle 9', XYZ = 4,25,11.9, ORIENTATION = 0,-0.5,-.866,
PROP_ID = 'Marioff Characteristics', QUANTITY ='TIME', SETPOINT =30. /

/x = 7 row

&DEVC ID ='Mist Nozzle 1', XYZ = 7,1,11.9, ORIENTATION = 0,0,-1, PROP_ID =
'Marioff Characteristics', QUANTITY ='TIME', SETPOINT =30. /
&DEVC ID ='Mist Nozzle 2', XYZ = 7,1,11.9, ORIENTATION = 0.5,0,-.866, PROP_ID
= 'Marioff Characteristics', QUANTITY ='TIME', SETPOINT =30. /
&DEVC ID ='Mist Nozzle 3', XYZ = 7,1,11.9, ORIENTATION = -0.5,0,-.866,PROP_ID
= 'Marioff Characteristics', QUANTITY ='TIME', SETPOINT =30. /
&DEVC ID ='Mist Nozzle 4', XYZ = 7,1,11.9, ORIENTATION = 0.3536,0.3563,-
.866,PROP_ID = 'Marioff Characteristics', QUANTITY ='TIME', SETPOINT =30. /
&DEVC ID ='Mist Nozzle 5', XYZ = 7,1,11.9, ORIENTATION = -0.3536,0.3536,-.866,
PROP_ID = 'Marioff Characteristics', QUANTITY ='TIME', SETPOINT =30./
&DEVC ID ='Mist Nozzle 6', XYZ = 7,1,11.9, ORIENTATION = 0.3536,-0.3536,-.866,
PROP_ID = 'Marioff Characteristics', QUANTITY ='TIME', SETPOINT =30./
&DEVC ID ='Mist Nozzle 7', XYZ = 7,1,11.9, ORIENTATION = -0.3536,-0.3536,-
.866,PROP_ID = 'Marioff Characteristics', QUANTITY ='TIME', SETPOINT =30. /
&DEVC ID ='Mist Nozzle 8', XYZ = 7,1,11.9, ORIENTATION = 0,0.5,-.866, PROP_ID
= 'Marioff Characteristics', QUANTITY ='TIME', SETPOINT =30. /
&DEVC ID ='Mist Nozzle 9', XYZ = 7,1,11.9, ORIENTATION = 0,-0.5,-.866,
PROP_ID = 'Marioff Characteristics', QUANTITY ='TIME', SETPOINT =30. /

&DEVC ID ='Mist Nozzle 1', XYZ = 7,4,11.9, ORIENTATION = 0,0,-1, PROP_ID =
'Marioff Characteristics', QUANTITY ='TIME', SETPOINT =30. /
&DEVC ID ='Mist Nozzle 2', XYZ = 7,4,11.9, ORIENTATION = 0.5,0,-.866, PROP_ID
= 'Marioff Characteristics', QUANTITY ='TIME', SETPOINT =30./
&DEVC ID ='Mist Nozzle 3', XYZ = 7,4,11.9, ORIENTATION = -0.5,0,-.866,PROP_ID
= 'Marioff Characteristics', QUANTITY ='TIME', SETPOINT =30. /
&DEVC ID ='Mist Nozzle 4', XYZ = 7,4,11.9, ORIENTATION = 0.3536,0.3563,-
.866,PROP_ID = 'Marioff Characteristics', QUANTITY ='TIME', SETPOINT =30. /
&DEVC ID ='Mist Nozzle 5', XYZ = 7,4,11.9, ORIENTATION = -0.3536,0.3536,-.866,
PROP_ID = 'Marioff Characteristics', QUANTITY ='TIME', SETPOINT =30./
&DEVC ID ='Mist Nozzle 6', XYZ = 7,4,11.9, ORIENTATION = 0.3536,-0.3536,-.866,
PROP_ID = 'Marioff Characteristics', QUANTITY ='TIME', SETPOINT =30./
&DEVC ID ='Mist Nozzle 7', XYZ = 7,4,11.9, ORIENTATION = -0.3536,-0.3536,-
.866,PROP_ID = 'Marioff Characteristics', QUANTITY ='TIME', SETPOINT =30. /
&DEVC ID ='Mist Nozzle 8', XYZ = 7,4,11.9, ORIENTATION = 0,0.5,-.866, PROP_ID
= 'Marioff Characteristics', QUANTITY ='TIME', SETPOINT =30. /
&DEVC ID ='Mist Nozzle 9', XYZ = 7,4,11.9, ORIENTATION = 0,-0.5,-.866,
PROP_ID = 'Marioff Characteristics', QUANTITY ='TIME', SETPOINT =30. /

&DEVC ID ='Mist Nozzle 1', XYZ = 7,7,11.9, ORIENTATION = 0,0,-1, PROP_ID =
'Marioff Characteristics', QUANTITY ='TIME', SETPOINT =30. /

&DEVC ID = 'Mist Nozzle 2', XYZ = 7,7,11.9, ORIENTATION = 0.5,0,-.866, PROP_ID = 'Marioff Characteristics', QUANTITY = 'TIME', SETPOINT = 30. /
&DEVC ID = 'Mist Nozzle 3', XYZ = 7,7,11.9, ORIENTATION = -0.5,0,-.866, PROP_ID = 'Marioff Characteristics', QUANTITY = 'TIME', SETPOINT = 30. /
&DEVC ID = 'Mist Nozzle 4', XYZ = 7,7,11.9, ORIENTATION = 0.3536,0.3563,-.866, PROP_ID = 'Marioff Characteristics', QUANTITY = 'TIME', SETPOINT = 30. /
&DEVC ID = 'Mist Nozzle 5', XYZ = 7,7,11.9, ORIENTATION = -0.3536,0.3536,-.866, PROP_ID = 'Marioff Characteristics', QUANTITY = 'TIME', SETPOINT = 30. /
&DEVC ID = 'Mist Nozzle 6', XYZ = 7,7,11.9, ORIENTATION = 0.3536,-0.3536,-.866, PROP_ID = 'Marioff Characteristics', QUANTITY = 'TIME', SETPOINT = 30. /
&DEVC ID = 'Mist Nozzle 7', XYZ = 7,7,11.9, ORIENTATION = -0.3536,-0.3536,-.866, PROP_ID = 'Marioff Characteristics', QUANTITY = 'TIME', SETPOINT = 30. /
&DEVC ID = 'Mist Nozzle 8', XYZ = 7,7,11.9, ORIENTATION = 0,0.5,-.866, PROP_ID = 'Marioff Characteristics', QUANTITY = 'TIME', SETPOINT = 30. /
&DEVC ID = 'Mist Nozzle 9', XYZ = 7,7,11.9, ORIENTATION = 0,-0.5,-.866, PROP_ID = 'Marioff Characteristics', QUANTITY = 'TIME', SETPOINT = 30. /

&DEVC ID = 'Mist Nozzle 1', XYZ = 7,10,11.9, ORIENTATION = 0,0,-1, PROP_ID = 'Marioff Characteristics', QUANTITY = 'TIME', SETPOINT = 30. /
&DEVC ID = 'Mist Nozzle 2', XYZ = 7,10,11.9, ORIENTATION = 0.5,0,-.866, PROP_ID = 'Marioff Characteristics', QUANTITY = 'TIME', SETPOINT = 30. /
&DEVC ID = 'Mist Nozzle 3', XYZ = 7,10,11.9, ORIENTATION = -0.5,0,-.866, PROP_ID = 'Marioff Characteristics', QUANTITY = 'TIME', SETPOINT = 30. /
&DEVC ID = 'Mist Nozzle 4', XYZ = 7,10,11.9, ORIENTATION = 0.3536,0.3563,-.866, PROP_ID = 'Marioff Characteristics', QUANTITY = 'TIME', SETPOINT = 30. /
&DEVC ID = 'Mist Nozzle 5', XYZ = 7,10,11.9, ORIENTATION = -0.3536,0.3536,-.866, PROP_ID = 'Marioff Characteristics', QUANTITY = 'TIME', SETPOINT = 30. /
&DEVC ID = 'Mist Nozzle 6', XYZ = 7,10,11.9, ORIENTATION = 0.3536,-0.3536,-.866, PROP_ID = 'Marioff Characteristics', QUANTITY = 'TIME', SETPOINT = 30. /
&DEVC ID = 'Mist Nozzle 7', XYZ = 7,10,11.9, ORIENTATION = -0.3536,-0.3536,-.866, PROP_ID = 'Marioff Characteristics', QUANTITY = 'TIME', SETPOINT = 30. /
&DEVC ID = 'Mist Nozzle 8', XYZ = 7,10,11.9, ORIENTATION = 0,0.5,-.866, PROP_ID = 'Marioff Characteristics', QUANTITY = 'TIME', SETPOINT = 30. /
&DEVC ID = 'Mist Nozzle 9', XYZ = 7,10,11.9, ORIENTATION = 0,-0.5,-.866, PROP_ID = 'Marioff Characteristics', QUANTITY = 'TIME', SETPOINT = 30. /

&DEVC ID = 'Mist Nozzle 1', XYZ = 7,13,11.9, ORIENTATION = 0,0,-1, PROP_ID = 'Marioff Characteristics', QUANTITY = 'TIME', SETPOINT = 30. /
&DEVC ID = 'Mist Nozzle 2', XYZ = 7,13,11.9, ORIENTATION = 0.5,0,-.866, PROP_ID = 'Marioff Characteristics', QUANTITY = 'TIME', SETPOINT = 30. /
&DEVC ID = 'Mist Nozzle 3', XYZ = 7,13,11.9, ORIENTATION = -0.5,0,-.866, PROP_ID = 'Marioff Characteristics', QUANTITY = 'TIME', SETPOINT = 30. /
&DEVC ID = 'Mist Nozzle 4', XYZ = 7,13,11.9, ORIENTATION = 0.3536,0.3563,-.866, PROP_ID = 'Marioff Characteristics', QUANTITY = 'TIME', SETPOINT = 30. /

&DEVC ID = 'Mist Nozzle 5', XYZ = 7,13,11.9, ORIENTATION = -0.3536,0.3536,-.866, PROP_ID = 'Marioff Characteristics', QUANTITY = 'TIME', SETPOINT = 30./
&DEVC ID = 'Mist Nozzle 6', XYZ = 7,13,11.9, ORIENTATION = 0.3536,-0.3536,-.866, PROP_ID = 'Marioff Characteristics', QUANTITY = 'TIME', SETPOINT = 30./
&DEVC ID = 'Mist Nozzle 7', XYZ = 7,13,11.9, ORIENTATION = -0.3536,-0.3536,-.866, PROP_ID = 'Marioff Characteristics', QUANTITY = 'TIME', SETPOINT = 30. /
&DEVC ID = 'Mist Nozzle 8', XYZ = 7,13,11.9, ORIENTATION = 0,0.5,-.866, PROP_ID = 'Marioff Characteristics', QUANTITY = 'TIME', SETPOINT = 30. /
&DEVC ID = 'Mist Nozzle 9', XYZ = 7,13,11.9, ORIENTATION = 0,-0.5,-.866, PROP_ID = 'Marioff Characteristics', QUANTITY = 'TIME', SETPOINT = 30. /

&DEVC ID = 'Mist Nozzle 1', XYZ = 7,16,11.9, ORIENTATION = 0,0,-1, PROP_ID = 'Marioff Characteristics', QUANTITY = 'TIME', SETPOINT = 30. /
&DEVC ID = 'Mist Nozzle 2', XYZ = 7,16,11.9, ORIENTATION = 0.5,0,-.866, PROP_ID = 'Marioff Characteristics', QUANTITY = 'TIME', SETPOINT = 30. /
&DEVC ID = 'Mist Nozzle 3', XYZ = 7,16,11.9, ORIENTATION = -0.5,0,-.866, PROP_ID = 'Marioff Characteristics', QUANTITY = 'TIME', SETPOINT = 30. /
&DEVC ID = 'Mist Nozzle 4', XYZ = 7,16,11.9, ORIENTATION = 0.3536,0.3563,-.866, PROP_ID = 'Marioff Characteristics', QUANTITY = 'TIME', SETPOINT = 30. /
&DEVC ID = 'Mist Nozzle 5', XYZ = 7,16,11.9, ORIENTATION = -0.3536,0.3536,-.866, PROP_ID = 'Marioff Characteristics', QUANTITY = 'TIME', SETPOINT = 30./
&DEVC ID = 'Mist Nozzle 6', XYZ = 7,16,11.9, ORIENTATION = 0.3536,-0.3536,-.866, PROP_ID = 'Marioff Characteristics', QUANTITY = 'TIME', SETPOINT = 30./
&DEVC ID = 'Mist Nozzle 7', XYZ = 7,16,11.9, ORIENTATION = -0.3536,-0.3536,-.866, PROP_ID = 'Marioff Characteristics', QUANTITY = 'TIME', SETPOINT = 30. /
&DEVC ID = 'Mist Nozzle 8', XYZ = 7,16,11.9, ORIENTATION = 0,0.5,-.866, PROP_ID = 'Marioff Characteristics', QUANTITY = 'TIME', SETPOINT = 30. /
&DEVC ID = 'Mist Nozzle 9', XYZ = 7,16,11.9, ORIENTATION = 0,-0.5,-.866, PROP_ID = 'Marioff Characteristics', QUANTITY = 'TIME', SETPOINT = 30. /

&DEVC ID = 'Mist Nozzle 1', XYZ = 7,19,11.9, ORIENTATION = 0,0,-1, PROP_ID = 'Marioff Characteristics', QUANTITY = 'TIME', SETPOINT = 30. /
&DEVC ID = 'Mist Nozzle 2', XYZ = 7,19,11.9, ORIENTATION = 0.5,0,-.866, PROP_ID = 'Marioff Characteristics', QUANTITY = 'TIME', SETPOINT = 30. /
&DEVC ID = 'Mist Nozzle 3', XYZ = 7,19,11.9, ORIENTATION = -0.5,0,-.866, PROP_ID = 'Marioff Characteristics', QUANTITY = 'TIME', SETPOINT = 30. /
&DEVC ID = 'Mist Nozzle 4', XYZ = 7,19,11.9, ORIENTATION = 0.3536,0.3563,-.866, PROP_ID = 'Marioff Characteristics', QUANTITY = 'TIME', SETPOINT = 30. /
&DEVC ID = 'Mist Nozzle 5', XYZ = 7,19,11.9, ORIENTATION = -0.3536,0.3536,-.866, PROP_ID = 'Marioff Characteristics', QUANTITY = 'TIME', SETPOINT = 30./
&DEVC ID = 'Mist Nozzle 6', XYZ = 7,19,11.9, ORIENTATION = 0.3536,-0.3536,-.866, PROP_ID = 'Marioff Characteristics', QUANTITY = 'TIME', SETPOINT = 30./
&DEVC ID = 'Mist Nozzle 7', XYZ = 7,19,11.9, ORIENTATION = -0.3536,-0.3536,-.866, PROP_ID = 'Marioff Characteristics', QUANTITY = 'TIME', SETPOINT = 30. /

&DEVC ID = 'Mist Nozzle 8', XYZ = 7,19,11.9, ORIENTATION = 0,0.5,-.866,
PROP_ID = 'Marioff Characteristics', QUANTITY = 'TIME', SETPOINT = 30. /
&DEVC ID = 'Mist Nozzle 9', XYZ = 7,19,11.9, ORIENTATION = 0,-0.5,-.866,
PROP_ID = 'Marioff Characteristics', QUANTITY = 'TIME', SETPOINT = 30. /

&DEVC ID = 'Mist Nozzle 1', XYZ = 7,22,11.9, ORIENTATION = 0,0,-1, PROP_ID =
'Marioff Characteristics', QUANTITY = 'TIME', SETPOINT = 30. /
&DEVC ID = 'Mist Nozzle 2', XYZ = 7,22,11.9, ORIENTATION = 0.5,0,-.866,
PROP_ID = 'Marioff Characteristics', QUANTITY = 'TIME', SETPOINT = 30. /
&DEVC ID = 'Mist Nozzle 3', XYZ = 7,22,11.9, ORIENTATION = -0.5,0,-
.866,PROP_ID = 'Marioff Characteristics', QUANTITY = 'TIME', SETPOINT = 30. /
&DEVC ID = 'Mist Nozzle 4', XYZ = 7,22,11.9, ORIENTATION = 0.3536,0.3563,-
.866,PROP_ID = 'Marioff Characteristics', QUANTITY = 'TIME', SETPOINT = 30. /
&DEVC ID = 'Mist Nozzle 5', XYZ = 7,22,11.9, ORIENTATION = -0.3536,0.3536,-
.866, PROP_ID = 'Marioff Characteristics', QUANTITY = 'TIME', SETPOINT = 30./
&DEVC ID = 'Mist Nozzle 6', XYZ = 7,22,11.9, ORIENTATION = 0.3536,-0.3536,-
.866, PROP_ID = 'Marioff Characteristics', QUANTITY = 'TIME', SETPOINT = 30./
&DEVC ID = 'Mist Nozzle 7', XYZ = 7,22,11.9, ORIENTATION = -0.3536,-0.3536,-
.866,PROP_ID = 'Marioff Characteristics', QUANTITY = 'TIME', SETPOINT = 30. /
&DEVC ID = 'Mist Nozzle 8', XYZ = 7,22,11.9, ORIENTATION = 0,0.5,-.866,
PROP_ID = 'Marioff Characteristics', QUANTITY = 'TIME', SETPOINT = 30. /
&DEVC ID = 'Mist Nozzle 9', XYZ = 7,22,11.9, ORIENTATION = 0,-0.5,-.866,
PROP_ID = 'Marioff Characteristics', QUANTITY = 'TIME', SETPOINT = 30. /

&DEVC ID = 'Mist Nozzle 1', XYZ = 7,25,11.9, ORIENTATION = 0,0,-1, PROP_ID =
'Marioff Characteristics', QUANTITY = 'TIME', SETPOINT = 30. /
&DEVC ID = 'Mist Nozzle 2', XYZ = 7,25,11.9, ORIENTATION = 0.5,0,-.866,
PROP_ID = 'Marioff Characteristics', QUANTITY = 'TIME', SETPOINT = 30. /
&DEVC ID = 'Mist Nozzle 3', XYZ = 7,25,11.9, ORIENTATION = -0.5,0,-
.866,PROP_ID = 'Marioff Characteristics', QUANTITY = 'TIME', SETPOINT = 30. /
&DEVC ID = 'Mist Nozzle 4', XYZ = 7,25,11.9, ORIENTATION = 0.3536,0.3563,-
.866,PROP_ID = 'Marioff Characteristics', QUANTITY = 'TIME', SETPOINT = 30. /
&DEVC ID = 'Mist Nozzle 5', XYZ = 7,25,11.9, ORIENTATION = -0.3536,0.3536,-
.866, PROP_ID = 'Marioff Characteristics', QUANTITY = 'TIME', SETPOINT = 30./
&DEVC ID = 'Mist Nozzle 6', XYZ = 7,25,11.9, ORIENTATION = 0.3536,-0.3536,-
.866, PROP_ID = 'Marioff Characteristics', QUANTITY = 'TIME', SETPOINT = 30./
&DEVC ID = 'Mist Nozzle 7', XYZ = 7,25,11.9, ORIENTATION = -0.3536,-0.3536,-
.866,PROP_ID = 'Marioff Characteristics', QUANTITY = 'TIME', SETPOINT = 30. /
&DEVC ID = 'Mist Nozzle 8', XYZ = 7,25,11.9, ORIENTATION = 0,0.5,-.866,
PROP_ID = 'Marioff Characteristics', QUANTITY = 'TIME', SETPOINT = 30. /
&DEVC ID = 'Mist Nozzle 9', XYZ = 7,25,11.9, ORIENTATION = 0,-0.5,-.866,
PROP_ID = 'Marioff Characteristics', QUANTITY = 'TIME', SETPOINT = 30. /

/x = 10 row

&DEVC ID = 'Mist Nozzle 1', XYZ = 10,1,11.9, ORIENTATION = 0,0,-1, PROP_ID = 'Marioff Characteristics', QUANTITY = 'TIME', SETPOINT = 30. /
&DEVC ID = 'Mist Nozzle 2', XYZ = 10,1,11.9, ORIENTATION = 0.5,0,-.866, PROP_ID = 'Marioff Characteristics', QUANTITY = 'TIME', SETPOINT = 30. /
&DEVC ID = 'Mist Nozzle 3', XYZ = 10,1,11.9, ORIENTATION = -0.5,0,-.866, PROP_ID = 'Marioff Characteristics', QUANTITY = 'TIME', SETPOINT = 30. /
&DEVC ID = 'Mist Nozzle 4', XYZ = 10,1,11.9, ORIENTATION = 0.3536,0.3563,-.866, PROP_ID = 'Marioff Characteristics', QUANTITY = 'TIME', SETPOINT = 30. /
&DEVC ID = 'Mist Nozzle 5', XYZ = 10,1,11.9, ORIENTATION = -0.3536,0.3536,-.866, PROP_ID = 'Marioff Characteristics', QUANTITY = 'TIME', SETPOINT = 30. /
&DEVC ID = 'Mist Nozzle 6', XYZ = 10,1,11.9, ORIENTATION = 0.3536,-0.3536,-.866, PROP_ID = 'Marioff Characteristics', QUANTITY = 'TIME', SETPOINT = 30. /
&DEVC ID = 'Mist Nozzle 7', XYZ = 10,1,11.9, ORIENTATION = -0.3536,-0.3536,-.866, PROP_ID = 'Marioff Characteristics', QUANTITY = 'TIME', SETPOINT = 30. /
&DEVC ID = 'Mist Nozzle 8', XYZ = 10,1,11.9, ORIENTATION = 0,0.5,-.866, PROP_ID = 'Marioff Characteristics', QUANTITY = 'TIME', SETPOINT = 30. /
&DEVC ID = 'Mist Nozzle 9', XYZ = 10,1,11.9, ORIENTATION = 0,-0.5,-.866, PROP_ID = 'Marioff Characteristics', QUANTITY = 'TIME', SETPOINT = 30. /

&DEVC ID = 'Mist Nozzle 1', XYZ = 10,4,11.9, ORIENTATION = 0,0,-1, PROP_ID = 'Marioff Characteristics', QUANTITY = 'TIME', SETPOINT = 30. /
&DEVC ID = 'Mist Nozzle 2', XYZ = 10,4,11.9, ORIENTATION = 0.5,0,-.866, PROP_ID = 'Marioff Characteristics', QUANTITY = 'TIME', SETPOINT = 30. /
&DEVC ID = 'Mist Nozzle 3', XYZ = 10,4,11.9, ORIENTATION = -0.5,0,-.866, PROP_ID = 'Marioff Characteristics', QUANTITY = 'TIME', SETPOINT = 30. /
&DEVC ID = 'Mist Nozzle 4', XYZ = 10,4,11.9, ORIENTATION = 0.3536,0.3563,-.866, PROP_ID = 'Marioff Characteristics', QUANTITY = 'TIME', SETPOINT = 30. /
&DEVC ID = 'Mist Nozzle 5', XYZ = 10,4,11.9, ORIENTATION = -0.3536,0.3536,-.866, PROP_ID = 'Marioff Characteristics', QUANTITY = 'TIME', SETPOINT = 30. /
&DEVC ID = 'Mist Nozzle 6', XYZ = 10,4,11.9, ORIENTATION = 0.3536,-0.3536,-.866, PROP_ID = 'Marioff Characteristics', QUANTITY = 'TIME', SETPOINT = 30. /
&DEVC ID = 'Mist Nozzle 7', XYZ = 10,4,11.9, ORIENTATION = -0.3536,-0.3536,-.866, PROP_ID = 'Marioff Characteristics', QUANTITY = 'TIME', SETPOINT = 30. /
&DEVC ID = 'Mist Nozzle 8', XYZ = 10,4,11.9, ORIENTATION = 0,0.5,-.866, PROP_ID = 'Marioff Characteristics', QUANTITY = 'TIME', SETPOINT = 30. /
&DEVC ID = 'Mist Nozzle 9', XYZ = 10,4,11.9, ORIENTATION = 0,-0.5,-.866, PROP_ID = 'Marioff Characteristics', QUANTITY = 'TIME', SETPOINT = 30. /

&DEVC ID = 'Mist Nozzle 1', XYZ = 10,7,11.9, ORIENTATION = 0,0,-1, PROP_ID = 'Marioff Characteristics', QUANTITY = 'TIME', SETPOINT = 30. /
&DEVC ID = 'Mist Nozzle 2', XYZ = 10,7,11.9, ORIENTATION = 0.5,0,-.866, PROP_ID = 'Marioff Characteristics', QUANTITY = 'TIME', SETPOINT = 30. /
&DEVC ID = 'Mist Nozzle 3', XYZ = 10,7,11.9, ORIENTATION = -0.5,0,-.866, PROP_ID = 'Marioff Characteristics', QUANTITY = 'TIME', SETPOINT = 30. /

&DEVC ID = 'Mist Nozzle 4', XYZ = 10,7,11.9, ORIENTATION = 0.3536,0.3563,-.866,PROP_ID = 'Marioff Characteristics', QUANTITY = 'TIME', SETPOINT = 30. /
&DEVC ID = 'Mist Nozzle 5', XYZ = 10,7,11.9, ORIENTATION = -0.3536,0.3536,-.866, PROP_ID = 'Marioff Characteristics', QUANTITY = 'TIME', SETPOINT = 30. /
&DEVC ID = 'Mist Nozzle 6', XYZ = 10,7,11.9, ORIENTATION = 0.3536,-0.3536,-.866, PROP_ID = 'Marioff Characteristics', QUANTITY = 'TIME', SETPOINT = 30. /
&DEVC ID = 'Mist Nozzle 7', XYZ = 10,7,11.9, ORIENTATION = -0.3536,-0.3536,-.866,PROP_ID = 'Marioff Characteristics', QUANTITY = 'TIME', SETPOINT = 30. /
&DEVC ID = 'Mist Nozzle 8', XYZ = 10,7,11.9, ORIENTATION = 0,0.5,-.866, PROP_ID = 'Marioff Characteristics', QUANTITY = 'TIME', SETPOINT = 30. /
&DEVC ID = 'Mist Nozzle 9', XYZ = 10,7,11.9, ORIENTATION = 0,-0.5,-.866, PROP_ID = 'Marioff Characteristics', QUANTITY = 'TIME', SETPOINT = 30. /

&DEVC ID = 'Mist Nozzle 1', XYZ = 10,10,11.9, ORIENTATION = 0,0,-1, PROP_ID = 'Marioff Characteristics', QUANTITY = 'TIME', SETPOINT = 30. /
&DEVC ID = 'Mist Nozzle 2', XYZ = 10,10,11.9, ORIENTATION = 0.5,0,-.866, PROP_ID = 'Marioff Characteristics', QUANTITY = 'TIME', SETPOINT = 30. /
&DEVC ID = 'Mist Nozzle 3', XYZ = 10,10,11.9, ORIENTATION = -0.5,0,-.866,PROP_ID = 'Marioff Characteristics', QUANTITY = 'TIME', SETPOINT = 30. /
&DEVC ID = 'Mist Nozzle 4', XYZ = 10,10,11.9, ORIENTATION = 0.3536,0.3563,-.866,PROP_ID = 'Marioff Characteristics', QUANTITY = 'TIME', SETPOINT = 30. /
&DEVC ID = 'Mist Nozzle 5', XYZ = 10,10,11.9, ORIENTATION = -0.3536,0.3536,-.866, PROP_ID = 'Marioff Characteristics', QUANTITY = 'TIME', SETPOINT = 30. /
&DEVC ID = 'Mist Nozzle 6', XYZ = 10,10,11.9, ORIENTATION = 0.3536,-0.3536,-.866, PROP_ID = 'Marioff Characteristics', QUANTITY = 'TIME', SETPOINT = 30. /
&DEVC ID = 'Mist Nozzle 7', XYZ = 10,10,11.9, ORIENTATION = -0.3536,-0.3536,-.866,PROP_ID = 'Marioff Characteristics', QUANTITY = 'TIME', SETPOINT = 30. /
&DEVC ID = 'Mist Nozzle 8', XYZ = 10,10,11.9, ORIENTATION = 0,0.5,-.866, PROP_ID = 'Marioff Characteristics', QUANTITY = 'TIME', SETPOINT = 30. /
&DEVC ID = 'Mist Nozzle 9', XYZ = 10,10,11.9, ORIENTATION = 0,-0.5,-.866, PROP_ID = 'Marioff Characteristics', QUANTITY = 'TIME', SETPOINT = 30. /

&DEVC ID = 'Mist Nozzle 1', XYZ = 10,13,11.9, ORIENTATION = 0,0,-1, PROP_ID = 'Marioff Characteristics', QUANTITY = 'TIME', SETPOINT = 30. /
&DEVC ID = 'Mist Nozzle 2', XYZ = 10,13,11.9, ORIENTATION = 0.5,0,-.866, PROP_ID = 'Marioff Characteristics', QUANTITY = 'TIME', SETPOINT = 30. /
&DEVC ID = 'Mist Nozzle 3', XYZ = 10,13,11.9, ORIENTATION = -0.5,0,-.866,PROP_ID = 'Marioff Characteristics', QUANTITY = 'TIME', SETPOINT = 30. /
&DEVC ID = 'Mist Nozzle 4', XYZ = 10,13,11.9, ORIENTATION = 0.3536,0.3563,-.866,PROP_ID = 'Marioff Characteristics', QUANTITY = 'TIME', SETPOINT = 30. /
&DEVC ID = 'Mist Nozzle 5', XYZ = 10,13,11.9, ORIENTATION = -0.3536,0.3536,-.866, PROP_ID = 'Marioff Characteristics', QUANTITY = 'TIME', SETPOINT = 30. /
&DEVC ID = 'Mist Nozzle 6', XYZ = 10,13,11.9, ORIENTATION = 0.3536,-0.3536,-.866, PROP_ID = 'Marioff Characteristics', QUANTITY = 'TIME', SETPOINT = 30. /

&DEVC ID = 'Mist Nozzle 7', XYZ = 10,13,11.9, ORIENTATION = -0.3536,-0.3536,-.866,PROP_ID = 'Marioff Characteristics', QUANTITY = 'TIME', SETPOINT = 30. /
&DEVC ID = 'Mist Nozzle 8', XYZ = 10,13,11.9, ORIENTATION = 0,0.5,-.866, PROP_ID = 'Marioff Characteristics', QUANTITY = 'TIME', SETPOINT = 30. /
&DEVC ID = 'Mist Nozzle 9', XYZ = 10,13,11.9, ORIENTATION = 0,-0.5,-.866, PROP_ID = 'Marioff Characteristics', QUANTITY = 'TIME', SETPOINT = 30. /

&DEVC ID = 'Mist Nozzle 1', XYZ = 10,16,11.9, ORIENTATION = 0,0,-1, PROP_ID = 'Marioff Characteristics', QUANTITY = 'TIME', SETPOINT = 30. /
&DEVC ID = 'Mist Nozzle 2', XYZ = 10,16,11.9, ORIENTATION = 0.5,0,-.866, PROP_ID = 'Marioff Characteristics', QUANTITY = 'TIME', SETPOINT = 30. /
&DEVC ID = 'Mist Nozzle 3', XYZ = 10,16,11.9, ORIENTATION = -0.5,0,-.866,PROP_ID = 'Marioff Characteristics', QUANTITY = 'TIME', SETPOINT = 30. /
&DEVC ID = 'Mist Nozzle 4', XYZ = 10,16,11.9, ORIENTATION = 0.3536,0.3563,-.866,PROP_ID = 'Marioff Characteristics', QUANTITY = 'TIME', SETPOINT = 30. /
&DEVC ID = 'Mist Nozzle 5', XYZ = 10,16,11.9, ORIENTATION = -0.3536,0.3536,-.866, PROP_ID = 'Marioff Characteristics', QUANTITY = 'TIME', SETPOINT = 30. /
&DEVC ID = 'Mist Nozzle 6', XYZ = 10,16,11.9, ORIENTATION = 0.3536,-0.3536,-.866, PROP_ID = 'Marioff Characteristics', QUANTITY = 'TIME', SETPOINT = 30. /
&DEVC ID = 'Mist Nozzle 7', XYZ = 10,16,11.9, ORIENTATION = -0.3536,-0.3536,-.866,PROP_ID = 'Marioff Characteristics', QUANTITY = 'TIME', SETPOINT = 30. /
&DEVC ID = 'Mist Nozzle 8', XYZ = 10,16,11.9, ORIENTATION = 0,0.5,-.866, PROP_ID = 'Marioff Characteristics', QUANTITY = 'TIME', SETPOINT = 30. /
&DEVC ID = 'Mist Nozzle 9', XYZ = 10,16,11.9, ORIENTATION = 0,-0.5,-.866, PROP_ID = 'Marioff Characteristics', QUANTITY = 'TIME', SETPOINT = 30. /

&DEVC ID = 'Mist Nozzle 1', XYZ = 10,19,11.9, ORIENTATION = 0,0,-1, PROP_ID = 'Marioff Characteristics', QUANTITY = 'TIME', SETPOINT = 30. /
&DEVC ID = 'Mist Nozzle 2', XYZ = 10,19,11.9, ORIENTATION = 0.5,0,-.866, PROP_ID = 'Marioff Characteristics', QUANTITY = 'TIME', SETPOINT = 30. /
&DEVC ID = 'Mist Nozzle 3', XYZ = 10,19,11.9, ORIENTATION = -0.5,0,-.866,PROP_ID = 'Marioff Characteristics', QUANTITY = 'TIME', SETPOINT = 30. /
&DEVC ID = 'Mist Nozzle 4', XYZ = 10,19,11.9, ORIENTATION = 0.3536,0.3563,-.866,PROP_ID = 'Marioff Characteristics', QUANTITY = 'TIME', SETPOINT = 30. /
&DEVC ID = 'Mist Nozzle 5', XYZ = 10,19,11.9, ORIENTATION = -0.3536,0.3536,-.866, PROP_ID = 'Marioff Characteristics', QUANTITY = 'TIME', SETPOINT = 30. /
&DEVC ID = 'Mist Nozzle 6', XYZ = 10,19,11.9, ORIENTATION = 0.3536,-0.3536,-.866, PROP_ID = 'Marioff Characteristics', QUANTITY = 'TIME', SETPOINT = 30. /
&DEVC ID = 'Mist Nozzle 7', XYZ = 10,19,11.9, ORIENTATION = -0.3536,-0.3536,-.866,PROP_ID = 'Marioff Characteristics', QUANTITY = 'TIME', SETPOINT = 30. /
&DEVC ID = 'Mist Nozzle 8', XYZ = 10,19,11.9, ORIENTATION = 0,0.5,-.866, PROP_ID = 'Marioff Characteristics', QUANTITY = 'TIME', SETPOINT = 30. /
&DEVC ID = 'Mist Nozzle 9', XYZ = 10,19,11.9, ORIENTATION = 0,-0.5,-.866, PROP_ID = 'Marioff Characteristics', QUANTITY = 'TIME', SETPOINT = 30. /

&DEVC ID = 'Mist Nozzle 1', XYZ = 10,22,11.9, ORIENTATION = 0,0,-1, PROP_ID = 'Marioff Characteristics', QUANTITY = 'TIME', SETPOINT = 30. /
&DEVC ID = 'Mist Nozzle 2', XYZ = 10,22,11.9, ORIENTATION = 0.5,0,-.866, PROP_ID = 'Marioff Characteristics', QUANTITY = 'TIME', SETPOINT = 30. /
&DEVC ID = 'Mist Nozzle 3', XYZ = 10,22,11.9, ORIENTATION = -0.5,0,-.866, PROP_ID = 'Marioff Characteristics', QUANTITY = 'TIME', SETPOINT = 30. /
&DEVC ID = 'Mist Nozzle 4', XYZ = 10,22,11.9, ORIENTATION = 0.3536,0.3563,-.866, PROP_ID = 'Marioff Characteristics', QUANTITY = 'TIME', SETPOINT = 30. /
&DEVC ID = 'Mist Nozzle 5', XYZ = 10,22,11.9, ORIENTATION = -0.3536,0.3536,-.866, PROP_ID = 'Marioff Characteristics', QUANTITY = 'TIME', SETPOINT = 30. /
&DEVC ID = 'Mist Nozzle 6', XYZ = 10,22,11.9, ORIENTATION = 0.3536,-0.3536,-.866, PROP_ID = 'Marioff Characteristics', QUANTITY = 'TIME', SETPOINT = 30. /
&DEVC ID = 'Mist Nozzle 7', XYZ = 10,22,11.9, ORIENTATION = -0.3536,-0.3536,-.866, PROP_ID = 'Marioff Characteristics', QUANTITY = 'TIME', SETPOINT = 30. /
&DEVC ID = 'Mist Nozzle 8', XYZ = 10,22,11.9, ORIENTATION = 0,0.5,-.866, PROP_ID = 'Marioff Characteristics', QUANTITY = 'TIME', SETPOINT = 30. /
&DEVC ID = 'Mist Nozzle 9', XYZ = 10,22,11.9, ORIENTATION = 0,-0.5,-.866, PROP_ID = 'Marioff Characteristics', QUANTITY = 'TIME', SETPOINT = 30. /

&DEVC ID = 'Mist Nozzle 1', XYZ = 10,25,11.9, ORIENTATION = 0,0,-1, PROP_ID = 'Marioff Characteristics', QUANTITY = 'TIME', SETPOINT = 30. /
&DEVC ID = 'Mist Nozzle 2', XYZ = 10,25,11.9, ORIENTATION = 0.5,0,-.866, PROP_ID = 'Marioff Characteristics', QUANTITY = 'TIME', SETPOINT = 30. /
&DEVC ID = 'Mist Nozzle 3', XYZ = 10,25,11.9, ORIENTATION = -0.5,0,-.866, PROP_ID = 'Marioff Characteristics', QUANTITY = 'TIME', SETPOINT = 30. /
&DEVC ID = 'Mist Nozzle 4', XYZ = 10,25,11.9, ORIENTATION = 0.3536,0.3563,-.866, PROP_ID = 'Marioff Characteristics', QUANTITY = 'TIME', SETPOINT = 30. /
&DEVC ID = 'Mist Nozzle 5', XYZ = 10,25,11.9, ORIENTATION = -0.3536,0.3536,-.866, PROP_ID = 'Marioff Characteristics', QUANTITY = 'TIME', SETPOINT = 30. /
&DEVC ID = 'Mist Nozzle 6', XYZ = 10,25,11.9, ORIENTATION = 0.3536,-0.3536,-.866, PROP_ID = 'Marioff Characteristics', QUANTITY = 'TIME', SETPOINT = 30. /
&DEVC ID = 'Mist Nozzle 7', XYZ = 10,25,11.9, ORIENTATION = -0.3536,-0.3536,-.866, PROP_ID = 'Marioff Characteristics', QUANTITY = 'TIME', SETPOINT = 30. /
&DEVC ID = 'Mist Nozzle 8', XYZ = 10,25,11.9, ORIENTATION = 0,0.5,-.866, PROP_ID = 'Marioff Characteristics', QUANTITY = 'TIME', SETPOINT = 30. /
&DEVC ID = 'Mist Nozzle 9', XYZ = 10,25,11.9, ORIENTATION = 0,-0.5,-.866, PROP_ID = 'Marioff Characteristics', QUANTITY = 'TIME', SETPOINT = 30. /

/x = 13 row

&DEVC ID = 'Mist Nozzle 1', XYZ = 13,1,11.9, ORIENTATION = 0,0,-1, PROP_ID = 'Marioff Characteristics', QUANTITY = 'TIME', SETPOINT = 30. /
&DEVC ID = 'Mist Nozzle 2', XYZ = 13,1,11.9, ORIENTATION = 0.5,0,-.866, PROP_ID = 'Marioff Characteristics', QUANTITY = 'TIME', SETPOINT = 30. /

&DEVC ID = 'Mist Nozzle 3', XYZ = 13,1,11.9, ORIENTATION = -0.5,0,-.866,PROP_ID = 'Marioff Characteristics', QUANTITY = 'TIME', SETPOINT = 30. /
&DEVC ID = 'Mist Nozzle 4', XYZ = 13,1,11.9, ORIENTATION = 0.3536,0.3563,-.866,PROP_ID = 'Marioff Characteristics', QUANTITY = 'TIME', SETPOINT = 30. /
&DEVC ID = 'Mist Nozzle 5', XYZ = 13,1,11.9, ORIENTATION = -0.3536,0.3536,-.866,PROP_ID = 'Marioff Characteristics', QUANTITY = 'TIME', SETPOINT = 30. /
&DEVC ID = 'Mist Nozzle 6', XYZ = 13,1,11.9, ORIENTATION = 0.3536,-0.3536,-.866,PROP_ID = 'Marioff Characteristics', QUANTITY = 'TIME', SETPOINT = 30. /
&DEVC ID = 'Mist Nozzle 7', XYZ = 13,1,11.9, ORIENTATION = -0.3536,-0.3536,-.866,PROP_ID = 'Marioff Characteristics', QUANTITY = 'TIME', SETPOINT = 30. /
&DEVC ID = 'Mist Nozzle 8', XYZ = 13,1,11.9, ORIENTATION = 0,0.5,-.866,PROP_ID = 'Marioff Characteristics', QUANTITY = 'TIME', SETPOINT = 30. /
&DEVC ID = 'Mist Nozzle 9', XYZ = 13,1,11.9, ORIENTATION = 0,-0.5,-.866,PROP_ID = 'Marioff Characteristics', QUANTITY = 'TIME', SETPOINT = 30. /

&DEVC ID = 'Mist Nozzle 1', XYZ = 13,4,11.9, ORIENTATION = 0,0,-1, PROP_ID = 'Marioff Characteristics', QUANTITY = 'TIME', SETPOINT = 30. /
&DEVC ID = 'Mist Nozzle 2', XYZ = 13,4,11.9, ORIENTATION = 0.5,0,-.866,PROP_ID = 'Marioff Characteristics', QUANTITY = 'TIME', SETPOINT = 30. /
&DEVC ID = 'Mist Nozzle 3', XYZ = 13,4,11.9, ORIENTATION = -0.5,0,-.866,PROP_ID = 'Marioff Characteristics', QUANTITY = 'TIME', SETPOINT = 30. /
&DEVC ID = 'Mist Nozzle 4', XYZ = 13,4,11.9, ORIENTATION = 0.3536,0.3563,-.866,PROP_ID = 'Marioff Characteristics', QUANTITY = 'TIME', SETPOINT = 30. /
&DEVC ID = 'Mist Nozzle 5', XYZ = 13,4,11.9, ORIENTATION = -0.3536,0.3536,-.866,PROP_ID = 'Marioff Characteristics', QUANTITY = 'TIME', SETPOINT = 30. /
&DEVC ID = 'Mist Nozzle 6', XYZ = 13,4,11.9, ORIENTATION = 0.3536,-0.3536,-.866,PROP_ID = 'Marioff Characteristics', QUANTITY = 'TIME', SETPOINT = 30. /
&DEVC ID = 'Mist Nozzle 7', XYZ = 13,4,11.9, ORIENTATION = -0.3536,-0.3536,-.866,PROP_ID = 'Marioff Characteristics', QUANTITY = 'TIME', SETPOINT = 30. /
&DEVC ID = 'Mist Nozzle 8', XYZ = 13,4,11.9, ORIENTATION = 0,0.5,-.866,PROP_ID = 'Marioff Characteristics', QUANTITY = 'TIME', SETPOINT = 30. /
&DEVC ID = 'Mist Nozzle 9', XYZ = 13,4,11.9, ORIENTATION = 0,-0.5,-.866,PROP_ID = 'Marioff Characteristics', QUANTITY = 'TIME', SETPOINT = 30. /

&DEVC ID = 'Mist Nozzle 1', XYZ = 13,7,11.9, ORIENTATION = 0,0,-1, PROP_ID = 'Marioff Characteristics', QUANTITY = 'TIME', SETPOINT = 30. /
&DEVC ID = 'Mist Nozzle 2', XYZ = 13,7,11.9, ORIENTATION = 0.5,0,-.866,PROP_ID = 'Marioff Characteristics', QUANTITY = 'TIME', SETPOINT = 30. /
&DEVC ID = 'Mist Nozzle 3', XYZ = 13,7,11.9, ORIENTATION = -0.5,0,-.866,PROP_ID = 'Marioff Characteristics', QUANTITY = 'TIME', SETPOINT = 30. /
&DEVC ID = 'Mist Nozzle 4', XYZ = 13,7,11.9, ORIENTATION = 0.3536,0.3563,-.866,PROP_ID = 'Marioff Characteristics', QUANTITY = 'TIME', SETPOINT = 30. /
&DEVC ID = 'Mist Nozzle 5', XYZ = 13,7,11.9, ORIENTATION = -0.3536,0.3536,-.866,PROP_ID = 'Marioff Characteristics', QUANTITY = 'TIME', SETPOINT = 30. /

&DEVC ID = 'Mist Nozzle 6', XYZ = 13,7,11.9, ORIENTATION = 0.3536,-0.3536,-.866, PROP_ID = 'Marioff Characteristics', QUANTITY = 'TIME', SETPOINT = 30. /
&DEVC ID = 'Mist Nozzle 7', XYZ = 13,7,11.9, ORIENTATION = -0.3536,-0.3536,-.866, PROP_ID = 'Marioff Characteristics', QUANTITY = 'TIME', SETPOINT = 30. /
&DEVC ID = 'Mist Nozzle 8', XYZ = 13,7,11.9, ORIENTATION = 0,0.5,-.866, PROP_ID = 'Marioff Characteristics', QUANTITY = 'TIME', SETPOINT = 30. /
&DEVC ID = 'Mist Nozzle 9', XYZ = 13,7,11.9, ORIENTATION = 0,-0.5,-.866, PROP_ID = 'Marioff Characteristics', QUANTITY = 'TIME', SETPOINT = 30. /

&DEVC ID = 'Mist Nozzle 1', XYZ = 13,10,11.9, ORIENTATION = 0,0,-1, PROP_ID = 'Marioff Characteristics', QUANTITY = 'TIME', SETPOINT = 30. /
&DEVC ID = 'Mist Nozzle 2', XYZ = 13,10,11.9, ORIENTATION = 0.5,0,-.866, PROP_ID = 'Marioff Characteristics', QUANTITY = 'TIME', SETPOINT = 30. /
&DEVC ID = 'Mist Nozzle 3', XYZ = 13,10,11.9, ORIENTATION = -0.5,0,-.866, PROP_ID = 'Marioff Characteristics', QUANTITY = 'TIME', SETPOINT = 30. /
&DEVC ID = 'Mist Nozzle 4', XYZ = 13,10,11.9, ORIENTATION = 0.3536,0.3563,-.866, PROP_ID = 'Marioff Characteristics', QUANTITY = 'TIME', SETPOINT = 30. /
&DEVC ID = 'Mist Nozzle 5', XYZ = 13,10,11.9, ORIENTATION = -0.3536,0.3536,-.866, PROP_ID = 'Marioff Characteristics', QUANTITY = 'TIME', SETPOINT = 30. /
&DEVC ID = 'Mist Nozzle 6', XYZ = 13,10,11.9, ORIENTATION = 0.3536,-0.3536,-.866, PROP_ID = 'Marioff Characteristics', QUANTITY = 'TIME', SETPOINT = 30. /
&DEVC ID = 'Mist Nozzle 7', XYZ = 13,10,11.9, ORIENTATION = -0.3536,-0.3536,-.866, PROP_ID = 'Marioff Characteristics', QUANTITY = 'TIME', SETPOINT = 30. /
&DEVC ID = 'Mist Nozzle 8', XYZ = 13,10,11.9, ORIENTATION = 0,0.5,-.866, PROP_ID = 'Marioff Characteristics', QUANTITY = 'TIME', SETPOINT = 30. /
&DEVC ID = 'Mist Nozzle 9', XYZ = 13,10,11.9, ORIENTATION = 0,-0.5,-.866, PROP_ID = 'Marioff Characteristics', QUANTITY = 'TIME', SETPOINT = 30. /

&DEVC ID = 'Mist Nozzle 1', XYZ = 13,13,11.9, ORIENTATION = 0,0,-1, PROP_ID = 'Marioff Characteristics', QUANTITY = 'TIME', SETPOINT = 30. /
&DEVC ID = 'Mist Nozzle 2', XYZ = 13,13,11.9, ORIENTATION = 0.5,0,-.866, PROP_ID = 'Marioff Characteristics', QUANTITY = 'TIME', SETPOINT = 30. /
&DEVC ID = 'Mist Nozzle 3', XYZ = 13,13,11.9, ORIENTATION = -0.5,0,-.866, PROP_ID = 'Marioff Characteristics', QUANTITY = 'TIME', SETPOINT = 30. /
&DEVC ID = 'Mist Nozzle 4', XYZ = 13,13,11.9, ORIENTATION = 0.3536,0.3563,-.866, PROP_ID = 'Marioff Characteristics', QUANTITY = 'TIME', SETPOINT = 30. /
&DEVC ID = 'Mist Nozzle 5', XYZ = 13,13,11.9, ORIENTATION = -0.3536,0.3536,-.866, PROP_ID = 'Marioff Characteristics', QUANTITY = 'TIME', SETPOINT = 30. /
&DEVC ID = 'Mist Nozzle 6', XYZ = 13,13,11.9, ORIENTATION = 0.3536,-0.3536,-.866, PROP_ID = 'Marioff Characteristics', QUANTITY = 'TIME', SETPOINT = 30. /
&DEVC ID = 'Mist Nozzle 7', XYZ = 13,13,11.9, ORIENTATION = -0.3536,-0.3536,-.866, PROP_ID = 'Marioff Characteristics', QUANTITY = 'TIME', SETPOINT = 30. /
&DEVC ID = 'Mist Nozzle 8', XYZ = 13,13,11.9, ORIENTATION = 0,0.5,-.866, PROP_ID = 'Marioff Characteristics', QUANTITY = 'TIME', SETPOINT = 30. /

&DEVC ID = 'Mist Nozzle 9', XYZ = 13,13,11.9, ORIENTATION = 0,-0.5,-.866,
PROP_ID = 'Marioff Characteristics', QUANTITY = 'TIME', SETPOINT = 30. /

&DEVC ID = 'Mist Nozzle 1', XYZ = 13,16,11.9, ORIENTATION = 0,0,-1, PROP_ID =
'Marioff Characteristics', QUANTITY = 'TIME', SETPOINT = 30. /

&DEVC ID = 'Mist Nozzle 2', XYZ = 13,16,11.9, ORIENTATION = 0.5,0,-.866,
PROP_ID = 'Marioff Characteristics', QUANTITY = 'TIME', SETPOINT = 30. /

&DEVC ID = 'Mist Nozzle 3', XYZ = 13,16,11.9, ORIENTATION = -0.5,0,-
.866,PROP_ID = 'Marioff Characteristics', QUANTITY = 'TIME', SETPOINT = 30. /

&DEVC ID = 'Mist Nozzle 4', XYZ = 13,16,11.9, ORIENTATION = 0.3536,0.3563,-
.866,PROP_ID = 'Marioff Characteristics', QUANTITY = 'TIME', SETPOINT = 30. /

&DEVC ID = 'Mist Nozzle 5', XYZ = 13,16,11.9, ORIENTATION = -0.3536,0.3536,-
.866, PROP_ID = 'Marioff Characteristics', QUANTITY = 'TIME', SETPOINT = 30. /

&DEVC ID = 'Mist Nozzle 6', XYZ = 13,16,11.9, ORIENTATION = 0.3536,-0.3536,-
.866, PROP_ID = 'Marioff Characteristics', QUANTITY = 'TIME', SETPOINT = 30. /

&DEVC ID = 'Mist Nozzle 7', XYZ = 13,16,11.9, ORIENTATION = -0.3536,-0.3536,-
.866,PROP_ID = 'Marioff Characteristics', QUANTITY = 'TIME', SETPOINT = 30. /

&DEVC ID = 'Mist Nozzle 8', XYZ = 13,16,11.9, ORIENTATION = 0,0.5,-.866,
PROP_ID = 'Marioff Characteristics', QUANTITY = 'TIME', SETPOINT = 30. /

&DEVC ID = 'Mist Nozzle 9', XYZ = 13,16,11.9, ORIENTATION = 0,-0.5,-.866,
PROP_ID = 'Marioff Characteristics', QUANTITY = 'TIME', SETPOINT = 30. /

&DEVC ID = 'Mist Nozzle 1', XYZ = 13,19,11.9, ORIENTATION = 0,0,-1, PROP_ID =
'Marioff Characteristics', QUANTITY = 'TIME', SETPOINT = 30. /

&DEVC ID = 'Mist Nozzle 2', XYZ = 13,19,11.9, ORIENTATION = 0.5,0,-.866,
PROP_ID = 'Marioff Characteristics', QUANTITY = 'TIME', SETPOINT = 30. /

&DEVC ID = 'Mist Nozzle 3', XYZ = 13,19,11.9, ORIENTATION = -0.5,0,-
.866,PROP_ID = 'Marioff Characteristics', QUANTITY = 'TIME', SETPOINT = 30. /

&DEVC ID = 'Mist Nozzle 4', XYZ = 13,19,11.9, ORIENTATION = 0.3536,0.3563,-
.866,PROP_ID = 'Marioff Characteristics', QUANTITY = 'TIME', SETPOINT = 30. /

&DEVC ID = 'Mist Nozzle 5', XYZ = 13,19,11.9, ORIENTATION = -0.3536,0.3536,-
.866, PROP_ID = 'Marioff Characteristics', QUANTITY = 'TIME', SETPOINT = 30. /

&DEVC ID = 'Mist Nozzle 6', XYZ = 13,19,11.9, ORIENTATION = 0.3536,-0.3536,-
.866, PROP_ID = 'Marioff Characteristics', QUANTITY = 'TIME', SETPOINT = 30. /

&DEVC ID = 'Mist Nozzle 7', XYZ = 13,19,11.9, ORIENTATION = -0.3536,-0.3536,-
.866,PROP_ID = 'Marioff Characteristics', QUANTITY = 'TIME', SETPOINT = 30. /

&DEVC ID = 'Mist Nozzle 8', XYZ = 13,19,11.9, ORIENTATION = 0,0.5,-.866,
PROP_ID = 'Marioff Characteristics', QUANTITY = 'TIME', SETPOINT = 30. /

&DEVC ID = 'Mist Nozzle 9', XYZ = 13,19,11.9, ORIENTATION = 0,-0.5,-.866,
PROP_ID = 'Marioff Characteristics', QUANTITY = 'TIME', SETPOINT = 30. /

&DEVC ID = 'Mist Nozzle 1', XYZ = 13,22,11.9, ORIENTATION = 0,0,-1, PROP_ID =
'Marioff Characteristics', QUANTITY = 'TIME', SETPOINT = 30. /

&DEVC ID = 'Mist Nozzle 2', XYZ = 13,22,11.9, ORIENTATION = 0.5,0,-.866,
PROP_ID = 'Marioff Characteristics', QUANTITY = 'TIME', SETPOINT = 30. /

&DEVC ID = 'Mist Nozzle 3', XYZ = 13,22,11.9, ORIENTATION = -0.5,0,-
.866,PROP_ID = 'Marioff Characteristics', QUANTITY = 'TIME', SETPOINT = 30. /
&DEVC ID = 'Mist Nozzle 4', XYZ = 13,22,11.9, ORIENTATION = 0.3536,0.3563,-
.866,PROP_ID = 'Marioff Characteristics', QUANTITY = 'TIME', SETPOINT = 30. /
&DEVC ID = 'Mist Nozzle 5', XYZ = 13,22,11.9, ORIENTATION = -0.3536,0.3536,-
.866, PROP_ID = 'Marioff Characteristics' , QUANTITY = 'TIME', SETPOINT = 30./
&DEVC ID = 'Mist Nozzle 6', XYZ = 13,22,11.9, ORIENTATION = 0.3536,-0.3536,-
.866, PROP_ID = 'Marioff Characteristics' , QUANTITY = 'TIME', SETPOINT = 30./
&DEVC ID = 'Mist Nozzle 7', XYZ = 13,22,11.9, ORIENTATION = -0.3536,-0.3536,-
.866,PROP_ID = 'Marioff Characteristics', QUANTITY = 'TIME', SETPOINT = 30. /
&DEVC ID = 'Mist Nozzle 8', XYZ = 13,22,11.9, ORIENTATION = 0,0.5,-.866,
PROP_ID = 'Marioff Characteristics', QUANTITY = 'TIME', SETPOINT = 30. /
&DEVC ID = 'Mist Nozzle 9', XYZ = 13,22,11.9, ORIENTATION = 0,-0.5,-.866,
PROP_ID = 'Marioff Characteristics', QUANTITY = 'TIME', SETPOINT = 30. /

&DEVC ID = 'Mist Nozzle 1', XYZ = 13,25,11.9, ORIENTATION = 0,0,-1, PROP_ID =
'Marioff Characteristics', QUANTITY = 'TIME', SETPOINT = 30. /
&DEVC ID = 'Mist Nozzle 2', XYZ = 13,25,11.9, ORIENTATION = 0.5,0,-.866,
PROP_ID = 'Marioff Characteristics', QUANTITY = 'TIME', SETPOINT = 30. /
&DEVC ID = 'Mist Nozzle 3', XYZ = 13,25,11.9, ORIENTATION = -0.5,0,-
.866,PROP_ID = 'Marioff Characteristics', QUANTITY = 'TIME', SETPOINT = 30. /
&DEVC ID = 'Mist Nozzle 4', XYZ = 13,25,11.9, ORIENTATION = 0.3536,0.3563,-
.866,PROP_ID = 'Marioff Characteristics', QUANTITY = 'TIME', SETPOINT = 30. /
&DEVC ID = 'Mist Nozzle 5', XYZ = 13,25,11.9, ORIENTATION = -0.3536,0.3536,-
.866, PROP_ID = 'Marioff Characteristics' , QUANTITY = 'TIME', SETPOINT = 30./
&DEVC ID = 'Mist Nozzle 6', XYZ = 13,25,11.9, ORIENTATION = 0.3536,-0.3536,-
.866, PROP_ID = 'Marioff Characteristics' , QUANTITY = 'TIME', SETPOINT = 30./
&DEVC ID = 'Mist Nozzle 7', XYZ = 13,25,11.9, ORIENTATION = -0.3536,-0.3536,-
.866,PROP_ID = 'Marioff Characteristics', QUANTITY = 'TIME', SETPOINT = 30. /
&DEVC ID = 'Mist Nozzle 8', XYZ = 13,25,11.9, ORIENTATION = 0,0.5,-.866,
PROP_ID = 'Marioff Characteristics', QUANTITY = 'TIME', SETPOINT = 30. /
&DEVC ID = 'Mist Nozzle 9', XYZ = 13,25,11.9, ORIENTATION = 0,-0.5,-.866,
PROP_ID = 'Marioff Characteristics', QUANTITY = 'TIME', SETPOINT = 30. /

/x = 16 row

&DEVC ID = 'Mist Nozzle 1', XYZ = 16,1,11.9, ORIENTATION = 0,0,-1, PROP_ID =
'Marioff Characteristics', QUANTITY = 'TIME', SETPOINT = 30. /
&DEVC ID = 'Mist Nozzle 2', XYZ = 16,1,11.9, ORIENTATION = 0.5,0,-.866,
PROP_ID = 'Marioff Characteristics', QUANTITY = 'TIME', SETPOINT = 30. /
&DEVC ID = 'Mist Nozzle 3', XYZ = 16,1,11.9, ORIENTATION = -0.5,0,-
.866,PROP_ID = 'Marioff Characteristics', QUANTITY = 'TIME', SETPOINT = 30. /
&DEVC ID = 'Mist Nozzle 4', XYZ = 16,1,11.9, ORIENTATION = 0.3536,0.3563,-
.866,PROP_ID = 'Marioff Characteristics', QUANTITY = 'TIME', SETPOINT = 30. /
&DEVC ID = 'Mist Nozzle 5', XYZ = 16,1,11.9, ORIENTATION = -0.3536,0.3536,-
.866, PROP_ID = 'Marioff Characteristics' , QUANTITY = 'TIME', SETPOINT = 30./

&DEVC ID = 'Mist Nozzle 6', XYZ = 16,1,11.9, ORIENTATION = 0.3536,-0.3536,-.866, PROP_ID = 'Marioff Characteristics', QUANTITY = 'TIME', SETPOINT = 30. /
&DEVC ID = 'Mist Nozzle 7', XYZ = 16,1,11.9, ORIENTATION = -0.3536,-0.3536,-.866, PROP_ID = 'Marioff Characteristics', QUANTITY = 'TIME', SETPOINT = 30. /
&DEVC ID = 'Mist Nozzle 8', XYZ = 16,1,11.9, ORIENTATION = 0,0.5,-.866, PROP_ID = 'Marioff Characteristics', QUANTITY = 'TIME', SETPOINT = 30. /
&DEVC ID = 'Mist Nozzle 9', XYZ = 16,1,11.9, ORIENTATION = 0,-0.5,-.866, PROP_ID = 'Marioff Characteristics', QUANTITY = 'TIME', SETPOINT = 30. /

&DEVC ID = 'Mist Nozzle 1', XYZ = 16,4,11.9, ORIENTATION = 0,0,-1, PROP_ID = 'Marioff Characteristics', QUANTITY = 'TIME', SETPOINT = 30. /
&DEVC ID = 'Mist Nozzle 2', XYZ = 16,4,11.9, ORIENTATION = 0.5,0,-.866, PROP_ID = 'Marioff Characteristics', QUANTITY = 'TIME', SETPOINT = 30. /
&DEVC ID = 'Mist Nozzle 3', XYZ = 16,4,11.9, ORIENTATION = -0.5,0,-.866, PROP_ID = 'Marioff Characteristics', QUANTITY = 'TIME', SETPOINT = 30. /
&DEVC ID = 'Mist Nozzle 4', XYZ = 16,4,11.9, ORIENTATION = 0.3536,0.3536,-.866, PROP_ID = 'Marioff Characteristics', QUANTITY = 'TIME', SETPOINT = 30. /
&DEVC ID = 'Mist Nozzle 5', XYZ = 16,4,11.9, ORIENTATION = -0.3536,0.3536,-.866, PROP_ID = 'Marioff Characteristics', QUANTITY = 'TIME', SETPOINT = 30. /
&DEVC ID = 'Mist Nozzle 6', XYZ = 16,4,11.9, ORIENTATION = 0.3536,-0.3536,-.866, PROP_ID = 'Marioff Characteristics', QUANTITY = 'TIME', SETPOINT = 30. /
&DEVC ID = 'Mist Nozzle 7', XYZ = 16,4,11.9, ORIENTATION = -0.3536,-0.3536,-.866, PROP_ID = 'Marioff Characteristics', QUANTITY = 'TIME', SETPOINT = 30. /
&DEVC ID = 'Mist Nozzle 8', XYZ = 16,4,11.9, ORIENTATION = 0,0.5,-.866, PROP_ID = 'Marioff Characteristics', QUANTITY = 'TIME', SETPOINT = 30. /
&DEVC ID = 'Mist Nozzle 9', XYZ = 16,4,11.9, ORIENTATION = 0,-0.5,-.866, PROP_ID = 'Marioff Characteristics', QUANTITY = 'TIME', SETPOINT = 30. /

&DEVC ID = 'Mist Nozzle 1', XYZ = 16,7,11.9, ORIENTATION = 0,0,-1, PROP_ID = 'Marioff Characteristics', QUANTITY = 'TIME', SETPOINT = 30. /
&DEVC ID = 'Mist Nozzle 2', XYZ = 16,7,11.9, ORIENTATION = 0.5,0,-.866, PROP_ID = 'Marioff Characteristics', QUANTITY = 'TIME', SETPOINT = 30. /
&DEVC ID = 'Mist Nozzle 3', XYZ = 16,7,11.9, ORIENTATION = -0.5,0,-.866, PROP_ID = 'Marioff Characteristics', QUANTITY = 'TIME', SETPOINT = 30. /
&DEVC ID = 'Mist Nozzle 4', XYZ = 16,7,11.9, ORIENTATION = 0.3536,0.3536,-.866, PROP_ID = 'Marioff Characteristics', QUANTITY = 'TIME', SETPOINT = 30. /
&DEVC ID = 'Mist Nozzle 5', XYZ = 16,7,11.9, ORIENTATION = -0.3536,0.3536,-.866, PROP_ID = 'Marioff Characteristics', QUANTITY = 'TIME', SETPOINT = 30. /
&DEVC ID = 'Mist Nozzle 6', XYZ = 16,7,11.9, ORIENTATION = 0.3536,-0.3536,-.866, PROP_ID = 'Marioff Characteristics', QUANTITY = 'TIME', SETPOINT = 30. /
&DEVC ID = 'Mist Nozzle 7', XYZ = 16,7,11.9, ORIENTATION = -0.3536,-0.3536,-.866, PROP_ID = 'Marioff Characteristics', QUANTITY = 'TIME', SETPOINT = 30. /
&DEVC ID = 'Mist Nozzle 8', XYZ = 16,7,11.9, ORIENTATION = 0,0.5,-.866, PROP_ID = 'Marioff Characteristics', QUANTITY = 'TIME', SETPOINT = 30. /

&DEVC ID = 'Mist Nozzle 9', XYZ = 16,7,11.9, ORIENTATION = 0,-0.5,-.866,
PROP_ID = 'Marioff Characteristics', QUANTITY = 'TIME', SETPOINT = 30. /

&DEVC ID = 'Mist Nozzle 1', XYZ = 16,10,11.9, ORIENTATION = 0,0,-1, PROP_ID =
'Marioff Characteristics', QUANTITY = 'TIME', SETPOINT = 30. /
&DEVC ID = 'Mist Nozzle 2', XYZ = 16,10,11.9, ORIENTATION = 0.5,0,-.866,
PROP_ID = 'Marioff Characteristics', QUANTITY = 'TIME', SETPOINT = 30. /
&DEVC ID = 'Mist Nozzle 3', XYZ = 16,10,11.9, ORIENTATION = -0.5,0,-
.866,PROP_ID = 'Marioff Characteristics', QUANTITY = 'TIME', SETPOINT = 30. /
&DEVC ID = 'Mist Nozzle 4', XYZ = 16,10,11.9, ORIENTATION = 0.3536,0.3563,-
.866,PROP_ID = 'Marioff Characteristics', QUANTITY = 'TIME', SETPOINT = 30. /
&DEVC ID = 'Mist Nozzle 5', XYZ = 16,10,11.9, ORIENTATION = -0.3536,0.3536,-
.866, PROP_ID = 'Marioff Characteristics', QUANTITY = 'TIME', SETPOINT = 30./
&DEVC ID = 'Mist Nozzle 6', XYZ = 16,10,11.9, ORIENTATION = 0.3536,-0.3536,-
.866, PROP_ID = 'Marioff Characteristics', QUANTITY = 'TIME', SETPOINT=30./
&DEVC ID = 'Mist Nozzle 7', XYZ = 16,10,11.9, ORIENTATION = -0.3536,-0.3536,-
.866,PROP_ID = 'Marioff Characteristics', QUANTITY = 'TIME', SETPOINT = 30. /
&DEVC ID = 'Mist Nozzle 8', XYZ = 16,10,11.9, ORIENTATION = 0,0.5,-.866,
PROP_ID = 'Marioff Characteristics', QUANTITY = 'TIME', SETPOINT = 30. /
&DEVC ID = 'Mist Nozzle 9', XYZ = 16,10,11.9, ORIENTATION = 0,-0.5,-.866,
PROP_ID = 'Marioff Characteristics', QUANTITY = 'TIME', SETPOINT = 30. /

&DEVC ID = 'Mist Nozzle 1', XYZ = 16,13,11.9, ORIENTATION = 0,0,-1, PROP_ID =
'Marioff Characteristics', QUANTITY = 'TIME', SETPOINT = 30. /
&DEVC ID = 'Mist Nozzle 2', XYZ = 16,13,11.9, ORIENTATION = 0.5,0,-.866,
PROP_ID = 'Marioff Characteristics', QUANTITY = 'TIME', SETPOINT = 30. /
&DEVC ID = 'Mist Nozzle 3', XYZ = 16,13,11.9, ORIENTATION = -0.5,0,-
.866,PROP_ID = 'Marioff Characteristics', QUANTITY = 'TIME', SETPOINT = 30. /
&DEVC ID = 'Mist Nozzle 4', XYZ = 16,13,11.9, ORIENTATION = 0.3536,0.3563,-
.866,PROP_ID = 'Marioff Characteristics', QUANTITY = 'TIME', SETPOINT = 30. /
&DEVC ID = 'Mist Nozzle 5', XYZ = 16,13,11.9, ORIENTATION = -0.3536,0.3536,-
.866, PROP_ID = 'Marioff Characteristics', QUANTITY = 'TIME', SETPOINT = 30./
&DEVC ID = 'Mist Nozzle 6', XYZ = 16,13,11.9, ORIENTATION = 0.3536,-0.3536,-
.866, PROP_ID = 'Marioff Characteristics', QUANTITY = 'TIME', SETPOINT = 30./
&DEVC ID = 'Mist Nozzle 7', XYZ = 16,13,11.9, ORIENTATION = -0.3536,-0.3536,-
.866,PROP_ID = 'Marioff Characteristics', QUANTITY = 'TIME', SETPOINT = 30. /
&DEVC ID = 'Mist Nozzle 8', XYZ = 16,13,11.9, ORIENTATION = 0,0.5,-.866,
PROP_ID = 'Marioff Characteristics', QUANTITY = 'TIME', SETPOINT = 30. /
&DEVC ID = 'Mist Nozzle 9', XYZ = 16,13,11.9, ORIENTATION = 0,-0.5,-.866,
PROP_ID = 'Marioff Characteristics', QUANTITY = 'TIME', SETPOINT = 30. /

&DEVC ID = 'Mist Nozzle 1', XYZ = 16,16,11.9, ORIENTATION = 0,0,-1, PROP_ID =
'Marioff Characteristics', QUANTITY = 'TIME', SETPOINT = 30. /

&DEVC ID = 'Mist Nozzle 2', XYZ = 16,16,11.9, ORIENTATION = 0.5,0,-.866,
PROP_ID = 'Marioff Characteristics', QUANTITY = 'TIME', SETPOINT = 30. /
&DEVC ID = 'Mist Nozzle 3', XYZ = 16,16,11.9, ORIENTATION = -0.5,0,-
.866,PROP_ID = 'Marioff Characteristics', QUANTITY = 'TIME', SETPOINT = 30. /
&DEVC ID = 'Mist Nozzle 4', XYZ = 16,16,11.9, ORIENTATION = 0.3536,0.3563,-
.866,PROP_ID = 'Marioff Characteristics', QUANTITY = 'TIME', SETPOINT = 30. /
&DEVC ID = 'Mist Nozzle 5', XYZ = 16,16,11.9, ORIENTATION = -0.3536,0.3536,-
.866, PROP_ID = 'Marioff Characteristics' , QUANTITY = 'TIME', SETPOINT = 30./
&DEVC ID = 'Mist Nozzle 6', XYZ = 16,16,11.9, ORIENTATION = 0.3536,-0.3536,-
.866, PROP_ID = 'Marioff Characteristics' , QUANTITY = 'TIME', SETPOINT = 30./
&DEVC ID = 'Mist Nozzle 7', XYZ = 16,16,11.9, ORIENTATION = -0.3536,-0.3536,-
.866,PROP_ID = 'Marioff Characteristics', QUANTITY = 'TIME', SETPOINT = 30. /
&DEVC ID = 'Mist Nozzle 8', XYZ = 16,16,11.9, ORIENTATION = 0,0.5,-.866,
PROP_ID = 'Marioff Characteristics', QUANTITY = 'TIME', SETPOINT = 30. /
&DEVC ID = 'Mist Nozzle 9', XYZ = 16,16,11.9, ORIENTATION = 0,-0.5,-.866,
PROP_ID = 'Marioff Characteristics', QUANTITY = 'TIME', SETPOINT = 30. /

&DEVC ID = 'Mist Nozzle 1', XYZ = 16,19,11.9, ORIENTATION = 0,0,-1, PROP_ID =
'Marioff Characteristics', QUANTITY = 'TIME', SETPOINT = 30. /
&DEVC ID = 'Mist Nozzle 2', XYZ = 16,19,11.9, ORIENTATION = 0.5,0,-.866,
PROP_ID = 'Marioff Characteristics', QUANTITY = 'TIME', SETPOINT = 30. /
&DEVC ID = 'Mist Nozzle 3', XYZ = 16,19,11.9, ORIENTATION = -0.5,0,-
.866,PROP_ID = 'Marioff Characteristics', QUANTITY = 'TIME', SETPOINT = 30. /
&DEVC ID = 'Mist Nozzle 4', XYZ = 16,19,11.9, ORIENTATION = 0.3536,0.3563,-
.866,PROP_ID = 'Marioff Characteristics', QUANTITY = 'TIME', SETPOINT = 30. /
&DEVC ID = 'Mist Nozzle 5', XYZ = 16,19,11.9, ORIENTATION = -0.3536,0.3536,-
.866, PROP_ID = 'Marioff Characteristics' , QUANTITY = 'TIME', SETPOINT = 30./
&DEVC ID = 'Mist Nozzle 6', XYZ = 16,19,11.9, ORIENTATION = 0.3536,-0.3536,-
.866, PROP_ID = 'Marioff Characteristics' , QUANTITY = 'TIME', SETPOINT = 30./
&DEVC ID = 'Mist Nozzle 7', XYZ = 16,19,11.9, ORIENTATION = -0.3536,-0.3536,-
.866,PROP_ID = 'Marioff Characteristics', QUANTITY = 'TIME', SETPOINT = 30. /
&DEVC ID = 'Mist Nozzle 8', XYZ = 16,19,11.9, ORIENTATION = 0,0.5,-.866,
PROP_ID = 'Marioff Characteristics', QUANTITY = 'TIME', SETPOINT = 30. /
&DEVC ID = 'Mist Nozzle 9', XYZ = 16,19,11.9, ORIENTATION = 0,-0.5,-.866,
PROP_ID = 'Marioff Characteristics', QUANTITY = 'TIME', SETPOINT = 30. /

&DEVC ID = 'Mist Nozzle 1', XYZ = 16,22,11.9, ORIENTATION = 0,0,-1, PROP_ID =
'Marioff Characteristics', QUANTITY = 'TIME', SETPOINT = 30. /
&DEVC ID = 'Mist Nozzle 2', XYZ = 16,22,11.9, ORIENTATION = 0.5,0,-.866,
PROP_ID = 'Marioff Characteristics', QUANTITY = 'TIME', SETPOINT = 30. /
&DEVC ID = 'Mist Nozzle 3', XYZ = 16,22,11.9, ORIENTATION = -0.5,0,-
.866,PROP_ID = 'Marioff Characteristics', QUANTITY = 'TIME', SETPOINT = 30. /
&DEVC ID = 'Mist Nozzle 4', XYZ = 16,22,11.9, ORIENTATION = 0.3536,0.3563,-
.866,PROP_ID = 'Marioff Characteristics', QUANTITY = 'TIME', SETPOINT = 30. /

&DEVC ID = 'Mist Nozzle 5', XYZ = 16,22,11.9, ORIENTATION = -0.3536,0.3536,-.866, PROP_ID = 'Marioff Characteristics', QUANTITY = 'TIME', SETPOINT = 30. /
&DEVC ID = 'Mist Nozzle 6', XYZ = 16,22,11.9, ORIENTATION = 0.3536,-0.3536,-.866, PROP_ID = 'Marioff Characteristics', QUANTITY = 'TIME', SETPOINT = 30. /
&DEVC ID = 'Mist Nozzle 7', XYZ = 16,22,11.9, ORIENTATION = -0.3536,-0.3536,-.866, PROP_ID = 'Marioff Characteristics', QUANTITY = 'TIME', SETPOINT = 30. /
&DEVC ID = 'Mist Nozzle 8', XYZ = 16,22,11.9, ORIENTATION = 0,0.5,-.866, PROP_ID = 'Marioff Characteristics', QUANTITY = 'TIME', SETPOINT = 30. /
&DEVC ID = 'Mist Nozzle 9', XYZ = 16,22,11.9, ORIENTATION = 0,-0.5,-.866, PROP_ID = 'Marioff Characteristics', QUANTITY = 'TIME', SETPOINT = 30. /

&DEVC ID = 'Mist Nozzle 1', XYZ = 16,25,11.9, ORIENTATION = 0,0,-1, PROP_ID = 'Marioff Characteristics', QUANTITY = 'TIME', SETPOINT = 30. /
&DEVC ID = 'Mist Nozzle 2', XYZ = 16,25,11.9, ORIENTATION = 0.5,0,-.866, PROP_ID = 'Marioff Characteristics', QUANTITY = 'TIME', SETPOINT = 30. /
&DEVC ID = 'Mist Nozzle 3', XYZ = 16,25,11.9, ORIENTATION = -0.5,0,-.866, PROP_ID = 'Marioff Characteristics', QUANTITY = 'TIME', SETPOINT = 30. /
&DEVC ID = 'Mist Nozzle 4', XYZ = 16,25,11.9, ORIENTATION = 0.3536,0.3536,-.866, PROP_ID = 'Marioff Characteristics', QUANTITY = 'TIME', SETPOINT = 30. /
&DEVC ID = 'Mist Nozzle 5', XYZ = 16,25,11.9, ORIENTATION = -0.3536,0.3536,-.866, PROP_ID = 'Marioff Characteristics', QUANTITY = 'TIME', SETPOINT = 30. /
&DEVC ID = 'Mist Nozzle 6', XYZ = 16,25,11.9, ORIENTATION = 0.3536,-0.3536,-.866, PROP_ID = 'Marioff Characteristics', QUANTITY = 'TIME', SETPOINT = 30. /
&DEVC ID = 'Mist Nozzle 7', XYZ = 16,25,11.9, ORIENTATION = -0.3536,-0.3536,-.866, PROP_ID = 'Marioff Characteristics', QUANTITY = 'TIME', SETPOINT = 30. /
&DEVC ID = 'Mist Nozzle 8', XYZ = 16,25,11.9, ORIENTATION = 0,0.5,-.866, PROP_ID = 'Marioff Characteristics', QUANTITY = 'TIME', SETPOINT = 30. /
&DEVC ID = 'Mist Nozzle 9', XYZ = 16,25,11.9, ORIENTATION = 0,-0.5,-.866, PROP_ID = 'Marioff Characteristics', QUANTITY = 'TIME', SETPOINT = 30. /

Appendix H: Additional Incident Heat Flux Results

H.1 Nozzle A Results

H.1.1 Simulation A.1

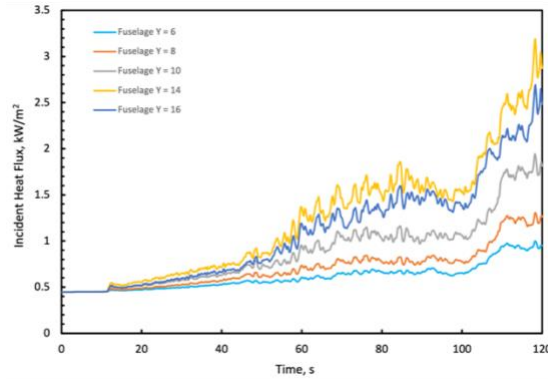


Figure 0-1 Incident Heat Flux versus time for various locations along the fuselage ($X=13$) for simulation A.1

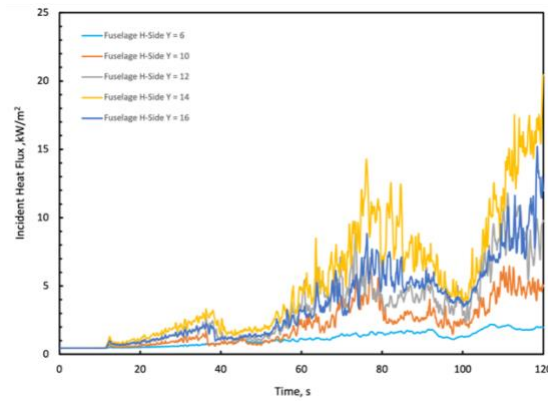


Figure 0-2 Incident Heat Flux versus time for various locations along the high side of the fuselage for simulation A.1

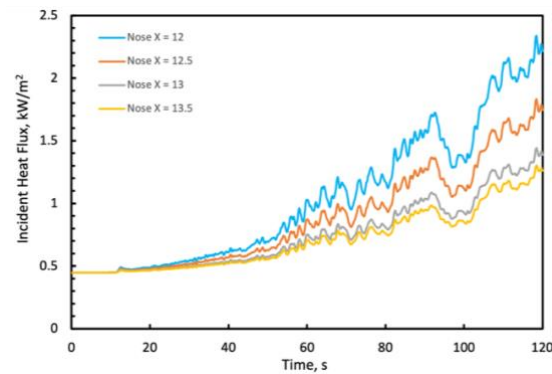


Figure 0-3 Incident Heat Flux versus time for various locations along the Nose of the aircraft ($Y = 20$) for simulation A.1

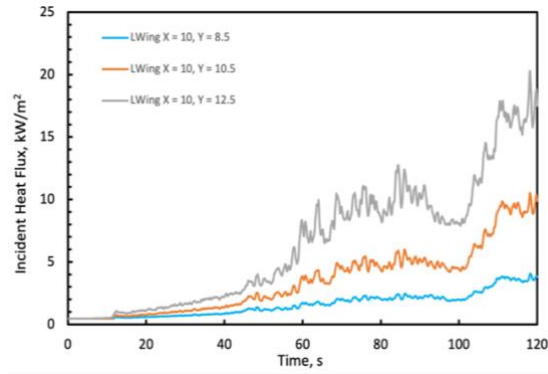


Figure 0-4 Incident Heat Flux versus time for various locations on the left wing ($X = 10$) for simulation A.1

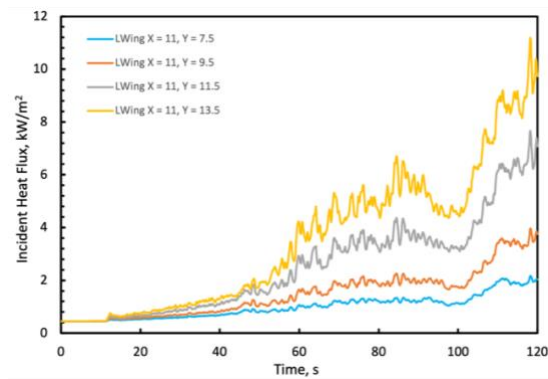


Figure 0-5 Incident Heat Flux versus time for various locations on the left wing ($X = 11$) for simulation A.1

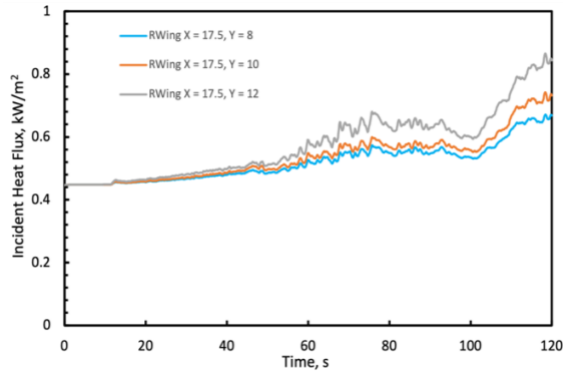


Figure 0-6 Incident Heat Flux versus time for various locations on the right wing ($X = 17.5$) for simulation A.1

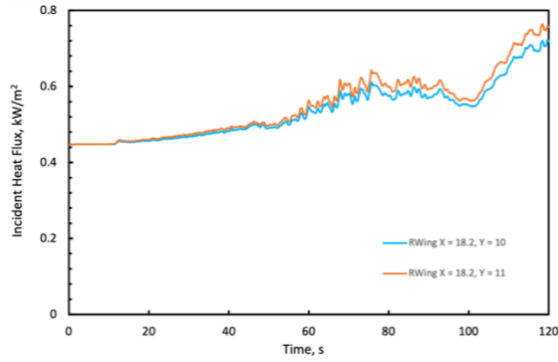


Figure 0-7 Incident Heat Flux versus time for various locations on the right wing ($X = 18.2$) for simulation A.1

H.1.2 Simulation A.2

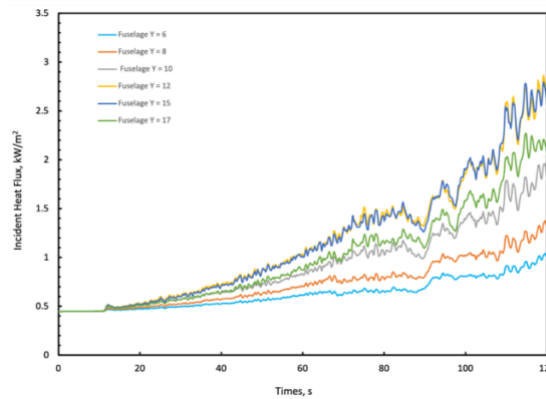


Figure 0-8 Incident Heat Flux versus time for various locations along the fuselage ($X=13$) for simulation A.2

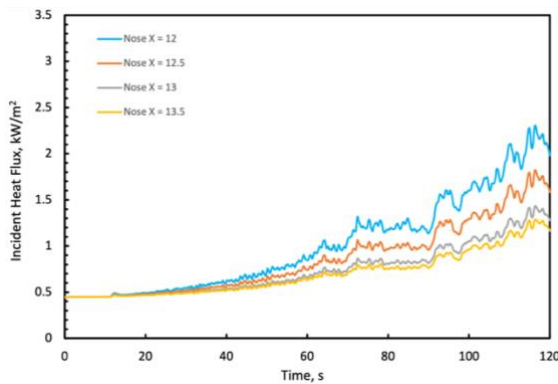


Figure 0-9 Incident Heat Flux versus time for various locations along the Nose of the aircraft ($Y = 20$) for simulation A.2

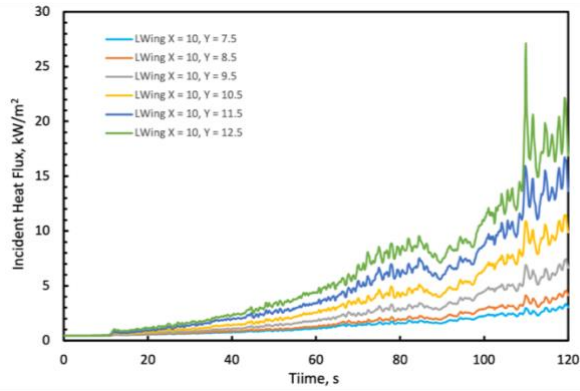


Figure 0-10 Incident Heat Flux versus time for various locations on the left wing ($X = 10$) for simulation A.2

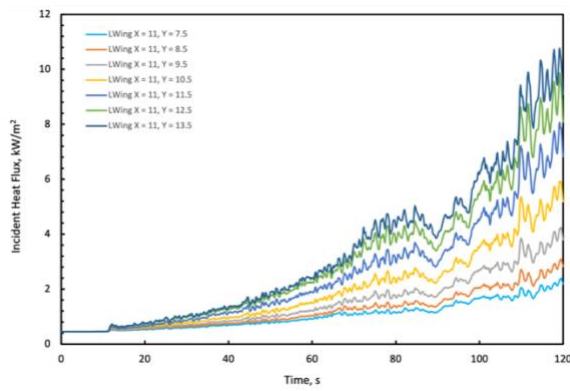


Figure 0-11 Incident Heat Flux versus time for various locations on the left wing ($X = 11$) for simulation A.2

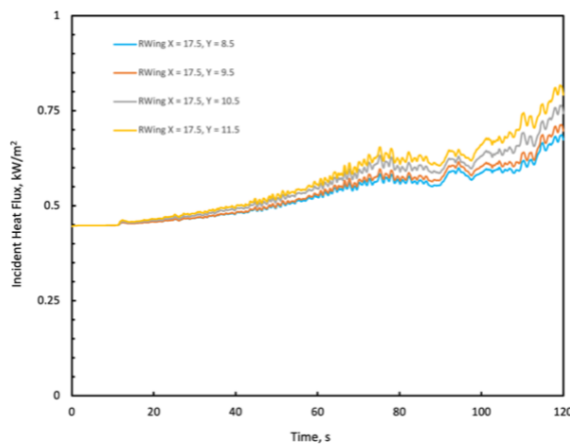


Figure 0-12 Incident Heat Flux versus time for various locations on the right wing ($X = 17.5$) for simulation A.2

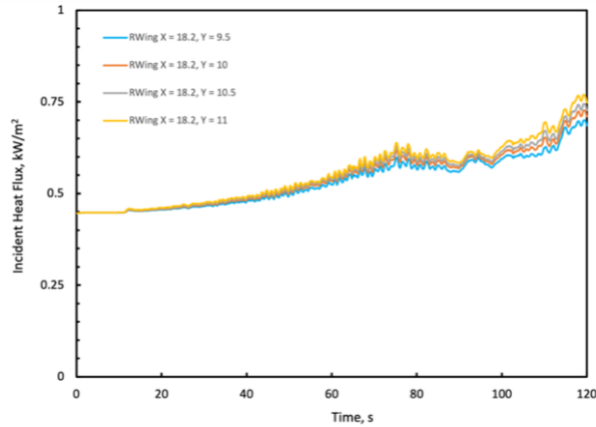


Figure 0-13 Incident Heat Flux versus time for various locations on the right wing ($X = 18.2$) for simulation A.2

H.2 Nozzle B Results

H.2.1 Simulation B.1.a

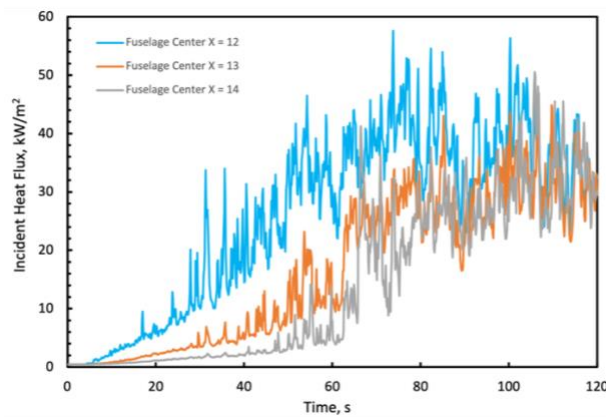


Figure 0-14 Incident Heat Flux versus time for various locations across the center of the fuselage ($Y = 13$) for simulation B.1.a

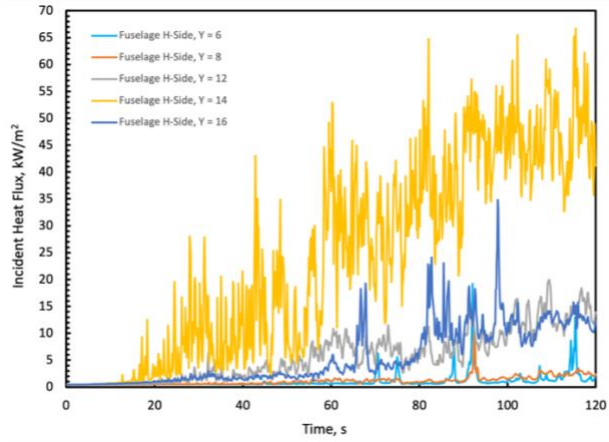


Figure 0-15 Incident Heat Flux versus time for various locations along the high side of the fuselage for simulation B.1.a

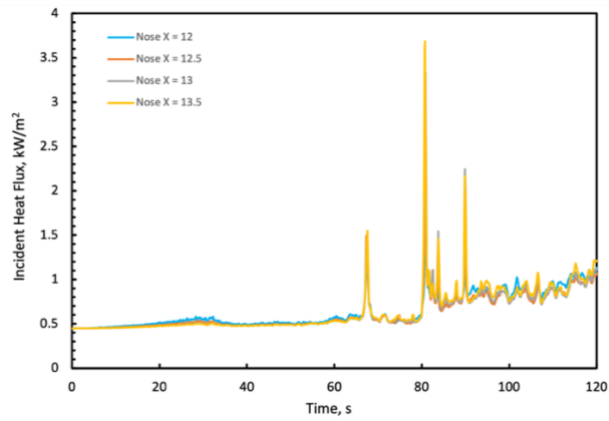


Figure 0-16 Incident Heat Flux versus time for various locations along the Nose of the aircraft ($Y = 20$) for simulation B.1.a

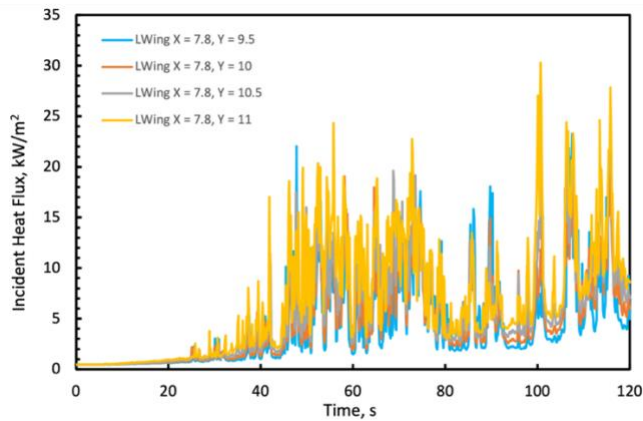


Figure 0-17 Incident Heat Flux versus time for various locations on the left wing ($X = 7.8$) for simulation B.1.a

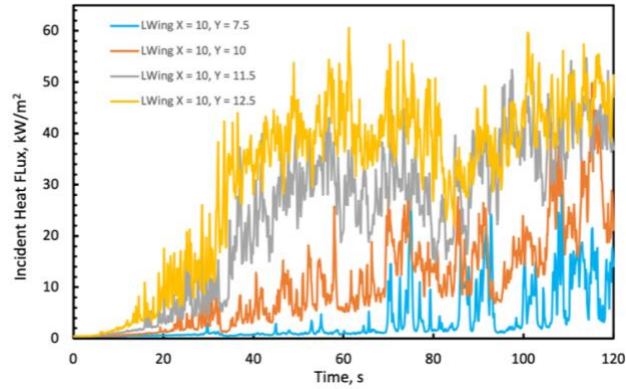


Figure 0-18 Incident Heat Flux versus time for various locations on the left wing ($X = 10$) for simulation B.1.a

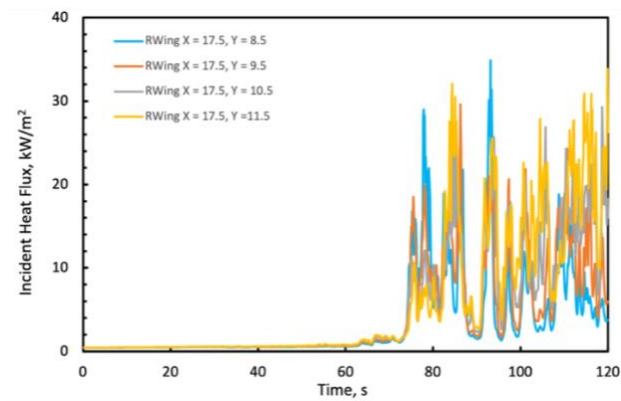


Figure 0-19 Incident Heat Flux versus time for various locations on the right wing ($X = 17.5$) for simulation B.1.a

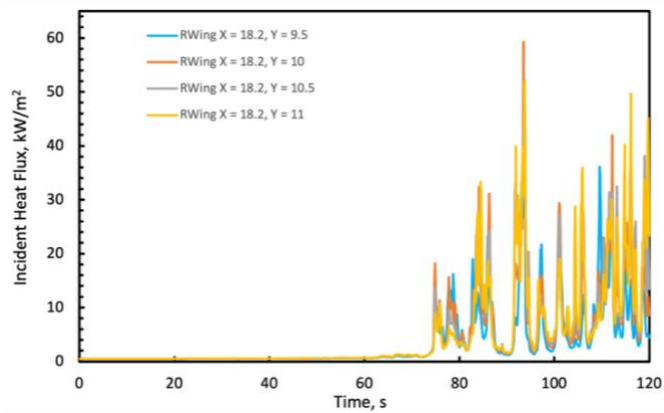


Figure 0-20 Incident Heat Flux versus time for various locations on the right wing ($X = 18.2$) for simulation B.1.a

H.2.2 Simulation B.1.b

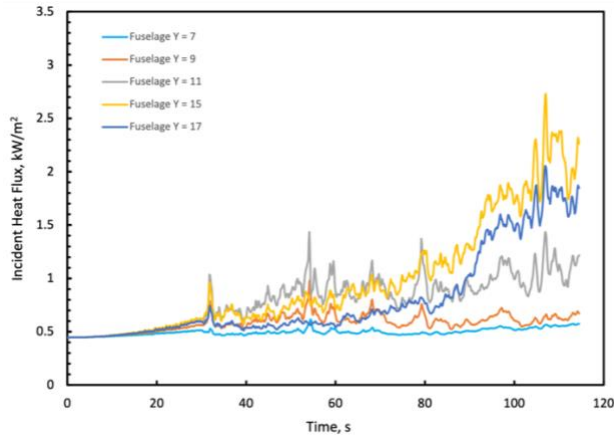


Figure 0-21 Incident Heat Flux versus time for various locations along the fuselage ($X=13$) for simulation B.1.b

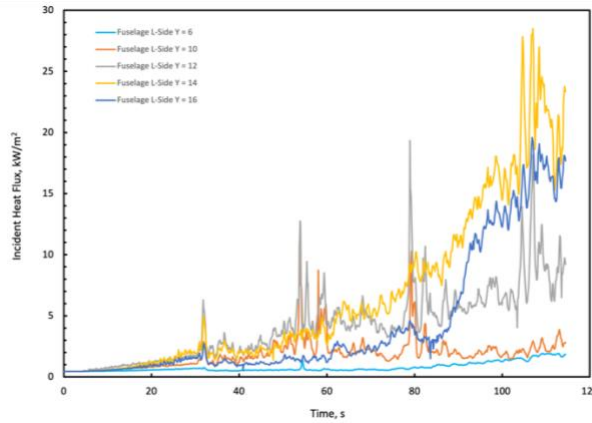


Figure 0-22 Incident Heat Flux versus time for various locations along the low side of the fuselage for simulation B.1.b

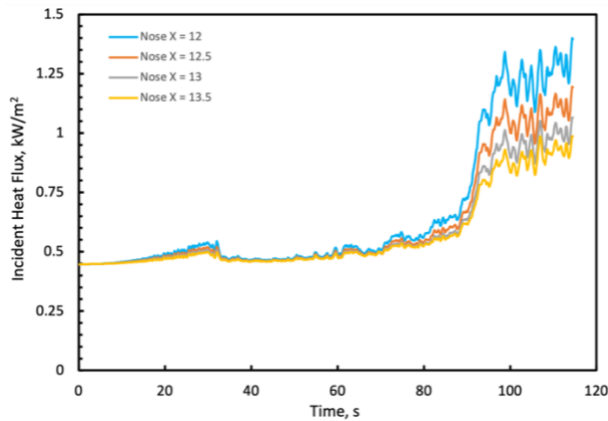


Figure 0-23 Incident Heat Flux versus time for various locations along the Nose of the aircraft ($Y = 20$) for simulation B.1.b

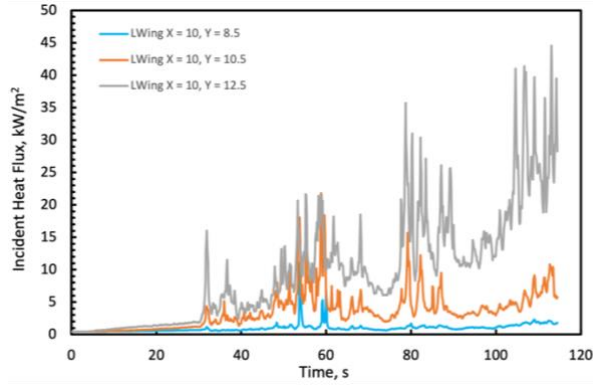


Figure 0-24 Incident Heat Flux versus time for various locations on the left wing ($X = 10$) for simulation B.1.b

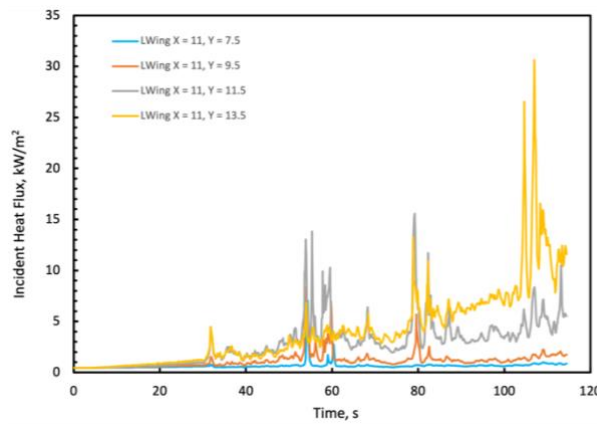


Figure 0-25 Incident Heat Flux versus time for various locations on the left wing ($X = 11$) for simulation B.1.b

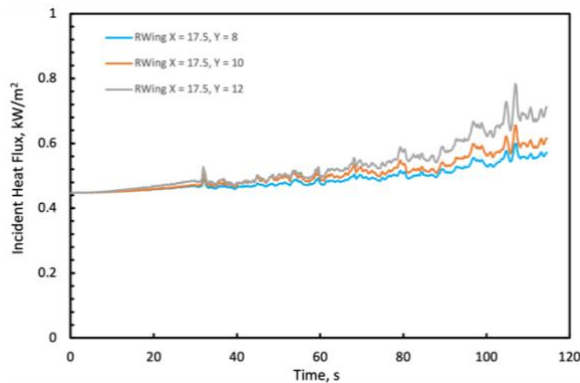


Figure 0-26 Incident Heat Flux versus time for various locations on the right wing ($X = 17.5$) for simulation B.1.b

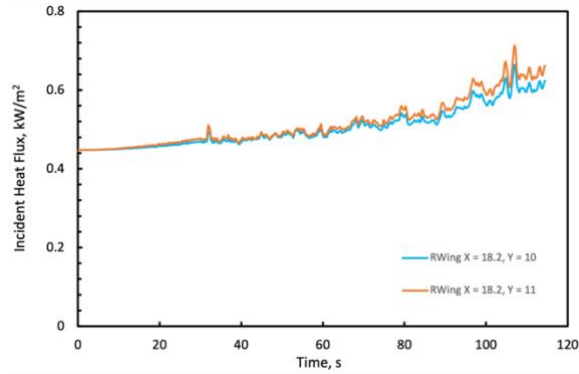


Figure 0-27 Incident Heat Flux versus time for various locations on the right wing ($X = 18.2$) for simulation B.1.b

H.2.3 Simulation B.2

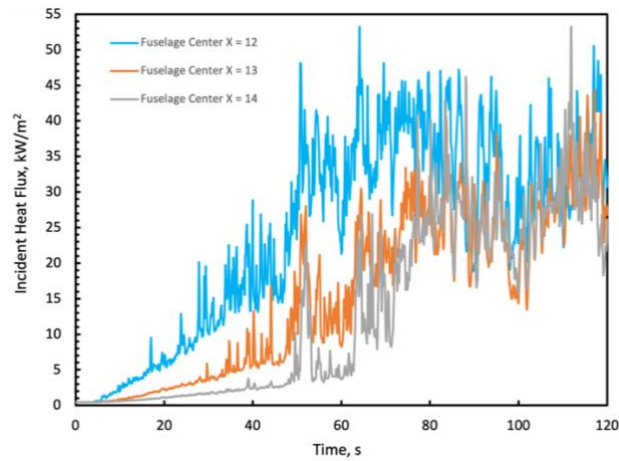


Figure 0-28 Incident Heat Flux versus time for various locations across the center of the fuselage ($Y=13$) for simulation B.2

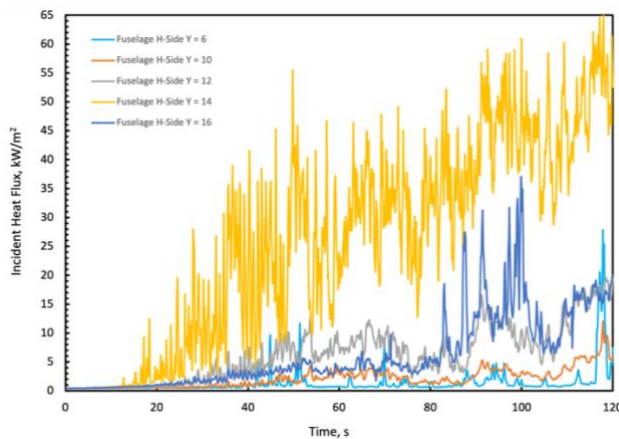


Figure 0-29 Incident Heat Flux versus time for various locations along the high side of the fuselage for simulation B.2

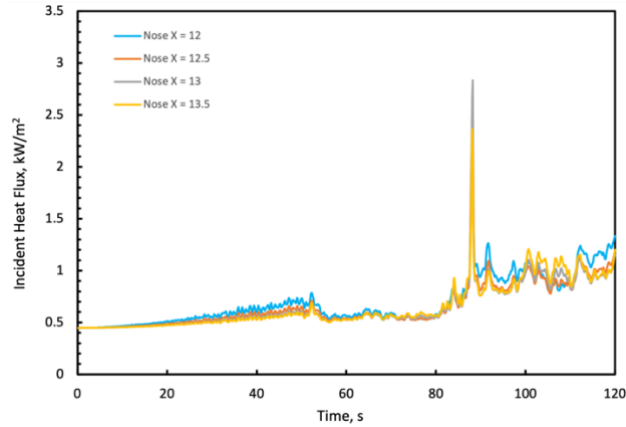


Figure 0-30 Incident Heat Flux versus time for various locations along the Nose of the aircraft ($Y = 20$) for simulation B.2

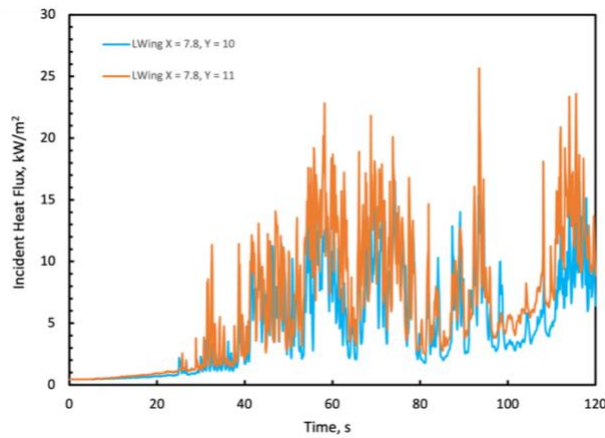


Figure 0-31 Incident Heat Flux versus time for various locations on the left wing ($X = 7.8$) for simulation B.2

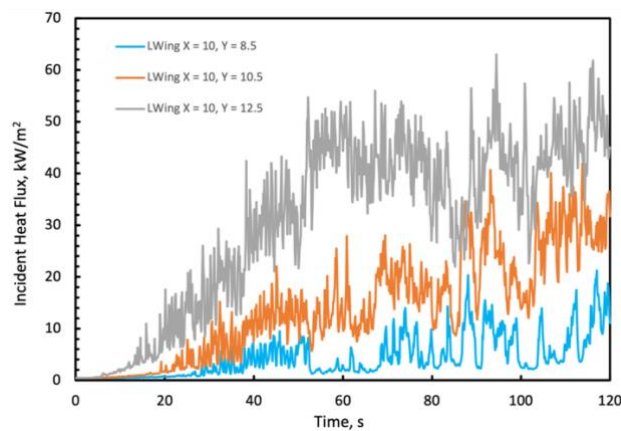


Figure 0-32 Incident Heat Flux versus time for various locations on the left wing ($X = 10$) for simulation B.2

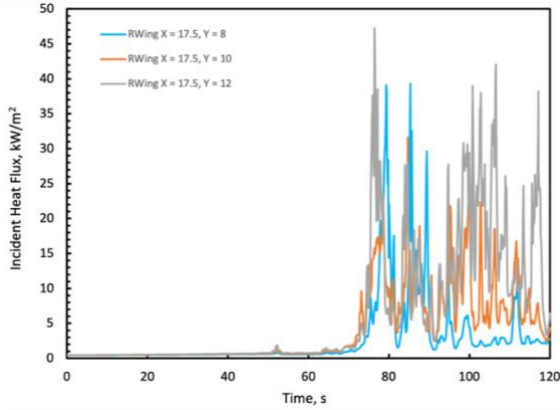


Figure 0-33 Incident Heat Flux versus time for various locations on the right wing ($X = 17.5$) for simulation B.2

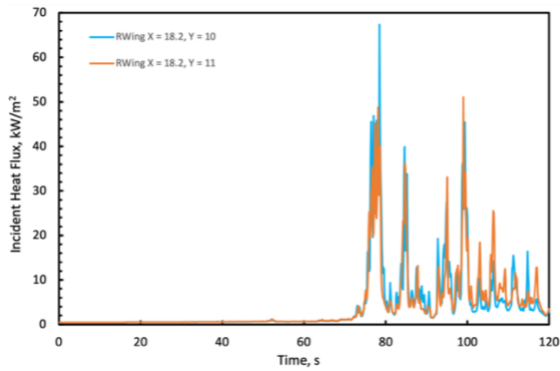


Figure 0-34 Incident Heat Flux versus time for various locations on the right wing ($X = 18.2$) for simulation B.2

H.3 Nozzle C Results

H.3.1 Simulation C.1

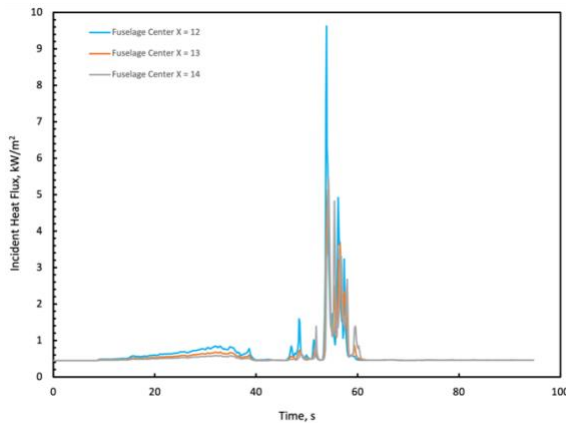


Figure 0-35 Incident Heat Flux versus time for various locations across the center of the fuselage ($Y = 13$) for simulation C.1

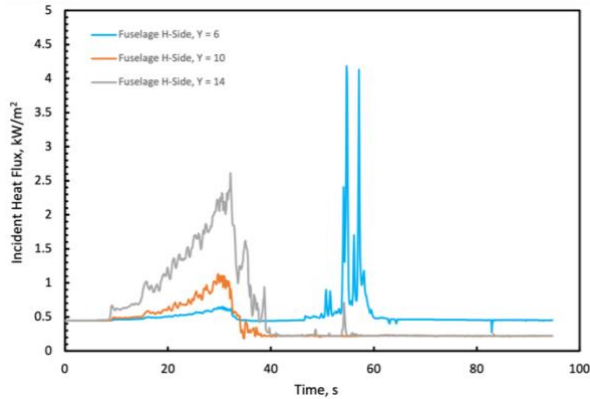


Figure 0-36 Incident Heat Flux versus time for various locations along the high side of the fuselage for simulation C.1

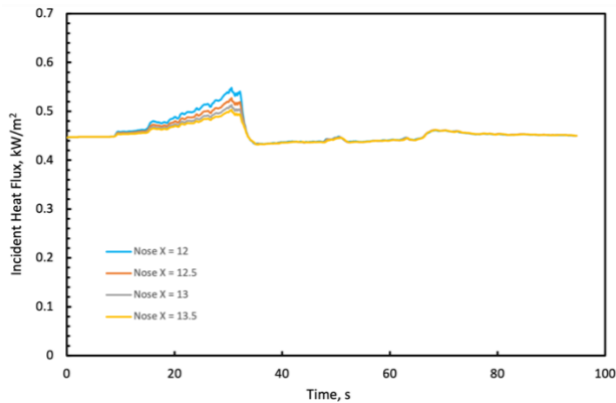


Figure 0-37 Incident Heat Flux versus time for various locations along the Nose of the aircraft ($Y = 20$) for simulation C.1

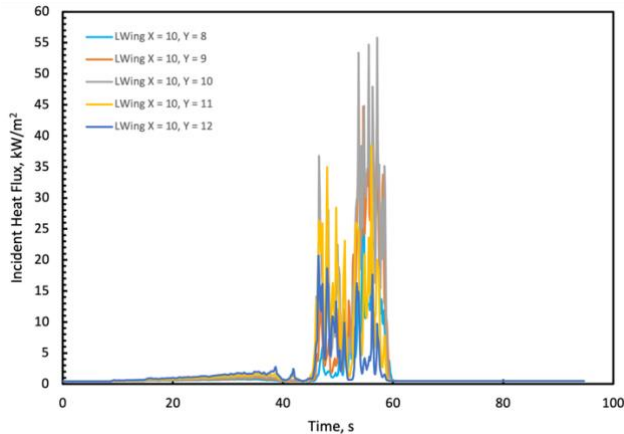


Figure 0-38 Incident Heat Flux versus time for various locations on the left wing ($X = 10$) for simulation C.1

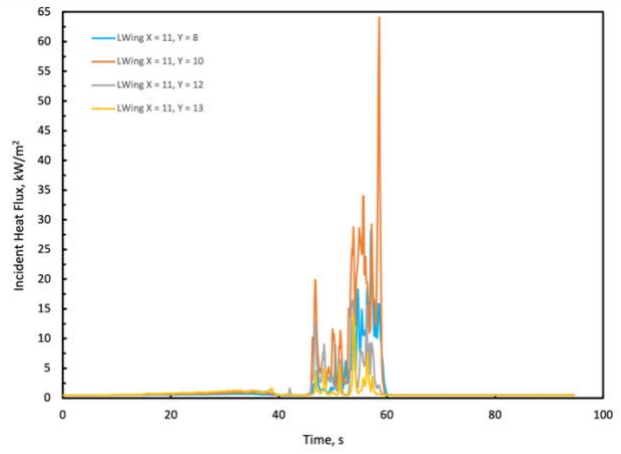


Figure 0-39 Incident Heat Flux versus time for various locations on the left wing ($X = 11$) for simulation C.1

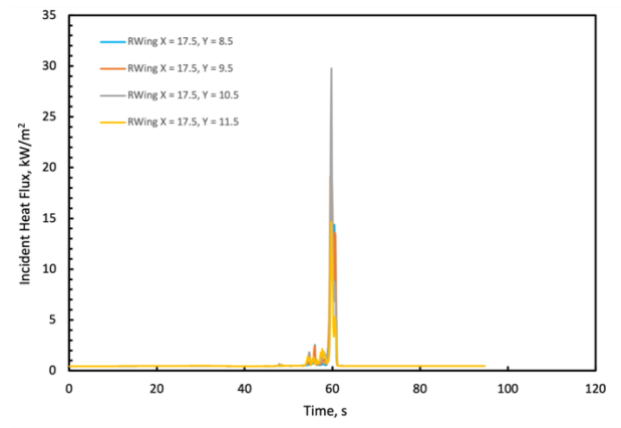


Figure 0-40 Incident Heat Flux versus time for various locations on the right wing ($X = 17.5$) for simulation C.1

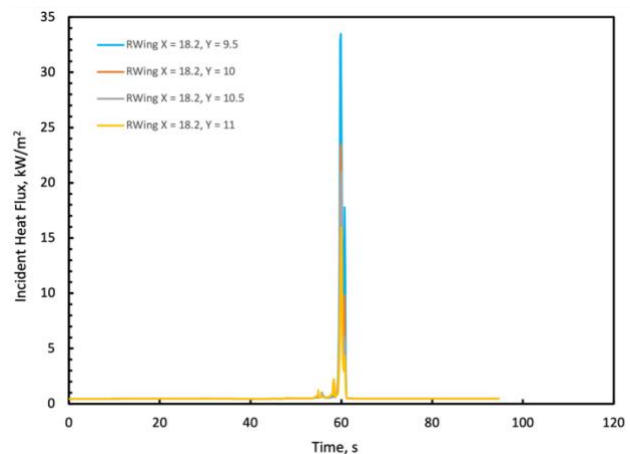


Figure 0-41 Incident Heat Flux versus time for various locations on the right wing ($X = 18.2$) for simulation C.1

H.3.2 Simulation C.2

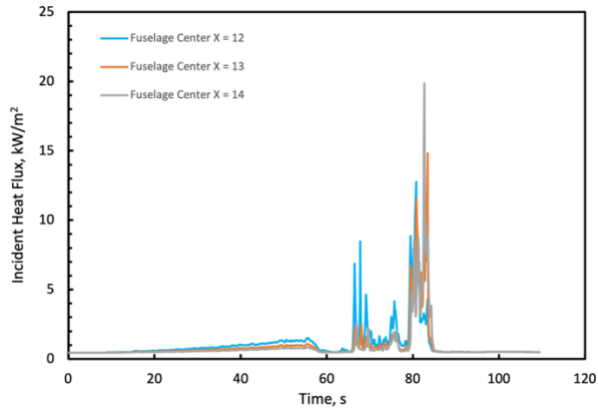


Figure 0-42 Incident Heat Flux versus time for various locations across the center of the fuselage (Y=13) for simulation C.2

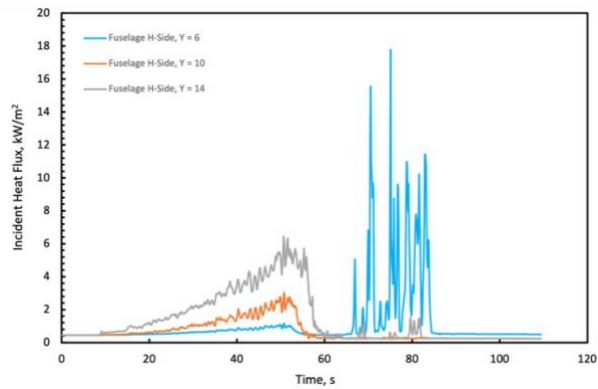


Figure 0-43 Incident Heat Flux versus time for various locations along the high side of the fuselage for simulation C.2

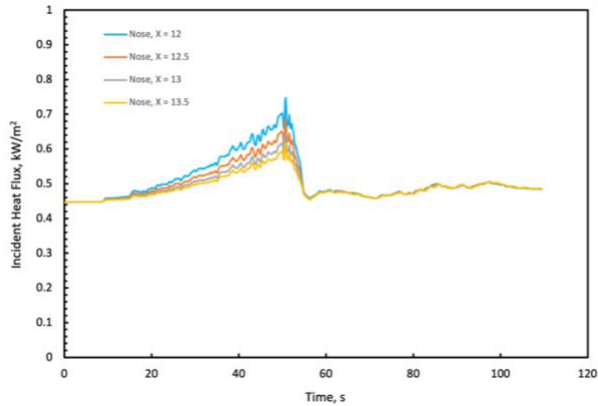


Figure 0-44 Incident Heat Flux versus time for various locations along the Nose of the aircraft (Y = 20) for simulation C.2

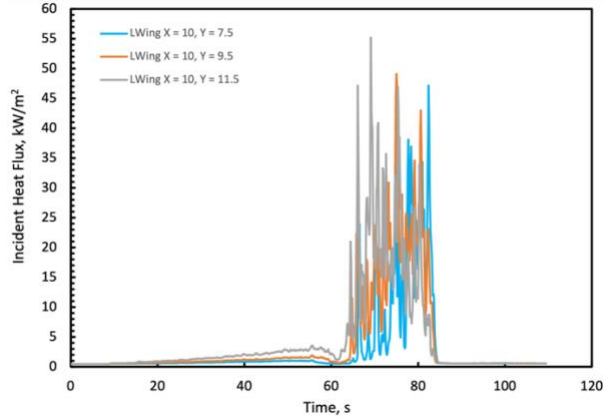


Figure 0-45 Incident Heat Flux versus time for various locations on the left wing ($X = 10$) for simulation C.2

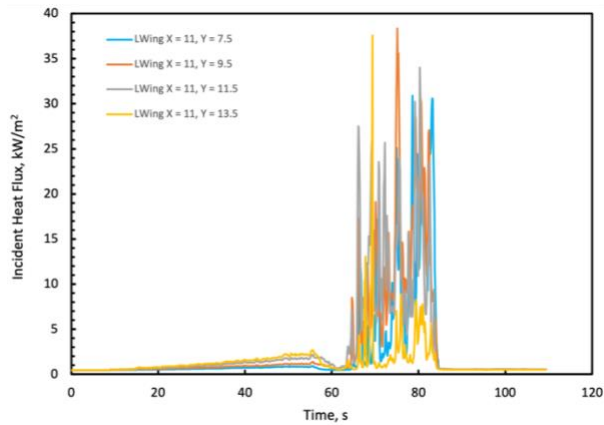


Figure 0-46 Incident Heat Flux versus time for various locations on the left wing ($X = 11$) for simulation C.2

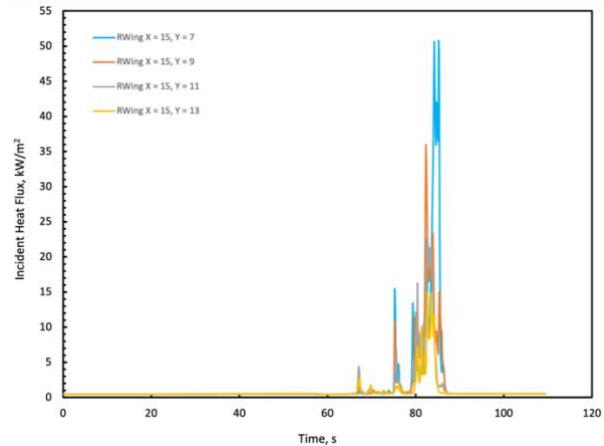


Figure 0-47 Incident Heat Flux versus time for various locations on the right wing ($X = 15$) for simulation C.2

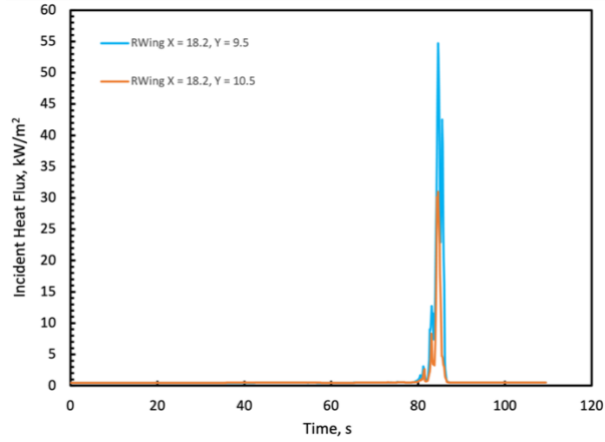


Figure 0-48 Incident Heat Flux versus time for various locations on the right wing ($X = 18.2$) for simulation C.2

References

1. Milke, J.A., Behera, S., Lee, K. and Slingsluff, C. (2019, November). *Review of Foam Fire Suppression System Discharges in Aircraft Hangars*. Retrieved from https://www.nata.aero/assets/Site_18/files/NFPA%20409/UMD%20Report%2011-12.pdf
2. *Standard on Aircraft Hangars*. (2011). Quincy, MA: National Fire Protection Association.
3. Milke, J.A., Brondum, N., Dunne, S., and Whitcomb, C. (2021, February 22). *Review of Foam Fire Suppression System Discharges in Aircraft Hangars*. Retrieved from https://www.nata.aero/assets/Site_18/files/NFPA%20409/UMD-Poole%20Hangar%20Research%20Report.pdf
4. McGrattan, K., Hostikka, S., Floyd, J., McDermott, R., Vanella, M. (2019). *Fire Dynamics Simulator: Technical Reference Guide*. Retrieved from <https://nvlpubs.nist.gov/nistpubs/Legacy/SP/nistspecialpublication1018.pdf>
5. McGrattan, K., Hostikka, S., Floyd, J., McDermott, R., Vanella, M. (2020). *Fire Dynamics Simulator Technical Reference Guide Volume 3: Validation*. Baltimore, MD: NIST Special Publication 1018-3.
6. *Types of Fire Suppression Systems*. (2020, October 20). Retrieved from <https://www.fike.com/knowledge-center/101/types-of-fire-suppression-systems/>
7. *FM Approval Guide*. (n.d.). Retrieved from https://www.approvalguide.com/CC_host/pages/custom/templates/FM/index.cfm?line=-1
8. Gottuk, D.T., White, D.A. (2016). "Liquid Fuel Fires," SFPE Handbook of Fire Protection Engineering, 5th edition, M. Hurley (ed.), New York: Springer.
9. Beyler, C. L. (2016). "Fire Hazard Calculations for Large, Open Hydrocarbon Fires," SFPE Handbook of Fire Protection Engineering, 5th edition, M. Hurley (ed.), New York: Springer.
10. Edwards, J. T. (2017). *Reference Jet Fuels for Combustion Testing*. *55th AIAA Aerospace Sciences Meeting*. doi:10.2514/6.2017-0146

11. Chickos, J. S., & Zhao, H. (2005). Measurement of the Vaporization Enthalpy of Complex Mixtures by Correlation-Gas Chromatography. The Vaporization Enthalpy of RP-1, JP-7, and JP-8 Rocket and Jet Fuels at T= 298.15 K. *Energy & Fuels*, 19(5), 2064-2073. doi:10.1021/ef050116m
12. McGrattan, K., Hostikka, S., Floyd, J., McDermott, R., Vanella, M. (2019) Fire Dynamics Simulator: User's Guide. Retrieved from <https://nvlpubs.nist.gov/nistpubs/legacy/SP/nistspecialpublication1019.pdf>
13. Gott, J. E., Lowe, D. L., Notarianni, K. A., & Davis, W. (1997). Analysis of High Bay Hangar Facilities for Fire Detector Sensitivity and Placement. NIST TN-1423, Gaithersburg, MD: National Institute of Standards and Technology.
14. Vaari, J., Hostikka, S., Sikanen, T., & Paajanen, A. (n.d.). *Numerical simulations on the performance of water-based fire suppressions systems* (Tech. No. ISBN 978-951-38-7882-5). JULKAISIJA – UTGIVARE. Retrieved from <http://www.vtt.fi/publications/index.jsp>
15. Table 6 Thermal Conductivity, Specific Heat Capacity and Density. (n.d.). Retrieved from https://help.iesve.com/ve2018/table_6_thermal_conductivity__specific_heat_capacity_and_density.htm
16. ASTM A525 Galvanized Steel. (n.d.). Retrieved from http://www.matweb.com/search/datasheet_print.aspx?matguid=abfb07b7f93a4c358a0ddd194f5c18be&n=1
17. Bocchieri, R., Cozart, K., Wells, S., Kirkpatrick, S., MacNeill, R., Dierdorf, D., Enlow, M. (2003, May). *Firefighting and Emergency Response Study of Advanced Composite Aircraft; Objective 1: Composite Material Damage in Minor Aircraft Fires*. Retrieved from <https://apps.dtic.mil/dtic/tr/fulltext/u2/a592381.pdf>
18. Choi, I., Chung, K., & Lee, H. (2017). Thermal and Mechanical Properties of Structural Steel SN400 at Elevated Temperatures. *International Journal of Steel Structures*, 17(3), 999-1007. doi:10.1007/s13296-017-9011-z
19. Material Thermal Properties Database. (n.d.). Retrieved from

https://ncfs.ucf.edu/burn_db/Thermal_Properties/databases.html

20. VID Fire Kill ApS. (2018, January) *Product Data Sheet Hangar Protection System Model F-102*. Retrieved from <https://vidaps.dk/wp-content/uploads/DS-171218-08-03-F102.pdf>